Hierarchical Flight Control System Synthesis for Rotorcraft-based Unmanned Aerial Vehicles

by

Hyunchul Shim

B.A. (Seoul National University, Seoul, South Korea) 1991
M.S. (Seoul National University, Seoul, South Korea) 1993

A dissertation submitted in partial satisfaction of the

requirements for the degree of

Doctor of Philosophy
in

Engineering-Mechanical Engineering

in the

GRADUATE DIVISION

of the

UNIVERSITY OF CALIFORNIA, BERKELEY

Committee in charge:

Professor S. Shankar Sastry, Chair
Professor Andrew K. Packard
Professor J. Karl Hedrick
Professor Edward A. Lee

Fall 2000

The dissertation of Hyunchul Shim is approved:

Chair Date

Date

Date

Date

University of California, Berkeley

Fall 2000

Hierarchical Flight Control System Synthesis
for Rotorcraft-based Unmanned Aerial Vehicles

by

Hyunchul Shim

Abstract

Hierarchical Flight Control System Synthesis for Rotorcraft-based Unmanned Aerial Vehicles

by

Hyunchul Shim

Doctor of Philosophy in Mechanical Engineering

University of California, Berkeley

Professor S. Shankar Sastry, Chair

The Berkeley Unmanned Aerial Vehicle (UAV) research aims to design, implement, and analyze a group of autonomous intelligent UAVs and UGVs (Unmanned Ground Vehicles). The goal of this dissertation is to provide a comprehensive procedural methodology to design, implement, and test rotorcraft-based unmanned aerial vehicles (RUAVs). We choose the rotorcraft as the base platform for our aerial agents because it offers ideal maneuverability for our target scenarios such as the pursuit-evasion game. Aided by many enabling technologies such as lightweight and powerful computers, high-accuracy navigation sensors and communication devices, it is now possible to construct RUAVs capable of precise navigation and intelligent behavior by the decentralized onboard control system. Building a fully functioning RUAV requires a deep understanding of aeronautics, control theory and computer science as well as a tremendous effort for implementation. These two aspects are often inseparable and therefore equally highlighted throughout this research.

The problem of multiple vehicle coordination is approached through the notion of a hierarchical system. The idea behind the proposed architecture is to build a hierarchical multiple-layer system that gradually decomposes the abstract mission objectives into the physical quantities of control input. Each RUAV incorporated into this system performs the given tasks and reports the results through the hierarchical communication channel back to the higher-level coordinator.

In our research, we provide a theoretical and practical approach to build a number of RUAVs based on commercially available navigation sensors, computer systems, and radio-controlled helicopters. For the controller design, the dynamic model of the helicopter is first built. The helicopter exhibits a very complicated multi-input multi-output, nonlinear, time-varying and coupled dynamics, which is exposed to severe exogenous disturbances. This poses considerable difficulties for the identification, control and general operation. A high-fidelity helicopter model is established with the lumped-parameter approach. With the lift and torque aerodynamic model of the main and tail rotors, a

nonlinear simulation model is first constructed. The control models of the RUAVs used in our research are derived by the application of a time-domain parametric identification method to the flight data of target RUAVs. Two distinct control theories, namely classical control theory and modern linear robust control theory, are applied to the identified model. The proposed controllers are validated in a nonlinear simulation environment and tested in a series of test flights.

With the successful implementation of the low-level vehicle controller, the guidance layer is designed. The waypoint navigator, which decides the adequate flight mode and the associated reference trajectory, serves as an intermediary between the low-level vehicle control layer and the high-level mission-planning layer. In order to interpret the abstract mission planning to commands that are compatible with the low-level structure, a novel framework called *Vehicle Control Language* (VCL) is developed. The key idea of VCL is to provide a mission-independent methodology to describe given flight patterns. The VCL processor and vehicle control layer are integrated into the hierarchical control structure, which is the backbone of our intelligent UAV system. The proposed idea is validated in the simulation environment and then fully tested in a series of flight tests.

S. Shankar Sastry
Chair

Contents

List of Figures

List of Tables

List of Symbols

a	: semimajor axis length of the ellipsoidal approximation of the Earth
a_0	: coning angle of main rotor
A_1	: lateral cyclic pitch
a_{1s}	: longitudinal flapping angle of main rotor
b	: semiminor axis length of the ellipsoidal approximation of the Earth
b	: number of blades in a rotor system
B_1	: longitudinal cyclic pitch
b_{1s}	: lateral flapping angle of main rotor
c_d	: drag coefficient of a blade
D	: drag force of rotor
$\frac{dM}{da_{1s}}$	: Flapping stiffness in pitch direction
$\frac{dR}{db_{1s}}$	: Flapping stiffness in roll direction
e	: eccentricity of the ellipsoidal approximation of the Earth
f	: flatness of the ellipsoidal approximation of the Earth
g	: gravitational acceleration
h	: vertical distance between the C.G. location and the acting point of a force
$K_{p_x}, K_{p_y}, K_{p_z}$	: Feedback gain for p_x, p_y, p_z channel, respectively
K_u, K_v, K_w	: Feedback gain for *u, v, w* channel, respectively
K_Φ, K_Θ, K_Ψ	: Feedback gain for roll, pitch, and yaw channel, respectively
l	: longitudinal distance between the C.G. location and the acting point of a force
m	: mass of helicopter
$m_{1,2,3,4,5,6}$	: temporary variables for closed-form thrust equation
m_b	: unit mass of blade
$n_{1,\cdots,10}$	: temporary variables for closed-form torque equation

p	: roll rate
Q	: anti-torque of rotor
$\mathbf{q}$	: quaternion
q	: pitch rate
$q_{1,2,3,4}$	: components of a quaternion
$Q_{M,T}$	: Torque of main and tail rotor, respectively
R	: radius of a rotor (often referring to the main rotor diameter)
r	: yaw rate
R_0	: inner radius of a rotor where the effective blade section starts
$\mathbf{R}_{A\to B}$	: rotational matrix from coordinate frame *A* to coordinate frame *B*
T	: thrust of a rotor
$T_{M,T}$	: Thrust of main and tail rotor, respectively
$u_{a_{1s}}$	: input to the longitudinal flapping
$u_{b_{1s}}$	: input to the lateral flapping
$u_{r_{ref}}$	: reference input to the yaw rate feedback system
u_{θ_M}	: input to the main rotor collective pitch
u_{θ_T}	: input to the tail rotor collective pitch
$\mathbf{V}$	: velocity vector
V_C	: vertical climb velocity of a helicopter
W_A	: Actuator weighting function
W_N	: Noise weighting function
W_P	: Performance weighting function
W_Q	: Handling quality weighting function
W_U	: Uncertainty weighting function
$\mathbf{X}$	: position vector
y	: lateral distance between the C.G. location and the acting point of a force
(I_{xx}, I_{yy}, I_{zz})	: mass moment of inertia in *x*,*y*,*z*-direction of body coordinate system
(p_x, p_y, p_z)	: position vector in local Cartesian coordinate
(R_i, M_i, N_i)	: moment in *x*, *y*, and *z*-direction exerting on *i*-component, respectively

(u, v, w) : body velocity in *x*, *y*, and *z*-direction

(X_i, Y_i, Z_i) : body force in *x*, *y*, and *z*-direction exerting on *i*-component, respectively

Φ : roll angle of Euler angle representation

ϕ : longitude in geodetic coordinate system

λ : latitude in geodetic coordinate system

μ : structured singular value

Θ : pitch angle of Euler angle representation

θ : pitch angle of rotor

ρ : density of air

σ : singular value of a matrix

τ_f : time constant of rotor flapping in the Bell-Hiller stabilizer system

Ψ : yaw angle of Euler angle representation; or azimuth angle of main rotor rotation

Ω : angular velocity of main and tail rotors

$\mathbf{\Omega}$: angular velocity tensor

$\boldsymbol{\omega}$: angular velocity vector

Superscripts

^{TP} : tangent-plane

^{b} : body frame

Subscripts

$_{M, T, H, V, F}$: main rotor, tail rotor, horizontal stabilizer, vertical stabilizer, and fuselage, respectively.

Acknowledgements

I believe that I am truly privileged to participate in this fascinating project as a founding member since 1996. I would like to give my deepest gratitude to Professor Shankar Sastry for his guidance, insight, and vision on this project. I would like to thank Professor Andy K. Packard, who has guided and encouraged my work with such passion and sincerity for knowledge, teaching and care. Also I would like to thank Professor J. Karl Hedrick and Professor Edward A. Lee for their time and valuable advices on my dissertation.

I would like to thank my research fellows Hoam Chung, Frank Hoffman, Jin Kim, John Koo, Cedric Ma, Omid Shakernia, Cory Sharp, Rene Vidal for their help, advice, and cooperation for many years.

I would like to thank Peter Ray in Electronics Research Laboratory of EECS department of UC Berkeley, whose trust and encouragement brought my research and our group this far. I am also very grateful to Judy Liebman, who proofread my dissertation in great detail.

I am pleased to acknowledge the financial support of the Army Research Office DAAH04-96-1-0341 and by the Office of Naval Research under Grants N00014-97-1-0946, and DARPA F33615-98-C-3614.

I would like to thank my previous advisor Professor Masayoshi Tomizuka in ME department for allowing my study in Berkeley. My experience in motion control in his laboratory is also a valuable part of my stay in Berkeley.

I would like to thank my research advisor back in my Master's degree, Professor Kyo-Il Lee in Seoul National University, Korea, for starting the pioneering research of helicopter control back in 1991. My experience in his lab certainly set the direction of my research. Also I would like to thank Eun-Ho Lee for his insight on the future of autonomous helicopter research.

My special thanks go to my family. I would like to thank my parents, who taught me to take chances for better things in my life. Also my gratitude to my late grandmother, who has offered me unconditional love and care. I thank my brothers for their care and wish the best in their career.

In retrospect, this project did start humble but have grown to be a great success as now. There are many happy times and many disappointing moments, but now I am very happy because all the hardship I had to go through mostly alone finally paid off.

Above all, all the glory to God for everything that He has provided in my life, especially during my years in Berkeley. "He who began a good work in you will complete it until the day of Jesus Christ."

Chapter 1

Introduction

The Berkeley UAV (Unmanned Aerial Vehicle) research aims to synthesize, implement, and analyze a hybrid system consisting of multiple agents. These agents actively operate, interact, cooperate, and achieve the given abstract tasks using the provided autonomy and intelligence in poorly known or completely unknown environment. This goal encompasses diverse fields of science and technology such as control theory, hybrid system theory, artificial intelligence, probabilistic reasoning, and vision-based servoing to name a few. Although the project was originally initiated for the creation of single UAV, it has diversified into many subgroups. Since the beginning of our project in 1996, remarkable research efforts have been made in many fields such as hybrid system theory and analysis [1], multiple agent coordination [2,3], map building, collision avoidance, and vehicle stabilization and control [4,5,6].

Among these many topics, the research on UAV flight system design remains the original and fundamental one because it is the cornerstone technology that provides the testbed upon which other abstract-level research can be implemented and evaluated. The UAV system design problem alone encompasses many challenging research topics such as system identification, feedback control system, navigation sensor design and implementation, hybrid systems, signal processing, realtime control software design, and component-level mechanical-electronic integration. Indeed, UAV development is a showcase of diverse fields of science and technology.

The Berkeley UAV team strives to construct a fleet of UAV systems that are endowed with intelligence and autonomy to independently accomplish the given abstract commands while interacting with other agents in the neighborhood. The UAV is built by putting together state-of-the-art navigation sensors and high-performance onboard computer systems with realtime software control and background optimization processes, on a commercially available radio-controlled small-size helicopter. The sensing capability of the vehicle is extended by additional sensor systems such as vision processor, laser range finder and so forth. The vehicle communicates with other agents and the ground posts through the broadband wireless communication device, which will be capable of dynamic network IP forwarding. The vehicle will be truly autonomous when it is capable of self-start and automatic recovery with a single click of a button on the screen of the vehicle-monitoring computer. The individual UAVs are integrated with the overall system through the hierarchical system structure so that they can perform the given task in a cooperative manner. A high-level mission command is decomposed into a set of low-level vehicle stabilization and control commands associated with the proper flight mode and reference trajectory. In the following, we briefly overview the relevant technologies of the UAV system and the hierarchical architecture.

1.1 Overview of UAV Research

A UAV indicates an airframe that is capable of performing given missions autonomously through the use of onboard sensors and manipulation systems. Any type of aircraft may serve as the base airframe for a UAV application. Traditionally, the fixed-wing aircraft have been favored as the platform because of many good reasons: they are simple in structure, efficient, and easy to build and maintain. The autopilot design is easier for fixed-wing aircrafts than for rotary-wing aircrafts because the fixed-wing aircrafts have relatively simple, symmetric, and decoupled dynamics. Some fixed-wing UAVs (FUAVs), Pioneer UAV from Israel for example, have very successful records in actual field operations. However, rotorcraft-based UAVs have been desirable for certain applications where the unique flight capability of the rotorcraft is required. The rotorcraft can take off and land within limited space. They can also hover, and cruise at very low speed. Research of Rotorcraft-based UAVs has finally become an active area during the last decade although one of the first RUAVs, Gyrodyne QH-50, made its debut in 1958. One of the driving forces of the overdue proliferation of RUAVs may be attributed to the maturing technologies that became available during the last 10 years, such as rotorcraft dynamics, control system theory and application, high-accuracy small navigation systems and GPS.

While building a fixed-wing aircraft that meets the given requirements such as payload is relatively easy, building a custom-designed helicopter requires tremendous knowledge, time, and effort. The market for the helicopter platform for RUAV development is very small and specialized. Most of the above reasons contribute to the general understanding that RUAVs are more expensive and more difficult to operate than FUAVs. However, only RUAVs can perform some applications such as low-speed tracking maneuvers in law-enforcement, reconnaissance, and operations where no runway is available for take-off and landing. Thanks to the vertical take-off and landing (VTOL) capability, rotorcrafts can take off and land on a very limited space such as a ship deck. Hover, low-speed flight and sideslip capabilities make the helicopter a perfect vehicle for tracking or searching out ground targets. This versatile flight capability is achieved at the expense of having complicated and inherently unstable dynamics, lower fuel-efficiency, and slower cruise speed. Furthermore, the helicopter powertrain and control mechanisms are heavier and more complicated. In summary, the characteristics of RUAVs are listed:

Advantages

- Small space is required for launch and retrieval
- Versatile flight modes: vertical take-off, landing, hover, pirouette, sideslip, low-speed cruise

Disadvantages

- More complicated mechanical structure
- Inefficient flight dynamics: lower maximum speed, shorter mission range
- More accurate and complicated navigation sensor requirement
- Inherently unstable and relatively poorly known dynamics→difficult control system design

Figure 1.1 First Navy RUAV: Gyrodyne QH-50 “DASH”

As pointed out above, the main challenges of the RUAV application come from the restrictive performance and the inherently unstable dynamics. There are some efforts to resolve the limitation of the cruise speed and mission radius caused by the inefficiency of the rotor in cruise mode. One of the candidates is the *tilt-rotor* aircraft, which has two propeller engine modules mounted at each end of the wing and it tilts the propellers from the vertical to the horizontal direction to obtain vertical lift to horizontal thrust while the stubby wing takes the responsibility to generate the lift (Figure 1.2). With this unique lift/thrust generation mechanism, the tilt-rotor aircraft satisfies the same requirements of FUAV in terms of maximum cruise speed and mission radius while it takes off and lands vertically. One of the major disadvantages of the tilt-rotor aircraft is the prohibitively high cost because of the complicated propulsion and actuation system as well as the exceptionally high requirement of structural strength.

Figure 1.2 Tilt-rotor UAV: The Bell Eagle Eye

Another drawback of RUAVs is the complex vehicle dynamics, which needs a more sophisticated control algorithm than that for a fixed-wing aircrafts. The helicopter dynamics are inherently unstable and it requires velocity feedback as well as attitude feedback to stabilize and control. Velocity feedback needs the accurate velocity estimates, which can be obtained by the use of an inertial navigation system. The inertial navigation system in turn requires external aids so that the velocity and position estimates do not diverge with the uncompensated bias and drift of the inertial instruments, i.e., accelerometers and rate gyroscopes. Another irony is that, even though UAVs are typically smaller than the full-size manned vehicles, they usually require more accurate sensors because the demanded sensor accuracy is higher when the vehicle is smaller. For example, the Boeing 747 would not require one-meter accuracy to guide it across the Pacific Ocean. On the contrary, a 1.5m long RUAV would not be able to accurately hover with a 1m-accuracy sensor about the given waypoint. This observation alone asserts the complication of the onboard navigation and control system required for helicopter control.

Fortunately, however, many of the obstacles to constructing an autopilot system for RUAVs are eliminated thanks to enabling technologies. In the sensor realm, inertial instruments fabricated by micromachining technology can be made small enough to fit on a monolithic chip die. The NAVSTAR GPS system has been another major thrust because it provides the position estimates with bounded error at any time on any location on the earth when a good view of the sky is available. In the year 2000, the Selective Availability (S/A), the intentionally injected noise for the degradation of position accuracy for those not authorized by the US Department of Defense, was finally eliminated and the accuracy without any differential GPS correction improved by roughly 10 times, making it possible to achieve 10-meter or better accuracy in SPS mode.

Another driving force is the ever-increasing computing power of microprocessors, whose speed of innovation is simply amazing. For example, the flight computer used to be overloaded just for the low-level control tasks because of the limited CPU processing power just a couple of years ago. Nowadays, with the fastest speed reaching a 1GHz clock speed, the onboard control system can execute complicated guidance and control algorithms running in realtime. In our experience, for example, the onboard computer using a Pentium 233MHz runs the discrete-time implementation of a robust controller of 50^{th} order in realtime.

Another supporting technology came from advanced wireless communication devices. These devices are vital for remote operation without cumbersome umbilical cords. The wireless LAN provides IEEE 802.11 compatible CSMA/CD protocol on wireless media. This allows peer-to-peer communication that is perfect for multi-agent scenarios.

The advances in modeling, identification and control of the helicopter are also a major contributing factor to the proliferation of RUAVs. With an accurate understanding of dynamics, the controller design and testing has become very straightforward and safe. The availability of fast, efficient, and accurate simulation environments such as MATLAB have also helped to speed up the development of RUAVs.

Overall, the helicopter is considered a promising VTOL UAV platform because the desired maneuverability can be achieved with an acceptable level of difficulties in terms of controller design and operation. In our research, the helicopter platform is particularly useful because it offers the maneuverability desirable for our target scenarios such as the *pursuit-evasion game*. In the Berkeley spirit, along the same lines as the invention of Cyclotron instead of a linear accelerator due to the limited space on the campus, one motivation to adopt the helicopter as the base airframe is that they do not require large open spaces with runways to take off and land. In addition, the RUAV serves as an excellent testbed for advanced identification, control, and hybrid system theories, which will be reviewed in the following sections.

1.2 Hierarchical Vehicle Management Structure

As mentioned above, we are aiming to construct a group of RUAVs that are capable of performing high-level tasks in an interactive manner. To achieve this level of autonomy, a more sophisticated approach than simple feedback control is necessary. In this research, we adopt the hierarchical vehicle management system. This system has been proven very effective for other hybrid systems problems such as the automated highway system [8] and the air traffic management system (ATMS) [9](Figure 1.3). The adopted structure allows good insight into how a UAV system should be constructed as a number of hierarchical layers interacting with each other in order to achieve the given high-level tasks. When we deal with a hierarchical structure, we can approach it with either a top-down approach or with a bottom-up approach. While the former advantageously allows a more systematic and orderly approach, it lacks in perceiving physical requirements and limitations. This approach often ends up with a total detachment from reality by introducing too many simplifying assumptions. The irony of idealization is that it yields often mathematically-beautiful-but-just-don't-work-in-reality situations. These situations are even more likely to come up when we deal with very complicated real systems like UAVs. Therefore, the bottom-up approach is chosen because the problem of UAV system construction is still under vigorous study and hence is not a well-established area. UAV system construction requires trial-and-error and feedback from the base vehicle construction problem. Indeed, there have been many instances when we had to go back to the conceptual design stage to tackle physical problems.

1.3 Relevant Research

There are a number of important fields of science and technology, which are directly related with this research: (1) general helicopter dynamics, (2) RUAV development, (3) system identification and (4) control.

Helicopter dynamics have been studied for many decades since its debut in the 1940s. The helicopter dynamics in theoretical and experimental field are well established [10,11] and it is usually directly applicable to RUAV study because RUAVs have a very similar configuration to full size helicopters. To be specific, many results such as rotor thrust and torque equations can be applied with minimal modification for our application. The flapping dynamics, which plays the crucial role for helicopter stability and control, show one critical difference due to the use of the *Bell-Hiller stabilizer*, which is widely used in small-size helicopters.

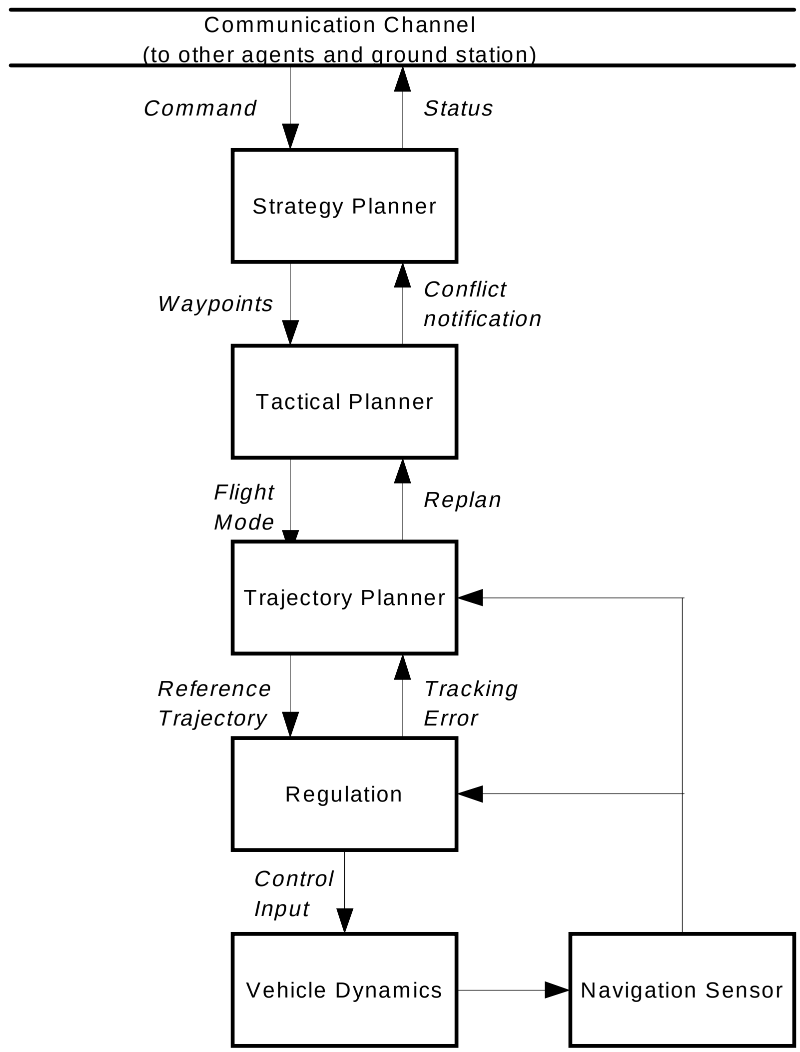

Figure 1.3 Hierarchical flight control system

Some of the earliest modern research on helicopter control is the application of LQR theory on helicopter control [12] and hover control with sling-load [13] from the 1960s. After these works, there has been much research in the area of helicopter control which uses various approaches. These approaches can be categorized into (1) classical control [14], (2) linear quadratic regulation [15], (3) Eigenstructure assignment [16], (4) robust control theory such as H_∞ [17,18,19] or μ-synthesis [20], and (5) rotor dynamics inclusion [21,22,23] . These results allow insights on how the control system should be synthesized for small-size helicopter dynamics.

Since the 1980s, a few research results on small-size helicopter control have begun to appear in publications [24]. During this time, while vast numbers of control theories were available, the experiments were severely limited by the lack of accurate navigation sensors. As an alternative approach, they often used a linkage system which is attached to the helicopter body to allow a free but limited range of motion while providing position and attitude measurements from the potentiometers installed at each joint [24,25,26,27,28,29]. Usually, the dynamics are additionally constrained to have freedom in attitude only. This makes the problem easier because the helicopter dynamics in attitude becomes marginally stable only when the translational motion is constrained [10]. In other research, ground-based cameras were employed to estimate the position of the helicopter in three-dimensional space by taking continuous images of the visual markers on the helicopter body. In either case, the accuracy of motion estimates and the degree-of-freedom of the test vehicle were significantly limited.

After 1990, flying RUAVs in full six degrees-of-freedom and without any constraints or umbilical cords finally became possible due to the advent of small-size, high-accuracy INS and GPS. With this break-through technology, a number of research efforts in similar topics of RUAV development were published [6,30,31,32]. Another driving force behind RUAV development was the International Aerial Robotics Competition. This competition has encouraged many research groups to build autonomous unmanned aerial vehicles designed to perform the given tasks, which require low-speed or hovering for ground scanning and target recognition.

In this area, Draper Laboratory at MIT, Team Hummingbird of Stanford University, the Robotics Institute at Carnegie-Mellon University, as well as Georgia Institute of Technology, the originator of the competition, have participated in the competitions and demonstrated their technologies of autonomous helicopter systems. Overseas, University of Berlin has been doing outstanding work for the 1999 and 2000 competitions. It is worthwhile to review how these groups approached the UAV design problem and understand key technologies they utilized.

The Hummingbird from Stanford won the competition in 1995 marking the milestone by demonstrating the first fully autonomous flight and fulfilling the rule, which required picking up disks on one side of a tennis court and dropping them on the other side. The vehicle platform was a hobby-purpose radio-controlled helicopter, Excel 60, which was heavily modified to carry a total weight of 46 pounds. The unique feature of this helicopter is the sole use of GPS as the navigation sensor. They wanted to demonstrate that GPS could replace the INS, which is conventionally favored as the primary navigation sensor. Their GPS system consisting of a common oscillator and four separate carrier-phase receivers with four antennae mounted at strategic points of the helicopter body provides the position, velocity, attitude and angular information for vehicle control.

The team from Draper Laboratory won the competition in 1996 by fulfilling the new rule, which required the autonomous vehicle to navigate the given field looking for barrels identifiable by the labels attached to their top and side and then report the position and type of each barrel to the ground base. Draper used a 60-class helicopter as their base platform. For the navigation system, they took the canonical approach of INS/GPS combination. Their navigation system consisted of a Systron-Donner MotionPak™ IMU, a NovAtel GPS, a digital compass and an ultrasonic altimeter. The flight computer was a standard PC104 system, which is PC-compatible. The inertial measurements were sampled and processed by the onboard computer running numerical integration, the Kalman filtering algorithm, and simple PID control as the low-level vehicle control. The control gain was determined by *tuning-on-the-fly* while the safety of the vehicle is at the hand of a very capable human pilot. The morale of the Draper approach is to demonstrate the possibility of building RUAVs using COTS components.

The winner in the year of 1997 was a group from the Robotics Institute at Carnegie-Mellon University. They built their RUAV on a Yamaha R-50, a helicopter developed for agricultural use such as crop-dusting because in Japan because of their tight regulations on the operation of full-size aircraft. Unlike the previous helicopters, their platform has a more-than-sufficient payload of 20 kg. The unique feature of their helicopter is the vision-only based navigation capability. The onboard DSP-based vision processor provides navigation information such as position, velocity and attitude at an acceptable delay on the order of 10ms. Their vision system is also capable of performing the target identification required by the same rule as in 1996. Their research is the showcase of an advanced vision system applied to the aerial vehicle control problem.

1.4 Project History

The Berkeley UAV research group has expanded its scope of interests from the design of a single UAV flight control system to a group of interacting agents. These agents include UAVs, UGVs and a ship-motion simulating landing deck. This project first started when our colleague Tak-kuen John Koo proposed the idea of building an autonomous helicopter system to Professor Shankar Sastry in the EECS department of UC Berkeley in 1996. He suggested the author to join this project because of my previous experience with the design and implementation of a hover control for a model helicopter using LQG/LTR during my Master’s program at Seoul National University in 1991 [26]. In the middle of 1996, the Berkeley UAV team made its humble start by John Koo, Ma Yi, Frank Hoffman and the author. Our first UAV platform was the Concept 60 SR II from Kyosho Industry, Japan. The *60*-class model helicopters are the largest commercially available radio-controlled helicopters for hobby use and it offers the largest payload without any modification on the powertrain and rotor blades. Among many helicopters in the 60-class, the Concept 60 from Kyosho Industry was chosen because of the author's previous experience with this model. The primary question during this early period of our research was where this 60-class hobby helicopter could be used for RUAV platform. The most pressing concern was the payload that this vehicle could handle. With the nominal output of 2.2 hp of the OS SX-61WC engine, it was observed that it could lift off with 5 kg of payload and stay *in* the ground effect region. Without fully understanding that the ground effect can boost the thrust significantly even up to 200%, it was concluded that the 60-class helicopters could handle 5 kg of payload or more. It turned out that the acceptable payload of the original 60-class engine is less than 4kg, which is somewhat less than the desired value of 5-6 kg. The first prototype was finished in late 1997. Since the symbol of UC Berkeley is a bear, this helicopter was named as *Ursa Minor 1*, which means "small bear" in Latin. This helicopter was slated to be the first testbed on which navigation and control system could be designed and tested. The flight computer system consists of PC104 compatible CPU and peripheral boards. The navigation system consists of a NovAtel RT-20 GPS board, a digital compass, and a custom INS system consisting of six accelerometers positioned in strategic points. The underlying idea of this special INS is that the six accelerometers can estimate translational acceleration and angular rates using the geometry of the sensor locations. Unfortunately, the person in charge of this type of INS left our project and a replacement for INS had to be sought. In early 1998, Systron-Donner MotionPak™ was adopted as the primary inertial measurement unit. This sensor unit exploits the latest piezoelectric technology yielding a compact, light-weight, and yet powerful INS solution. It consists of three accelerometers and three rate gyros in orthogonal configuration and measures the translational accelerations and angular rates on x, y, and z axis. The raw sensor output, analog voltage from 0V to 10V, is read by an A/D conversion circuit in the flight computer and then processed to obtain the navigation solution for identification and control. The inertial navigation integration equation using quaternion was offered by John Koo and then implemented in MS-DOS and subsequently in QNX. After intense testing for about a year, it is concluded that the custom INS code lacks a proper sensor bias estimation routine and cannot be used to obtain a high-accuracy navigation solution. As an alternative solution, John Koo purchased an INS unit, DQI-NP from Boeing, in late 1998. This INS consists of a piezoelectric inertial sensor unit and a DSP board to process the inertial measurements at very high rate. The navigation solution computed by the DSP chip is available on the RS-232 serial port or a custom high speed synchronized serial port. This system allowed the high accuracy navigation estimates and it boosted to our research progress. The Boeing DQI-NP system is fully integrated with our existing helicopter platform with substantial modification of the navigation software in early 1999.

The excess payload problem seriously delayed the progress of research since the beginning of the project. When fully equipped, *Ursa Minor 2*, the successor of *Ursa Minor 1*, could not reach an altitude outside of the ground effect. Many attempts such as using high-lift main rotor blades or high nitrogen compound composition fuel were made, mostly in vain, to obtain more lift from the same 2-cycle glow engine with 0.60 cubic inch displacement. The clean answer would be to use a replacement engine with higher power. This solution, although not impossible, involves redesigning the engine mount and machining a new gear. These modifications would have exceeded the capabilities and resources available to us.

The breakthrough was made by the adoption of a 0.91 cubic inch engine originally designed for hobby aircraft, with a minor modification of the engine shaft. With this more powerful engine providing 2.8 hp, *Ursa Minor 2* could easily fly out of the ground effect. In parallel to the quest for a more powerful engine, a larger helicopter platform was also sought. In the middle of 1998, a more powerful helicopter, Bergen Industrial Twin, joined the Berkeley RUAV fleet. It is equipped with twin four-stroke gasoline engines welded together for more power. Thanks to this design, the helicopter offers an available payload of 10kg, which is sufficient for most RUAV applications. However, a potential structural problem was anticipated because most of the helicopter parts including the control linkage and the main rotor grips were originally designed for a 60 class engine and they would not withstand the excessive loading by the oversized engine. The payload problem was finally solved by adding Yamaha agricultural helicopters R-50 and their successor RMAX to our Berkeley UAV fleet. Two Yamaha R-50s arrived at Berkeley in June 1999 and two RMAXs in December 1999. At the expense of the extremely high cost, the Yamaha helicopters offer high reliability and generous payload of 20kg-30kg. They now serve as the ultimate platform for diverse UAV research such as vision-based navigation, dynamic wireless network system and advanced control law testbeds.

After the two major problems, the INS and the available payload problems, were solved, the Berkeley *BEAR* project finally began to see results. In early 1999, a newer version of the Kyosho helicopter, Concept 60 SR II Graphite, was built as the primary testbed for control system design. Joining as the third 60-class helicopter, it was named as *Ursa Minor 3*. Boeing DQI-NP was mounted at the tip of the nose using special gel-type mounting to minimize the transmission of the severe engine and rotor vibration. A more powerful CPU, Cyrix MediaGX233, was used in the flight computer. For GPS, NovAtel MillenRT-2 was adopted for its unsurpassed accuracy of 2cm. In July

1999, this configuration tested on *Ursa Minor 3* and then ported to the Yamaha R-50, named as *Ursa Magna*.After intensive work during the summer break of 1999, the *Ursa Magna 2* was equipped with a basic navigation suite, a main flight computer and a vision-processing computer. In August 1999, the first identification flight with active YACS (will be discussed later) was flown. The flight experiment was performed smoothly and high quality flight data was obtained.

The final breakthrough for the control system was made during October 1999. This time, *Ursa Minor 3* was used again as the main experimental platform because it is easy to manage and repair in the case of a crash. However, a more adequate mounting could be used with *Ursa Magna*, thanks to its size and payload. The result is more stable INS/GPS operation. A similar identification flight, applying a frequency-sweeping input, was performed during October 1999. The gathered data was processed using the UAV model proposed by Mettler from Carnegie-Mellon UAV research [**7**]. The greatest advantage of his model is the explicit compensation for the Bell-Hiller stabilizer dynamics. This model was able to predict the stabilizer bar response accurately and the whole model was able to produce estimates closely matching the flight data. One major difference in the identification process from the Carnegie-Mellon team was the numerical tool used for the identification process. While they used the optimization package called CIPHER, which was not available to Berkeley UAV team, I had to use existing tools such as the MatLAB™ Identification Toolbox™ written by Ljung [34]. While CIPHER identifies the model in the frequency-domain, the numerical tool offered by Identification Toolbox™ uses the prediction-error method (PEM) [35]. This approach produced a reasonably accurate model which is valid for hover. Furthermore, a basic multi-loop controller could be designed using the classical root-locus method. From late October to late November of 1999, the basic hovering controller which regulates position in the x, y, and z axis as well as the heading, was designed. The controller showed superior hovering performance with ±20cm accuracy in the x-y plane.

Once the basic controller design/implementation/testing was accomplished, the research effort was steered to the automation of the Yamaha R-50. Many parts of the work for R-50 could be adapted from Ursa Minor 3 with very minor modifications because they share identical sensors, i.e., Boeing DQI-NP and NovAtel MillenRT-2 GPS, and the servomotors accept the same PWM signal. Differences come from the extended sensor suite such as the ultrasonic height meter, the vision computer and the ground contact switch sets. As most of the work had been finished in the summer of 1999, only a small amount of modifications and improvements were made in March 2000. One major difference was the adoption of the Lucent™ (later renamed to Orinoco™) WaveLAN system as the primary communication device. WaveLAN is a wireless local network device supporting popular protocols such as TCP/UDP/IP in IEEE 802.11 compatible CSMA/CD format. Before this, a wireless modem with the maximum throughput of somewhere between 57,600-115,200 bps was used for wireless communication between the ground station and the onboard flight computer. While it offered reliable performance from the beginning of the project, the radio signal of the wireless modem at 900 MHz might have been strong enough to cause jamming with the NovAtel GPS which is receiving signals in the 1 GHz band from the GPS satellites more than 20,000 km away. On the other hand, WaveLAN™ trades range with bandwidth. With the new communication system, the ground station display station, running in Microsoft Window 98, was modified to use the WaveLAN™.

The controller design of the Yamaha R-50 was based on the new system model of this aircraft. The system model of Yamaha R-50 in hover was identified using a similar approach as was used with the case of Kyosho Concept 60. This time, a procedure that is more systematic was developed to identify the model using PEM tool of the MATLAB System Identification Toolbox™. Based on the identified model, the controller was designed and tested during April to May 2000. The designed controller for hovering was validated during flight and it showed satisfactory response *as is,* without any “tweaking” of the controller gain during the test flight.

During May 2000, a novel concept called *Vehicle Control Language* (VCL) was conceived for describing a given mission. As will be discussed later in more detail, VCL is human-understandable ASCII script-type language, which specifies the helicopter mission at the waypoint level. Different flight modes such as take-off, hover, turn, cruise and land are specified with coordinates and options and saved as text files. These VCL files are then uploaded to the target UAV and then executed. The VCL can be generated by typing the commands or by using the convenient graphical user interface offered as a part of the ground station program. In July and August 2000, the first-generation VCL interpreter was tested in a series of test flights and proved the anticipated effectiveness.

1.5 Contributions

This project was funded by Army Research Office (ARO), Office of Naval Research (ONR), and Defense Advanced Research Project Agency (DARPA). Professor S. Shankar Sastry is in charge of the whole project. Peter Ray, a staff of Electronics Research Laboratory (ERL) of Electric, Electronic and Computer Science (EECS) Department of University of California, Berkeley (UCB) is in charge of financial management. Tak-kuen John Koo, a graduate student of EECS department proposed, initiated and led the project until 1999. The project was co-founded by Yi Ma, Frank Hoffman, Kiril Mostov and myself in 1996.

The concept of hierarchical structure and hybrid system were contributed by the previous works of PATH project and ATMS projects. In the beginning, the selection of essential avionic systems was influenced by the previous works of PATH. With the assist of these works, I achieved the following works:

- Assembly of Ursa Minor 1 (Kyosho Concept 60 SR-II) (Fall 1996)
- Assembly of Ursa Minor 2 (Kyosho Concept 60 SR-II) (Summer, 1998)
- Assembly of Ursa Minor 3 (Kyosho Concept 60 SR-II Graphite) (Fall 1998)
- Assembly of Kyosho Caliber 60 (Fall 1999)
- Design, fabrication and assembly of avionics electronics for Ursa Minor 1 (Fall 1997)
- Design, fabrication and assembly of avionics electronics for Ursa Minor 2 (1998)
- Design, fabrication and assembly of avionics electronics for Ursa Minor 3 (Spring 1999)
- Design, fabrication and assembly of avionics for Ursa Magna 2 (Yamaha R-50) (Summer 1999~)
- Design and partial assembly of the avionics for Ursa Maxima 2 (Yamaha RMAX) (Summer 2000~)
- Mechanical part design of tail servo mounting, custom IMU mounting, GPS mounting, etc
- Mounting and enclosure design and machining for Ursa Minor 1, Ursa Minor 2, Ursa Minor 3, Ursa Magna 2 and partial work on Ursa Maxima 3
- Circuit design, layout and fabrication of custom take-over board (TOB) for Ursa Minor 1, Ursa Minor 2, Ursa Minor 3, and Ursa Magna 2
- Programming for early version of navigation algorithm in MS-DOS and QNX
- System identification of Ursa Minor 3 and Ursa Magna 2
- Simulation model derivation and programming in MATLAB/Simulink for Ursa Minor 2, Ursa Minor 3, and Ursa Magna 2
- Classical multi-loop controller design for Ursa Minor 3 and Ursa Magna 2
- μ-Synthesis controller design for Ursa Minor 2 and Ursa Magna 2
- Design, programming, and testing of vehicle management software (VMS) for Ursa Minor 2 (December 1998~April 1999)
- Design, programming, and testing of VMS for Ursa Minor 3 (April 1999~March 2000)
- Design, programming, and testing of VMS for Ursa Magna 2 (June 1999~)

- Design, programming, and testing of VMS for Ursa Maxima 2 (May 2000~)
- Integration of INS/GPS using Systron-Donner MotionPak IMU and NovAtel GPS MillenRT-2 for Ursa Minor 2 (June 1998~April 1999)
- Integration of INS/GPS using Boeing DQI-NP INS and NovAtel GPS MillenRT-2 for Ursa Minor 3 and Ursa Magna 2 (January 1999~)
- Identification flight of Ursa Minor 3 (October 1999)
- Test flight of Ursa Minor 3 (October 1999~March 2000)
- Test flight of Ursa Magna 2 (March 2000~current)
- Creation, programming, simulation, and test flight of VCL-based waypoint navigator (May 2000~)

John Koo is responsible for the shaping-up of the project from the beginning to summer 1999. William Morrison, a graduate student in Mechanical Engineering (ME), designed and machined the mounting of an INS, ultrasonic sensor mounting, battery tray, avionics mounting, and contact switch fixture of Ursa Magna 2.

Santosh Phillip (ME) wrote the driver for Senix ultrasonic sensor.

Shahid Rashid (EECS) and Santosh Phillip wrote a TCP/IP driver for QNX. Shahid also wrote a GUI using LabWindows®.

Cedric Ma (EECS) wrote OpenGL-based software for three-dimensional visualization of helicopter control simulation results. He also performed the system identification test flight of Ursa Magna 2 twice (one time with YACS on and the other time with YACS off).

Hoam Chung (ME) fabricated the majority of the avionics of Ursa Maxima 2. He also assisted many important flight tests such as waypoint navigation and μ-Synthesis attitude controller on Ursa Magna 2 since June 2000.

While not introduced in detail in this dissertation, the vision system and the UGV system are related with this work. Omid Shakernia (EECS), Cory Sharp (EECS), and Rene Vidal (EECS) are responsible for the color tracking vision system on Ursa Magna 2 and UGVs. Cory Sharp wrote the guidance software for Pioneer outdoor UGVs and developed, programmed, and tested a special vision algorithm on Ursa Magna 2. Tullio Celano III (US Navy) constructed two ship-motion simulators based on Stuart platform: the earlier version with electric motors (Fall 1999) and the later and larger version with hydraulic cylinders (Winter 1999~2000). A number of joint works were performed with them: the semi-automatic landing with Ursa Minor 3 (December 1999) and color-based UGV tracking with Ursa Magna 2 (August 2000).

1.6 Scope of This Dissertation

The research presented in this dissertation finds its significance in the establishment of a systematic methodology for the development of RUAVs by the use of commercial off-the shelf (COTS) components such as radio-controlled helicopters, navigation sensors, computers, and communication devices. With the ultimate goal of fully autonomous flight capability from take-off to landing, each step towards the goal has been developed, implemented and tested on three RUAVs. These steps are (1) helicopter dynamics modeling, (2) parametric system identification, (3) hardware integration, (4) software design, and (5) flight test. In the following chapters, the developed technologies for these stages are presented.

The helicopter model is derived from a general full-size helicopter model with the augmentation of the servorotor dynamics. The acquired nonlinear model is directly used for simulation model and it is further simplified through linearization in order to obtain a linear model for controller design. Helicopter platforms are integrated with navigation sensors and onboard flight computers. Once the hardware and software are ready, a number of identification flights, manual flights with certain inputs exciting each flight mode of roll, pitch, yaw and heave, were flown. The input and output of the helicopter was sensed, sampled, downloaded and recorded for processing. The parametric helicopter model for hover is identified by running an identification algorithm with the collected data. After a high-fidelity model was found, both classical control theory and state-space based linear robust control theory are applied for helicopter stabilization. The proposed controllers were tested on Berkeley RUAVs and they showed satisfactory results.

Based on the successful controller for the low-level vehicle stabilization, a vehicle guidance logic is developed. A unique approach proposed in this research is the novel concept of *Vehicle Control Language (VCL)*. VCL is a middle-level vehicle guidance layer in the hierarchical structure shown in Figure 1.3. This approach provides the isolation and abstraction between the low-level vehicle control and the mission-level condition. In this framework, the onboard autopilot system can perform any given feasible mission without any reprogramming of onboard software as the mission changes. The sequence of motion commands is described in a script language form understandable to humans. The VCL module consists of a user interface part on the ground station, a language interpreter, and a sequencer on the UAV side.

It should be stressed that all of the proposed idea in this dissertation were fully tested repeatedly in the actual flight tests. From this point, it is asserted that all of the proposed methodologies in this paper can be repeated on the other RUAV platforms with proper minor modifications.

This dissertation is organized in the following order: in Chapter 2, the general helicopter dynamics are overviewed and the nonlinear simulation model and linear control model are established. Chapter 3 introduces the hardware and software implementation of Berkeley RUAVs in detail. In Chapter 4, the autopilot system design in the context of multi-layer hierarchical structure is addressed. For the low-level control, two distinct approaches of classical control and modern linear robust control are applied for the design of the stabilizing controller using the system model identified in Chapter 2. To bridge the low-level vehicle regulation layer and the high-level strategic coordination, the novel approach of Vehicle Control Language is introduced and the experiment results are shown. Detailed technical information about the RUAVs used in this research is given in the Appendix.

Chapter 2

Helicopter Dynamics Modeling and System Identification

To design an effective autopilot system for a RUAV system, we should first understand the dynamics of the target vehicle platform. The helicopter dynamics are derived by establishing the equations of motion by aerodynamic analysis of the whole system. The dynamics of the helicopter have been well studied over decades and abundant theoretical as well as experimental results are available [10,11]. A nonlinear model to our best knowledge is desired for high-fidelity simulations upon which the proposed controllers are validated. For controller design, the model may be simplified to the detail level that the applied control theory requires

Helicopter dynamics are nonlinear, inherently unstable, coupled, input-saturated, MIMO, and time-varying system with changing parameters. It is exposed to unsteady disturbances such as wind gust and cross wind while operating in diverse flight modes such as take-off, landing, hover, forward flight, bank-to-turn, and even inverted flight. Due to the complicated and almost chaotic behavior involved with the aerodynamics of a helicopter, it is virtually impossible to obtain fully accurate dynamic equations valid for all the aforementioned flight modes. Theoretical model often has rather large errors and has to be adjusted with the experimental data. Therefore, we often have to compromise to obtain models with moderate accuracy for simulation and control design.

In this chapter, we first briefly overview the coordinate systems that are used as the reference frame for the description of helicopter motion. Then, we develop a fully nonlinear model of the helicopter dynamic by lumped-parameter approach. The results derived for full-size helicopters are adapted to account for the specific dynamic behavior of the servorotor of small-size helicopters. The general dynamics are simplified to a model valid for hover and low-velocity motion. The theoretical model derived by aerodynamic equations oftentimes include rather large error due to the inaccurate knowledge about the actual parameters of aerodynamic components and has to be reconciled with the actual experimental results. This process requires certain experiment facilities such as wind tunnel or whirl tower. In many cases, however, these facilities are not easy to access and it would take tremendous time and effort for a small research group in a university. Therefore, we are forced to find some other way to find a model for controller design. For this reason, we adopt the parametric linear time-invariant model proposed by Mettler [**7**] and seek to identify the parameters in the model using the flight data from our RUAVs.

2.1 Coordinate Systems and Transformations

A number of coordinate systems are introduced to describe the motion of RUAV in three-dimensional space.

- Inertial reference system
- Earth-Centered Earth-Fixed (ECEF) system
- Tangent-plane coordinate system
- Body-coordinate system

2.1.1 Inertial Reference System and ECEF System

The inertial reference system is the hypothetical coordinate system where the classical Newtonian mechanics is assumed to hold true. For describing motion bound to the Earth, the inertial reference system is not very convenient because the Earth rotates with respect to the inertial frame. In this application, the ECEF coordinate system, which is not an inertial reference frame, is more convenient. The ECEF coordinate system is, as the name implies, attached to the center of the earth and rotates together as the Earth rotates. Hence, any fixed geographical location on the Earth has constant coordinates with respect to the ECEF system. In the ECEF coordinate system, a given point is expressed in either Cartesian coordinates or geodetic coordinates. The coordinate in the ECEF system is specified by (x_e, y_e, y_e) in the Cartesian coordinate system. The geodetic coordinate system employs certain hypothetical ellipsoid to approximate the complex surface shape of the Earth. A geodetic ellipsoid is defined by its semimajor axis length (a), eccentricity (e), inertial rate of rotation (ω_{ie}), and equatorial effective gravity (γ_e) [36]. There are a number of standard ellipsoids and hence it should be specified when the geodetic coordinates are used in literature. For now, the WGS-84 ellipsoid is commonly used in literature for describing the operation of INS and GPS. In WGS-84 standard, the semimajor and semiminor axes are defined as

Semimajor axis length: a=6378137.0 m

Semiminor axis length: b=6356752.3142 m

In the geodetic system, a coordinate is described by latitude, longitude and absolute height, i.e., $(\lambda, \phi, h)_e$. There is a transformation relationship between the Cartesian coordinates and geodetic coordinates. In WGS-84 standard, the flatness of the ellipsoid is defined as

$$f = \frac{a-b}{a} = 0.0034 \tag{2.1}$$

The eccentricity of the ellipsoid is defined as

$$e = \sqrt{f(2-f)} \tag{2.2}$$

The length of the normal to the ellipsoid, from the surface of the ellipsoid to its intersection with the ECEF z-axis, is

$$N(\lambda) = \frac{a}{\sqrt{1-e^2 \sin^2 \lambda}} \tag{2.3}$$

With given $(\lambda, \phi, h)_e$ and f, e, and N (2.1), (2.2) and (2.3), the Cartesian coordinates are found by the following equations.

$$x = (N+h)\cos\lambda\cos\phi \tag{2.4}$$

$$y = (N+h)\cos\lambda\sin\phi \tag{2.5}$$

$$z = [N(1-e^2)+h]\sin\lambda \tag{2.6}$$

The transformation in the other direction, i.e., geodetic to Cartesian, is rather complicated but exists as well [36].

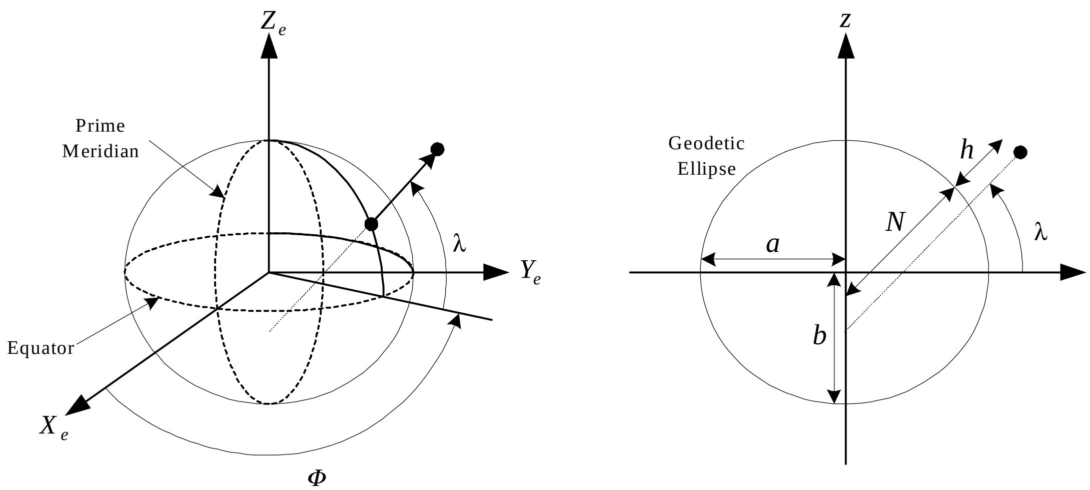

Figure 2.1 Geodetic reference coordinate system

2.1.2 Tangent Plane Coordinate System

The tangent-plane frame is also called the local Cartesian coordinate system. Its origin is located on a certain point of interest and its *x*, *y*, *z* axes align respectively with the north, east and downward direction of the ECEF frame (Figure 2.2). In localized navigation, other than global-scale navigation, it is often more convenient to refer to this coordinate system than geodetic coordinates or Cartesian coordinates in the ECEF frame. Since GPS measurements refers to the ECEF coordinate, we need a transformation from ECEF to the tangent plane coordinate system as following.

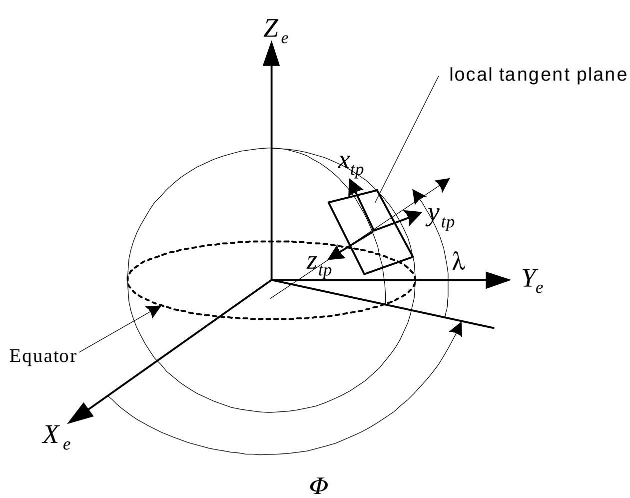

Figure 2.2 Tangent plane coordinate system

The transformation depends on the origin, whose coordinate is denoted as $(x_o, y_o, z_o)_{ECEF}$ or equivalently $(\lambda_{o,}\phi_o, h_o)$ in geodetic frame. With a given point whose coordinate is $(x, y, z)_{ECEF}$ in ECEF coordinates, its transformed coordinate $(x, y, z)_{tp}$ in the tangent plane system is given as following:

$$\begin{aligned}\begin{bmatrix} x \\ y \\ z \end{bmatrix}_{TP} &= \mathbf{R}_{ECEF\to TP}\mathbf{\Delta X}_{ECEF} \\ &= \begin{bmatrix} -\sin\lambda\cos\phi & -\sin\lambda\sin\phi & \cos\lambda \\ -\sin\phi & \cos\phi & 0 \\ -\cos\lambda\cos\phi & -\cos\lambda\sin\phi & -\sin\lambda \end{bmatrix}\left(\begin{bmatrix} x \\ y \\ z \end{bmatrix}_{ECEF} - \begin{bmatrix} x_o \\ y_o \\ z_o \end{bmatrix}_{ECEF}\right)\end{aligned} \tag{2.7}$$

$\mathbf{R}_{ECEF\to TP}$ in equation (2.7) denotes the transformation from ECEF to the tangent-plane system. The inverse transformation is simply the transpose of $\mathbf{R}_{ECEF\to TP}$ because it is, like any other rotational matrix, unitary.

As we are currently interested in local navigation while using global coordinates from GPS and INS, the waypoints usually refer to tangent-plane coordinates and the transformation of equation (2.7) is routinely applied for the processing of GPS measurements by the onboard navigation algorithm.

2.1.3 Body Coordinate System

The body coordinate system is a special coordinate system, whose origin is usually attached to the center of mass of a rigid body of interest and rotates with the body of interest. Trivially, any component rigidly attached to the vehicle, which is assumed as a rigid body, would have a constant coordinate in the body coordinate system. This coordinate system is very important as the reference frame for (1) system dynamic equations, (2) the measurements by strap-down inertial instruments such as accelerometers and GPS, and (3) lever-arm compensation of GPS measurement for INS update.

By the convention of aeronautics, the body coordinate system is attached to the center of mass of the airframe x, y, and z axes point to the nose of airframe, right side, and *downward* respectively, as shown in Figure 2.4.

The transformation between the body coordinate system and the tangent plane system is also needed. This transformation involves the translation and rotation of the rigid body representation of airframe with respect to the tangent plane reference coordinate system. In vector geometry, any point on the rigid body, denoted by $\mathbf{X}_{TP}$, can be represented by vector sum as shown in the following:

$$\begin{aligned}\mathbf{X}_{TP}^{P} &= \mathbf{X}_{TP}^{O} + \mathbf{X}_{TP}^{O\to P} \\ &= \mathbf{X}_{TP}^{O} + \mathbf{R}_{B\to TP}\mathbf{X}_{B}^{O\to P}\end{aligned} \tag{2.8}$$

There are three representations for the rotation transformation $\mathbf{R}_{B\to TP}$.

2.1.3.1 Euler Angles

The rotational matrix commonly represented by the Euler angle of (roll, pitch, yaw), denoted by (Φ,Θ,Ψ), respectively, is given as:

$$\begin{aligned}&\mathbf{R}_{B\to TP} \\ &= \begin{bmatrix} \cos\Psi\cos\Theta & \sin\Psi\cos\Theta & -\sin\Theta \\ -\sin\Psi\cos\Phi+\cos\Psi\sin\Theta\sin\Phi & \cos\Psi\cos\Phi+\sin\Psi\sin\Theta\sin\Phi & \cos\Theta\sin\Phi \\ \sin\Psi\cos\Phi+\cos\Psi\sin\Theta\cos\Phi & -\cos\Psi\sin\Phi+\sin\Psi\sin\Theta\cos\Phi & \cos\Theta\cos\Phi \end{bmatrix}\end{aligned} \tag{2.9}$$

Again, the transformation $\mathbf{R}_{B\to TP}$ is unitary and the inverse transformation is simply

$$\mathbf{R}_{TP\to B} = \mathbf{R}_{B\to TP}^{-1} = \mathbf{R}_{B\to TP}^{T} \tag{2.10}$$

Another important equation is the differential equation relating (*p*, *q*, *r*), the angular rates in the *x*, *y*, and *z* direction, with the Euler angle (Φ,Θ,Ψ):.

$$\frac{d}{dt}\begin{bmatrix}\Phi\\ \Theta\\ \Psi\end{bmatrix} = \begin{bmatrix}1 & \sin\Phi\tan\Theta & \cos\Phi\tan\Theta \\ 0 & \cos\Phi & -\sin\Phi \\ 0 & \sin\Phi/\cos\Theta & \cos\Phi/\cos\Theta\end{bmatrix}\begin{bmatrix}p\\ q\\ r\end{bmatrix} \tag{2.11}$$

The inertial navigation algorithm can compute the attitude of the vehicle by solving the differential equation (2.11). It should be noted, however, that the matrix has singularity at $\Theta = \pm 90°$, when the vehicle is upside down. In normal operation of the helicopter, this is not a serious problem, but it can still pose serious limitations in some cases. Indeed, small-size hobby helicopters are capable of hovering upside down. While the Euler angle representation is intuitively appealing and convenient for dynamic equations, representations without any singularities, such as direction-cosine or quaternion, are preferred for the implementation of INS.

2.1.3.2 Quaternion Representation

Quaternion parametrization is a favored method to represent the rotation of a rigid body because it is free from singularities and it is computationally efficient. A quaternion is a vector of four entities obeying generalized complex algebraic rules:

$$\mathbf{q} = q_1\mathbf{i} + q_2\mathbf{j} + q_3\mathbf{k} + q_4 \tag{2.12}$$

where

$$\|\mathbf{q}\| = 1$$

$$\begin{array}{lll} \mathbf{i}\circ\mathbf{i} = -1 & \mathbf{j}\circ\mathbf{j} = -1 & \mathbf{k}\circ\mathbf{k} = -1 \\ \mathbf{i}\circ\mathbf{j} = \mathbf{k} & \mathbf{j}\circ\mathbf{k} = \mathbf{i} & \mathbf{k}\circ\mathbf{i} = \mathbf{j} \\ \mathbf{j}\circ\mathbf{i} = -\mathbf{k} & \mathbf{k}\circ\mathbf{j} = -\mathbf{i} & \mathbf{i}\circ\mathbf{k} = -\mathbf{j} \end{array}$$

A quaternion is equivalently represented by a vector: $\mathbf{q} = [q_1 \quad q_2 \quad q_3 \quad q_4]^T$.

The angular motion is described entirely by the quaternion representation as shown below:

$$\begin{aligned} \dot{\mathbf{q}} &= \mathbf{\Psi}\mathbf{q} \\ &= \frac{1}{2}\begin{bmatrix} 0 & r & -q & p \\ -r & 0 & p & q \\ q & -p & 0 & r \\ -p & -q & -r & 0 \end{bmatrix}\mathbf{q} \\ &= \frac{1}{2}\begin{bmatrix} q_4 & -q_3 & q_2 \\ q_3 & q_4 & -q_1 \\ -q_2 & q_1 & q_4 \\ -q_1 & -q_2 & -q_3 \end{bmatrix}\begin{bmatrix} p \\ q \\ r \end{bmatrix} \end{aligned} \tag{2.13}$$

Obviously, integrating equation (2.13) is much more efficient than (2.11) because it does not involve computationally expensive trigonometric functions. The rotational transformation matrix $\mathbf{R}_{B\to TP}$ can be directly found with quaternion:

$$\mathbf{R}_{B\to TP} = \begin{bmatrix} q_1^2+q_4^2-q_2^2-q_3^2 & 2(q_1q_2-q_3q_4) & 2(q_1q_3+q_2q_4) \\ 2(q_1q_2+q_3q_4) & q_2^2+q_4^2-q_1^2-q_3^2 & 2(q_2q_3-q_1q_4) \\ 2(q_1q_3-q_2q_4) & 2(q_2q_3+q_1q_4) & q_3^2+q_4^2-q_1^2-q_2^2 \end{bmatrix} \tag{2.14}$$

The major advantage of using quaternion is, although it is not intuitive at all, the computational efficiency and the absence of the singularities that the Euler angles have. In some situations, vehicle feedback control for example, Euler angles are still necessary and the relationship is given as follows:

$$\begin{aligned} \sin\Theta &= -2(q_2q_4+q_1q_3) \\ \Phi &= \arctan 2\left[2(q_2q_3-q_1q_4), -2(q_1^2+q_2^2)\right] \\ \Psi &= \arctan 2\left[2(q_1q_2-q_3q_4), -2(q_2^2+q_3^2)\right] \end{aligned} \tag{2.15}$$

2.1.3.3 Direction Cosine

The direction cosine matrix is widely used in aerospace applications, especially in the design of inertial navigation systems [37]. Any two vectors in three-dimensional space, denoted by $\mathbf{r}_1$ and $\mathbf{r}_2$, intersect with angle θ, which can be found by the inner product relationship:

$$\theta = \cos^{-1}\left[\frac{\mathbf{r}_1 \circ \mathbf{r}_2}{\|\mathbf{r}_1\|\|\mathbf{r}_2\|}\right] \tag{2.16}$$

Suppose there are two coordinate systems, denoted by superscript *a* and *b*. A vector **X** can be represented by two coordinate systems *a* and *b* denoted by $\mathbf{X}^a$ and $\mathbf{X}^b$, respectively. There exists a unique transformation between these two coordinate systems satisfying

$$\mathbf{X}^b = \mathbf{R}_a^b \mathbf{X}^a \tag{2.17}$$

The transformation can be found by the following idea. We can find the intersection angles among the orthogonal unit vectors of two frames, denoted by $\left(\mathbf{i}_x^a, \mathbf{i}_y^a, \mathbf{i}_z^a\right)$ and $\left(\mathbf{i}_x^b, \mathbf{i}_y^b, \mathbf{i}_z^b\right)$, and then cast into the matrix form

$$\mathbf{R}_a^b = \begin{bmatrix} \mathbf{i}_x^b \circ \mathbf{i}_x^a & \mathbf{i}_x^b \circ \mathbf{i}_y^a & \mathbf{i}_x^b \circ \mathbf{i}_z^a \\ \mathbf{i}_y^b \circ \mathbf{i}_x^a & \mathbf{i}_y^b \circ \mathbf{i}_y^a & \mathbf{i}_y^b \circ \mathbf{i}_z^a \\ \mathbf{i}_z^b \circ \mathbf{i}_x^a & \mathbf{i}_z^b \circ \mathbf{i}_y^a & \mathbf{i}_z^b \circ \mathbf{i}_z^a \end{bmatrix} \tag{2.18}$$

In fact, the transformation matrix (2.18) is the identical rotational matrix presented earlier in equation (2.9).

Another important relationship is the time derivative of the transformation matrix (2.18). The transformation matrix changes as a function of time when the vehicle rotates as a function of time with respect to the inertial frame. The derivative can be found by

$$\begin{aligned} \frac{d\mathbf{R}_a^b(t)}{dt} &= \mathbf{R}_a^b \mathbf{\Omega}_{ab}^b \\ &= \mathbf{R}_a^b \begin{bmatrix} 0 & -\omega_3 & \omega_2 \\ \omega_3 & 0 & -\omega_1 \\ -\omega_2 & \omega_1 & 0 \end{bmatrix} \end{aligned} \tag{2.19}$$

$\mathbf{\Omega}_{ab}^b$ denotes the angular change of the b-frame relative to the a-frame, coordinatized in the b-frame. Note that the skew-symmetric matrix $\mathbf{\Omega}_{ab}^b$ can be represented by a vector $\boldsymbol{\omega} = [\omega_1 \quad \omega_2 \quad \omega_3]^T$ with outer-product operator.

When $\boldsymbol{\omega}$ is constant, the solution of the differential equation (2.19) is

$$\begin{aligned} \mathbf{R}_a^b(t) &= \mathbf{R}_a^b(t_0)\exp(\mathbf{\Omega}_{ab}^b t) \\ &= \mathbf{R}_a^b(t_0)\left[\mathbf{I} + \left(\frac{\sin\|\boldsymbol{\omega}\|t}{\|\boldsymbol{\omega}\|}\right)\mathbf{\Omega}_{ab}^b + \left(\frac{1-\cos\|\boldsymbol{\omega}\|t}{\|\boldsymbol{\omega}\|^2}\right)\left(\mathbf{\Omega}_{ab}^b\right)^2\right] \end{aligned} \tag{2.20}$$

The rotational matrix at every time t may be found by calculating the solution (2.20). Comparing the dual approaches, it is known that the quaternion approach is numerically efficient and yields lower error solutions [36].

2.2 General Helicopter Model

The helicopter is capable of vertical take-off/landing, hover, and pirouette as well as cruising like a conventional airplane. While fixed-wing aircrafts obtain lift with their wings when they propel through the air with sufficient speed, helicopters use rotors to generate lift and other control forces and moments. A rotor consists of a number of spinning blades symmetrically installed in a plane, which are attached to a shaft perpendicular to the blades. The circular plane that the blades sweep through is called *rotor disc*. The blade has certain cross-sectional shape, called airfoil, which is suitable for the generation of lift. When a rotor rotates by external torque, the blade pushes the air down and generates lift as Newton's law dictates. At the same time, the blade receives resisting torque in the opposite direction of rotor revolution, which is transmitted to the fuselage and causes spin in the opposite direction of the rotor revolution. This type of torque is called *anti-torque* and has to be cancelled by an additional mechanism. The most common solution is the tail rotor whose shaft is installed along the y-axis in the body coordinate system. The tail rotor is installed at the end of fuselage so that the resultant moment, the outer product of moment arm and the tail rotor thrust, is large enough to cancel the anti-torque. An undesirable side effect of this configuration is the unbalanced thrust in the y-direction, which acts to drift the helicopter sideway and to tip off the helicopter when it is on the ground. Nonetheless, due to its simple construction, it is the most popular configuration.

Figure 2.3 Helicopters with different configuration
Left: Tandem helicopter Boeing CH-47 "Chinook"
Right: Coaxial helicopter Kamov Ka-52

Other configurations are (1) tandem type and (2) coaxial type. These designs have two identical rotors rotating in opposite direction so that the anti-torque of each rotor disc cancels the other. Yaw motion is obtained by controlling the difference of the anti-torque of each rotor. Coaxial-rotor helicopters have two main rotors attached to a coaxial shaft rotating in opposite directions. This approach results in a shorter body without a tail boom at the expense of a very complicated power transmission and control structure of the main rotor. Tandem helicopters, take the Boeing CH-47 for example, have two identical rotors rotating in opposite direction on the front and the rear top of the fuselage.

All of the Berkeley UAV fleet, i.e., Kyosho Concept 60 SR II, Bergen Industrial Twin, Yamaha R-50 and RMAX, have the configuration of one-main-rotor and one-tail-rotor, which was pioneered by Igor Sikorsky in the 1940s. In the following, we concentrate on the dynamics of main-tail rotor configuration helicopters.

2.2.1 Kinematic-Dynamic Equation of the Helicopter

The motion of a rigid body in three-dimensional space is characterized by the position $\mathbf{X}^{TP}$ of the center of mass and the Euler angles (Φ, Θ, Ψ) for rotation of the helicopter with respect to the tangent-plane frame. In the following formulation, we employ the tangent plane coordinate system as the inertial reference frame by neglecting the rotation of the Earth. The rigid body obeys the following kinematic equations:

$$\dot{\mathbf{X}}^{TP} = \mathbf{V}^{TP} \tag{2.21}$$

$$\frac{d}{dt}\begin{bmatrix} \Phi \\ \Theta \\ \Psi \end{bmatrix} = \begin{bmatrix} 1 & \sin\Phi\tan\Theta & \cos\Phi\tan\Theta \\ 0 & \cos\Phi & -\sin\Phi \\ 0 & \sin\Phi/\cos\Theta & \cos\Phi/\cos\Theta \end{bmatrix} \boldsymbol{\omega}^b \tag{2.22}$$

where

$\mathbf{X}^{TP} \triangleq \begin{bmatrix} x^{TP} & y^{TP} & z^{TP} \end{bmatrix}^T \in \mathscr{R}^3$

$\mathbf{V}^{TP}$: velocity of center of mass in the tangent plane frame

Helicopter dynamics obey the Newton-Euler equation for rigid body in translational and rotational motion. The dynamic equation is conveniently described with respect to the body coordinate system.

$$\dot{\mathbf{V}}^b = \frac{1}{m}\mathbf{F}_{ext} - \boldsymbol{\omega}^b \times \mathbf{V}^b \tag{2.23}$$

$$\mathbf{I}_b \dot{\boldsymbol{\omega}}^b = \mathbf{M}_{ext} - \boldsymbol{\omega}^b \times \mathbf{I}_b \boldsymbol{\omega}^b \tag{2.24}$$

where

$$\mathbf{V}^b \triangleq \begin{bmatrix} u & v & w \end{bmatrix}^T$$

$$\boldsymbol{\omega}^b \triangleq \begin{bmatrix} p & q & r \end{bmatrix}^T$$

$$\mathbf{I}_b = \begin{bmatrix} I_{xx} & I_{xy} & I_{xz} \\ I_{yx} & I_{yy} & I_{yz} \\ I_{zx} & I_{zy} & I_{zz} \end{bmatrix}$$

The kinematic-dynamic relationship from (2.21) to (2.24) holds true for any rigid body motion. $\mathbf{F}_{ext}$ and $\mathbf{M}_{ext}$ in (2.23) and (2.24) stand for the sum of the external forces and moments that the rigid body receives and they are specific to the dynamics of the vehicle. In other words, the main problem of modeling is to find $\mathbf{F}_{ext}$ and $\mathbf{M}_{ext}$. Helicopter dynamics can be studied by employing the lumped-parameter approach, which considers the helicopter as the composition of the following major components: main rotor, tail rotor, fuselage, horizontal stabilizer, and vertical stabilizer. These components are considered as the source of forces and moments. The free-body diagram of helicopter is as shown in Figure 2.4. The diagram depicts the coordinate system, geometric constants, and force and moment terms acting on those components. The force terms in the *x, y,* and *z* direction are denoted by *X, Y,* and *Z* respectively. The moment terms in roll, pitch and yaw direction are denoted by *R, M,* and *N*, respectively. The subscripts *M, T, F, H* and *V* denote main rotor, tail rotor, fuselage, horizontal stabilizer and vertical stabilizer, respectively. In the rotational terms, the cross inertia terms of the inertia tensor are assumed negligible. Based on these notation, we can write the force and moment equations as following:

$$\dot{\mathbf{V}}_b = \frac{1}{m}\begin{bmatrix} X_M + X_T + X_H + X_V + X_F \\ Y_M + Y_T + Y_V + Y_F \\ Z_M + Z_T + Z_H + Z_V + Z_F \end{bmatrix} + \mathbf{R}_{TP\to B}\begin{bmatrix} 0 \\ 0 \\ g \end{bmatrix} + \begin{bmatrix} -vr - wq \\ -ur + wp \\ uq - vp \end{bmatrix} \tag{2.25}$$

$$\begin{aligned} \dot{\boldsymbol{\omega}}^b = \mathbf{I}_b^{-1} & \begin{bmatrix} R_M + Y_M h_M + Z_M y_M + Y_T h_T + Y_V h_V + Y_F h_F + R_F \\ M_M - X_M h_M + Z_M l_M + M_T - X_T h_T + Z_T h_T - X_H h_H + Z_H l_H - X_V h_V + M_F \\ N_M - Y_M l_M - Y_T l_T - Y_V l_V + N_F - Y_F l_F \end{bmatrix} \\ + \mathbf{I}_b^{-1} & \begin{bmatrix} qr(I_{yy} - I_{zz}) \\ pr(I_{zz} - I_{xx}) \\ pq(I_{xx} - I_{yy}) \end{bmatrix} \end{aligned} \tag{2.26}$$

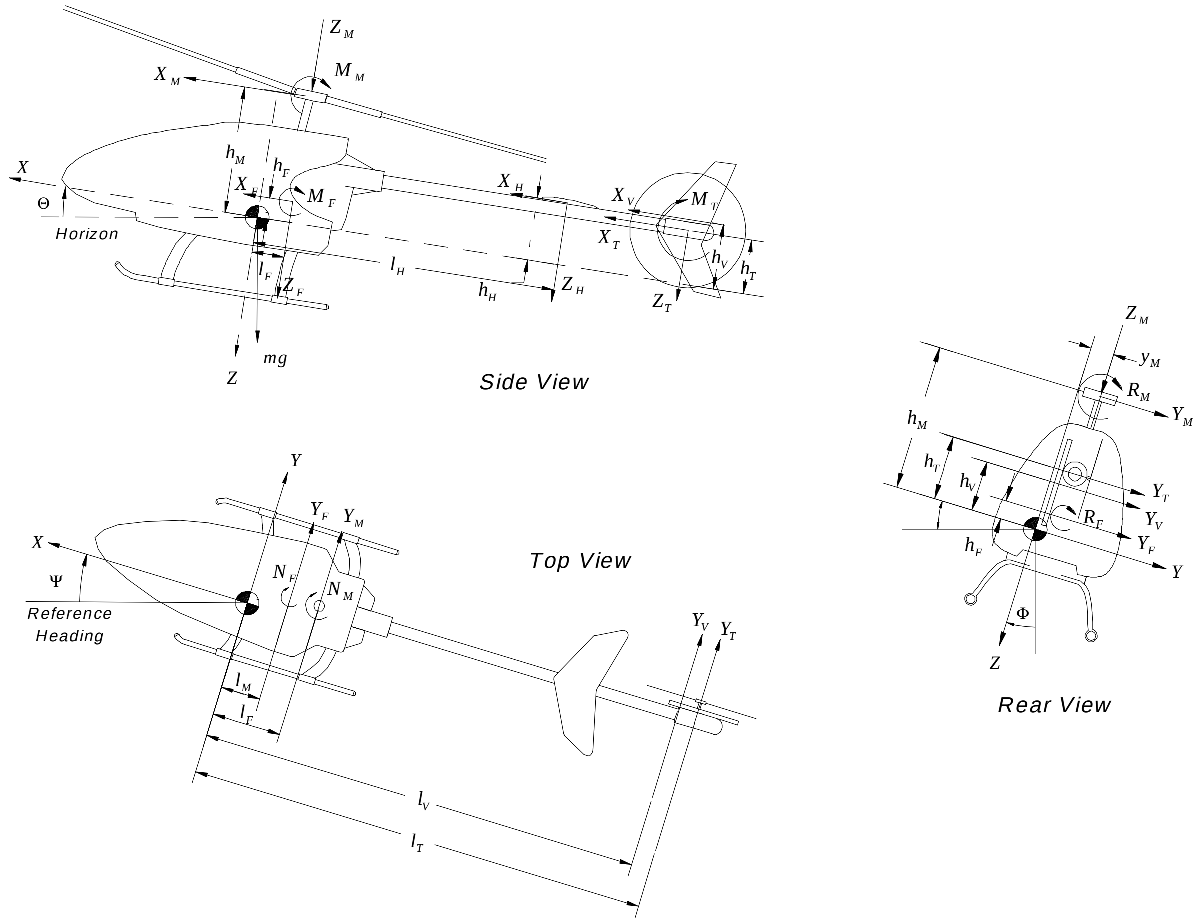

Figure 2.4 Free body diagram of helicopter with respect to body coordinate system

Now the problem reduces to the formulation of each force and moment term and the measurements of the geometric constants specific to the location of center of mass and the location of main rotor, tail rotor, and stabilizer fins. In the following sections, we seek to find the equations for each force and moment term following the results by Prouty [10]. This is not a trivial task because the aerodynamics involved are very complicated and the resulting equations may be in implicit form and/or involve look-up tables and graphs. The overall accuracy may fall below the demanded accuracy. Still, this process is valuable to gain insight of the overall helicopter dynamics, which are helpful to design control systems and operate the vehicle. Once we finish finding these terms, we can construct a simulation model and a control model.

2.2.2 Main Rotor

The main rotor is the most crucial part of the helicopter dynamics. It generates the vertical thrust, or *lift*, to act against gravity. The main rotor system is also the most complicated mechanical part of the entire helicopter system. A main rotor typically has two to six blades in radial configuration separated by an equal angle. A blade is bolted to the blade grip, which is attached to the main rotor head through a bearing system (articulated) or strap (hingeless). The lift generated by the blade is the function of many factors including relative air speed, air density, airfoil shape, angle-of-attack and so forth. The main rotor system also has a mechanism called swashplate which changes the blade pitch simultaneously or as the function of the angular position of the main rotor shaft. The former is called collective pitch and the latter is called cyclic pitch. The collective pitch changes the pitch of all blades to control vertical lift. The cyclic pitch changes the distribution of the lift force over the disc so that the direction of the thrust vector can be tilted from the upright direction. It also generates rolling and/or pitching moment to cause the fuselage to tilt and the inclination in roll and/or pitch induces lateral and/or longitudinal motion respectively.

The dynamic equation of the main rotor can be obtained by an analysis called *blade-element method* [10]. It starts with the analysis of an infinitesimal blade element on which various forces such as lift, drag, and centrifugal force act. The overall dynamics of the main rotor can be found by integrating the force and moment terms along the blade length.

In Figure 2.5, the geometry and the free-body diagram for the blade element method is given. The lift generated on the blade element is a function of the local dynamic pressure, lift coefficient and the width of the blade.

$$\Delta L = q c_i c \Delta r \tag{2.27}$$

where q : local dynamic pressure

c_i : local lift coefficient

c : width of blade

The local dynamic pressure q and the local lift coefficient c_i are given by

$$q = \tfrac{1}{2}\rho\left(\Omega r\right)^2 \tag{2.28}$$

$$c_i = a\alpha \tag{2.29}$$

where ρ : air density

Ω : angular velocity of rotor

a : slope of the lift curve

α : local angle of attach

With the given geometry in Figure 2.5, the following relationships are found:

$$\alpha = \theta - \phi \tag{2.30}$$

$$\phi = \tan^{-1}\frac{v_1}{\Omega r} \simeq \frac{v_1}{\Omega r} \tag{2.31}$$

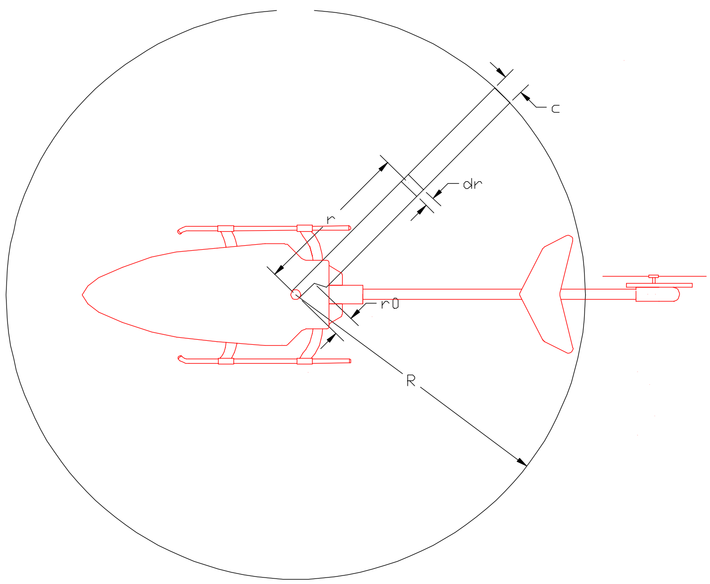

(a)Geometry of a Blade Element

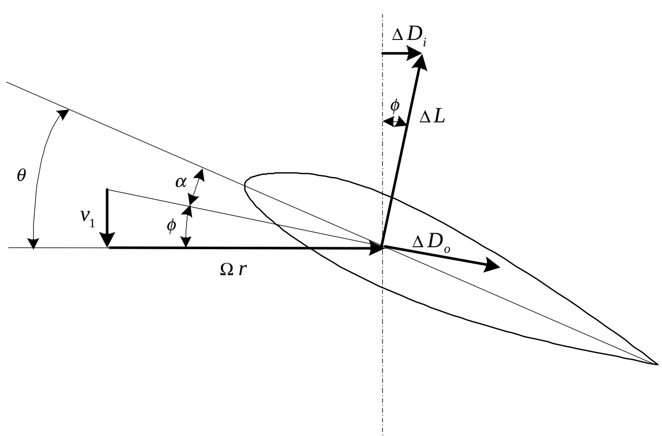

(b) Free body diagram of blade method

Figure 2.5 Blade element method

The total thrust of the rotor can be found by the following integration

$$T = bL = \frac{\rho}{2}\Omega^2 abc\int_{R_0}^{R}\left(\theta r^2 - \frac{v_1(r)}{\Omega}r\right)dr \tag{2.32}$$

v_1 in equation (2.32) is the induced velocity of air volume pushed down by the revolving blade. It is a function of *r*. In hover, when there is no additional relative air speed from horizontal or vertical velocity, it has the implicit form with the thrust *T:*

$$\overline{v}_1 = -\frac{V_c}{2} + \sqrt{\left(\frac{V_c}{2}\right)^2 + \frac{T}{2\rho A}} \tag{2.33}$$

where V_c : climb velocity of the rotor

Note that v_1 in equation (2.33) is in fact the *averaged* induced velocity of the rotor disc and it yields approximated results when solved in an iterative manner [11] or in closed form after certain manipulation [26]. For more accurate analysis, the following equation for v_1 as the function of *r* is used.

$$v_1(r) = \frac{-\left(\frac{\Omega}{2}abc + 4\pi V_c\right) + \sqrt{\left(\frac{\Omega}{2}abc + 4\pi V_c\right)^2 + 8\pi abc\Omega^2 r\left(\theta - \frac{V_c}{\Omega r}\right)}}{8\pi} \tag{2.34}$$

Plugging equation (2.34) into (2.32), after a long manipulation, *T* in closed form is given as follows with some constant variables introduced for simplicity in manipulation:

$$\begin{aligned} T = {} & \frac{R^3 - R_0^3}{3}m_3\theta + \frac{m_3 m_6}{2}\left(R^2 - R_0^2\right) \\ & - \frac{m_3}{8\pi\Omega^2}\left\{\frac{2}{15m_2^2\theta^2}\left(\left(3m_2R\theta - 2m_5\right)\left(m_2R\theta + m_5\right)^{3/2} - \left(3m_2R_0\theta - 2m_5\right)\left(m_2R_0\theta + m_5\right)^{3/2}\right)\right\} \end{aligned} \tag{2.35}$$

where

$$
\begin{aligned}
m_1 &= \frac{\Omega}{2} abc + 4\pi V_c \\
m_2 &= 8\pi\Omega^2 abc \\
m_3 &= \frac{\rho}{2}\Omega^2 abc \\
m_5 &= m_1^2 - \frac{V_c m_2}{\Omega} \\
m_6 &= \frac{1}{\Omega}\left(\frac{m_1}{8\pi} - V_c\right)
\end{aligned} \tag{2.36}
$$

As obvious in equation (2.35) and (2.36), T is a function of many geometric parameters: the main rotor (b, c, R R_0), the aerodynamic parameters of the blade (ρ, a) and the operational parameters (θ, V_c, Ω). Once the rotor geometry is determined, then the rotor thrust can be controlled by the collective pitch θ and the rotor RPM Ω. As mentioned earlier, full-size helicopters have an engine governor to regulate the rotor RPM to a constant speed. Small size helicopters usually do not have the luxury of a governor. Instead, the radio controller has special mixing capability to simultaneously control the collective pitch and the engine throttle opening in preprogrammed mapping so that the engine can keep up with the varying load by the rotor. Since this mapping is preset, the engine RPM does fluctuate upon the change of the load on the engine. This method does not impose too much difficulty on human pilots. For automatic control, the engine governor is desired to keep the helicopter dynamics less perturbed for model-based controllers. In our research, engine governors are built using an optical encoder, which picks up the difference of reflectivity of a marker on the flywheel. The engine governor for hobby purpose (Futaba GV-1) is also available.

Another important contribution of main rotor is the torque Q, which can be computed by the similar blade element approach. As can be seen in the free-body diagram in Figure 2.5, there are two sources of horizontal drag force, induced drag and profile drag, whose outer product with the moment arm r acts as the anti-torque:

$$
\Delta Q = \left(\Delta L \phi + \Delta D\right) r \tag{2.37}
$$

The induced drag is the horizontal component of the lift, which is perpendicular to the direction of local flow. The profile drag is the air resistance force parallel to the local flow. Substituting the expression for ΔL and ΔD, equation (2.37) becomes

$$\Delta Q = r\left[\frac{\rho}{2}(\Omega r)^2 c_l c\phi\Delta r + \frac{\rho}{2}(\Omega r)^2 c_c c\Delta r\right] \tag{2.38}$$

After substituting (2.31) and (2.34) into (2.38), and enormous manipulation, we obtain Q:

$$\begin{aligned}
Q &= n_1 n_7 \frac{R^3 - R_0^3}{3} \\
&+ \frac{2n_1 n_8}{105 m_4^3}\left\{\left(15m_4^2R^2 - 12m_4m_5R + 8m_5^2\right)\left(m_4R + m_5\right)^{3/2}\right. \\
&\left.-\left(15m_4^2R_0^2 - 12m_4m_5R_0 + 8m_5^2\right)\left(m_4R_0 + m_5\right)^{3/2}\right\} \\
&- \frac{n_1 n_9}{2}\left(R^3 - R_0^3\right) + \\
&\frac{2n_1 n_{10}}{15m_4^3}\left\{\left(3m_4R - 2m_5\right)\left(m_4R + m_5\right)^{3/2} - \left(3m_4R_0 - 2m_5\right)\left(m_4R_0 + m_5\right)^{3/2}\right\} \\
&+ \frac{c_d n_1}{4}\left(R^4 - R_0^4\right)
\end{aligned} \tag{2.39}$$

where

$$\begin{aligned}
n_1 &= \frac{\rho}{2}\Omega^2 bc & n_6 &= a\left(\frac{V_c}{\Omega}\right)^2 \\
n_2 &= V_c - \frac{m_1}{8\pi} & n_7 &= \frac{a\theta}{\Omega}n_2 - n_3 m_4 \\
n_3 &= \frac{a}{(8\pi\Omega)^2} & n_8 &= \frac{a\theta}{8\pi\Omega} \\
n_4 &= m_1^2 + m_5 & n_9 &= n_3 n_4 - n_5 m_1 + n_6 \\
n_5 &= \frac{aV_c}{4\pi\Omega^2} & n_{10} &= 2m_1 n_3 - n_5
\end{aligned} \tag{2.40}$$

Closed-form equations with rather overwhelming complexity have been derived. One discouraging aspect of this approach is that aerodynamic equations usually contain 5~20% error due to the imperfect knowledge of the involved aerodynamic quantities and the chaotic nature of fluid dynamics. Still, these equations allow us certain insights in a qualitative way when used with realistic measurements.

To gain some insight from the very complicated thrust equation, we plot the value evaluated using the quantities for *Ursa Minor 3*. In Figure 2.6, the thrust is plotted versus, (a) collective pitch and (b) the climb velocity. In (a), as expected, the thrust increases proportional to the increase of collective pitch. Rather surprisingly, unlike the complicated thrust equation, the lift curve is almost linear with slight concavity. This inspires the approximation of thrust with simpler function as done by many researchers, e.g. [6]. In (b), the thrust decreases slightly when the helicopter soars up. This is the clue to the inherent stability of vertical response. When the helicopter climbs, the lift generated by the rotor decreases and the helicopter drops, and consequentially the helicopter gains more lift and climbs back. This holds true for tail thrust as well so the yaw dynamics is inherently stable.

The thrust equation developed before is quasi-static form and only the influence of vertical velocity is accounted for. As a matter of fact, the aerodynamics involved with the rotor thrust are very complicated and it is also a function of the direction and magnitude of inflow along the x, y, and z axis (so far we considered z direction only) and even the rate of the pitch change. Experiments show that blade pitch changes in large amount within short time induces large amount of peak thrust and settles down.

The dependency on the inflow has significant effect on the stability of vehicle speed. First of all, as shown above, the vertical dynamics is stable. The lift would increase with increasing horizontal velocity u and v because there is the more inflow per unit time. However, the overall vehicle stability is not only a function of lift, but also of the flapping action as will be discussed below. Jumping to the conclusion, the forward (or lateral) velocity dynamics is governed by the thrust, flapping and the pitch angle of the body and it is known to be stable in the usual configuration (no oversize horizontal stabilizer and so on). This stability in larger scale is known as *speed stability* [10] and it indicates that the helicopter converges to a certain forward velocity with a certain pitch angle of the fuselage. It does not mean, of course, the helicopter is stable at hover. Hovering is an unstable equilibrium and the vehicle has certain stable equilibrium of non-zero cruising velocity. If the helicopter is left uncontrolled at hover, it would start an oscillatory motion in the altitude-velocity-attitude channel known as phugoid, and it eventually would go unstable. This is the reason why helicopters need stabilizing control either by a human pilot or an automatic feedback controller.

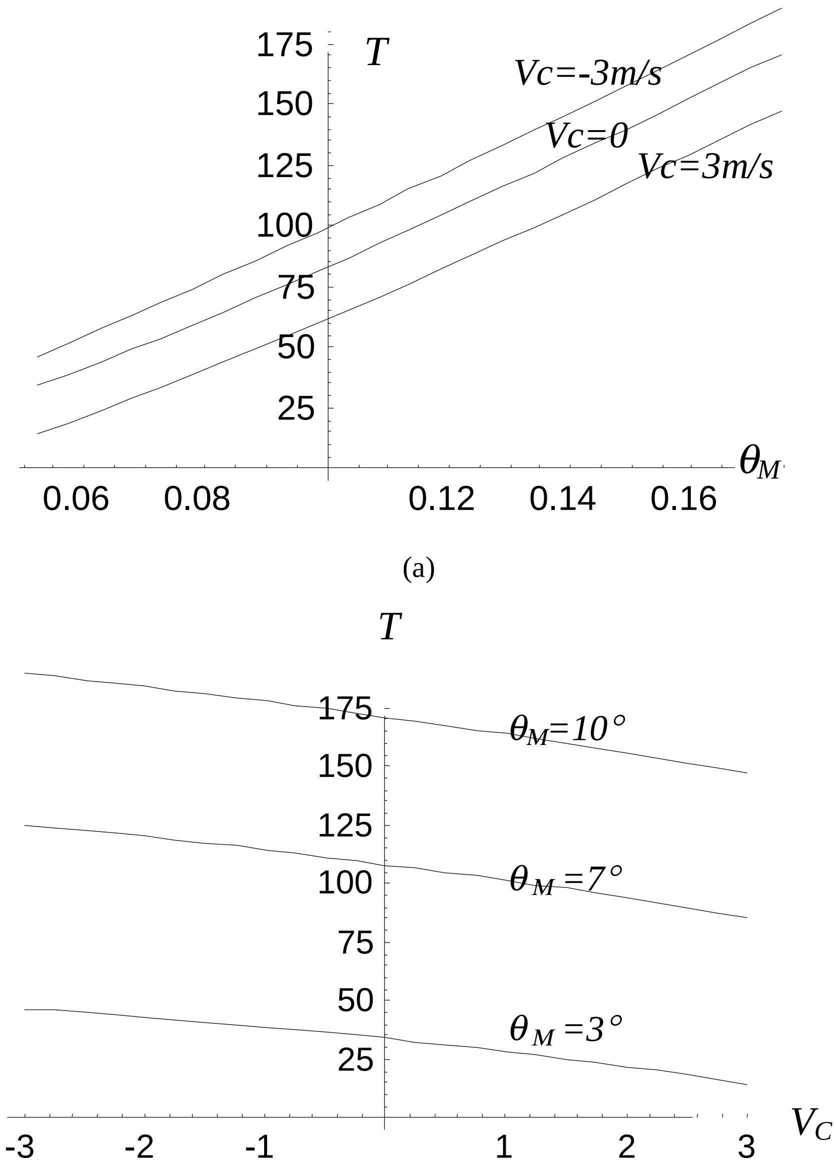

(a)

(b)

Figure 2.6 Thrust vs (a) θ_{0m} , (b) V_c

Another important characteristic of the main rotor, in addition to thrust and anti-torque, is the flapping. Flapping indicates the oscillatory motion of the main rotor blades about the hinges, which allows the perpendicular motion to the rotor disc. This notion is due to the fluctuating thrust that is caused by the change of the angle of the attack of blades, the velocity, and direction of local flow. Since the lift is perpendicular to the blade surface, if the blade is flapping along the flapping hinge, the overall lift over the blade has a vertical and a horizontal component. Hence, the horizontal component acts as the moment in rolling and pitching as well as the horizontal force in the *x* and *y*-

axis. The original concept of flapping was devised by an aerodynamicist Juan de la Cierva, who conducted extensive study on autogiro. After experiencing mysterious rollover of his test autogiro, he discovered that the unbalanced lift on the rotor disc was due to the increased forward velocity of the vehicle. He thought that the unbalance could be alleviated by installing hinges for the blade grips to allow blades to climb up and down by the amount of generated lift. Since helicopters have the same problem with the unbalanced lift when they attain forward velocity, flapping is an important feature in all helicopters. In addition to the flapping caused by the forward flight, flapping is also induced by the mechanism called *cyclic pitch*. Cyclic pitch forces the blade to have a certain pitch angle which is a function of azimuth, i.e., the rotation angle of the main rotor with respect to the fuselage. Cyclic pitch is created by tilting the swashplate. The pitch lever attached to the blade follows the tilt angle of the swashplate and forces the blade to have the cyclic pitch angle. In a full-size helicopter, the blade pitch angle follows 90° in advance of the swashplate angle in order to compensate for the 90° phase delay of gyroscopic effect. In other words, when the blade rotates and receives upward force due to the increased lift by flapping, the blade starts tilting upward and reaches the maximum angle approximately after one-quarter turn of the blade. Therefore, the longitudinal swashplate tilt induces the pitch angle of the blade while the blade is still over the side. The maximum flapping is achieved when the blade reaches the longitudinal position.

The cyclic pitch is produced by the ingenious linkage system and swashplate. The mechanism of full-size helicopter is rather simple because the blade pitch level is directly connected to the swashplate. The blade pitch can be written in terms of a Fourier series. While the blade pitch has fixed geometric relationship with the swashplate, the flapping dynamics depend on the blade pitch, the local flow, the helicopter body pitch and roll rate and so on. We will not go any further into the flapping dynamics of full-size helicopters here because there are very different from that of small-size helicopters[1].

$$\theta = \theta_0 + \frac{r}{R}\theta_1 - A_1 \cos\Psi - B_1 \sin\Psi \tag{2.41}$$

where

θ : local blade pitch

θ_1 : blade twist(typically 0 in radio control helicopters)

A_1 : lateral cyclic pitch

[1] Confusion arises due to the different direction of rotation of main rotor. Most civilian and military helicopters manufactured in the US has counterclockwise rotation viewed above. Most hobby helicopters and full-size helicopters manufactured outside of the US including those used in this research have clockwise rotation when viewed from above. The clockwise rotation is consistently assumed in the following including Figure 2.7 and Figure 2.8.

B_1 : longitudinal cyclic pitch

Ψ : azimuth angle

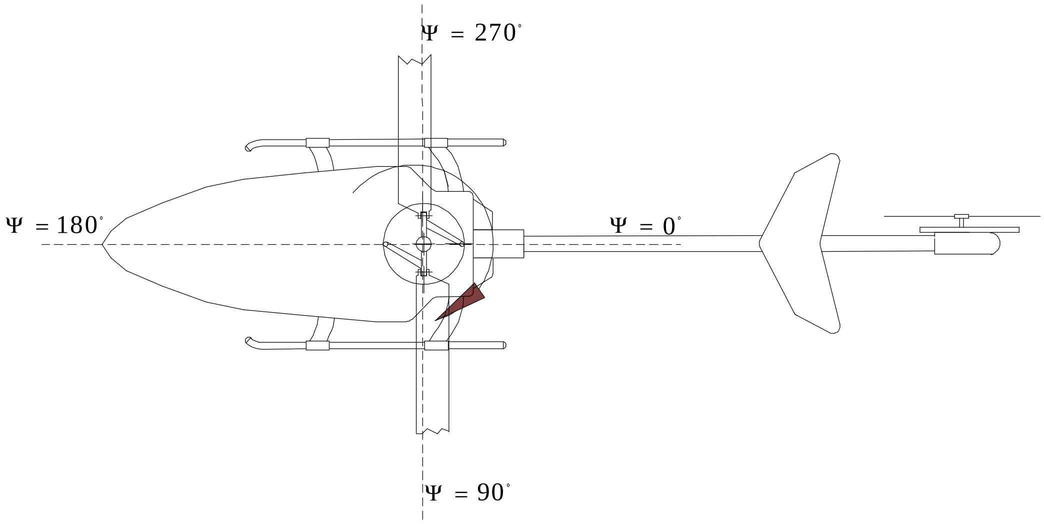

Figure 2.7 Swashplate and pitch level configuration

A_1 is positive when the pitch at $\Psi = 180°$ is larger. B_1 is positive when the pitch on the retreating blade is greater than the pitch on the advancing blade.

With the alternating blade pitch θ, the blade flaps up and down during its revolution with angle β to the plane perpendicular to main rotor shaft. The angle β can be represented by Fourier series and we can truncate the series by ignoring the higher order terms:

$$\begin{aligned}\beta &= a_0 - a_{1s}\cos\Psi - b_{1s}\sin\Psi - a_{2s}\cos 2\Psi - b_{2s}\sin 2\Psi \cdots\cdots \\ &\simeq a_0 - a_{1s}\cos\Psi - b_{1s}\sin\Psi\end{aligned} \tag{2.42}$$

In the series (2.42), the constant term a_0 is called coning, and only the first order coefficients are used for flapping analysis. a_{1s} is called the longitudinal flapping with respect to a plane perpendicular to the shaft defined as positive when the blade flaps down at the tail and up at the nose. b_{1s} is called the lateral flapping defined as positive when the blade flaps down on the advancing side and up on the retreating side(Figure 2.8).

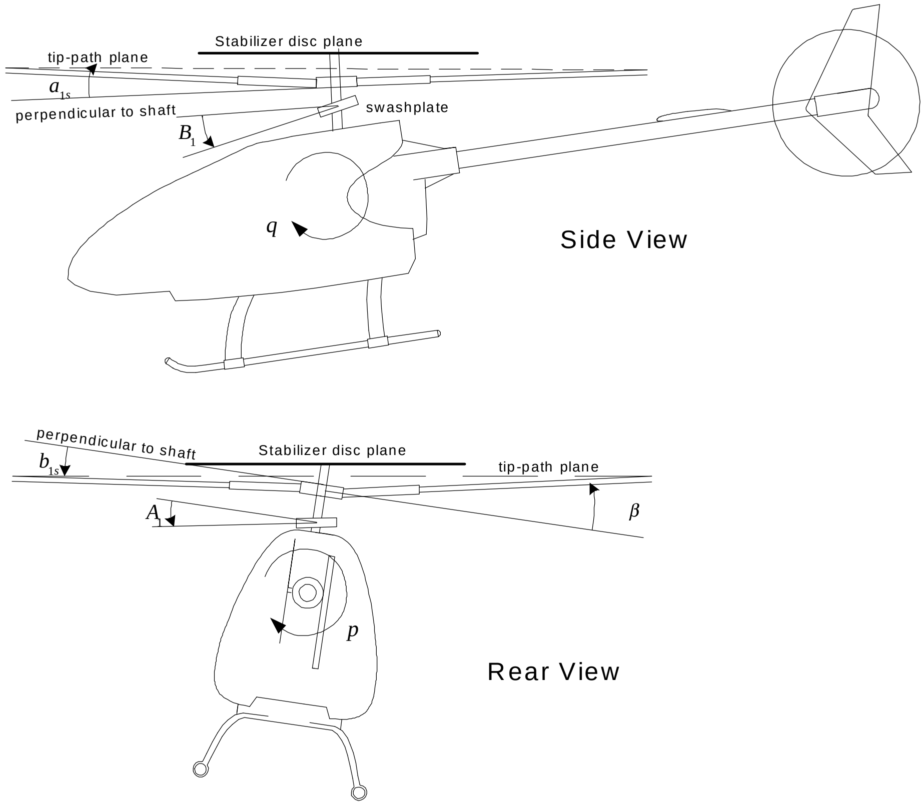

Figure 2.8 Rotor swashplate and flapping angles relationship

It is known that the flapping action of a full-size helicopter finds the equilibrium in less than one rotor revolution when the rotor disc is perturbed by a sudden tilt of the body [10]. Considering that the average main rotor speed is around 350RPM, the response time is less 0.2 second. Small size radio helicopters usually have a very high rotor speed around 1500 RPM, and they would have response time in less than 40 ms. This is an extremely short time for the radio control pilots on the ground. The dynamics of small-size helicopters would be correspondingly very fast because they have a smaller inertia. For this reason, almost all small-size radio helicopters have a mechanism to artificially introduce damping.

A stabilizer mechanism introduces stability to the helicopter dynamics through the use of the gyroscopic effect or the aerodynamic effect of servorotors or both. Bell stabilizer, which was invented by Arthur Young in 1940s and widely used in the Bell UH-1H helicopters, utilizes the gyroscopic effect of the stabilizer bar with weights at its tips. When it rotates, the bar earns gyroscopic effect and it tends to remain in the same plane of rotation by resisting external torque. The main rotor blade pitch levers are connected to the stabilizer bar through linkages and its gyroscopic effect acts as the mechanical feedback source of roll and pitch rate. The Hiller stabilizer utilizes the aerodynamic force exerted on the stabilizer blades, which have a symmetric airfoil shape. The main rotor blade pitch is controlled through the teetering motion of the stabilizer bar and the response of the blade is aerodynamically damped. As the name implies, the Bell-Hiller stabilizer is a combination of two distinct stabilizer mechanisms, i.e., the Bell-stabilizer and the Hiller stabilizer. This clever combination of these two mechanisms has a stabilizer bar with stabilizer blades as well as the weights. The role of Bell-Hiller stabilizer is also dual: the mechanical stabilization by gyroscopic effect of the tip weights and the mechanical servoing by the use of aerodynamic force on the stabilizer blades.

This stabilizer mechanism consists of two paddle-shape blades attached to a rod hinged in its middle on the tip of the main rotor shaft and other mixing linkages connecting from the swashplate to the main rotor blade pitch control lever. In Figure 2.9, the Bell-Hiller stabilizer mechanism of the Yamaha R-50 and the Kyosho Concept 60 are shown. The actual implementation of the stabilizer mechanism differs slightly because the R-50 has a vertically moving swashplate and the Concept 60 has vertically fixed swashplate.

When the stabilizer bar rotates together with the main rotor blades, the stabilizer bar with weights and blades develops gyroscopic action and aerodynamic force. The former reacts against any external torque acting on the stabilizer disc and it retains the current attitude of rolling and pitching for substantial time. The motion of the stabilizer bar is connected to the main rotor pitch levers through a series of linkages.

The blades receive aerodynamic force proportional to their pitch angle. This aerodynamic force exerts the teetering moment of the bar. The teetering motion is converted to the change of the main rotor pitch. Due to the configuration of the blade pitch axis and the point where lift exerts on the blade, the blade pitch has a restoring moment, which in turn acts to restore the teetering motion to rest. These two moments seek the equilibrium between the teetering motion and the restoring torque of the rotor blades at significantly slower rate than the time constant of the rotor system without the stabilizer mechanism. Therefore, the servomotors that actuate the swashplate do not have to supply a large amount of force to overcome the restoring torque of the main rotor blades as the servomotors in the full-size helicopters have to do. This unique approach of the use of aerodynamic force on the stabilizer blades as the blade actuation force earned the name *servorotor*.

The teetering motion is a damped oscillatory motion, whose characteristic is determined by the aerodynamic properties of the stabilizer blades and the main rotor blades. The amount of teetering is determined by the rotor speed and the pitch angle of the stabilizer blades and it is the same as the tilt angle of the swashplate.

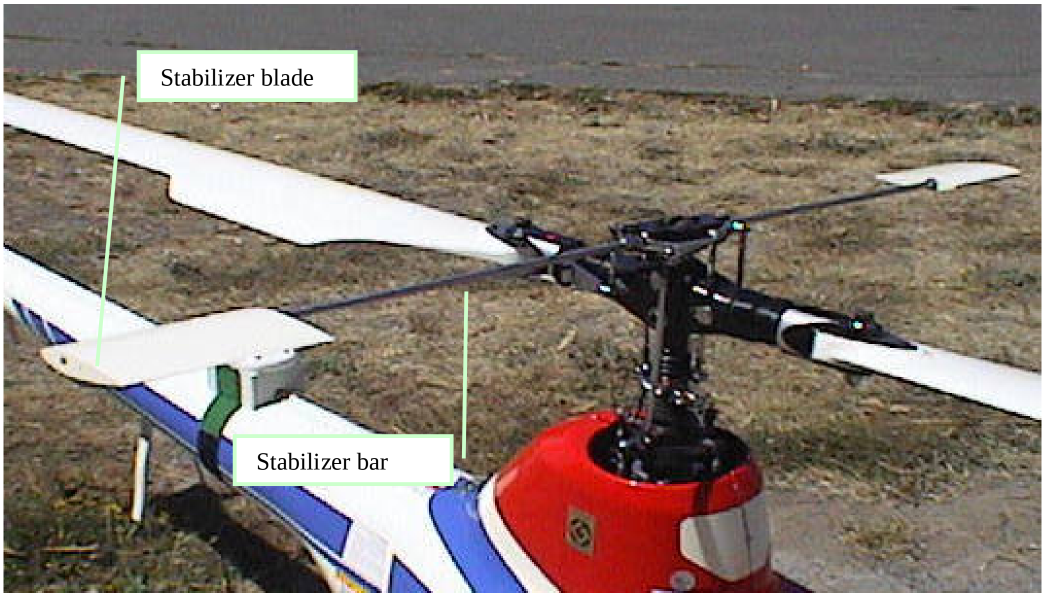

(a) Yamaha R-50

(b) Kyosho Concept 60

Figure 2.9 Bell-Hiller Stabilizer system

The stabilizer dynamics can be modeled in a second order differential equation involving the stabilizer bar and the rotor blade inertia, the aerodynamic force on the stabilizer blades and the rotor blades and the mechanical feedback term from the gyroscopic effect of the stabilizer bar. Mettler [7] proposed first-order model that characterizes the behavior of the Bell-Hiller stabilizer as shown in (2.43).

$$\dot{a}_{1s} = -\frac{a_{1s}}{\tau_f} - q + A_{b_{1s}} b_{1s} + A_{u_{a1s}} u_{a_{1s}} + A_{u_{b1s}} u_{b_{1s}}$$

$$\dot{b}_{1s} = -\frac{b_{1s}}{\tau_f} - p + B_{a_{1s}} a_{1s} + B_{u_{a1s}} u_{a_{1s}} + B_{u_{b1s}} u_{b_{1s}} \tag{2.43}$$

Equation (2.43) is a first-order model of the flapping rotor dynamics, which accounts for the coupled servorotor dynamics and mechanical feedback by the gyroscopic effect of the stabilizer bar. τ_f is the time constant of the servorotor response to the swashplate tilt angles. The body rate p and q appear as feedback terms due to the gyroscopic effect of the stabilizer bar of the servorotor system. The equations also include the input coupling terms, which are not small as shown later. The angular rate dynamics are coupled with blade flapping angles (a_{1s}, b_{1s}) and body velocities (*u, v*). *u* and *v* mainly are affected by the tilt angle pitch and roll, respectively and also by the flapping angles.

Research [**7**] shows this time constant τ_f introduced by the use of the Bell-Hiller stabilizer is approximately equal to five revolutions of the main rotor. For the Kyosho Concept 60 helicopter, τ_f is about $5/(1500\text{RPM}/60) = 0.2$ second. For the Yamaha R-50, $\tau_f = 5/(900\text{RPM}/60) = 0.333$.

As the closing remarks, it should be noted that the stabilizer bar does not *stabilize* the overall vehicle dynamics. It merely introduces further damping to slow down the response so that the ground-based pilot can control the vehicle with greater ease. Another observation is that the stabilizer mechanism is not used for full-size helicopters any more because the stabilizer mechanism sacrifices maneuverability for the additional stability. The dynamic characteristics of the vehicle can be significantly improved by the use of electronic stability and control augmentation system (SCAS) in more versatile manner.

2.2.3 Tail Rotor

The primary role of tail rotor is to generate horizontal thrust varying by the collective pitch of the tail rotor blades. With the moment arm provided by the tail boom, the tail rotor provides yawing moment to counteract the anti-torque of the main rotor. It also produces the unbalanced horizontal force, which acts as a drifting force in the *y*-direction. In hover, the helicopter tilts slightly in roll so that the horizontal component of the main rotor thrust in the *y*-direction counteracts to the tail rotor force.

The tail rotor consists of two or more symmetrically placed blades, a shaft and pitch control mechanism. The configuration is simpler than the main rotor because they do not have cyclic pitch control mechanisms, or stabilizer bars. Although small-size helicopters usually do not have flapping hinges, the blades do undergo elastic deflection by the fluctuating aerodynamic force. In simplified analysis, the tail rotor contributes to the yaw moment, sideslip and rolling moment depending on the location of center of mass. The thrust and torque can be computed with equations (2.35) and (2.39) with different values for tail rotor. The thrust dynamics with the sideslip or yaw is similar to the main rotor dynamics in vertical motion, and hence it shows inherent stability. However, when the helicopter has significant cruise speed, the downwash from the main rotor as well as the inflow affects the tail rotor and the horizontal stabilizer fin and resulting dynamics can be quite complicated.

2.2.4 Stabilizer Fins

The Horizontal and vertical stabilizer fins, which are attached to the tail boom, exert the restoring moments in the pitching and the yawing directions, respectively when the vehicle has forward velocity or head wind blows. Their role is similar to the role of their counterpart of fixed-wing aircraft: to provide mechanical stabilization when the vehicle has sufficient forward velocity or it is exposed to headwind. The contribution of the fins appears as the forces and moments caused by the aerodynamic lift and drag that are generated when the incoming airflow passes through these components. The airflow around the fins becomes very complicated when the effect of inflow and the downwash of the main rotor interact in high-speed cruise. In low velocity cruise or hover, they do not have significant role and hence we can ignore the effect of the fins in the subsequent modeling.

While the fins of fixed-wing aircrafts always offer positive stabilizing effects, the fins in helicopters may cause adversary effects when the helicopter experiences tail wind or side wind during low-speed flight or hover. For example, when the tail wind blows a helicopter in hover, the vertical stabilizer fin forces the yawing to deviate further. The horizontal fin shows similar effects in pitching motion. Therefore, similar to airplanes, it is safe for helicopters to take off with head wind. In hover, when there is no wind, the fins do not contribute to the helicopter in any significant way except to create the vertical drag of the horizontal fin due to the main rotor downwash. In some designs including the Yamaha industrial helicopters used for our research, the stabilizer fins are omitted or miniaturized if the helicopter is not intended to fly at high speed.

Figure 2.10 Stabilizer fins of R-50 (left) and Concept 60 (right)

2.2.5 Fuselage

The fuselage receives drag and lift forces in all direction. The downward drag is produced by blocking the inner part of the downwash of the main rotor. The horizontal lift and drag are produced when the helicopter gains speed or it is exposed to the wind. Definitely, the drag and the lift of the fuselage are the function of the geometric shape. The horizontal drag of the fuselage is one of the major factors for engine output and the maximum cruise speed. The vertical drag by the partial blockage of the downwash acts as a parasite load. One interesting observation is that the helicopter hovers with lesser power in the inverted flight, i.e., the helicopter flies upside down with the strong negative pitch of the main rotor. In this state, the downwash of the main rotor is not blocked by the body anymore and slight decrease of the power requirement for hover is observed. This has been never attempted by the full-size helicopters, but it is one of the popular stunt flights by the advanced hobby radio-controlled helicopter fliers.

The behavior of the drag and lift of the fuselage can be measured by the use of a wind tunnel or estimated by the projected blocking area of the fuselage. However, similar to the stabilizer fins, the horizontal and the vertical drag do not have the significant effect on the vehicle dynamics especially when the helicopter is in hover. Therefore, it is also ignored in the simulation modeling in our study.

2.2.6 External Factors

The helicopter dynamics undergoes a transition when it takes off from the ground or lands back on the earth. The ground exerts supporting force when all or some part of the landing gear touches the ground. With a certain assumption, the ground support can be modeled into the simulation. Another important factor is the *ground effect*, which indicates the phenomenon that less power is required to generate a certain amount of lift when the helicopter is closer to the ground than the power required for same amount of lift far from the ground [10,39]. The source of the ground effect is the decreased magnitude of the induced velocity at the blade element, due to the blockage of the downwash by the ground. The ground effect usually lasts up to the altitude of roughly the length of the main rotor diameter. When the helicopter is very close to the ground, the ground effect can boost the thrust up to 100% more than the nominal thrust out of the ground effect region. Indeed, this is the underlying theory of hovercraft, which floats only few inches over the ground by blowing air down. Ursa Minor 1, the first test RUAV for the Berkeley UAV research, could hover only in the ground effect region because the engine could not keep up with the required load for ground effect-free flight.

Obviously, the ground effect is a very complicated and strongly nonlinear dynamic effect, which is very hard to model analytically. From the viewpoint of controller design, the rotor efficiency boost under the ground effect appears as larger control input gain. In the ground effect region, the helicopter drifts more or feels like it is “riding on air” due to the unsteady wake of the main rotor which is reflected on the ground. From these observations, the proposed controller should be robust to the change of rotor efficiency as well as to the disturbance when the helicopter is in the ground effect. The landing controller should be able to control the vertical descent following the landing profile while minimizing the longitudinal and lateral drift to prevent tip-off of the helicopter.

2.2.7 Helicopter Hover Model

The Newton-Euler dynamic equations in (2.25) and (2.26) is valid throughout the entire flight envelop as long as the accurate force and moment terms are found and used. It is often impossible to find the force and moment terms that are accurate over the entire flight envelop. Therefore, we need to limit the flight range to a certain flight mode to obtain more accurate and simpler equation form for analysis. In our research, as has been implied so far, we start with hover mode because it is one of the most important maneuvers of helicopter and low velocity horizontal/vertical motion and pirouette can be considered as the extension of hover. In hover, the helicopter dynamics simplify in the following ways:

- Since the vehicle has a very low velocity in every direction and the attitude deviation is small, we can ignore the effect of the fuselage, the horizontal stabilizer and the vertical stabilizer.

$$\begin{aligned}(X,Y)_F &= 0\\ (X,Y)_H &= 0\\ (X,Y,Z)_V &= 0\end{aligned} \tag{2.44}$$

- The tail rotor shaft is aligned along the +*y* axis and it does not generate any significant forces by the local inflow in other direction. In other words, the tail rotor generates the lateral thrust, and yaw moment and anti-torque in pitch axis only.

$$\begin{aligned}(X,Z)_T &= 0\\ (R,N)_T &= 0\end{aligned} \tag{2.45}$$

Under the assumption (2.44) and (2.45), the differential equation (2.25) simplifies to:

$$\dot{\mathbf{V}}_b = \frac{1}{m}\begin{bmatrix} X_M \\ Y_M + Y_T \\ Z_M + Z_H + Z_F \end{bmatrix} + \mathbf{R}_{TP\to B}\begin{bmatrix} 0 \\ 0 \\ g \end{bmatrix} + \begin{bmatrix} vr - wq \\ wp - ur \\ uq - vp \end{bmatrix} \tag{2.46}$$

$$\dot{\boldsymbol{\omega}} = \mathbf{I}_b^{-1}\begin{bmatrix} R_M + Y_M h_M + Z_M y_M + Y_T h_T \\ M_M - X_M h_M + Z_M l_M + M_T + Z_H l_H \\ N_M - Y_M l_M - Y_T l_T \end{bmatrix} + \mathbf{I}_b^{-1}\begin{bmatrix} qr(I_{yy} - I_{zz}) \\ pr(I_{zz} - I_{xx}) \\ pq(I_{xx} - I_{yy}) \end{bmatrix} \tag{2.47}$$

With the simplified system equation for hover, we find the aerodynamic equations for variables in equation (2.47).

- **Main rotor**

  The main rotor is the source of vertical lift, horizontal force, and anti-torque. It also generates the rolling and pitching moment by flapping, known as *rotor stiffness*, which is produced by the vertical component of the blade centrifugal force acting at the hinge offset. The overall contribution of the main rotor can be written as follows:

$$
\begin{aligned}
X_M &= -T_M \sin a_{1s} \\
Y_M &= -T_M \sin b_{1s} \\
Z_M &= -T_M \cos a_{1s} \cos b_{1s} \\
R_M &= -\left(\frac{dR}{db_{1s}}\right) b_{1s} - Q_M \sin a_{1s} \\
M_M &= \left(\frac{dM}{da_{1s}}\right) a_{1s} - Q_M \sin b_{1s} \\
N_M &= -Q_M \cos a_{1s} \cos b_{1s}
\end{aligned}
\tag{2.48}
$$

where the rotor stiffness term can be found by

$$
\frac{dR}{db_{1s}} = \frac{dM}{da_{1s}} = \frac{1}{4}\frac{e}{R} b m_b R \left(\Omega R\right)^2 \tag{2.49}
$$

Note that the rotor stiffness is identical in roll and pitch direction because of the symmetry of the rotor.

- **Tail rotor**

As reviewed above, the tail rotor is considered to provide the lateral force as well as the anti-torque.

$$
\begin{aligned}
Y_T &= -T_T \\
M_T &= -Q_T
\end{aligned}
\tag{2.50}
$$

The sign of M_T depends on the direction of the tail rotor revolution. The sign is minus for both Kyosho Concept 60 and Yamaha R-50 helicopters

- **Vertical Drag on fuselage and horizontal stabilizer**

These terms, Z_F and Z_H can be obtained by experiments or some estimation using the cross-sectional area of these components in the rotor downwash.

Substituting (2.48) and (2.50) to (2.46) and (2.47), we obtain the nonlinear model for hover as following:

$$\dot{\mathbf{V}}_b = \frac{1}{m}\begin{bmatrix} -T_M \sin a_{1s} \\ -T_M \sin b_{1s} - T_T \\ -T_M \cos a_{1s} \cos b_{1s} + Z_H + Z_F \end{bmatrix} + \mathbf{R}_{TP\to B}\begin{bmatrix} 0 \\ 0 \\ g \end{bmatrix} + \begin{bmatrix} vr - wq \\ wp - ur \\ uq - vp \end{bmatrix} \tag{2.51}$$

$$\dot{\boldsymbol{\omega}} = \mathbf{I}_b^{-1}\begin{bmatrix} -\left(\dfrac{dR}{db_{1s}}\right)b_{1s} - T_M h_M \sin b_{1s} - Q_M \sin a_{1s} - T_M y_M - T_T h_T \\ \left(\dfrac{dM}{da_{1s}}\right)a_{1s} + T_M h_M \sin a_{1s} - Q_M \sin b_{1s} + T_M l_M - Q_T + Z_H l_H \\ -Q_M \cos a_{1s} \cos b_{1s} + T_M \sin b_{1s} l_M + T_T l_T \end{bmatrix} + \mathbf{I}_b^{-1}\begin{bmatrix} qr(I_{yy} - I_{zz}) \\ pr(I_{zz} - I_{xx}) \\ pq(I_{xx} - I_{yy}) \end{bmatrix} \tag{2.52}$$

We can complete the simulation model with the knowledge of each force and moment terms T_M, T_T, Q_M, and Q_T are found by the equations developed in Section 2.2.2. In evaluating equations (2.46) to (2.50), we need to know geometric, aerodynamic and mechanical parameters specific to the helicopter system. Some of these can be easily measured, some of these can be obtained from experimental data sources such as NACA and some of these have to be decided by approximation and estimation. Usually the most troublesome parts are the aerodynamic properties especially when we do not have access to certain test equipment. Another difficulty is the measurement of the mass moment of inertia. For smaller helicopters, we can directly estimate the quantity through the pendulum test [26]. For larger helicopters, such as the Yamaha helicopters, this process is usually cumbersome. Solid modeling using computer design software could be employed with moderate accuracy. However, the latter approach requires extensive knowledge of the helicopter components that only the manufacturers are likely to have. Furthermore, many manufacturers do not even keep track of this information. Because of this complication, we did not find the CG location and mass moment of inertial of for the R-50 and the RMAX. This was another reason that we had to resort to the experimental parametric identification approach.

In the development of the simulation model for the *Ursa Minor 2*, we were able to perform extensive parameter measurements as shown in Table 2-1. These parameters have not been reconciled with the actual flight data because the flight experiments provide the system response which is a mixture of all components, i.e., main rotor, tail rotor and so on. Therefore, it is necessary to test the individual components using aerodynamic test facilities. Because of this difficulty, we did not attempt to find the nonlinear model with this approach and we took an alternative way that is presented in the next section.

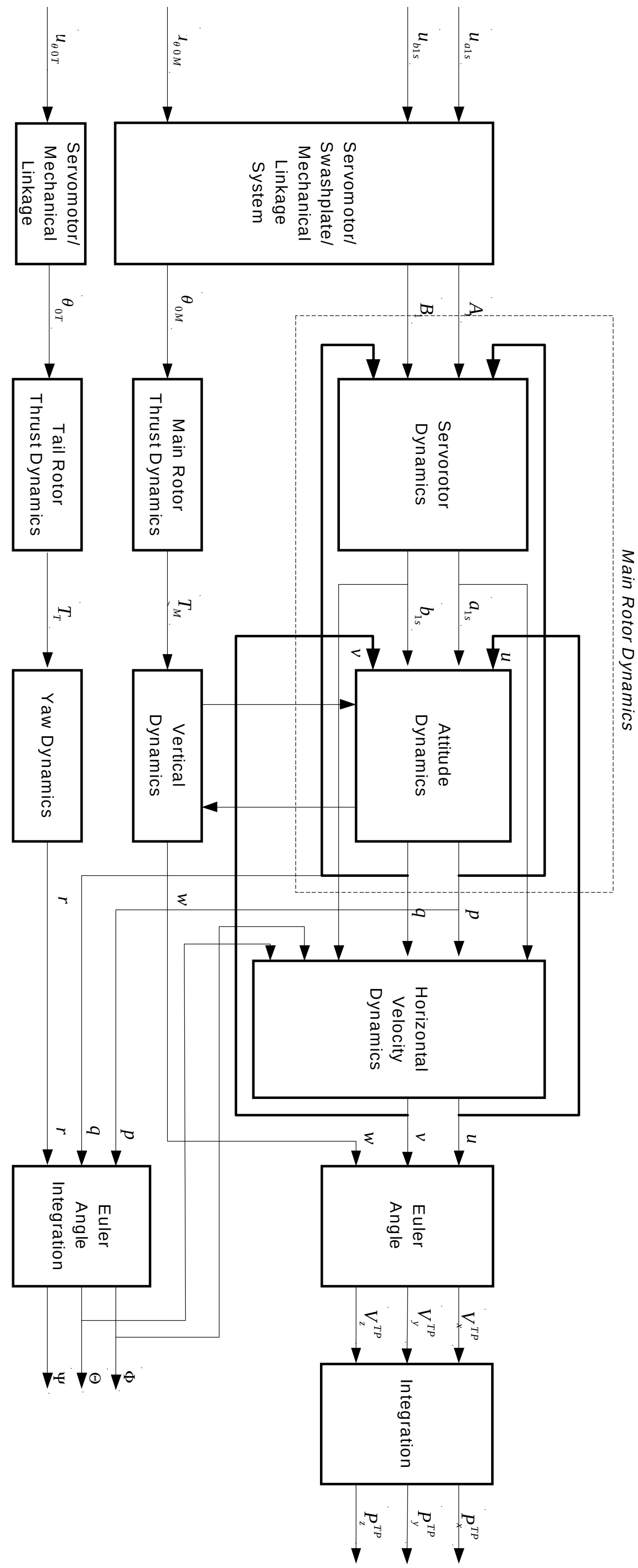

Figure 2.11 Block diagram representation of helicopter dynamics

The vehicle model developed so far can be implemented in a simulation environment. In choosing the simulation environment, there are a number of choices available. MATLAB is one of the most popular design and simulation environments because it offers abundant numerical algorithms and design tools as well as nice visualization functions. For the simulation, MATLAB offers graphical user interface-based numerical simulation environment, Simulink®. In this research, MATLAB/Simulink is consistently used for controller design and simulation. In the Simulink environment, the helicopter dynamics developed so far is cast into Simulink S-functions in the C language, which is chosen for faster execution time.

The helicopter equations that have been formulated so far can be represented in the following block diagram. It should be noted that, quite contrary to some understandings, the helicopter dynamics are *not* a cascade of servomotor-attitude-translational sub-dynamics. The feedback of angular rates p and q due to the Bell-Hiller stabilizer system modifies the dynamics substantially. The horizontal velocity u and v also affects the attitude dynamics. If the helicopter is constrained in the translational motion and only the attitude motion is allowed, the attitude dynamics is stable. However, when it is allowed to move freely in the horizontal direction, the vehicle dynamics becomes unstable due to the interaction of the lift and the inflow.

As can be seen in the block diagram, the helicopter system has four inputs while the helicopter has the freedom in $\mathscr{R}^3 \times \mathrm{SO}(3)$. Therefore, the helicopter is an *underactuated* system, which implies that the vehicle dynamics has internal constraints so that only four DOF can be arbitrarily achieved while the other two are constrained by the configuration of the helicopter. The helicopter achieves the longitudinal motion and the lateral motion by tilting the body first in pitch and roll direction, respectively. The attained velocity in x and y direction has certain relationship with the amount of the angle tilted in pitch and roll direction, respectively. In normal situation, this would not pose any significant restriction in navigation. The peculiar situation occurs during the landing: due to the dynamic relationship between the attitude and the translational velocities in the x and y direction, the helicopter has difficulties to land on a slanted surface. This has been known to be a problem when a helicopter attempts to land on a rolling and pitching deck of a ship.

- **Linearized Model**

The nonlinear model (2.46) for hover is valuable for the nonlinear simulation model and it can be further simplified to obtain the linear model. A linear dynamic model for helicopter is needed for the design of linear feedback control system. As shown in Figure 2.11, the helicopter dynamics can be decomposed into three parts: (1) servoactuator-mechanical linkage system, (2) aerodynamics system, and (3) kinematic system. In the previous sections, the kinematic-dynamic relationship for (2) and (3) are developed. The subsystem (1) is relatively easier to identify and the response time is usually faster than that of the aerodynamic systems. Therefore, in the subsequent analysis, the servoactuation dynamics is embedded in the much slower-to-respond consequential dynamics and will be identified together. With this consideration, we define the following nonlinear helicopter dynamics

$$\dot{\mathbf{x}} = \mathbf{F}(\mathbf{x}, \mathbf{u}) \tag{2.53}$$

where

$$\mathbf{x} = [u \quad v \quad w \quad \Phi \quad p \quad \Theta \quad q \quad \Psi \quad r \quad a_{1s} \quad b_{1s}]^T \tag{2.54}$$

$$\mathbf{u} = [u_{a_{1s}} \; u_{b_{1s}} \; u_{\theta_M} \; u_{\theta_T}]^T \tag{2.55}$$

$u_{a_{1s}}$: input to the lateral cyclic pitch

$u_{b_{1s}}$: input to the longitudinal cyclic pitch

u_{θ_M} : input to the main rotor collective pitch

u_{θ_T} : input to main rotor collective pitch

For the nonlinear control model, we can directly use the nonlinear simulation model or a model with simplifications and/or approximations of the thrust and torque terms. In this research, we are interested in finding the linear time invariant model for LTI identification and controller design for hover. Therefore, we introduce the following assumptions:

- The velocity and attitude angles are assumed to be very small so that the following simplifications are valid:

$$\sin x \simeq x, \quad \cos x \simeq 1 \tag{2.56}$$

- With the assumption that the rigid body has small velocity and attitude angles in every direction, the Coriolis' acceleration terms and gyroscopic terms are ignored.

$$\begin{gathered} \dot{y}r - \dot{z}q \simeq 0 \qquad -\dot{x}r + \dot{z}p \simeq 0 \qquad \dot{x}q - \dot{y}p \simeq 0 \\ \frac{I_{yy} - I_{zz}}{I_{xx}} qr \simeq 0 \quad \frac{I_{zz} - I_{xx}}{I_{yy}} pr \simeq 0 \quad \frac{I_{xx} - I_{yy}}{I_{zz}} pq \simeq 0 \end{gathered} \tag{2.57}$$

Applying (2.56) and (2.57) to the original equation, we obtain the differential equation

$$
\dot{\mathbf{x}} = \mathbf{F}(\mathbf{x},\mathbf{u})
= \begin{bmatrix}
-\frac{1}{m} T_M a_{1s} - g\Theta \\
-\frac{1}{m}\left(T_M b_{1s} + T_T\right) + g\Phi \\
\frac{1}{m}\left(-T_M + Z_H + Z_F\right) + g \\
p \\
\frac{1}{I_{xx}}\left[-\left\{\left(\frac{dR}{db_{1s}}\right) + T_M h_M\right\} b_{1s} - Q_M a_{1s} - T_M y_M - T_T h_T\right] \\
q \\
\frac{1}{I_{yy}}\left[\left\{\left(\frac{dM}{da_{1s}}\right) + T_M h_M\right\} a_{1s} - Q_M b_{1s} + T_M l_M - Q_T + Z_H l_H\right] \\
r \\
\frac{1}{I_{zz}}\left(-Q_M + T_M b_{1s} l_M + T_T l_T\right) \\
-\frac{a_{1s}}{\tau_f} - q + A_{b_{1s}} b_{1s} + A_{u_{a1s}} u_{a_{1s}} + A_{u_{b1s}} u_{b_{1s}} \\
-\frac{b_{1s}}{\tau_f} - p + B_{a_{1s}} a_{1s} + B_{u_{a1s}} u_{a_{1s}} + B_{u_{b1s}} u_{b_{1s}}
\end{bmatrix} \tag{2.58}
$$

Note that the force and moment terms are the function of a number of parameters as following:

$$
\begin{aligned}
& f_{T_M} : (u, v, w, \theta_M) \mapsto T_M \\
& f_{Q_M} : \theta_M \mapsto Q_M \\
& f_{T_T} : (v, r, \theta_T) \mapsto T_T \\
& f_{Q_T} : \theta_T \mapsto Q_T
\end{aligned} \tag{2.59}
$$

The linearized system equation is defined as the Jacobian matrices in the following:

$$
\delta\dot{\mathbf{x}} = \left[\frac{\partial F_j}{\partial x_i}\right]_{\substack{\mathbf{x}=\mathbf{x}_{trim} \\ \mathbf{u}=\mathbf{u}_{trim}}} \delta\mathbf{x} + \left[\frac{\partial F_j}{\partial u_i}\right]_{\substack{\mathbf{x}=\mathbf{x}_{trim} \\ \mathbf{u}=\mathbf{u}_{trim}}} \delta\mathbf{u} \tag{2.60}
$$

where

$$\delta\mathbf{x} = \mathbf{x} - \mathbf{x}_{trim}$$
$$\delta\mathbf{u} = \mathbf{u} - \mathbf{u}_{trim}$$

$$\left[\frac{\partial F_j}{\partial x_i}\right] = \begin{bmatrix} \frac{\partial F_u}{\partial u} & \frac{\partial F_u}{\partial v} & \frac{\partial F_u}{\partial w} & 0 & 0 & -g & 0 & 0 & \frac{\partial F_u}{\partial a_{1s}} & 0 \\ \frac{\partial F_v}{\partial u} & \frac{\partial F_v}{\partial v} & \frac{\partial F_v}{\partial w} & g & 0 & 0 & 0 & 0 & 0 & \frac{\partial F_v}{\partial b_{1s}} \\ \frac{\partial F_w}{\partial u} & \frac{\partial F_w}{\partial v} & \frac{\partial F_w}{\partial w} & 0 & 0 & 0 & 0 & 0 & 0 & 0 \\ 0 & 0 & 0 & 0 & 1 & 0 & 0 & 0 & 0 & 0 \\ \frac{\partial F_p}{\partial u} & \frac{\partial F_p}{\partial v} & \frac{\partial F_p}{\partial w} & 0 & 0 & 0 & 0 & 0 & \frac{\partial F_p}{\partial a_{1s}} & \frac{\partial F_p}{\partial b_{1s}} \\ 0 & 0 & 0 & 0 & 0 & 0 & 1 & 0 & 0 & 0 \\ \frac{\partial F_q}{\partial u} & \frac{\partial F_q}{\partial v} & \frac{\partial F_q}{\partial w} & 0 & 0 & 0 & 0 & 0 & \frac{\partial F_q}{\partial a_{1s}} & \frac{\partial F_q}{\partial b_{1s}} \\ \frac{\partial F_r}{\partial u} & \frac{\partial F_r}{\partial v} & \frac{\partial F_r}{\partial w} & 0 & 0 & 0 & 0 & \frac{\partial F_r}{\partial r} & 0 & \frac{\partial F_r}{\partial b_{1s}} \\ 0 & 0 & 0 & 0 & 0 & 0 & -1 & 0 & \frac{\partial F_{a_{1s}}}{\partial a_{1s}} & \frac{\partial F_{a_{1s}}}{\partial b_{1s}} \\ 0 & 0 & 0 & 0 & -1 & 0 & 0 & 0 & \frac{\partial F_{b_{1s}}}{\partial a_{1s}} & \frac{\partial F_{b_{1s}}}{\partial b_{1s}} \end{bmatrix} \quad (2.61)$$

$$\left[\frac{\partial F_j}{\partial u_i}\right] = \begin{bmatrix} 0 & 0 & \frac{\partial F_u}{\partial \theta_M} & 0 \\ 0 & 0 & \frac{\partial F_v}{\partial \theta_M} & \frac{\partial F_v}{\partial \theta_T} \\ 0 & 0 & \frac{\partial F_w}{\partial \theta_M} & 0 \\ 0 & 0 & 0 & 0 \\ 0 & 0 & \frac{\partial F_p}{\partial \theta_M} & \frac{\partial F_q}{\partial \theta_T} \\ 0 & 0 & 0 & 0 \\ 0 & 0 & \frac{\partial F_q}{\partial \theta_M} & \frac{\partial F_q}{\partial \theta_T} \\ 0 & 0 & \frac{\partial F_r}{\partial \theta_M} & \frac{\partial F_r}{\partial \theta_T} \\ \frac{\partial F_{a_{1s}}}{\partial u_{a_{1s}}} & \frac{\partial F_{a_{1s}}}{\partial u_{b_{1s}}} & 0 & 0 \\ \frac{\partial F_{b_{1s}}}{\partial u_{a_{1s}}} & \frac{\partial F_{b_{1s}}}{\partial u_{b_{1s}}} & 0 & 0 \end{bmatrix} \quad (2.62)$$

The Jacobian, often referred to as the *stability derivatives* in the aerospace community, can be found by the partial differentiation of the system equation $\mathbf{F}(\mathbf{x},\mathbf{u})$ as shown in (2.61) and (2.62). The terms with negligible contributions are displayed with smaller fonts. The valuable results on calculating the Jacobian were suggested by Prouty [10]. Using his work, the Jacobian matrices can be computed by simply plugging in the parameters of the target helicopter as shown in Table 2-1. Most of his work is directly applicable to our research with the exception of the flapping characteristics. The Jacobian in (2.61) and (2.62) provides us the insights on the relationship between the contribution of each term and the overall vehicle dynamics. This analysis is particularly useful for the vehicle design and tuning process to meet the handling quality requirements.

In Table 2-1, the various parameters of Ursa Minor 2 are listed. The meanings of these parameters are mostly self-explanatory. The inertia terms are measured by a simple pendulum test. The geometric terms are determined easily once the location of C.G. is found. The airfoil of the main rotor of the Ursa Minor 2 is assumed NACA0012 and its aerodynamic parameters are determined by the experiments by NACA in 1950s. The airfoil of the tail rotor is close to NACA0014 and the aerodynamic parameters are determined in a similar way. The operational parameters such as the angular velocity of main rotor and the hover pitch are found by a series of test flights.

As mentioned earlier, we have difficulty directly pursuing this approach because, in the case of Yamaha R-50 for example, most of the aerodynamic and mechanical parameters are difficult to find. R-50 is too large and heavy to measure the inertia directly. The aerodynamic property of the custom-shape blades of R-50 is difficult to estimate without any test facility. Therefore, we seek an alternative way to find a system model directly using the flight data.

Table 2-1 Parameters for Ursa Minor 2 for simulation model

Rotor	**CW**						
Rho	**1.18**	c					
Vertical Drag/mg H	**0**						
Vertical Drag/mg F	**0.02**						
Weight	**93.12**		9.5				
Ixx	**0.1634**	c					
Iyy	**0.5782**	c					
Izz	**0.6306**	c					
Mass of main blade	**0.178**	c					
Ibm	**0.0280**	c	******				
Qm	**2.5110**	c					
Angular Vel. of M.Rotor	**171.1**		**1634.32**	RPM	MACH Number	0.39766199144	
Radius of M.Rotor	**0.79**	c					
Inner radius of M.Rotor	**0.196**	c					
Pitch angle at root	**0.1257**		7.2	deg			
Twist of Main blade	**0**	c			**Normalization Numbers**		
a0	**0.04674**	c					
Sigma of M.Rotor	**0.04980**	c			**Max.Vx**	**5**	m/s
Pitch angle at 75%	**0.1257**	c			**Max.Vy**	**5**	m/s
Flapping offset ratio (e/R)	**0.05063**	c			**Max.Vz**	**5**	m/s
Slope of lift curve of M.Rotor	**5.40**	s			**Max.Roll_angle**	**0.3491**	rad
Drag coefficient Cd of M.Rotor	**0.006400**	s			**Max.Roll_rate**	**0.3491**	rad/s
# of M.blade	**2**	c			**Max.Pitch_angle**	**0.3491**	rad
width of M.Rotor	**0.058**	c			**Max.Pitch_rate**	**0.3491**	rad/s
Area of M.blade	**0.0916**	c			**Max.Yaw_angle**	**0.3491**	rad
iM	**-0.03491**	c			**Max.Yaw_rate**	**0.3491**	rad/s
hM	**0.2340**	c			**Max.Collective_pitch**	**0.0873**	rad
yM	**0**	c			**Max.Tail_pitch**	**0.4363**	rad
lM	**0.01**	c			**Max.Lateral_cyclic_pitch**	**0.3491**	rad
lF	**-0.1**	c			**Max.Longitudinal_cyclic_pitch**	**0.4363**	rad
lH	**0.00**	N/A			**Servo_Corner_Frequency**	**6.2832**	Hz
Angular Vel. of T.Rotor	**920.8**		8792.646	RPM	**Servo_Gain**	**66.82**	
Radius of T.Rotor	**0.1290**	c			**Max.Servo_Pulse_width**	**800**	
Inner radius of T.Rotor	**0.042**	c					
Slope of lift curve of T.Rotor	**5.40**	s			MACH Number	0.34934857633	
Drag coefficient Cd of T.Rotor	**0.006400**	s					
Sigma of T.Rotor	**0.1198**	c					
#.of Blade T.Rotor	**2**	c			**Linkage Gain**		
width of T.Rotor	**0.028**	c			**Main**	1.9248	
Area of Blade T.Rotor	**0.0056**	c			**Tail**	2.3955	
F to T ratio	**0.053**	s			**Lingitudinal**	1.9289	
Thrust of T.Rotor	**5.553**	c			**Lateral**	1.5431	
V1t	**7.095**	c					
Torque of T.Rotor	**0.02965**	c					
Pitch angle at 75% T.Rotor	**0.1414**		8.1		**0**		
ht	**0.0620**	c					
lt	**0.8980**	c					
Gear Ratio (Main Rotor/Engine)	9.79						
Gear Ratio (Tail Rotor/Engine)	5.38						
Angular Vel. of Engine	**1675.5**		16000				

2.2.8 Experimental Hover Model

In the previous sections, a general nonlinear system model for hover has been developed. This model is very useful for the construction of simulation model if and only if the accurate knowledge over numerous system parameters and rotor force and moment models is available. In our research, we estimated the full set of parameters for Ursa Minor 2 as shown in Table 2-1. As mentioned above, the estimated parameters were not reconciled with the flight data and the obtained nonlinear model may not correctly describe the actual helicopter dynamics. The major difficulty of this approach is that the accurate knowledge of the aerodynamic parameters as well as some other mechanical parameters are hard to obtain and the reconciliation of the theoretical model with the experimental data is impossible without proper experimental setup. In our research, this situation forced us to resort to the empirical parametric identification method instead of the theoretical model approach. The parameters that have to be identified are the Jacobians in the linearized model. While the parameters of the nonlinear model developed above are physical mechanical or aerodynamic parameters, the parameters in the Jacobian are the first-order derivative of the complicated nonlinear functions in (2.58). As we decided to identify the helicopter model as is, a number of changes are made to the original nonlinear or linear models proposed in Section 2.2.7. In the following, the template model for the LTI MIMO parametric identification is given. This model is proposed by Mettler *et al* in 1999: it is a simplified version of (2.61) and (2.62) obtained by discarding terms of negligible contributions. This model also includes the servorotor dynamics as a first-order approximation. The servomotor models for the control surfaces are embedded in the system matrices and identified together because the bandwidths of the servomotors are sufficiently higher than the retarded response speed of the servorotor and lift dynamics of main and tail rotors. Another major modification is the inclusion of the built-in rate gyroscope compensator model. As will be explained in a greater detail in Section 3.1, the rate gyroscope senses the yaw rate and superpose the yaw compensation signal on the pilot's command. The feedback system attenuates the effect of the anti-torque fluctuation on the yaw response so that the ground pilot to control the vehicle with ease. It was decided to leave the built-in gyroscope in the loop because of the two reasons: (1) the yaw response can be improved without additional yaw rate feedback if tuned correctly, and (2) it helps the human pilot to take over the control of the vehicle in emergency.

With these factors, the template model has the input to the servomotor as the control input variables. In the yaw channel, the input is no longer the tail collective pitch: it is now the input to the yaw rate compensator. By having the servomotor PWM input as the control input, we do not need to identify the servomotors and the linkage gains separately: they are identified as a whole in the identification process. In the following, the template model is shown:

$$\dot{\mathbf{x}} = \mathbf{A}\mathbf{x} + \mathbf{B}\mathbf{u} \tag{2.63}$$

where

$$\mathbf{x} = [u\ v\ p\ q\ \Phi\ \Theta\ a_{1s}\ b_{1s}\ w\ r\ r_{fb}]^T \tag{2.64}$$

$$\mathbf{u} = [u_{a_{1s}}\ u_{b_{1s}}\ u_{\theta_M}\ u_{r_{ref}}]^T \tag{2.65}$$

where

r_{fb} : feedback gyro system state

$$\mathbf{A} = \begin{bmatrix} X_u & 0 & 0 & 0 & 0 & -g & X_{a_{1s}} & 0 & 0 & 0 & 0 \\ 0 & Y_v & 0 & 0 & g & 0 & 0 & Y_{b_{1s}} & 0 & 0 & 0 \\ L_u & L_v & 0 & 0 & 0 & 0 & L_{a_{1s}} & L_{b_{1s}} & 0 & 0 & 0 \\ M_u & M_v & 0 & 0 & 0 & 0 & M_{a_{1s}} & M_{b_{1s}} & 0 & 0 & 0 \\ 0 & 0 & 1 & 0 & 0 & 0 & 0 & 0 & 0 & 0 & 0 \\ 0 & 0 & 0 & 1 & 0 & 0 & 0 & 0 & 0 & 0 & 0 \\ 0 & 0 & 0 & -1 & 0 & 0 & -1/\tau_f & A_{b_{1s}} & 0 & 0 & 0 \\ 0 & 0 & -1 & 0 & 0 & 0 & B_{a_{1s}} & -1/\tau_f & 0 & 0 & 0 \\ 0 & 0 & 0 & 0 & 0 & 0 & Z_{a_{1s}} & Z_{b_{1s}} & Z_w & Z_r & 0 \\ 0 & 0 & N_p & 0 & 0 & 0 & 0 & 0 & N_w & N_r & N_{rff} \\ 0 & 0 & 0 & 0 & 0 & 0 & 0 & 0 & 0 & K_r & K_{rfb} \end{bmatrix} \tag{2.66}$$

$$\mathbf{B} = \begin{bmatrix} 0 & 0 & 0 & 0 \\ 0 & 0 & 0 & 0 \\ 0 & 0 & 0 & 0 \\ 0 & 0 & 0 & 0 \\ 0 & 0 & 0 & 0 \\ 0 & 0 & 0 & 0 \\ A_{u_{a1s}} & A_{u_{b1s}} & 0 & 0 \\ B_{u_{a1s}} & B_{u_{b1s}} & 0 & 0 \\ 0 & 0 & Z_{u_{\theta M}} & 0 \\ 0 & 0 & N_{u_{\theta M}} & N_{u_{\theta T}} \\ 0 & 0 & 0 & 0 \end{bmatrix} \tag{2.67}$$

A MIMO model can be identified with a number of numerical optimization algorithms. In our research, a time-domain based optimization tool is used as will be explained in detail.

To identify the parameters in the system matrices (2.66) and (2.67), we need to collect flight data first. The UAV platforms are equipped, as will be explained in detail in next chapter, with hardware and software that measure the pilot's control input and the vehicle response. During the test flight, the pilot issues frequency-sweeping control input in each channel, namely roll, pitch, yaw, and vertical and the vehicle response was recorded. Although the task sounds straightforward, the actual experiment is more involved and risky due to the unstable helicopter response, the complication of platform/hardware/software reliability, and the perturbed vehicle response due to many factors such as wind and temperature.

In a certain interval, longitudinal and lateral controls are issued in mixed way to capture the cross-coupling of these two channels. One flight data is shown in Figure 2.12: in the first stage, the controls in the longitudinal and the lateral channels are given simultaneously in order to capture the coupling between these axes, while other channels are controlled to maintain constant altitude and heading. In the latter two stages, the main rotor collective pitch or the tail collective pitch are perturbed. Finally, the control signal is issued into all channels simultaneously to check the validity of the cross-coupling term. It should be noted that, due to the coupled and unstable dynamics, the pilot has to issue a stabilizing command to keep the helicopter in a confined area. This hinders the data collection of a one-channel-at-a-time response.

Once adequate flight data has been collected, we identify the parameters in the system matrices using an identification algorithm. Before feeding the data into the numerical tool, the data is preprocessed. The angular rate measurements are filtered by zero-phase non-causal discrete-time filters to filter out high frequency noise without introducing phase delay. The roll and pitch angle measurements are detrended because the helicopter has a trim condition, i.e., the equilibrium with certain nonzero states. In this research, the prediction-error method (PEM) in the MATLAB System Identification Toolbox is chosen.

- Prediction-error method [34]

Suppose we consider a discrete-time state space model

$$\begin{aligned} x(k+1) &= Ax(k) + Bu(k) + Ke(k) \\ y(k) &= Cx(k) + Du(k) + e(k) \end{aligned} \tag{2.68}$$

where

$$x \in \mathscr{R}^{n_x}$$

$$y \in \mathscr{R}^{n_y}$$

$$e \in \mathscr{R}^{n_y}$$

q: one time-step delay operator

From (2.68), the transfer function from u to y and the transfer function from e to y are

$$G(q) = C(qI_{nx} - A)^{-1}B + D \tag{2.69}$$

$$H(q) = C(qI_{nx} - A)^{-1}K + I_{ny} \tag{2.70}$$

respectively.

Define the prediction error $e(k)$ such that

$$\begin{aligned} \tilde{y}(k) &= y(k) - \hat{y}(k) \\ &= G(q)u(k) + H(q)e(k) - G(q)u(k) \\ &= H(q)e(k) \end{aligned} \tag{2.71}$$

$$\therefore e(k) = H^{-1}(q)\left[y(k) - G(q)u(k)\right] \tag{2.72}$$

The PEM seeks to minimizes the quadratic error function

$$V_N(G,H) = \sum_{k=1}^{N} e^2(k) \tag{2.73}$$

to find the system model G and the error model H such that

$$\left[\hat{G}_N, \hat{H}_N\right] = \arg\min V_N(G,H) \tag{2.74}$$

The minimization problem (2.74) is solved by the iterative Gauss-Newton algorithm. The PEM tool in the System Identification Toolbox accepts both continuous and discrete time representation of MIMO parametric system matrices. In our work, we chose the continuous-time template because it is more intuitive. Once the problem is cast into the framework of the PEM tool, we can start solving the minimization problem.

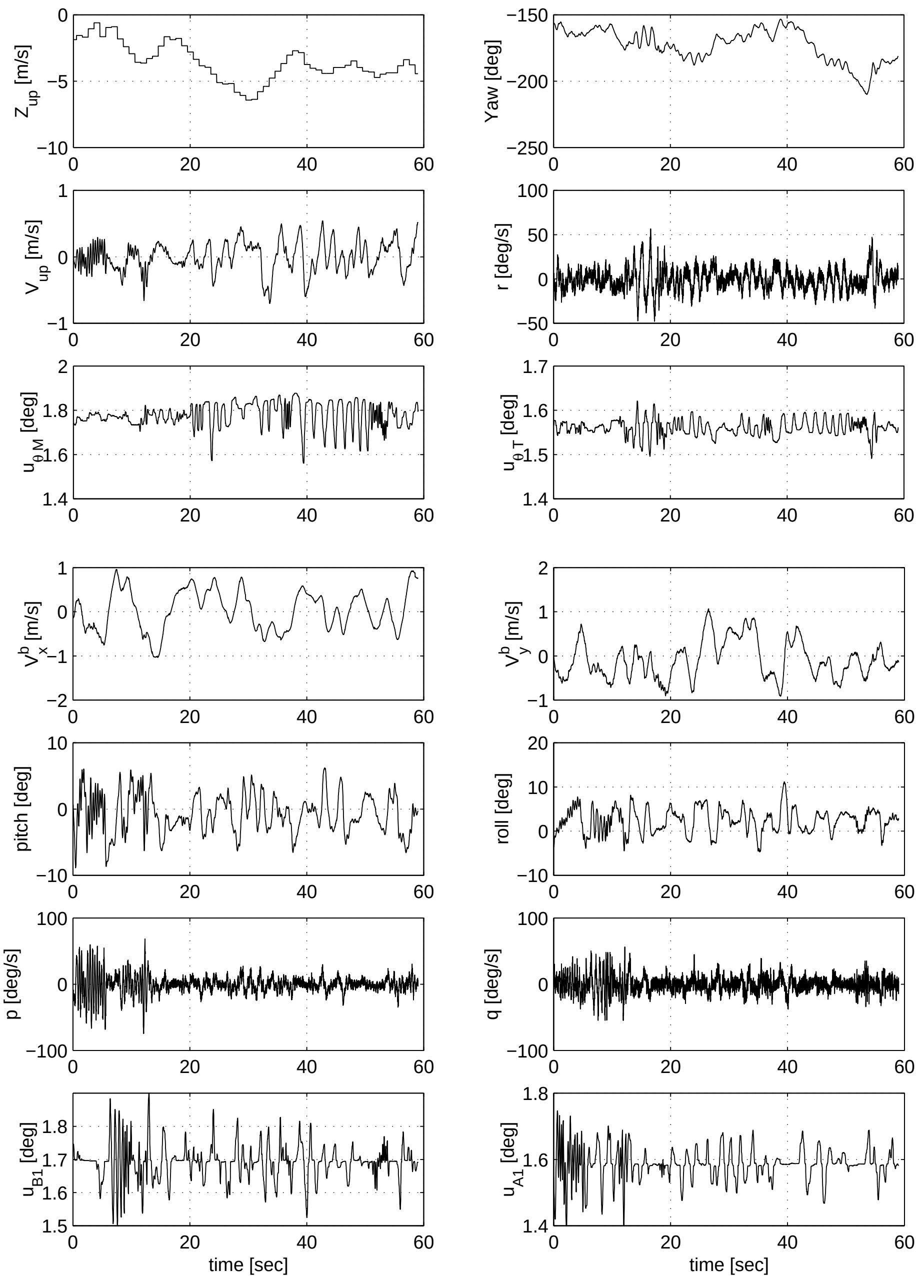

Figure 2.12 Sample flight data for system identification of Ursa Magna 2

It should be noted that this method is extremely sensitive to the initial guess of the parameters. It is also easily trapped in local minima of the parameter hypersurface. To obtain meaningful results and not some parameter set that blindly matches the time history while avoiding these weaknesses, the following technique is devised. First, the angular dynamics, which are augmented with the rotor dynamics, is identified using an initial guess. Since the angular rate/rotor dynamics are known to be stable and only a small number of parameters are involved, the numerical solution converges to consistent solutions. Then the horizontal dynamics, i.e., the longitudinal and lateral dynamic with linear velocity terms u and v are identified while the parameters for angular dynamics are fioxe This stage is rather challenging due to the unstable linear velocity dynamics. A shorter length of experimental data should be used to avoid the instability of the predictor and the divergence of the prediction error with a small mismatch of the initial condition and the parameters. The solution is found after a large number of iterations using the experimental data from different time intervals. Separate from the longitudinal and lateral dynamics, the heave and yaw dynamics is identified in a similar manner. The inherent stability of yaw and heave allows a nice convergence of these parameters. Once these two subsystems are identified, they are combined to form the full-model dynamics. Then the cross-coupling terms are estimated. Finally, a small number of iterations are performed to recalibrate the parameters in the subsystems. This procedure is illustrated in Figure 2.13.

3 Influence of velocity to the attitude dynamics

$$\mathbf{A} = \begin{bmatrix} X_u & 0 & 0 & 0 & 0 & -g & X_{a_{1s}} & 0 & 0 & 0 & 0 \\ 0 & Y_v & 0 & 0 & g & 0 & 0 & Y_{b_{1s}} & 0 & 0 & 0 \\ L_u & L_v & 0 & 0 & 0 & 0 & L_{a_{1s}} & L_{b_{1s}} & 0 & 0 & 0 \\ M_u & M_v & 0 & 0 & 0 & 0 & M_{a_{1s}} & M_{b_{1s}} & 0 & 0 & 0 \\ 0 & 0 & 1 & 0 & 0 & 0 & 0 & 0 & 0 & 0 & 0 \\ 0 & 0 & 0 & 1 & 0 & 0 & 0 & 0 & 0 & 0 & 0 \\ 0 & 0 & 0 & -1 & 0 & 0 & -1/\tau_f & A_{b_{1s}} & 0 & 0 & 0 \\ 0 & 0 & -1 & 0 & 0 & 0 & B_{a_{1s}} & -1/\tau_f & 0 & 0 & 0 \\ 0 & 0 & 0 & 0 & 0 & 0 & Z_{a_{1s}} & Z_{b_{1s}} & Z_w & Z_r & 0 \\ 0 & 0 & N_p & 0 & 0 & 0 & 0 & 0 & N_w & N_r & N_{rff} \\ 0 & 0 & 0 & 0 & 0 & 0 & 0 & 0 & 0 & K_r & K_{rfb} \end{bmatrix}$$

Velocity Dynamics (u,v) 2

Attitude Dynamics (roll, pitch)

Servorotor Dynamics

1

Vertical-Yaw Dynamics 4

5 Influence of attitude dynamics on vertical and yaw

i Order of identification using PEM

Figure 2.13 The procedure of system identification using PEM

Figure 2.14 shows the original system response and the predicted system response of the identified model. We can observe that the roll and pitch rate show superb matching because of the explicit servorotor model. The angle shows mostly good matching, but it deviates from the original response in some intervals because of the nonlinearity and the slightly mismatched trim angles. The vertical model shows rather poor matching in some intervals because the actual vertical dynamics is a very complicated combination of the engine, the transient lift, and the cross-coupling with the roll, pitch and yaw. A higher-order model may be used to account for the transient behavior of the lift dynamics. In the following, the identified system matrices for Ursa Magna 2 are shown.

$$\mathbf{A} = \begin{bmatrix} -0.1257 & 0 & 0 & 0 & 0 & -g & -g & 0 & 0 & 0 & 0 \\ 0 & -0.4247 & 0 & 0 & g & 0 & 0 & g & 0 & 0 & 0 \\ -0.1677 & 0.0870 & 0 & 0 & 0 & 0 & 36.7050 & 161.1087 & 0 & 0 & 0 \\ -0.0823 & -0.0518 & 0 & 0 & 0 & 0 & 63.5763 & -19.4931 & 0 & 0 & 0 \\ 0 & 0 & 1 & 0 & 0 & 0 & 0 & 0 & 0 & 0 & 0 \\ 0 & 0 & 0 & 1 & 0 & 0 & 0 & 0 & 0 & 0 & 0 \\ 0 & 0 & 0 & -1 & 0 & 0 & -3.4436 & 0.8287 & 0 & 0 & 0 \\ 0 & 0 & -1 & 0 & 0 & 0 & 0.3611 & -3.4436 & 0 & 0 & 0 \\ 0 & 0 & 0 & 0 & 0 & 0 & 0 & 9.6401 & -0.7598 & 8.4231 & 0 \\ 0 & 0 & -1.3300 & 0 & 0 & 0 & 0 & 0 & 0.0566 & -5.5105 & -44.8734 \\ 0 & 0 & 0 & 0 & 0 & 0 & 0 & 0 & 0 & 1.8157 & -11.0210 \end{bmatrix} \quad (2.75)$$

$$\mathbf{B} = \begin{bmatrix} 0 & 0 & 0 & 0 \\ 0 & 0 & 0 & 0 \\ 0 & 0 & 0 & 0 \\ 0 & 0 & 0 & 0 \\ 0 & 0 & 0 & 0 \\ 0 & 0 & 0 & 0 \\ -0.8417 & 2.8231 & 0 & 0 \\ -2.4090 & -0.3511 & 0 & 0 \\ 0 & 0 & 70.5041 & 0 \\ 0 & 0 & 23.6260 & 44.8734 \\ 0 & 0 & 0 & 0 \end{bmatrix} \quad (2.76)$$

Table 2-2 Eigenvalues of the identified helicopter system

Mode	**Value**	**Damping**	**Frequency (rad/s)**
Phugoid 1	-0.5262±0.0755j	0.990	0.532
Phugoid 2	0.2458±0.0279j	-0.994	0.247
Roll	-1.5725±12.2567j	0.127	12.4
Pitch	-1.8659±8.2757j	0.220	8.48
Yaw	-8.2845±8.5845j	0.694	11.9
Heave	-0.7223	1	0.722

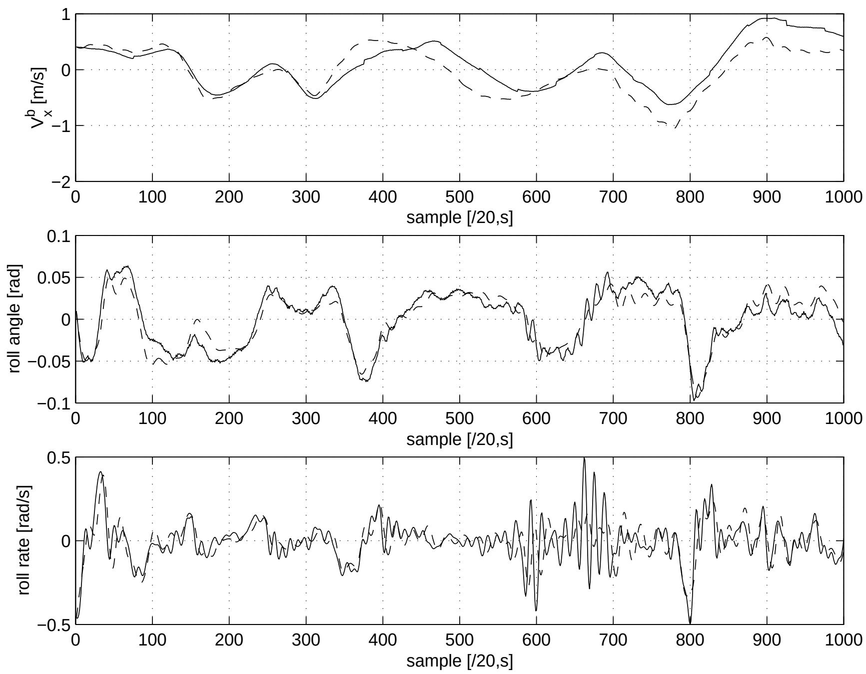

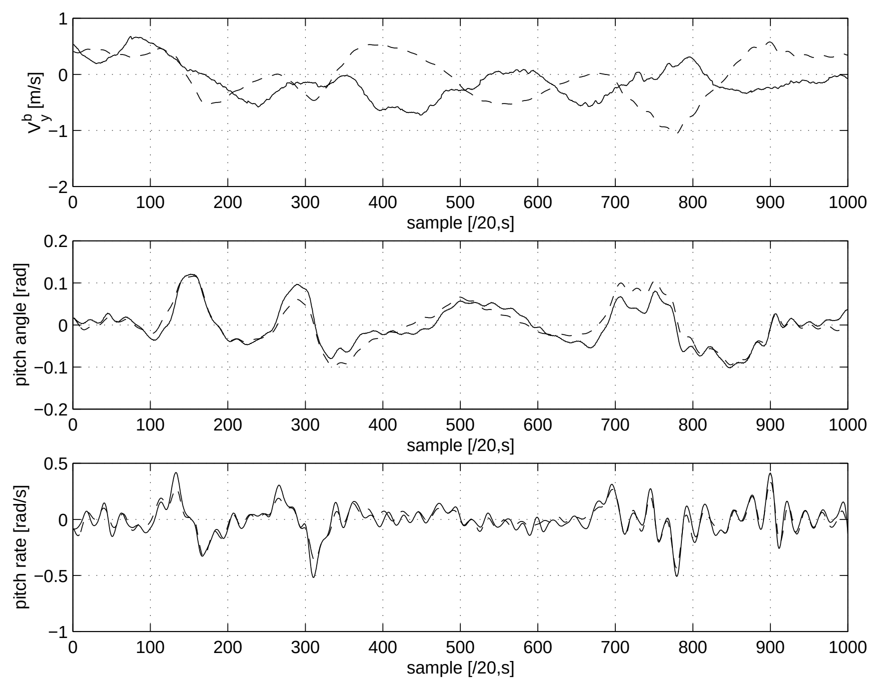

Figure 2.14 The original response and estimated response by the identified model (solid: original; dashed: estimates)

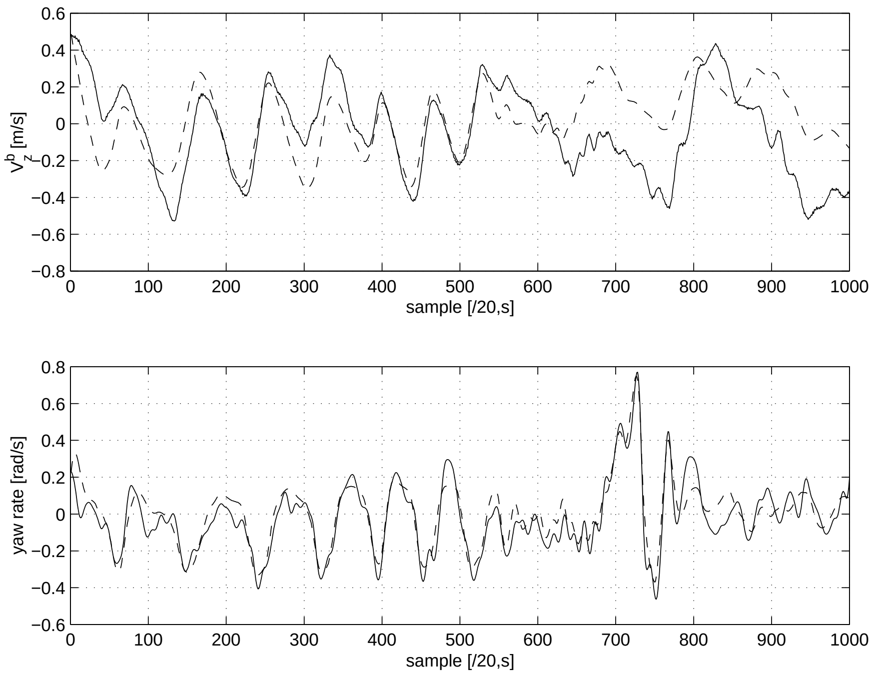

Figure 2.14 ('cont)

The eigenvalues of the identified model are listed in Table 2-2.The linearized system model has stable eigenvalues except for only one pair of complex conjugate in right half plane, which renders the whole helicopter dynamics unstable. This unstable mode is the coupled motion in u and v channels and it shows almost pure divergence because time constant is very large (25 seconds). The responses in all other channels are stable. The roll and pitch responses are weakly damped and their time constants are about 0.51 and 0.74 second, respectively. The rotor dynamics is essentially symmetric and the difference between them is generated by the different values of the mass moment of inertia in the roll and the pitch axis.

The yaw response is moderately damped and the response is fast. This well-tuned response is due to the built-in yaw rate damping gyro system. The heave response shows pure convergence in the first-order quasi-static model and the time constant is about 8.7 seconds. This is anticipated by the experience in manual control of R-50.

Chapter 3

Hardware, Software, and Vehicle Integration

One of the main goals of the Berkeley UAV research effort is to develop and establish a comprehensive and practical methodology to design and implement multiple number of RUAVs equipped with a reliable high-accuracy autopilot. To demonstrate this idea, we need to integrate the vehicle platform with the proper hardware and software so that the vehicle can perform the desired autonomous maneuvers. The integration process is not trivial in every detail because there are many limits and unforeseen interactions when individual components are installed and connected together mechanically and electronically. Indeed, an RUAV is a very tightly integrated embedded electro-mechanical system: every onboard component has an impact on the mechanical aspects such as mass, rotational inertia, and the center of gravity shift of the overall vehicle. In electronic aspects, electromagnetic interference may be a problem for sensitive devices such as the GPS and the digital compass. The small-size radio-controlled helicopters have very limited payload and mounting spaces, and hence we do not have the luxury to apply high-grade protection materials and mountings in order to isolate problems. In many cases, we are forced to provide minimal protection against vibration, heat, and EMI.

The operation of the helicopter platform is hazardous. The high-speed rotor blades pose significant potential threats on ground crew, any other people in the area, and buildings or any properties nearby because the main and tail rotor blades rotate at very high speeds. Moreover, unlike other experimental testbeds that are typically operated in isolated and stable indoor environments, RUAVs operate in a hostile environment. Another demanding factor is that experimental RUAVs require a very high level of reliability, which is only possible from higher standards of engineering and craftsmanship. Hence, utmost care should be exercised in the design, construction and operation of the vehicle to ensure exceptional reliability and robustness to shock, vibration, high temperature, dust, etc. In the Berkeley RUAV research, every effort has been made to reach an extremely high level of reliability of the onboard avionics. In this section, we present the detailed information of the airframe, the hardware, and the software of the Berkeley RUAVs.

3.1 Vehicle Platform

We have adopted four different sizes of model helicopters based on the payload and mission requirements: Kyosho Concept 60SR II, Bergen Industrial Twin, Yamaha R-50 and Yamaha RMAX. All of these helicopters have one main rotor/one tail rotor configuration and share very similar dynamics because of the common usage of the Bell-Hiller stabilizer system. Therefore, it is possible to develop and apply a set of common technologies for all airframes. Detailed information about mechanical specifications and onboard components is given in

Table 3-1. Other than these helicopters, another 60-class helicopter, Kyosho Caliber 60, has been tested as a potential platform for RUAV application. This rather expensive helicopter model features a high-stiffness aluminum body construction, high-accuracy all-metal linkage control and other luxurious options that are suitable for a highly maneuverable RUAV system. Currently, preliminary analysis of the feasibility of the Caliber 60 as a future RUAV platform is underway.

3.1.1 *Ursa Minor Series*-Kyosho Concept 60

Concept 60SR II from Kyosho Industry, Japan is a hobby-purpose radio-controlled helicopter. The main fuselage is constructed with sturdy ABS composite body or high stiffness-graphite plates. The model is powered by a 0.60 cubic-inch glow plug engine, which generates 2.2 hp at 16,000 rpm. BEAR team has acquired three Concept 60 series helicopters, two Concept 60SR-II and one Concept 60SR-II Graphite for RUAV development. Currently two Concept models, one ABS body and one graphite body, are implemented as RUAV platform and the first Concept 60 has retired and now serves as the training vehicle.

This helicopter consists of a fuselage, a main rotor, a tail boom/tail rotor assembly, and landing gear. The Bell-Hiller stabilizer system, often called *flybar* by hobbyists, is factory-tuned on the conservative side for beginners. The glow engine is mounted upside-down below the transmission case for compact design and can only be accessed from the bottom, left, or behind. This prohibits mounting any avionic systems in these areas and leaves this vehicle less attractive for tight component installation. The engine is started by first preheating the glow plug with a low-voltage high-current battery (typically 1.5V, 1500mA) and then cranking the engine by applying a DC-motor starter to the aluminum cone screwed to the end of the engine crankshaft.

The Concept series helicopters have five servomotor systems (commonly called *servos*) to control the main rotor collective pitch, the longitudinal cyclic pitch, the lateral cyclic pitch, the tail collective pitch and the engine throttle. Each of these control surfaces is controlled by one independent servo. Such a control system design is straightforward, unlike other helicopters, whose swashplates are actuated by a simultaneous motion of three servos to achieve main rotor collective/cyclic pitch. In addition, the simple control scheme of the Kyosho Concept 60 makes it possible to switch the control command source between the human pilot and the onboard automatic control channel by channel. Tail collective control is originally performed by a servo system mounted on the fuselage with a long and flexing control rod that yields undesirable hysteresis. A custom tail servo control mounting is machined to attach the servo close to the tail collective pitch linkage, resulting in a control action that is free from hysteresis. Since the vehicle has to carry an additional payload, which was not intended by the manufacturer, FRP main rotor blades, oversized and reinforced tail rotor blades, metal rotor grip, a lightweight engine cooling fan and shock-resistance aftermarket landing gear are used to enhance the overall reliability of the vehicle platform.

One of the earliest experiments to check the payload of the helicopter with the original configuration was performed in the spring of 1996. We validated that the Kyosho Concept 60 could lift 5 kg *within* the ground effect region (Figure 3.1). It should have been realized that, however, the helicopter can lift the 200% of its nominal payload (measured outside of ground effect region) when it is very close to ground [39]. Later on, it became obvious that acquiring or building high payload vehicle platform is *the* major challenge of the project. To overcome this payload barrier, a more powerful glow engine, OS FX91, which generates 2.8 hp output at 15,000 rpm, was tested on Ursa Minor 2 and 3 in April, 1999. This test showed that it could carry acceptable payload by flying well beyond the ground effect with 5 kg of avionics. Once the payload problem was solved, the project began to see huge progress in conjunction with the maturing identification and control techniques.

The avionics is integrated with the vehicle using custom mounting parts. The flight computer system, which consists of a stack of five or six PC104 cards, is housed in custom crafted aluminum enclosure and mounted on the left side of the vehicle using four aluminum mounting tubes and vibration-absorbing grommets. The communication devices and the GPS card are mounted on the right side of the vehicle in a similar manner in order to maintain balance. In later implementation, the GPS card is relocated on the tail boom. The INS is mounted on the nose of helicopter body using a special vibration isolating mounting. The GPS antenna is mounted on the tail boom where the GPS signal is received with less blocking.

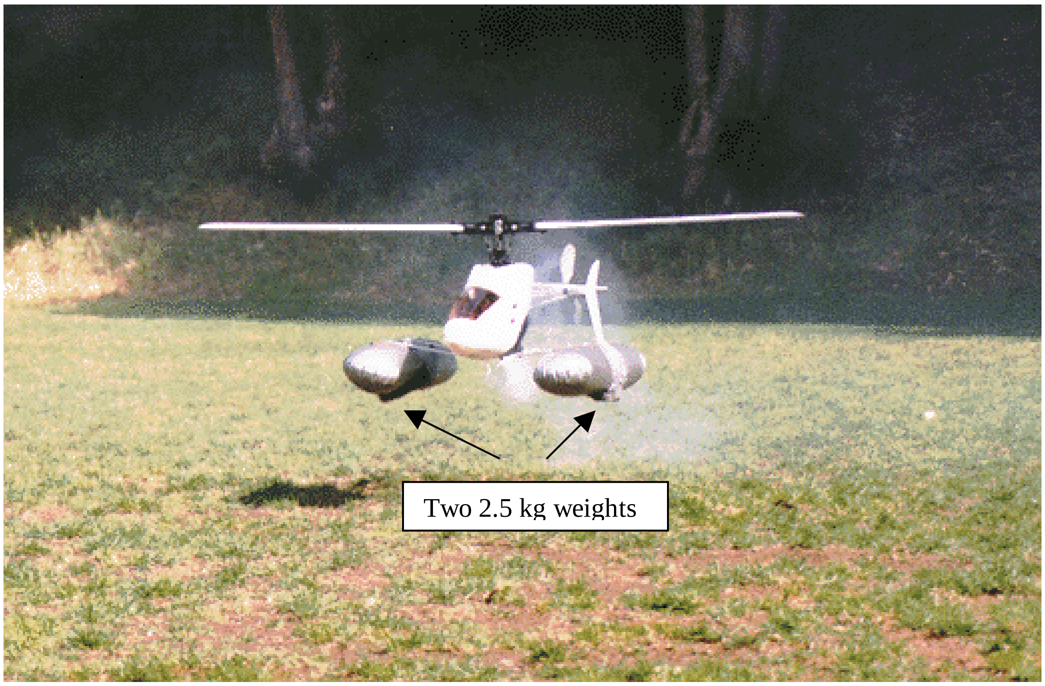

Figure 3.1 Ursa Minor 1 in the payload test (April 1997)

Ursa Minor 1 and *Ursa Minor 2* served a crucial role of paving the way to build successful RUAVs, such as *Ursa Minor 3* and *Ursa Magna 2*. Valuable knowledge and experience about hardware integration with an airframe ware gained during the construction and flight tests of *Ursa Minor 1* and *2*. A number of different configurations were implemented and tested on Ursa Minor 1 and Ursa Minor 2 (Figure 3.3). In the first configuration, Ursa Minor 2 was equipped with Systron-Donner MotionPak as the IMU. The GPS antenna is mounted right above the IMU to minimize the error from the lever arm compensation. The flight computer is housed in 8” ×6”×4.5” aluminum case, which is mounted on a custom aluminum mounting. It is also equipped with a special landing gear to protect the vehicle from shock landings. The major problem of the first configuration is the excessive weight for the 60-class engine. In the second configuration, the weight reduction was the primary objective. The custom aluminum mounting was replaced with light aluminum tubing. The original landing gear was restored to reduce the weight further. The original 60-class engine was replaced with the more powerful 90-class engine. With these improvements, Ursa Minor 2 was finally able to fly beyond the ground effect region. Until the second version, the IMU was mounted on a plastic part that is supported in a cantilever configuration, which is vulnerable to the vertical vibration. In the third configuration, the IMU was directly mounted on the fuselage to improve the vibration characteristics. On Ursa Minor 2, the first attitude controller designed by μ-synthesis was first tested in March 1999 but the result was not successful due to insufficient knowledge of the system model and the defective implementation of the controller.

The airframe for *Ursa Minor 3* (Kyosho Concept 60 Graphite) was purchased in October 1998 and later fully implemented as the primary testbed for the development of the basic autonomous navigation system. For this purpose, Boeing DQI-NP INS, NovAtel MillenRT-2 GPS, a PC104 flight computer, and wireless modems were installed during the first quarter of 1999. Based on the knowledge and experiences gained from building and operating Ursa Minor 1 and 2, the Ursa Minor 3 was designed and integrated. Ursa Minor 3 has been used as a valuable testbed for prototyping the flight system design: a multi-loop classical SISO position/velocity/attitude controller has been designed and tested on this vehicle successfully.

Figure 3.2 Ursa Minor 1 configured as a trainer

(a) February 1999

(b) April 1999

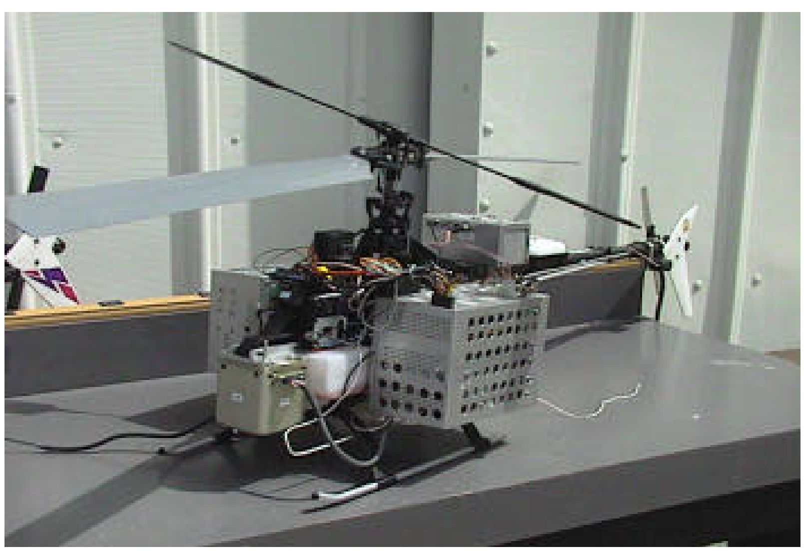

(c) August 1999

Figure 3.3 Ursa Minor 2 in different configurations

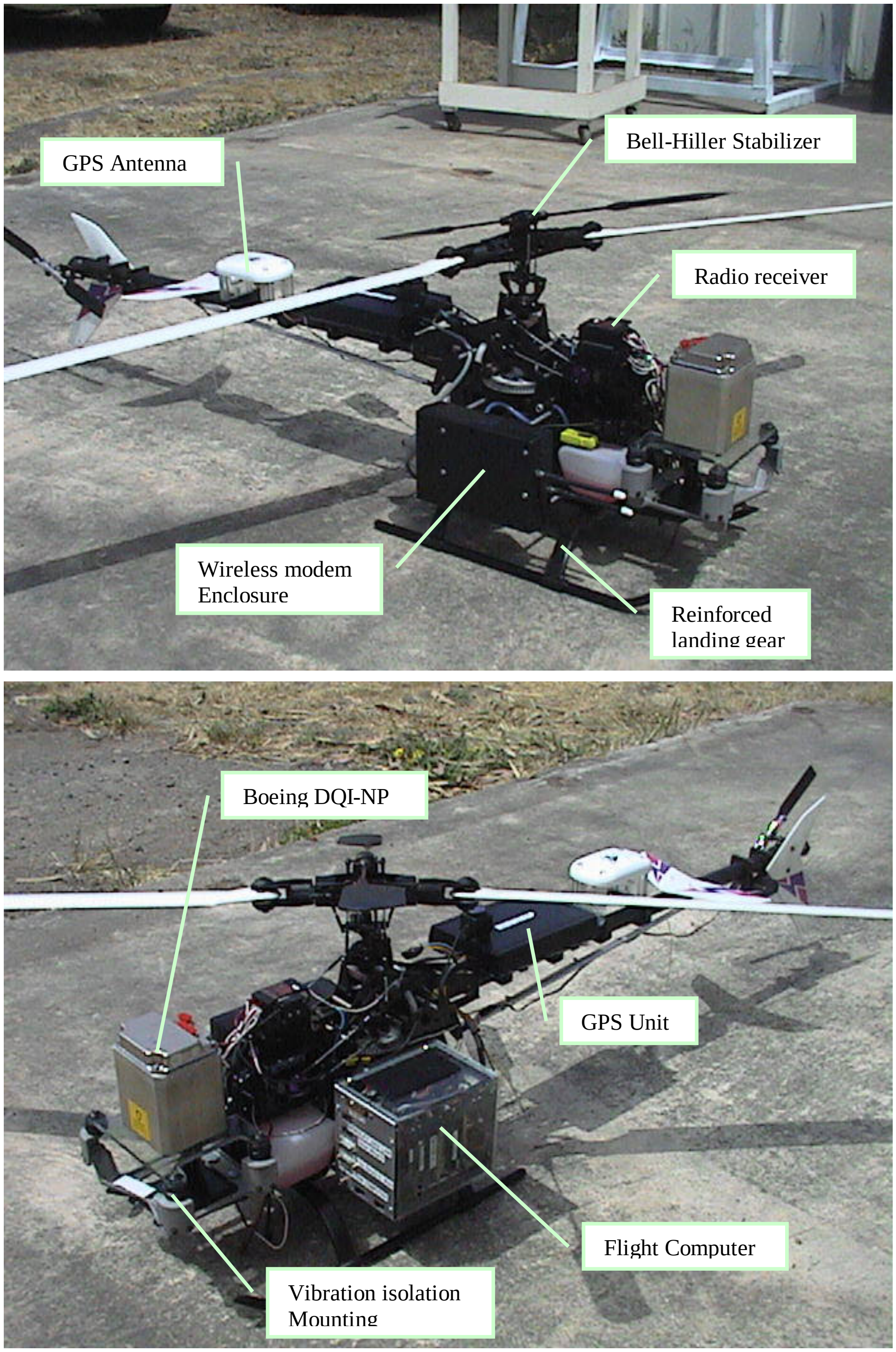

Figure 3.4 ***Ursa Minor 3*** based on Kyosho Concept 60SR II Graphite
(Configuration as of August 1999)

3.1.2 *Ursa Major Series*-Bergen Industrial Twin

The Bergen Industrial Twin is essentially a heavily modified 60-class helicopter powered by two 2-cycle gasoline engines. Two identical engines are attached together through a custom crankcase to generate massive horsepower. The vehicle has an oversized main rotor for additional payload. The tailboom is significantly elongated to compensate the increased anti-torque of the main rotor. This mutated helicopter can be the answer to the demands for higher payload helicopters at an affordable price. The payload of the Bergen helicopter is known to be around 10 kg, which is sufficient to carry the basic navigation system as well as some additional sensors such as a camera and ultrasonic sensors to name a few. However, the load factor on the main rotor shaft and the control linkages is expected to be dangerously high because the shafts and linkages are originally designed for 60 class helicopters weighing 5-6 kg at most while typical RUAV based on Bergen would weight around 15-20kg. Nonetheless, a number of successful RUAV implementations have been reported. For our research, we find Bergen helicopters as a reasonable platform for vision-based ship deck landing experiments because the host vehicle offers enough payload to carry a vision processing computer and a camera as well as the flight control computer. For this application, a special shock-absorbing landing gear is employed as shown in Figure 3.5.

Figure 3.5 Bergen Industrial Twin helicopter with shock absorbing landing gear

3.1.3 Ursa Magna Series-Yamaha R-50

Yamaha R-50 was originally developed in Japan as an efficient alternative for pesticide spraying in rice fields. Reflecting this design concept, the helicopter features rugged construction, simple operation, and easier control characteristics. It has high-clearance skid-type landing gear to allow the mounting of chemical dispensing pumps. This space is ideal for mounting our custom onboard avionics. The R-50 is powered by a water-cooled, single cylinder, 12-hp, 98 cc two-stoke gasoline engine. The engine requires a special external engine starter. The engine is very reliable and it is powerful enough to carry 20 kg of payload. Thanks to the ample payload, it serves as a platform for very extensive and versatile RUAV applications.

The control system consists of five servomotors: three for the actuation of the main rotor collective/cyclic pitches, one for the tail rotor collective pitch, and one for the engine throttle control. Unlike Kyosho, the swashplate is actuated by a coordinated motion of three servos, i.e., left, right, and back straight servos. The main rotor collective and cyclic pitch control obeys the following relationship with the servo action and the obtained pitches:

$$
\begin{aligned}
Collective\ pitch &= \left(L_{LSS} + L_{RSS}\right)/2 \\
Longitudinal\ cyclic\ picth &= L_{BSS} - \left(L_{LSS} + L_{RSS}\right)/2 \\
Lateral\ cyclic\ pitch &= \left(L_{LSS} - L_{RSS}\right)/2
\end{aligned}
\tag{3.1}
$$

where

LSS: Left straight servo

RSS: Right straight servo

BSS: Back straight servo

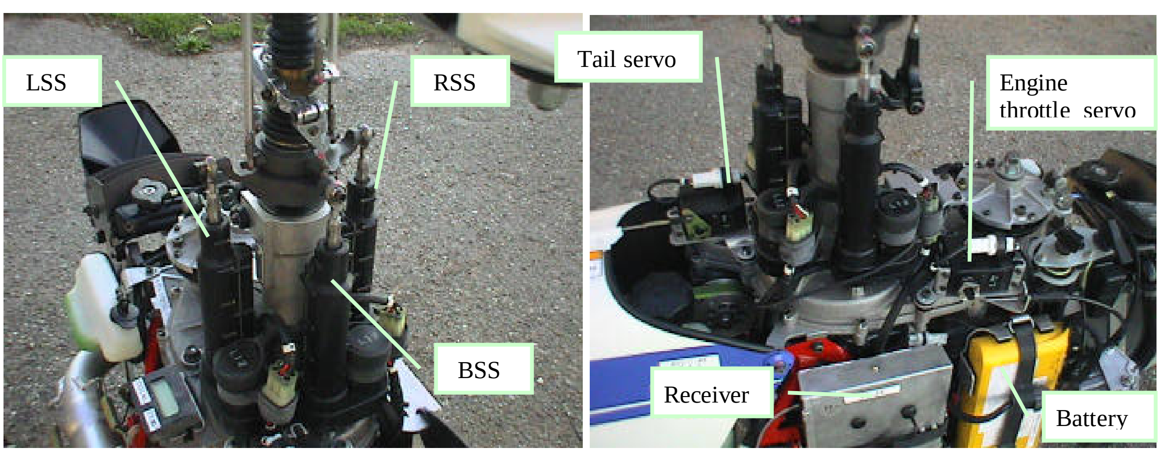

Figure 3.6 The servomotor configuration for swashplate actuation of Yamaha R-50

The onboard servos are also controlled by PWM signals. The control signal is intercepted at the bypass connector and fed through the custom control circuit. Special care is taken to build the custom circuit, wire harness, and connectors to guarantee reliable operation over time. The R-50 is also equipped with a Bell-Hiller stabilizer mechanism to introduce damping and aerodynamic servoing action. Hence, the dynamics is expected to be similar to other small-size helicopters.

Another advanced feature of the R-50 is the custom Stability Augmentation System (SAS) called YACS (Yamaha Attitude Control System), located approximately at the center of gravity of the helicopter body. This system was originally developed to aid inexperienced pilots, typically farmers, to fly the vehicle with greater ease. The YACS for the R-50 is designed as an optional add-on unit, which is plugged between the receiver and the servos through a bypass connector.

In appearance, the YACS is a compact aluminum alloy box mounted on four vibration-isolators filled with synthetic shock-absorbing gel. The YACS contains three accelerometers and three fiber-optic gyroscopes for inertial measurements and a microcomputer for sensor processing and control. The YACS superimposes the stabilizing command of attitude feedback over the pilot's command. This compensation stabilizes the attitude dynamics, which is marginally stable. The acceleration measurements in the x, y, and z axis directions also fed back to introduce further damping in each channel and also to function as automatically tuned trim. The attitude angles in the roll and pitch axis are estimated by the inertial measurements. Since the YACS is not aided by any external sensors such as GPS, the accuracy of the translational velocity and position estimation degrades quickly as a function of time in an unbounded manner due to the sensor bias and drift. This makes it impossible for the YACS to feed back the velocity to fully stabilize the vehicle dynamics. Instead, it uses the acceleration feedback to minimize the deviation of the acceleration in all three axes. Attitude estimates diverge relatively slower than velocity and position estimates do, and hence it is acceptable to introduce attitude feedback for short-term flight. This clever design achieves a self-contained and effective SAS for most missions. Additionally, YACS provides a self-diagnostic capability that monitors the radio signal strength, the integrity of the servo control signal, the engine stall and other vital information for safe operation of the vehicle. The YACS can be disengaged, if desired, by a toggle switch on the ground pilot's radio transmitter. Obviously, the YACS does not provide full autopilot capability and we chose to bypass it in our research to avoid artificial dynamic behavior introduced by the YACS.

Figure 3.7 ***Ursa Magna 2*** based on Yamaha R-50 industrial helicopter

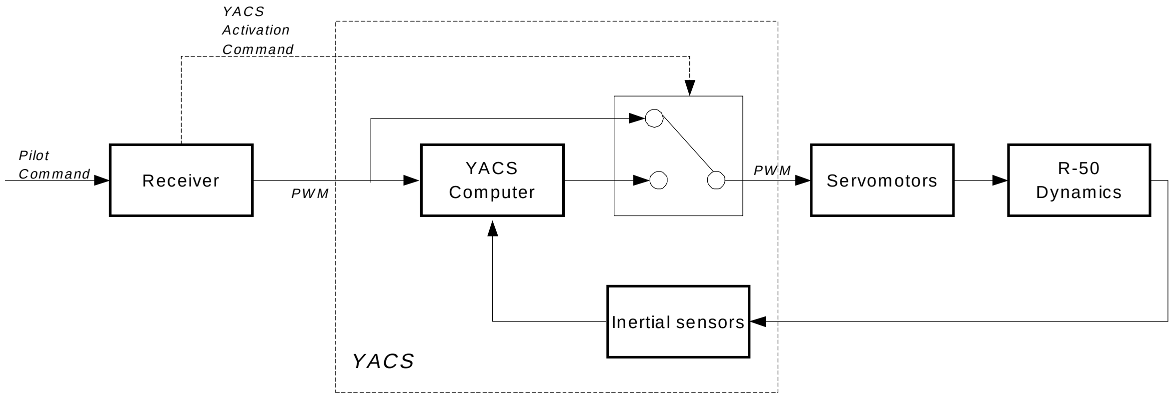

Figure 3.8 Block diagram of control signal flow in Yamaha R-50

3.1.4 Ursa Maxima Series-Yamaha RMAX

Yamaha RMAX is the successor of Yamaha R-50. It has an improved body construction, a new and more powerful engine for more payload, a built-in engine starter, an alternator and a more tightly integrated avionics system. The structure of the airframe is completely redesigned to accommodate the new horizontally opposed two-cylinder two-stroke gasoline engine with 21 hp output. Thanks to the more powerful engine, the vehicle is capable of carrying 30 kg of payload as well as its own weight of 58kg. This new engine is started by the built-in engine starter with one press of a button on the control panel. The engine runs the built-in alternator to power the onboard avionics system. The receiver battery used for the R-50 is replaced by a high capacity 12V lead-acid battery. The stock alternator can be replaced with a higher-capacity custom alternator so that it can provide enough electricity to power our custom avionic system as well as the built-in Yamaha avionics.

The YACS became a standard feature of the integrated radio-controlled system for the RMAX (Figure 3.9). The functionality of the YACS remains very similar to that of the R-50. In the system configuration, however, it is tightly integrated into the onboard radio receiver, feedback control, and servo driver system and it cannot be disconnected electronically as was possible with the R-50. Still, however, the YACS for the RMAX can be disengaged with a push of a button on the transmitter in similar manner to the R-50. The YACS is now mounted in the avionics compartment located in the lower part of the main body. The engineers at Yamaha added a custom serial port for more convenient interfacing with our autopilot system. The serial port has two output channels and one input channel. One serial output conveys the information about the stick command of the ground pilot. The other serial output contains the on-duty duration of PWM signals going out to the onboard servos as well as some part of the vehicle status such as a fuel warning and certain important switch positions on the radio transmitter of the ground pilot. Custom servo control can be performed by pushing a pushbutton on the transmitter and then writing a certain value in the predefined structure for the outgoing stream of serial port. Using serial communication for servo actuation eliminates sources of malfunctions such as exposed PWM signal lines, custom circuits, wire harness and connectors. It should be noted, however, that the serial communication introduces a significant time delay of approximately 14ms, which is 70% of the sampling time (20ms), when sending and receiving a data packet with the YACS, respectively. This substantial amount of phase delay may cause degradation of control performance and imposes a limit on the closed-loop bandwidth.

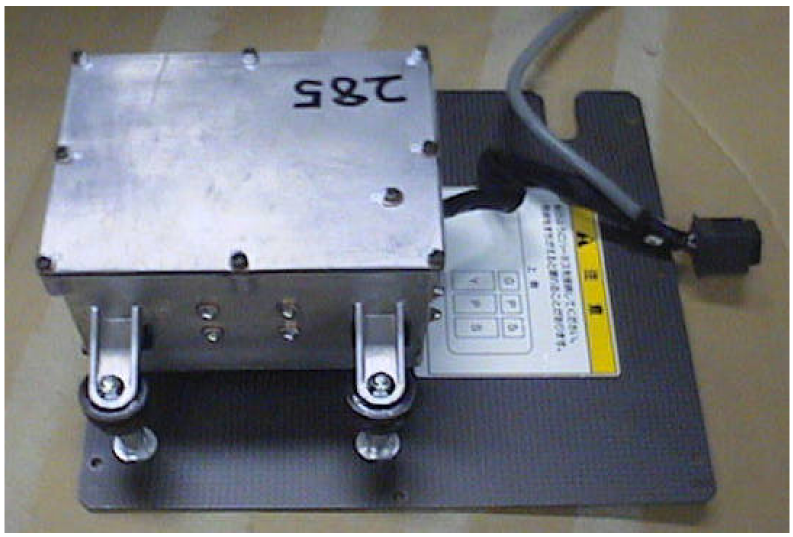

(a) Inertial sensor unit for YACS

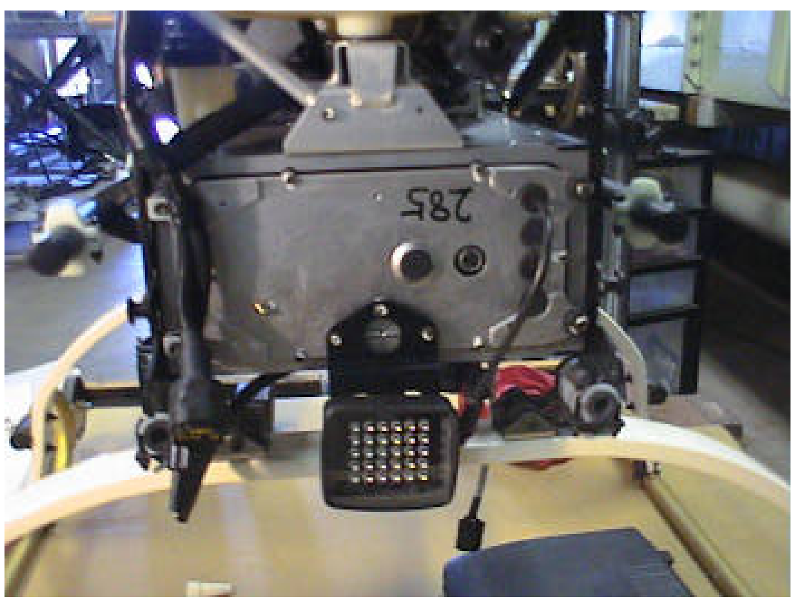

(b) YACS processor enclosure with special interface connector

Figure 3.9 YACS system for Yamaha RMAX

The rotor head features rigid blade grippers with a pre-built fixed coning angle. While the length of the blades is almost same with the R-50, probably to retain transportability, the width is significantly increased to generate more lift. This yields a higher disc loading. Other than this modification to meet the higher payload rating, the linkage and control mechanism is almost identical to that of the R-50.

The ample payload and other useful features such as the built-in starter and onboard alternator, allow the building of an RUAV capable of fully automatic operation for an extensive amount of time. The current plan is to build the RMAX to be able to start the operation with an automatic engine start and carry out the given mission over a longer period of time with a high-capacity fuel tank. The RUAV will be able to land, stop the engine automatically, and then resume the operation.

Figure 3.12 shows three Berkeley RUAVs constructed during the last two years. *Ursa Maxima 2* will soon undergo a series of test flight for onboard system reliability, system identification, and controller design.

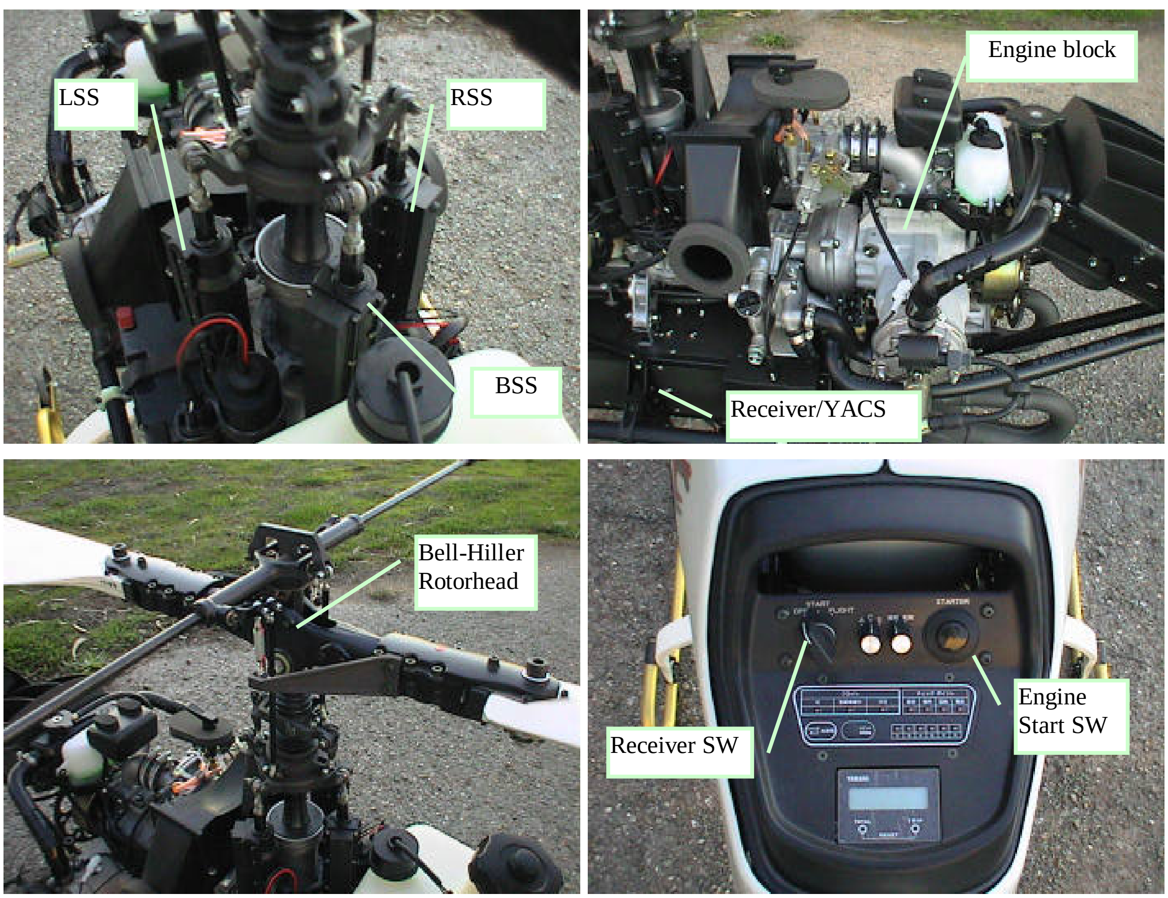

Figure 3.10 Detailed views of Yamaha RMAX

Figure 3.11 ***Ursa Maxima 2*** based on Yamaha RMAX industrial helicopter

Table 3-1 Specifications of Berkeley RUAV platform

		Ursa Minor 3 Kyosho Concept 60SR II	**Ursa Major** Bergen Industrial Twin	**Ursa Magna** Yamaha R-50	**Ursa Maxima** Yamaha RMAX
Length		1.4m	1.5m	3.58m	3.63m
Width		0.47m	0.3m	0.7m	0.72m
Height		0.39m	0.7m	1.08m	1.08m
Rotor diameter		1.5m	1.778m	3.070m	3.115m
Weight	**Dryweight**	4.5kg	7kg	44kg	58kg
	Payload	<5kg	10kg	20kg	30kg
	Avionics	4.8kg	N/A	10kg	15kg
Engine	**Type**	OS FX-91 Glow engine	Twin Genoa gasoline engines	Water-cooled 2 stroke 1 cylinder gasoline engine	Water-cooled 2 stroke 2 cylinder gasoline engine
	Displacement	14.9cc		98cc	256cc
	Power	2.8ps		12ps	21ps
Flight computer		Cyrix MediaGX233MHz	N/A	Intel Pentium 233MHz	Dual computer system (AMD) Primary: K6-400 Secondary: K6-400
Navigation Sensor		Boeing DQI-NP NovAtel GPS MillenRT-2	N/A	Boeing DQI-NP NovAtel MillenRT-2 Ultrasonic(x2) Ground contact SW	Boeing DQI-NP NovAtel GPS MillenRT-2 Digital compass
Wireless Communication		Lucent Orinoco Broze card+EC/S	N/A	Lucent Orinoco Broze card+EC/S	Lucent Orinoco Broze card+EC/S Dynamic IP Router (Cyrix MediaGX)
Vision System		N/A	N/A	Intel Pentium 266MHz Frame grabber Sony Camera with Pan/Tilt/Zoom	Intel Pentium 266MHz Stereo camera with Pan/Tilt/Verge
Power supply		Two Li-Ion 10.8V 3600mAh	N/A	Two Li-Ion 10.8V 3600mAh	Dual power system Onboard alternator +Four Li-Ion 10.8V 3600mAh
Operation Time	**Airframe**	20 min	N/A	30 min	60 min
	Avionics	60 min	N/A	60 min	60+ min
Application		Basic autopilot development	Vision-based Ship-deck landing	Advanced autopilot development Pursuit-evasion game Vision-based landing OCP testbed	Advanced autopilot development Pursuit-evasion game Vision-based landing Dynamic network OCP testbed

Figure 3.12 Fully equipped RUAV fleet at UC Berkeley
(left to right: *Ursa Magna 2, Ursa Minor3 , Ursa Maxima 2*)

3.2 Navigation and Control System

The Flight Control System (FCS) is the onboard component that is responsible for the overall vehicle management tasks such as vehicle guidance, control and communication. The main task of the flight computer is, as once put very eloquently, to 1) aviate, 2) navigate, and 3) communicate. In other words, the vehicle should be able to sustain its flight by proper stabilization and control of the vehicle dynamics and then should be guided along the desired waypoints and trajectories. Finally, the vehicle should communicate with the ground monitoring station and other aerial or ground-based agents if presented or required. Hence, the flight computer should 1) manage the sensor system, 2) stabilize and control the host vehicle at a low or high-level, and 3) communicate with other agents of the entire UAV system including the ground station. Among the many aspects of the operation of the flight computer, the realtime performance is one of the most important parts. In the following, a detailed description of the flight control system is given at the component level.

3.2.1 Flight Computer System

The flight computers used in this research are PC-compatibles in the PC104 standard. Although PC compatibles were not designed for a realtime control tasks, they can achieve a decent realtime performance when combined with realtime timing circuitry and a meticulous scheduling algorithm. A flight computer typically consists of one CPU board and other peripheral boards such as RS-232/422 communication board, Ethernet board, PWM generation board, DC-DC power supply and so on. In this research, the PC boards complying with the PC104 industrial standard are chosen due to their higher level of reliability and robustness than normal desktop boards, their wide variety of supporting functions, and their availability. The PC104 features a 3.55”×3.775” footprint circuit board that has the ISA bus or sometimes with the PCI bus of the Intel x86 based PCs (the system with PCI bus is called PC104-*plus)*. The only difference is the shape of the ISA bus connector. The boards are interconnected through the PC104 bus, which is almost identical to ISA bus with a different connector of 104 pins (hence the name). The CPU board is expanded by other peripheral boards and forms a stack as shown in Figure 3.13. This configuration accomplishes more ruggedness and reliability than the standard motherboard-daughterboard configuration found in desktop computers.

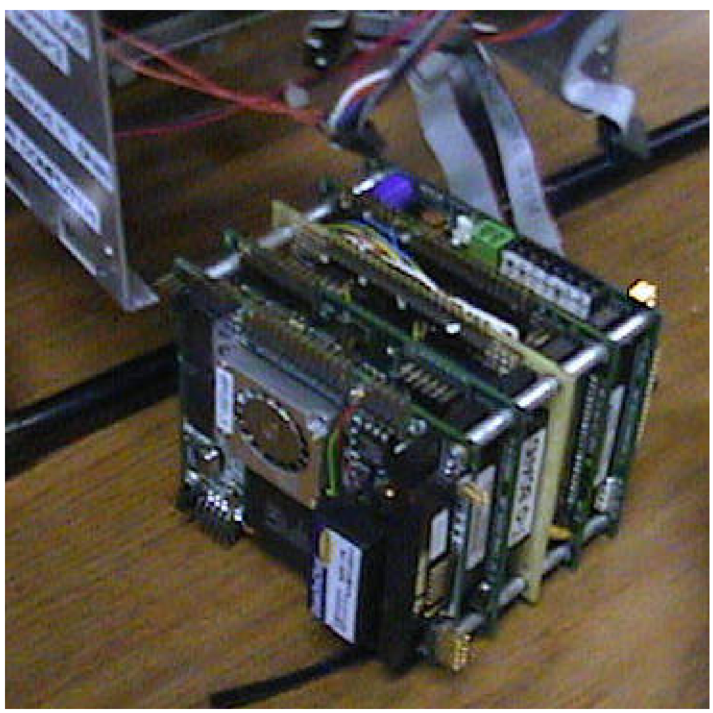

Figure 3.13. PC 104 stack (flight computer for Ursa Minor 3)

In this research, slightly different combinations of PC104 cards are used for each RUAV depending on their payload and application. More powerful CPUs are usually desired for improved realtime performance and future expandability. For the Kyosho Concept series helicopters, where the payload is the most limiting factor in the design, smaller CPU boards are preferred. In the beginning of the research back in 1996, a 586 CPU running at 133MHz was adopted for the *Ursa Minor 1*. Later it is replaced with a Pentium 233MHz because the 586 board could not handle the realtime computational load of the INS/GPS integration algorithm. The Pentium board used in this research is in the 8”×6” “Littleboard” format, which is in fact larger and heavier than a normal PC104 board and offers more onboard peripherals such as four serial ports, SCSI, dual IDE, a video adapter and a 10BaseT Ethernet port. For *Ursa Minor 3*, a standard PC104 CPU board with a Cyrix MediaGX 233MHz is used because of its smaller size and improved speed over the early 586 CPU.

For *Ursa Magna 2*, whose payload is not a limiting factor at all, a heavier and more powerful Littleboard from Ampro is used again because Pentium offers the fastest floating-point computation. For *Ursa Maxima 2*, more ambitious configuration of multiple flight computers for advanced flight control is laid out. Two AMD K6-400MHz CPU boards called *Panther board*[1] in standard PC104 format are used because their smaller footprint enables a multiple CPU configuration in a slightly larger enclosure than that of R50. The Panther board shows execution speed comparable with that of Pentium 233MHz. Because the floating point unit of AMD K6-400 is known to be slower than that of the Pentium running at the same clock speed. The latest AMD board consists of two PC104 boards featuring many useful peripheral ports including solid-state disk (SSD) support, two serial ports, two USB ports, one 10BaseT Ethernet port and one IDE interface.

Table 3-2 shows that the flight computer systems for different helicopters have many peripheral boards in common. The main difference comes from the configuration of the base CPU board. For *Ursa Minor 3* and *Ursa Magna 2,* the counter/timer card and custom take-over boards are commonly used for PWM signal reading and generation. Serial port expanders are commonly used by all configurations because many navigation sensors communicate via serial port.

The flight computer needs hard drive or some other equivalent mass-storage device for booting and running an operating system. Solid-state devices are preferred for their robustness against severe vibration. The DiskOnChip™ by M-Systems is a flash RAM device and is suitable for this type of operational environment. They are used on the MediaGX board and the Panther™ AMD boards. Ampro Littleboards do not support DiskOnChip currently and the PCMCIA FlashDisk card is used instead through a special adapter card.

[1] Versalogic Inc. (http://www.versalogic.com)

Table 3-2 Specification of FCS

	Ursa Minor3 Kyosho Concept 60	**Ursa Magna2** Yamaha R-50	**Ursa Maxima2** Yamaha RMAX
Flight Control System	CPU board (Realtime Devices USA) - Cyrix MediaGX233MHz - VGA - 2 serial ports - DiskOnChip 40MB Take-over board Counter/Timer board 4-Serial port expander DC/DC converter Ethernet 10BaseT card	Multi-functional CPU board (Ampro Littleboard) - Intel Pentium 233MHz - VGA - 4 serial ports - 10 BaseT Ethernet port - SCSI - Dual IDE Take-over board Counter/Timer board 4-Serial port expander DC/DC converter FlashDisk Carrier (SanDisk 72MB)	**Primary Flight Computer** Multi-functional CPU board (VersaLogic Patherboard) - AMD K6-400 - VGA - DiskOnChip 85MB - 10/100 BaseT Ethernet - 2 serial ports 4-Serial port expander Counter/Timer board A/D conversion board DC/DC converter **Secondary Flight Computer** Multi-functional CPU board (same as above) Hard drive carrier card (6GB) PCMCIA interface card DC/DC converter
OS	QNX	QNX	PFC: QNX SFC: MS-Windows 98
Nav. Sensors	INS (Boeing DQI-NP) GPS (NovAtel MillenRT-2)	INS (Boeing DQI-NP) GPS (NovAtel MillenRT-2) Ultrasonic sensor (x2) Ground contact switch (x4)	INS (Boeing DQI-NP) GPS (NovAtel MillenRT-2) Digital Compass Ground contact switch (x4) Height sensor (Ultra or Laser)

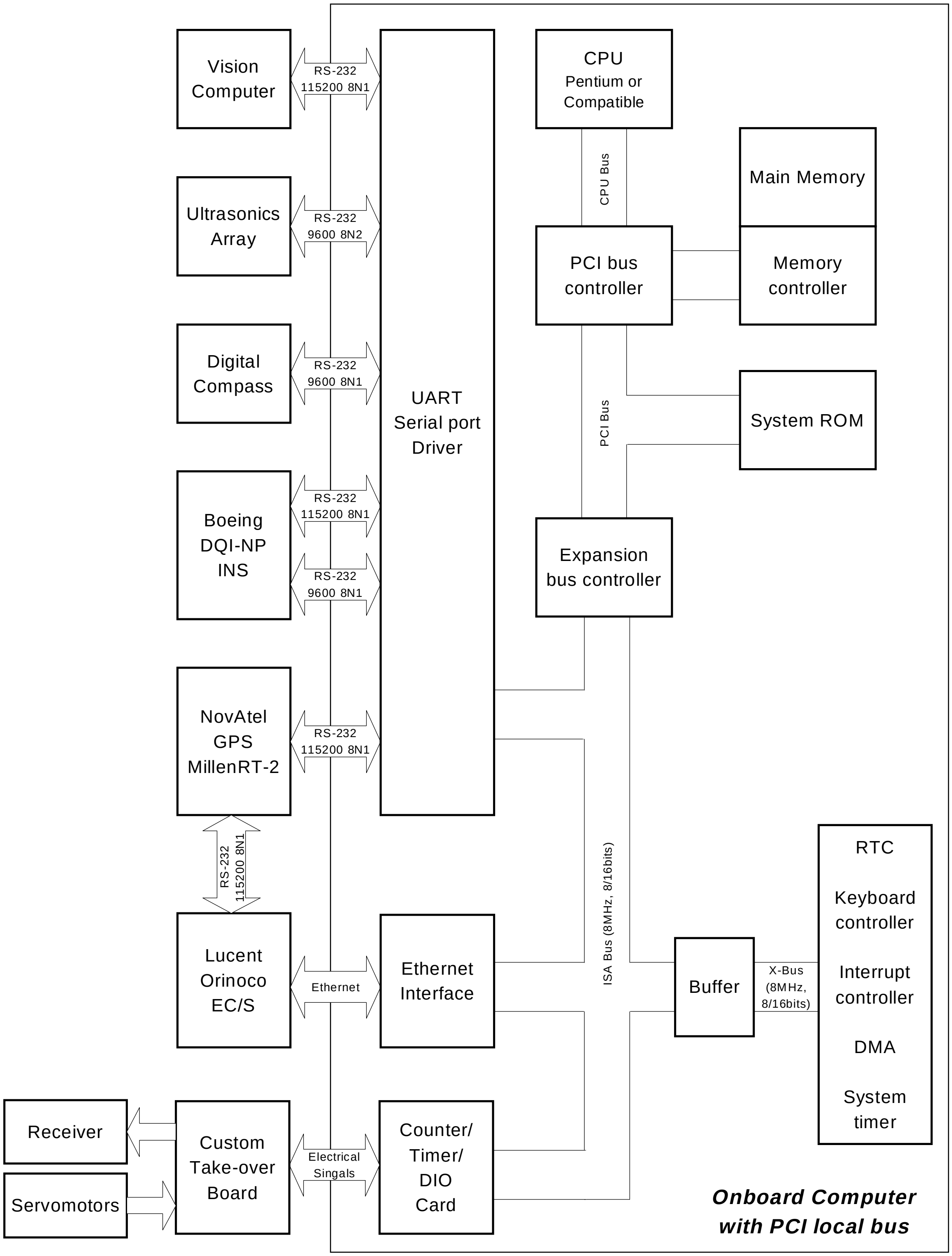

Figure 3.14 Interconnection diagram of onboard flight computer based on PCI local bus (Ursa Magna 2)

In Figure 3.14, the interconnection diagram of the onboard flight computer and other sensors is shown. Serial port communication constitutes the backbone of inter-device connection. In this research, RS-232, which uses single-ended transmission/reception lines and supplementary control lines, is universally used instead of RS-422, which uses differential voltage signal lines. All flight computers are equipped with a 4-port serial port expansion board so as to accommodate the demanded number of serial ports. In the hardware as well as the software aspect, it is very important to understand how the serial communication works. Since the data is decoded and transferred as a stream of bits accompanied by a start bit, stop bit(s) and in some cases parity bits, it takes longer than parallel ports to transfer the same amount of data. Also, the transmission time for 1 bit is limited by 1/115200 second that is longer than other protocols such as USB (Universal Serial Bus) or Ethernet, and hence the overall communication time causes delay which degrades realtime performance. The actual realtime performance measured in *Ursa Magna 2* will be given in Section 3.5.

3.2.2 Navigation Sensors

To navigate following a given trajectory while stabilizing the vehicle, the information about vehicle position, velocity, attitude, and angular rates should be known to the guidance and control system. The RUAVs are equipped with a number of complementary navigation sensors to obtain accurate information about the motion of the vehicle in association with environmental information, such as the relative distance to the ground surface to other objects near the vehicle.

The navigation sensors can be categorized as (1) environment-independent sensors and (2) environment-dependent sensors. The former includes INS and GPS, which compute the motion estimates regardless of the surrounding. The latter includes ultrasonic sensors, laser range finders and vision sensors. These sensors rely on the surrounding objects, which reflect the active probing signals such as an ultrasonic wave or laser beam, or on natural lights to form an image on the CCD receptors of the camera. These sensors are necessary to determine the relative distance from the vehicle to its surrounding objects or the ground surface for take-off/landing, collision avoidance or evasive maneuvers. The characteristics of these sensors are reviewed in the following sections.

3.2.2.1 Inertial Navigation System

The inertial navigation system is the central part of the navigation sensor system of the Berkeley RUAV system. Inertial navigation is a method which provides the motion estimates such as position, velocity and attitude by processing the inertial quantities sensed by inertial instruments. An INS consists of three accelerometers and three gyroscopes which measure the linear acceleration and angular rates. There are two types of INS: the *mechanized-platform* type and the *strap-down* type. The former consists of a mechanized gimbal platform, which aligns itself consistently along the reference inertial coordinate system regardless of the base vehicle's attitude change. The accelerometers are mounted on this platform. The velocity in the inertial coordinate system can be easily found by integration in each channel. The overall accuracy of the sensor system depends on the alignment of the instrument platform. The alignment requires a very precise sensing and actuation ot the mechanism. The strap-down type of INS utilizes three accelerometers and three rate gyroscopes, which are installed in the precise orthogonal *x, y,* and *z* direction. The inertial measurement unit is mounted on the vehicle without any actuation, and hence the inertial quantities are measured in the body-coordinate system. Transforming the inertial estimates into the spatial coordinates becomes the full responsibility of the inertial processing unit of the strap-down type INS. This process involves the integration of the accelerations measured in the body coordinate frame as well as the transformation into the spatial coordinates using the estimated Euler angles or other equivalents. The attitude angles are estimated by numerically integrating the differential equations in equation (2.11) or (2.13). In summary, the inertial estimates can be found by the following equation:

$$\begin{aligned} \dot{\mathbf{P}} &= \mathbf{V}^{TP} \\ \dot{\mathbf{V}}^{TP} &= \mathbf{R}_{B\to TP}(q_1, q_2, q_3, q_4)\mathbf{A}^b \\ \dot{\mathbf{q}} &= \mathbf{\Psi}\mathbf{q} \end{aligned} \tag{3.2}$$

The equations in (3.2) are pure kinematical relationships which hold true. However, the actual numerical integration is far less than ideal due to many error sources such as bias, drift, scaling error of the inertial sensors, imperfect integration by numerical algorithms and so forth. Hence, equation (3.2) should be augmented with a dynamic error model to minimize the deviation of the solution as time lapses. All the measurements of linear acceleration and angular rates are contaminated by noise, scaling error, bias and drift. Without proper calibration and compensation, the inertial estimates diverge very quickly. These error sources have a stochastic nature, and hence the unit should be initialized every time it is turned on. The best method of initialization is to measure the accelerations while keeping the unit stationary, in all channels, and calibrate them by comparing the values with the gravitational force. Unfortunately, the noise characteristics of these sensors change after the initialization. The bias swing, known as *drift*, slowly changes over time as a function of many factors, including the temperature. Therefore, high-accuracy INS cannot be built without the proper initialization and continuous compensation of the drift. While initial roll and pitch angles can be estimated approximately by computing the inclination angles using the measurements of the acceleration caused by the gravitational force, the initial heading is not observable at all by the inertial measurements. External information should be provided from such aids as heading sensors. This process is called the *alignment process*. The calibration and alignment processes can be performed without leaving the sensor unit stationary by using accurate external sensors such as GPS. If GPS is used, the sensor unit should be moved around so that the inertial estimates can be compared with GPS and then used for inertial sensor calibration.

The strap-down IMU is the main trend these days. They are particularly suitable for small-size vehicle applications because they are more advantageous than the mechanized-platform INS in terms of size and weight. The additional computational load for the strap-down system can be easily taken care of by today's powerful and small microprocessors. In the Berkeley RUAV research, we have consistently used a strap-down IMU for this reason. Most small-size strap-down IMUs contain the inertial sensors that are manufactured using micromachining and hence they are very small and light. Accelerometers are usually made of solid-state MEMS (Micro Electro-Mechanical Systems) using pitchfork technology. For rate gyroscopes, solid-state MEMS sensors or more accurate (and expensive) fiber-optic gyroscopes (FOG) are used.

In the Berkeley RUAV research, except for the brief period during which a special type of INS was investigated using six accelerometers, two types of inertial instruments have been consistently used. At first, MotionPak™ from Systron-Donner was used. MotionPak contains three accelerometers and three rate gyroscopes that output analog voltages. It is the user's responsibility to properly calibrate, filter the noise and compensate the bias as described above. Unfortunately, the Berkeley UAV team could not spend enough time and effort to develop and implement the proper compensation and alignment algorithm, and so we looked for an alternative. The Boeing DQI-NP (Digital Quartz IMU-Navigation Processor) offers fully integrated digital signal processors (DSP) for the full set of inertial estimates of position, velocity, and attitude as well as the raw sensor outputs of accelerometers and rate gyroscopes. Inertial measurements are easily acquired by reading the serial port output in the RS-232 or RS-422 protocol, which is user-selectable. Another attractive feature is the GPS integration capability: DQI-NP accepts the position update from GPS every second and updates the internal Kalman filter for loosely coupled INS/GPS compensation. It supports a limited number of GPS models and unfortunately, the GPS system used in our research, NovAtel MillenRT-2, is not among them for now. Therefore, an emulation program has to read the GPS output, cast it into one of the supported GPS message format, and feed it into the DQI-NP. The detailed information about this program will be discussed in Section 3.5

Figure 3.15 Inertial instruments: Boeing DQI-NP (left) Systron-Donner MotionPak™ (right)

Care should be taken with the mounting of DQI-NP. It is known that the inertial sensors inside the DQI-NP sensor module has an excitation frequency of 100 Hz. Coincidently, the RPM of the tail rotor of Ursa Minor 3 is around 6000 RPM (=100Hz) in hover and it was discovered that the navigation solution of DQI-NP diverges frequently. This problem was solved by the special shock-absorbing mounting for DQI-NP as shown in Figure 3.16.

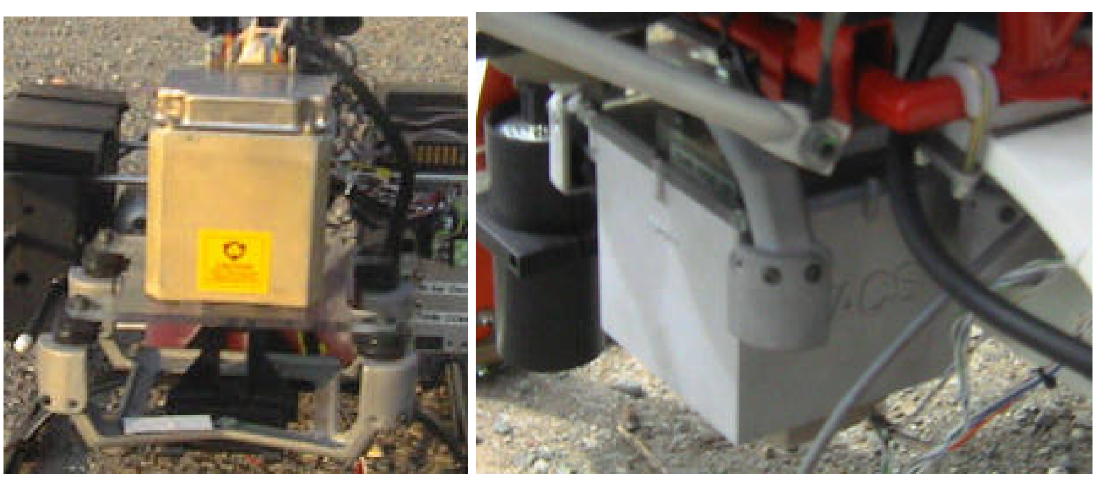

Figure 3.16 Boeing INS DQI-NP installed on *Ursa Minor3*(left) and *Ursa Magna2* (right)

The DQI-NP operates on a DC power source ranging between 20-34V. The Lithium-ion batteries used for our research are rated 10.8 V and two batteries are put in series so that the overall voltage is high enough to power the DQI-NP. The battery power source is shared with other onboard systems such as the flight computer and other navigation sensors. For Ursa Maxima helicopters, the input voltage for the avionics is fixed at 12V by the onboard lead-acid battery and a separate DC-DC converter is used to escalate the 12V input to 24V for DQI-NP.

3.2.2.2 Global Positioning System

NAVSTAR GPS is a space-based satellite radio navigation system developed by the United States Department of Defense. GPS provides three-dimensional position and time with the deduced estimates of velocity and heading. The GPS system consists of three major segments: Space, Control and User. The space segment consists of 24 satellites in circular orbits 20,200 km above the Earth's surface, with a 12-hour orbital period and an inclination angle of 55 degrees. This configuration intends to provide at least five satellites in view from any point on Earth at any time.

Each satellite continuously broadcasts radio signals at two L-band frequencies: L1 at 1575.42 MHz and L2 at 1227.6 MHz. The L1 frequency contains Precise ranging signal (P-code) modulated by 10.23 MHz as well as 1.023 MHz Coarse/Acquisition Code (C/A-code). The L2 frequency contains P-code only, which used to be dedicated for military GPS use only. L2 frequency used to be degraded with an certain encryption, which deterred non-authorized users from obtaining the utmost accuracy from the GPS. This process, known as *Selective Availability* (S/A), was known to inject as much error as 30m. It was finally eliminated in May of 2000. In our field experience, GPS accuracy has been significantly improved from a standard deviation of 25m to 2.5 m. The navigation data from each satellite contains time, clock correction, ephemeris parameters, almanac data, and health status. Based on this information, the user segment, i.e., the GPS receiver, computes the current position of each satellite. Actually, the receiver computes the elapsed time of each signal set to travel the distance from the source satellite to the receiver antenna. Stemming from the simple concept of triangular survey, with the additional unknown variable for time drift of the internal clock of the GPS receiver, four measurements, i.e., at least four satellites are required. The distance estimated in this manner is called the *pseudorange*. It earned its name because it contains errors from many sources. This process, relying on the NAVSTAR satellites only for positioning, is known as Single Position Station (SPS). Now that S/A has been eliminated, pseudoranging offers improved accuracy.

When two GPS systems are operated in the same vicinity, the overall accuracy of GPS can be significantly improved by canceling the common errors of those two systems. One receiver, the *reference station*, is positioned at a precisely known location and computes the pseudorange and correction information, and broadcasts it via radio link. The rover station computes its location and corrects it with the additional correction information it gains from the radio link. This scheme is called differential GPS (DGPS). Significantly more accurate position is estimated if the two receivers are located within 50 km with each other. It should be noted that precise knowledge of the position coordinates of the reference station directly impacts the rover's accuracy.

Further accuracy can be achieved with a method known as the *carrier-phase* algorithm. In this approach, the receiver monitors the number of wavelengths that the radio signal has to travel from the satellite to the antenna. The L1 frequency has a wavelength of 19 cm and the L2 is 24 cm. The distance divided by the wavelength will be the sum of an integer and a fractional component. Determining the integer portion is not straightforward and hence it is called *ambiguity*. A GPS can improve the accuracy significantly by looking for the integer using the lane search problem on both L1 and L2 frequencies. When it is locked in the *narrow-lane solution*, the accuracy of the baseline, the vector from the reference station to the rover station, can be as accurate as 1~2 cm.

The global positioning system (GPS) used in this research is the NovAtel MillenRT-2, which achieves this remarkable accuracy of 2cm through the use of DGPS and a carrier-phase algorithm. The NovAtel GPS provides position estimates at up to 10 Hz. We configured the receiver to generate the position log at 4 Hz. The flight control computer acquires the position, linear/angular velocity and attitude from the DQI-NP, and high accuracy position estimates from the NovAtel RT-2 via RS-232. It also relays the converted position estimate message packet from the GPS to the DQI-NP every second.

The actual operation of GPS takes caution and sometimes can be very frustrating. Our research used the NovAtel MillenRT-2, which requires a couple of minutes to lock itself onto the *narrow lane solution*. The necessary time for the lock-up depends on many factors such as the number of satellites in the sky view, the elevation angle of the satellites, and the ambient radio activity near the L1 and L2 frequencies and so forth. During experiments, the GPS often causes trouble because it is not able to sequence into the narrow-lane solution in a reasonable time. Theoretically, the floating-point solution can still be used as the position estimates. The only problem is that the position estimates have sudden jumps whenever the solution type changes. This may cause undesirable transient behavior in the INS, and if the loop is closed, the control system would react to this sudden jump and produce large jump in the control output. Therefore, fail-safety coding should be programmed for guaranteed operation.

For operation, the GPS antenna and the process card are installed on the host vehicle. With this setup alone, the GPS operates as a single positioning system (SPS). To exploit the DGPS capability, a base station that consists of a GPS receiver, an antenna, and a radio broadcasting system such as wireless modem or wireless LAN is set up.

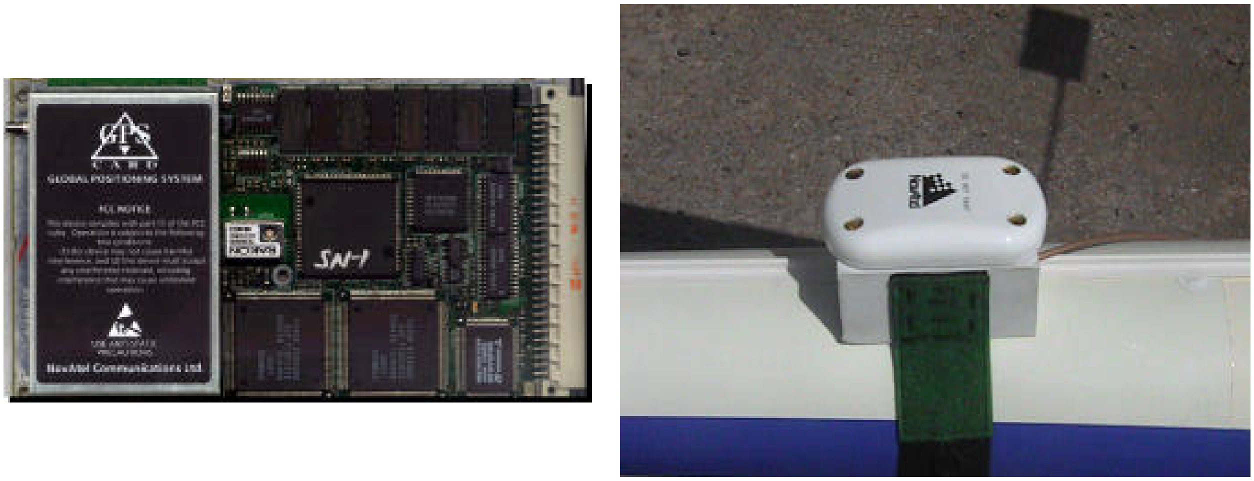

Figure 3.17 NovAtel GPS Card (left) and L1/L2 antenna installed on R-50 (right)

3.2.2.3 INS/GPS Combination

The INS alone has an unavoidable error in its integrated solution that grows unbounded as time lapses. Hence, the INS must be periodically corrected by external aids. The favored method nowadays is correction with the GPS, which provides estimation information with bounded error all the time. The shortcoming of the GPS is that it only provides the position estimate at relatively slower rate. Because of their complementary nature, the INS/GPS system offers very attractive features:

- The overall accuracy improves considerably than INS or GPS alone.
- It has a higher fault-tolerant property because one sensor can still provide (part of) the navigation solution while the other is temporarily unavailable because of jamming, GPS signal blockage, or any other reason. It should be noted that, however, INS will eventually diverge as a matter of time.
- GPS may be used for the initialization process of the INS and even for calibration on-the-fly capability.

When the INS is integrated with the GPS, the INS accepts the position measurement from GPS updates at slower rates. The Kalman filter integrates the raw inertial sensor measurements and corrects its solution with the GPS position updates. The combinatory system outputs the compensated position, velocity, and attitude estimates at high speed with bounded error.

There are two types of integration of INS/GPS [36]: loosely-coupled GPS aided INS and tightly-coupled GPS aided INS. In the former approach, only the position or range information from the GPS is fed into the INS to correct the position estimates. This method is computationally light and easy to implement. In the latter scheme, the acceleration information from INS is used by the carrier-tracking loop and this improves the signal-to-noise ratio and makes the overall system more robust to jamming and interference. While the latter may be more effective, it requires a full access to INS and GPS. This is not usually possible when using COTS INS and GPS.

DQI-NP provides loosely coupled GPS integration. In our experience, the performance of DQI-NP is acceptable when it is used in INS/GPS combination. One major deficiency of the DQI-NP is that it is impossible to specify that the standard deviation of position error is less than 1 meter because the data field for this information is defined as an integer variable in meter. In addition, the position update from DQI is 1Hz, which is too slow for high-accuracy position control. Therefore, an additional Kalman filter is implemented on the flight computer in order to generate high-speed position updates at 50 Hz. The Kalman filter performs numerical integration of the velocity estimates of the DQI-NP and correct it with the GPS measurements, which are available at 4Hz.

Since it is impossible to install the antenna and the IMU at the same location, there is always the offset between these two points. Therefore, the position of GPS should be compensated for the offset to the INS position. These two positions have a fixed distance if we assume they are attached to a rigid body. This distance is called *lever-arm* and its compensation involves the transformation between the body coordinate system and the inertial coordinate system such that

$$\mathbf{X}_{TP}^{INS} = \mathbf{X}_{TP}^{GPS} + \mathbf{R}_{B\rightarrow TP}\mathbf{X}_{B}^{GPS\rightarrow INS} \tag{3.3}$$

where

$\mathbf{X}_{TP}^{GPS}$: GPS location in the inertial frame

$\mathbf{X}_{TP}^{INS}$: INS location in the inertial frame

$\mathbf{X}_{B}^{GPS\rightarrow INS}$: the relative coordinate of INS with respect to GPS in the body coordinate system

This transformation requires knowledge of the Euler angles, which are the estimates of the INS. Therefore the GPS measurement is degraded further by the attitude estimate error of the INS. In order to minimize the error, it is desired to locate the INS and GPS antenna as close to each other as possible (Figure 3.18).

Figure 3.18 Desirable INS/GPS installation on Ursa Minor 3

3.2.2.4 Ultrasonic Sensors

Ultrasonic sensors estimate the distance from the surface of the ultrasonic transducer to the nearest object, which reflects the ultrasonic pulse, by measuring the elapsed time from the trigger to the reception of the echo. They are widely used for diverse applications including collision avoidance and local map building of UGVs. For RUAV applications, ultrasonic sensors measure the distance from the ground, or *relative altitude*, for automatic take-off/landing and ground collision avoidance. This information is very important for landing because the vehicle controller needs to know its relative distance from the ground in order to generate the landing profile. The accuracy and the reliability of ultrasonic sensors are usually worse than the INS/GPS sensor.

An ultrasonic sensor consists of the ultrasonic transducer and the processing board. In our research, we chose the ultrasonic sensor unit from Senix Inc[1]. The specific board we used for our

[1] http://www.senix.com

application has voltage, current and serial port outputs. In our application, the serial port output is used because this module supports communication of multiple ultrasonic sensors in a daisy-chain configuration through one communication channel.

Care should be exercised when mounting ultrasonic transducers because the sensor often gives faulty reading when it is exposed to harmful vibration. Rigid mountings should be avoided by all means and a flexible mounting for the transducer is highly recommended. The severe structural vibration of aircraft may inject excessive noise to the ultrasonic transducer and disturb the estimation algorithm. In addition to the vehicle vibration, the irregular or porous surface such as grass or dirt field may cause faulty readings. Since the relative altitude information is very important for landing, two ultrasonic sensors are installed for redundancy. In Figure 3.19, the ultrasonic sensor output during a test flight of Ursa Magna 2 is shown. The ultrasonic sensors have a roughly 300ms update cycle and their output is moderately accurate except for a few irregularities. These irregularities may be detected and eliminated by comparing the two measurements from the ultrasonic sensors and the INS/GPS.

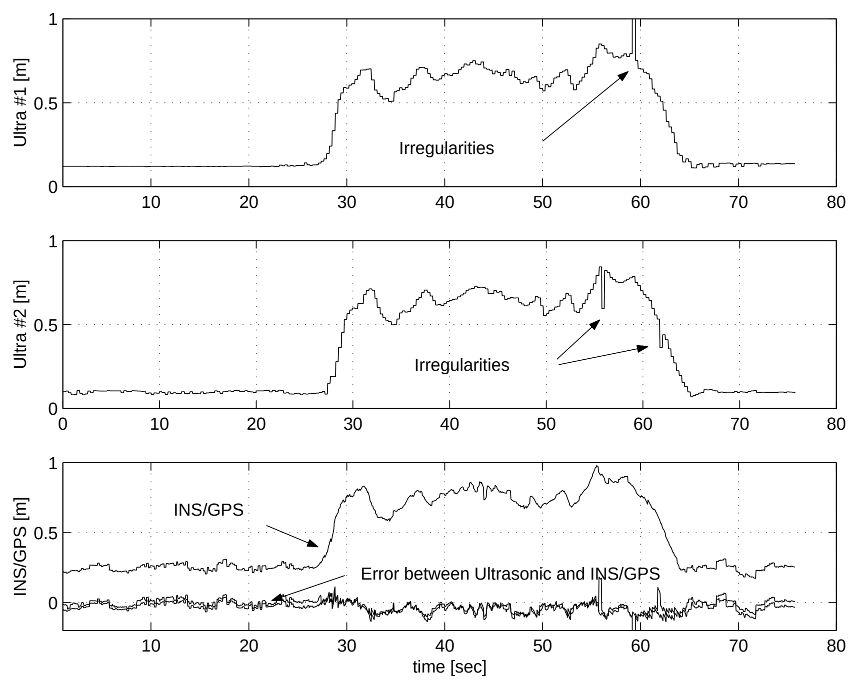

Figure 3.19 The measurement from two ultrasonic sensors of Ursa Magna 2

While the ultrasonic sensor is a low-cost solution for relative distance measurement, its occasional faulty behavior makes it less dependable as a navigational sensor. More accurate relative altitude information may be obtained from laser range finder. The laser range finder measures the distance from the laser generator to a point on the target surface by measuring the time for the laser beam to travel back and forth between these points. Therefore, it requires highly a precise mechanical and electrical system and is usually heavy, large, and expensive. When the laser range finder is combined with the INS/GPS, it serves as a superb sensor for building a local geographic map.

3.2.3 Servomotor Control

The final stage of the flight control is the actuation of the servomotors installed on the helicopter. Radio-controlled helicopters are typically equipped with five servomotors that actuate the main rotor swash plate, the tail collective pitch yoke and the engine throttle. Usually the engine control and the tail control are similar among helicopters, the mechanism for main rotor swashplate differs from model to model.

A servomotor is a compact electromechanical device consisting of a DC motor with a built-in feedback circuit. These servomotors accept pulse-width modulation (PWM) signals as the reference input. The flight control system should be able to generate the compatible PWM signal for servo actuation. It is also very desirable to read the incoming PWM signals from the receiver for system identification introduced in Section 2.2.8. The detailed information of the PWM reading and generation is listed in Appendix A.4.

3.3 Wireless Communication

Since the vehicle is operated in free space without any umbilical cords for power or communication, the onboard avionics should be equipped with some wireless communication device. In the early part of the research, 900MHz wireless modems were used for avionics data communication and DGPS correction broadcasting. Ursa Minor 1, 2 and 3 as well as Ursa Magna 2 were equipped with two wireless modems. The wireless modems used for this research are manufactured by FreeWave Inc[1]. They offer very reliable communication link with throughput somewhere between 57.6 kbps ~ 115.2 kbps. They also offer very long-range communication with a maximum of 1 watt power. It utilizes frequency-hopping TDMA protocol and supports a number of configurations such as master-to-slave, master-to-multiple-slave, multiple-master-to-slave and so on. Master-to-slave is the basic configuration for one-to-one communication such as flight data

[1] http://www.freewave.com

downloading. Master-to-multiple-slave is ideal for broadcasting DGPS corrections to multiple numbers of vehicles with GPS system.

Although the wireless modem functioned flawlessly many times, there were three limiting factors: (1) the limited bandwidth, (2) the limited protocol, and (3) possible interference with GPS. The first two factors are the natural consequences of serial port communications. The third factor raised curiosity because the wireless modem does not operate in the GPS L1 or L2 bands. It was discovered that the built-in automatic gain control (AGC) amplifier of NovAtel GPS in its RF circuit is the source of the problem. When the change of the RF activity in the neighboring bands is above certain level, which might interfere the GPS operation, the NovAtel GPS temporarily outputs an unusable data set with the error indication in GPS logging and resumes the normal operation as soon as an adjustment is made. If this condition is prolonged, the GPS loses the tracking and resumes the integer searching.

For multi-agent scenarios, one-to-one communication regime offered by radio modems is severely restrictive to access the peer-to-peer communication protocol. The need for higher throughput is another reason to abandon the conventional wireless serial communication. As an alternative for the wireless modem, the Lucent WaveLAN®, later renamed to Orinoco®, is chosen. Orinoco is a 2.4GHz wireless Ethernet system compatible with IEEE 802.11b. Packaged in a PC Card, it is a compact, portable and very powerful solution for wireless LAN in *ad-hoc* mode or in infrastructure mode. In either mode, the wireless Ethernet provides considerably faster throughput ranging from 1Mbps to 11 Mbps. The maximum range, seriously traded off with the throughput, is less than 1 mile depending on the efficiency of antennae. . In our application, however, the reduction of range is not a significant issue yet because our RUAVs are operated in a confined area no larger than half mile. Currently, all new RUAVs and UGVs are equipped with the Orinoco system for peer-to-peer communication in multi-agent scenarios. Due to the absence of the support for Orinoco PC card via PCMCIA bus by QNX RTOS, the card is accessed through an add-on product Ethernet and Serial Converter (EC/S). An EC/S offers a transparent interface between the Ethernet 10BaseT port on computer side and the Orinoco PC Card. The EC/S also offers the serial port interface and the two data streams of Ethernet and RS-232 are multiplexed in a 2.4GHz carrier. The serial port multiplex capability is extremely useful for DGPS broadcast and simplifies the onboard communication setup. This is especially advantageous for smaller UAV platforms with less available payloads.

In Figure 3.20, the entire communication system set up is shown. The communication system consists of a vehicle data communication channel and the DGPS broadcasting channel. The data channel is now based on the Orinoco system, but the 900MHz wireless modem can be operated concurrently as long as the interference with Orinoco can be kept minimal. The DGPS broadcast is now made in both the 900MHz wireless modem channel and the 2.4GHz Orinoco wireless LAN channel because some of UGVs are equipped with a wireless modem while all of the UAVs are now equipped with the Orinoco system only.

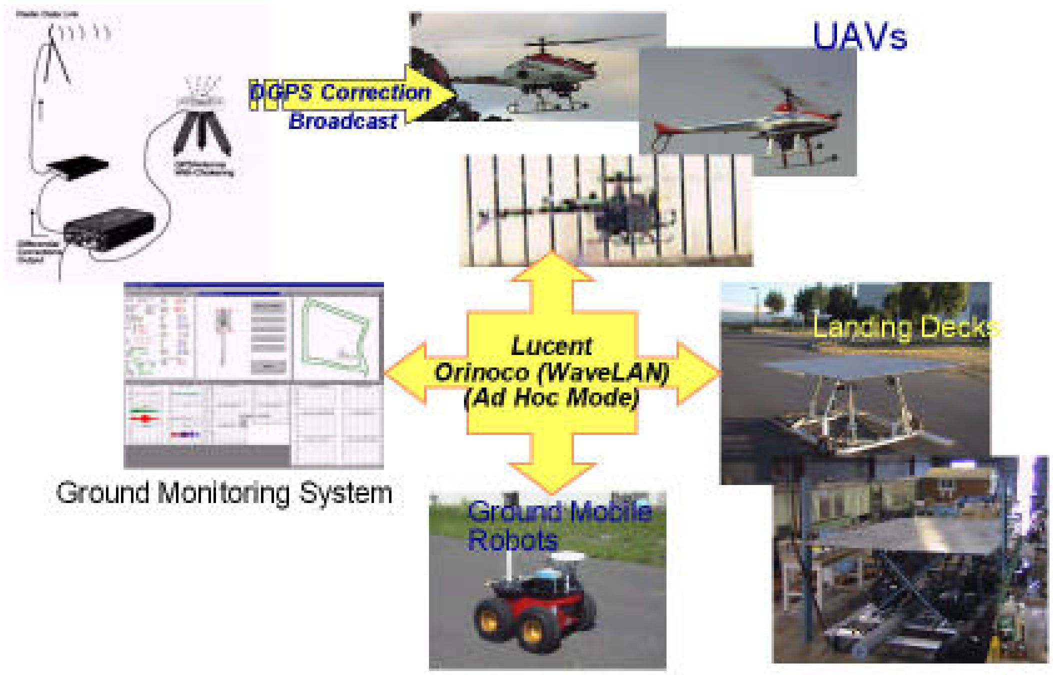

Figure 3.20 Communication architecture of Berkeley UAV/UGV/SMS Testbed

3.4 Ground Station

The ground station consists of a DGPS base station with broadcasting equipment and a portable computer connected to a communication device such as a wireless modem or wireless Ethernet. The ground station monitors and stores the flight data of the UAV and sends the navigation commands such as controller activation/ deactivation.

The base station is a multi-functional user interface that serves as the command post, realtime visualization station of the vehicle status, and the data logging system. The base station uses either wireless modem through a serial port or the Orinoco system. The software runs on Microsoft Windows 98, which is chosen for its outstanding graphics support and its compatibility with the Lucent Orinoco wireless LAN system. The software consists of a number of child windows in multi-document interface (MDI) and it displays the text-based INS/GPS status, the vehicle status, the control buttons, the 2-D map of the experiment site, the graphics-based navigation measurement, the control output, and the graphical display of the vehicle status. All the information is downloaded from the helicopter via the wireless network and is displayed in realtime. The incoming data may be saved, if the save option is activated, retrieved for off-line view later and exported in ASCII text form to other applications such as MATLAB for further processing and analysis.

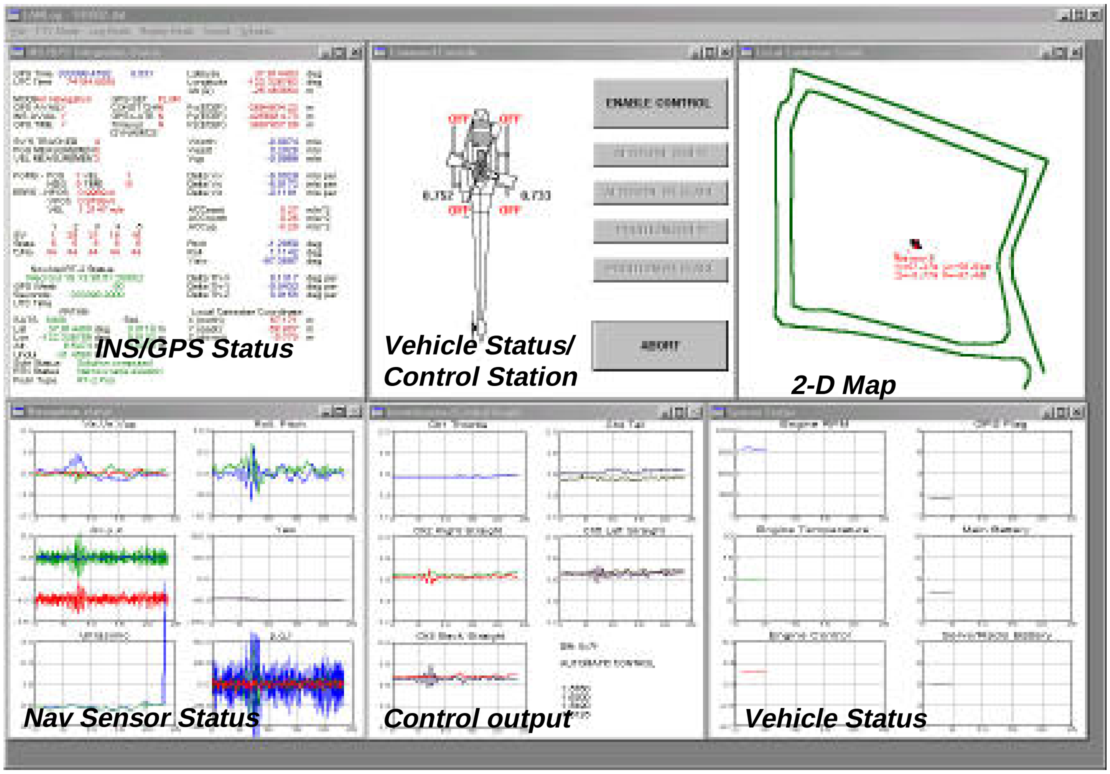

Figure 3.21 Ground monitoring station enhanced with GUI

3.5 Software Architecture

Vehicle management system software (VMSS) development is another very important stage for RUAV construction. The VMSS resides in the onboard flight control computer and manages the operation of the host RUAV. The VMSS is typically implemented on a realtime operating system (RTOS) to guarantee the demanding hard realtime requirements. The VMSS consists of a number of processes running at different rates to facilitate the needs of sensors and actuators. The design of the VMSS is closely related with the setup of the flight computer and the navigation sensors. As quoted above, the VMSS should perform the three tasks: (1) aviate, (2) navigate, and (3) communicate. The task of aviation in the perspective of the VMSS involves the trajectory generation and the hard realtime feedforward/feedback control of the vehicle through the aforementioned PWM generation circuit. The task of navigation involves initialization, calibration, acquisition and fault-toleration of the various onboard navigation sensors typically through serial ports. Finally, the communication is performed through the onboard wireless communication devices such as the wireless modem or the wireless LAN. These three tasks interact very closely: the low-level stabilization is activated regularly at its sampling rate and performs the INS reading, control output calculation, and download the flight status to the ground. This is the main loop of the VMSS and other auxiliary processes such as INS/GPS management, ultrasonic sensor polling, and the communication with the vision computer run concurrently. All of these “user processes” run on the application program interface (API) of the host RTOS. Because of the stringent requirements of the feedback control, the realtime support of the host OS is highly emphasized. The timing jittering should be kept in a minimal range for an accurate discrete controller realization. Since VMSS runs many tasks at different timing rates, the OS is desired to offer multitasking environment with synchronization and interprocess communication (IPC) capabilities. The support of multiple serial ports is also an important factor appears as a trivial requirements

Since VMSS takes the full responsibility of a remote mission, VMSS serves as an operating system of the vehicle/electronics/software integration. Since the target RUAV platform should perform the given high-level mission with the minimal support from the ground operator, the onboard system management software should perform a broad level of work from control output generation to the complex intelligent behavior in a robust manner. The tasks of VMSS are characterized as following:

- Sensor management

Many onboard sensors, the DQI-NP INS and the NovAtel MillenRT-2GPS for example, need to be properly initialized and maintained. The DQI-NP should be started following the strict initialization procedure and it needs position updates at a regular rate. The GPS card should also be initiated following a certain procedure. Although GPS runs quite independently, its operation can be erratic sometimes due to external mechanical vibration, radio activity in adjacent bands, or partial blockage of the GPS signal. Ultrasonic sensors should be polled and read regularly by sending special characters. The sensor readings are transferred mainly via RS-232 serial ports.

- Control output computation and signal generation

The main task of the FCS is the generation of the control output to the five servos installed on the helicopter system. The control output is calculated using either a classical multi-loop SISO control or a MIMO μ-synthesis control. Then the output values are sent to the counter board and the corresponding PWM signal is generated and sent to the servomotors.

- Communication

The onboard FCS should report the flight system status to the ground station for monitoring. The information is transferred via a wireless communication method such as wireless modem or wireless LAN. This task also includes the onboard communication with the vision computer via RS-232. The VMSS should satisfy the following requirements:

- Reliability

Reliability is one of the most important factors for successful, repeatable, and consistent operation of a RUAV system. Any accident during the test flight caused by a unreliable flight control software can be very disastrous because any damage to the delicate sensors/computer systems is very costly and more importantly the rotating blades can cause lethal damage to anything in their path. Hence, thorough validation of the flight control software should be performed before any real test flight. The code should be able to handle any run-time errors ranging from purely software problem (segment fault, memory overflow) to vehicle-originated faults (a severed wire connection, engine failure).

- Real-time

Some part of the task of VMSS requires hard-realtime performance. Sampling the sensor data and generation of the control output at every sample time with small *jittering* is the typical example. The VMSS should be able to meet the realtime requirement with minimal error. There are also numerous soft realtime tasks such as polling sensors and wireless communications. Even though these kind of jobs do not require as stringent of a performance as the hard-realtime tasks, these jobs should be processed with reasonable delay.

- Readability

This applies not only to the VMSS, but also to the general software development. The software should be readable by teammates other than the programmer him/herself for further development. Many and proper comments are strongly recommended for future references. The software can also be expandable whenever higher layers are added to the lower level software block.

These tasks require realtime operation to guarantee stable and reliable operation. For example, the control output generation requires a stringent sampling at a certain rate. Hence, we need a programming environment to guarantee acceptable realtime performance. Since the PC architecture is

Intel based, a number of OS are available: MS-DOS, MS-Windows 98/NT, QNX, VxWorks are candidates. In this research, the QNX realtime operating system (RTOS) is chosen and used throughout this research.

Based on the timing requirement and the assigned task, four concurrent processes are created and communicate with one another via the interprocess communication (IPC) scheme provided by QNX RTOS. The four processes are named *DQIGPS, DQICONT, VCOMM* and *ULREAD* after their functions.

The VMSS is initiated in the following order. At first, the wireless communication link from the ground station to the FCS is established. The ground operator logs into the QNX session and starts the parent process *DQIGPS* with the appropriate options. Then the *DQIGPS* starts and spawns the *DQICONT*. The *DQICONT* in turn spawns two more child processes: *VCOMM* and *ULREAD*. These processes runs concurrently with shared-memory and proxy based IPC as shown in Figure 3.23. Each process runs at its own rate, which is mainly determined by the requirements of the external sensors and actuators. The *DQIGPS* runs at 4Hz because the GPS outputs the RTK position data at 4Hz. The *DQICONT* runs at 100Hz because the DQI-NP outputs the navigation data at 100Hz. *VCOMM* and *ULREAD* run in an aperiodic manner: *VCOMM* is a server running on FCS and sends the current flight status to the vision computer via RS-232. *ULREAD* polls the daisy-chain ultrasonic sensors at approximately every 300 ms. Flowcharts for these processes are given in Figure 3.24 ~ Figure 3.27.

It is very important to check that the VMSS runs at the required timing within acceptable timing jittering. Since QNX does not offer rigorous scheduling analysis software tools, we had to devise some *ad hoc* way. In the main loop of *DQICONT*, a number of `outp` functions are inserted. These lines output one byte to the digital output port of the counter/timer board and we can monitor the status via oscilloscope. This method is not so elegant, but it is a very efficient and accurate way to monitor the realtime performance. It is validated that the processes run at excellent timing as shown in Figure 3.28. The main loop of *DQICONT* runs every 10ms and the entering point is approximately 0.5 millisecond after the end of the RS-232 transmission of the navigation data format M3512 of the DQI-NP. Then the *DQICONT* executes a series of functions: Kalman filtering, control output computation, wireless communication via TCP/IP, and the IPC. The overall user load is less than about 10% and it allows enough time to run other system processes.

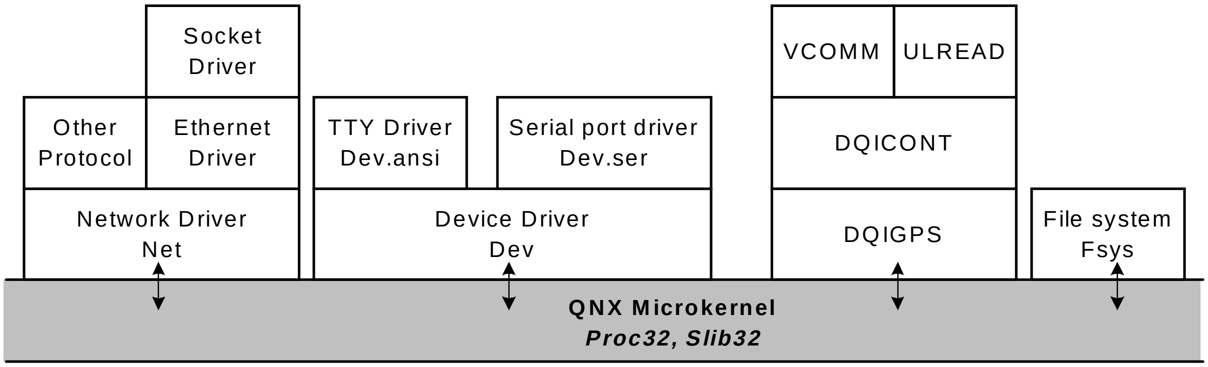

Figure 3.22 System architecture of QNX RTOS

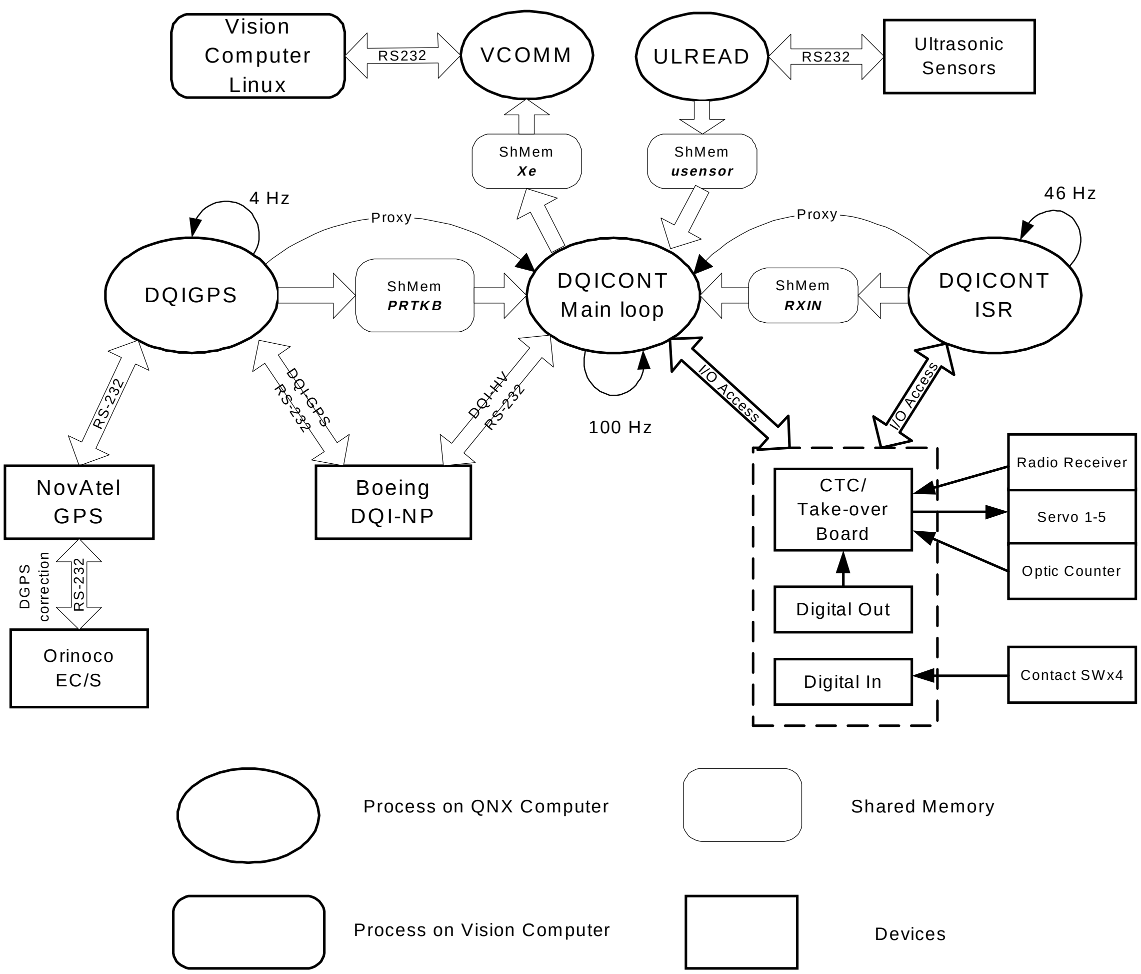

Figure 3.23. Block diagram of VMS

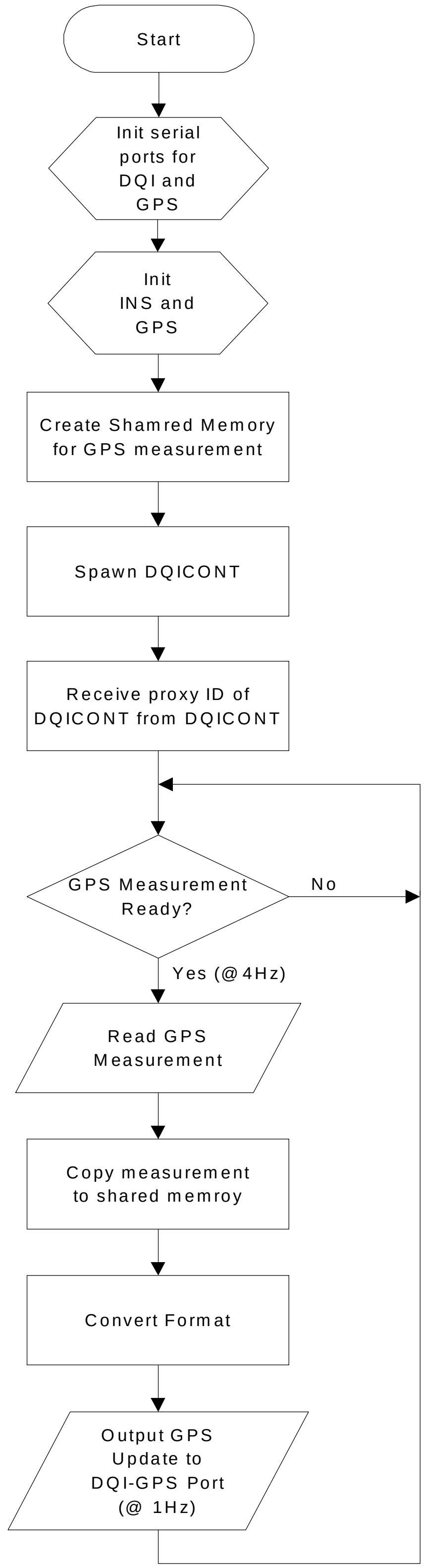

Figure 3.24 Flowchart of process DQIGPS

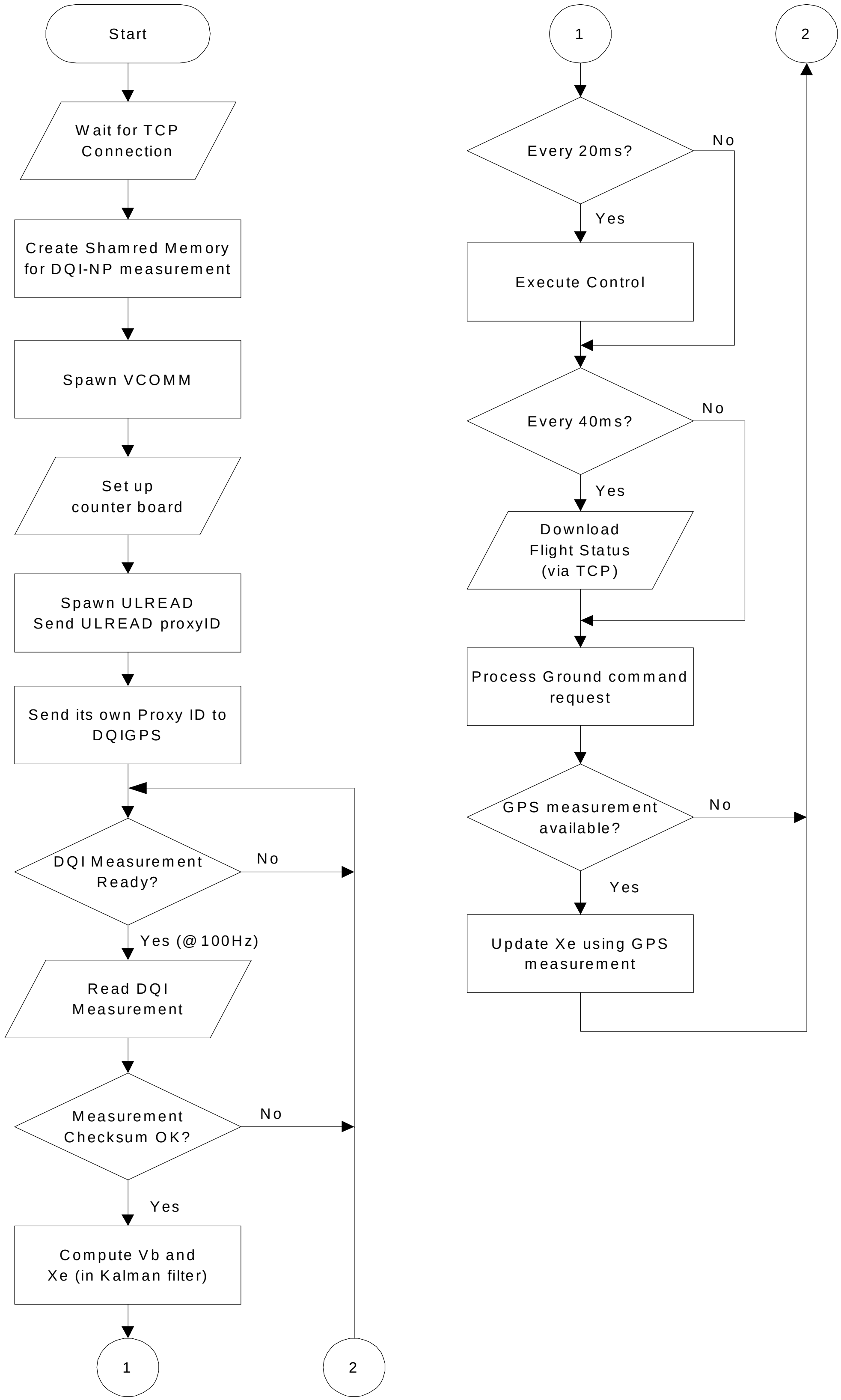

Figure 3.25 Flowchart of DQICONT

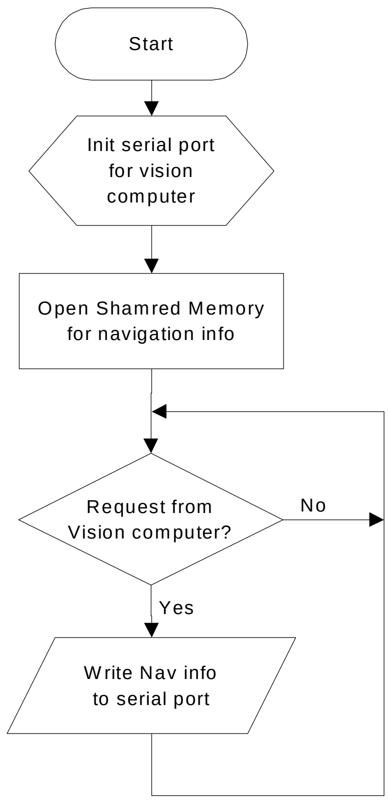

Figure 3.26 Flowchart for VCOMM

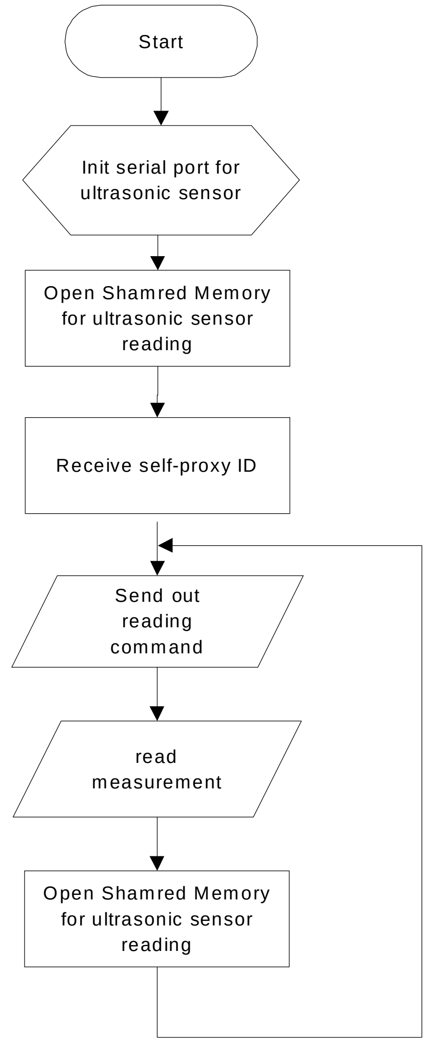

Figure 3.27 Flowchart for ULREAD

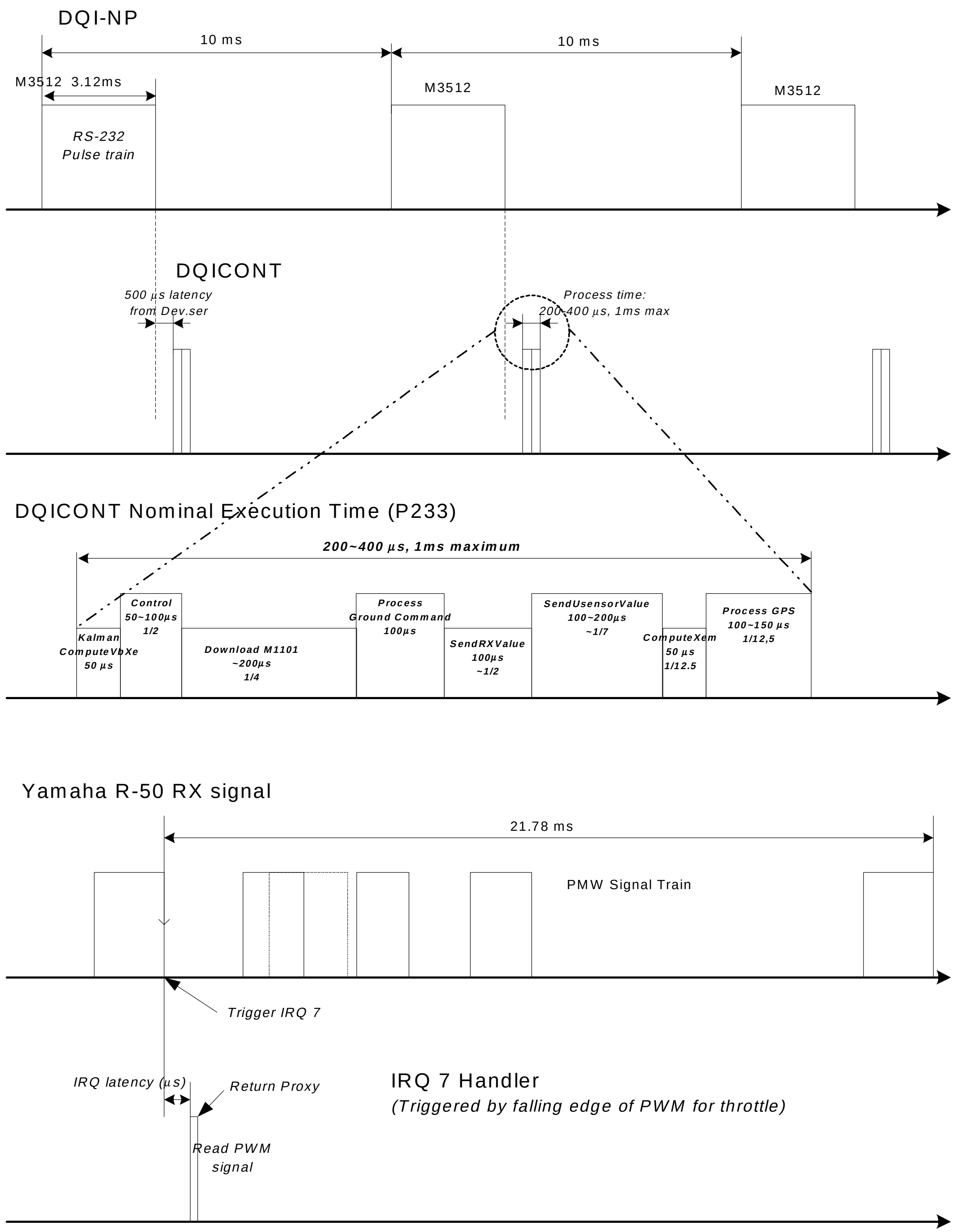

Figure 3.28 Real-time performance of onboard flight control software

Chapter 4

Hierarchical Flight Control System Synthesis

In this part of the research, we aim to construct a controller architecture that conforms to the hierarchical structure presented in Figure 1.3. The idea of the architecture is to build a hierarchical multiple-layer structure that decomposes the abstract mission objectives into physical quantities of control input. At the highest level, is the strategic planner, which determines the desired motion of the RUAV for a finite horizon based on the mission objective and the current navigation status. In the middle of the hierarchy, an intermediate layer interprets the output of the strategic planner and chooses the current flight mode and the associated reference trajectory in realtime. In the lower part, the regulation layer reads the realtime reference trajectory and issues the feedforward/feedback control output for the helicopter airframe in realtime. At the lowest level is the physical helicopter system. The helicopter responds to the control input from the regulation layer and the vehicle response is measured by the navigation sensors and fed back to the regulation layer and the waypoint navigator. The waypoint navigator monitors the navigation and the vehicle status to determine if the current flight mode is being realized correctly or if there is some fault or exogenous disturbance in the system. Based on the waypoint navigator's decision, the given task is carried on or aborted.

In Figure 4.1, the hierarchical structure that has been developed for our RUAV application is presented, As can be noticed, the proposed structure is slightly differently structure than the original structure shown in Figure 1.3. The major difference is that the tactical planner and the trajectory generator in Figure 1.3 are combined into a single layer. The reason for this modification is that the reference trajectory is completely dependent on the current flight mode and it is more reasonable to generate both the trajectory and the flight mode in a single module.

In this research, the lower two layers, the waypoint navigator and the regulation layer, are mainly developed while maintaining compatibility with the hierarchical structure. The waypoint navigator receives the motion command from the strategic planner and determines the appropriate flight mode and the associated reference trajectory. The waypoint navigator activates the proper control sets and sends the reference trajectory data in real time. In order to integrate these two layers with the strategic planner, a methodology to convey the necessary information independent of the mission and specific vehicle type is desired. To address this abstraction, the novel concept of *Vehicle Control Language* (VCL) is developed. VCL is a script-type human understandable language that encapsulates the flight mode, waypoint coordinates and other optional specifiers. Through the use of VCL, the autopilot system becomes independent of the detail of the mission. As a direct consequence, a more versatile flight control system can be implemented. These two major tasks of building the regulation layer and the waypoint navigator are discussed in this chapter. In accordance with the consistently used bottom-up approach, we first develop the stabilizing feedback control systems for hover. These systems are fully tested in a series of the test flights. In the next step, the waypoint navigator is developed using the framework of the VCL.

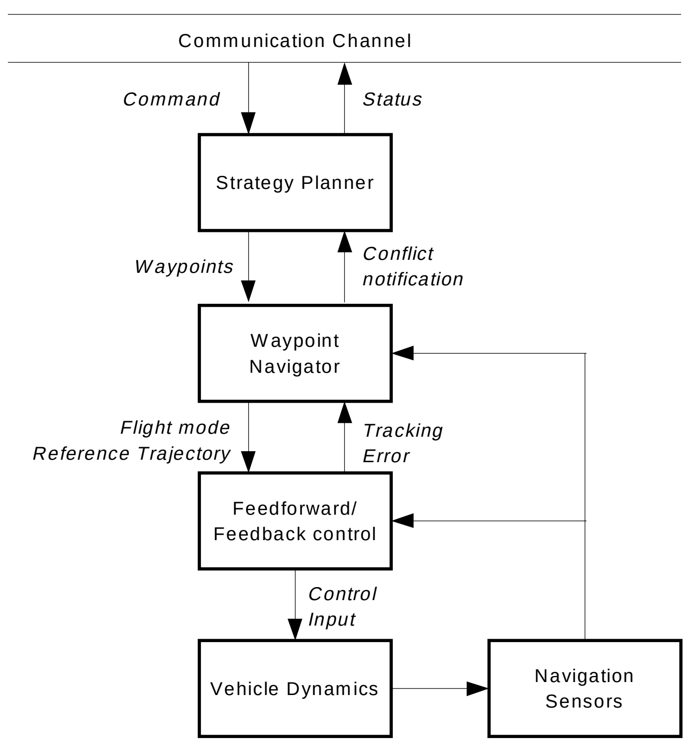

Figure 4.1 Modified hierarchical vehicle control system

4.1 Regulation Layer

The helicopter has inherently unstable, complicated, and nonlinear dynamics under the significant influence of exogenous disturbances and parameter perturbations. The system has to be stabilized by using a feedback controller. The stabilizing controller may be designed by the model-based mathematical approach or by heuristic control algorithms. Due to the complexity of the helicopter dynamics, there have been efforts to apply non-model-based approaches such as fuzzy-logic control, neural network control, or a combination of these [6]. While these approaches are attractive because no identification is required, they do not guarantee closed-loop stability while they are being tuned or being learning. The mathematical model-based approach assumes the availability of a linear or nonlinear system model for the controller design. In this case, the system identification process takes the significant amount out of the whole research effort of building a RUAV. As our goal is to provide a feedback controller that is consistently reliable, we seek a suboptimal controller using the model-base approach. In the early part of the Berkeley UAV research, three different approaches were chosen: (1) linear robust control using μ-synthesis, (2) feedback linearization, and (3) genetic fuzzy approach [6]. All of these controllers showed satisfactory stabilization and tracking performance when working with the nominal plant with acceptable level although certain differences are observed with plant perturbation and/or exogenous disturbance are introduced. While the genetic-fuzzy logic and the μ-synthesis control showed robustness to those adversary effects, the performance of the feedback linearization controller degraded considerably with the increased uncertainty and the external disturbance. In fact, the feedback linearization control theory can be applied, as for now, to very limited class of simple nonlinear systems. In efforts to cast the realistic nonlinear model into such a framework, extreme simplification and misleading assumptions have been introduced in many previous works. The resulting control law obtained by this approach would not be able to perform as promised by the simulation when in the presence of the neglected dynamics, model perturbations, or sensor noise.

The linear control theory has drawbacks of its own. First of all, the helicopter model is not linear by any means. The dynamics feature strongly nonlinear effects and the equations of motion are governed by the nonlinear kinematic relationship. Nonetheless, it has been proved that linear control theory is able to stabilize unstable nonlinear dynamics consistently, as long as the system stays in the region where the linearity assumption holds. The deficiency of the linear approach in the coordinate transformation should be taken care of by a separate algorithm. For example, the linear controller does not understand the heading other than 0°. The forward flight with a fixed heading of other than 0° is realized only through an explicit coordinate transformation of the tangent plane position coordinates back to the body coordinates. Even with these difficulties, gain-scheduled linear controllers have been widely accepted as the mainstream approach by many practitioners in industry. It is rather hard to understand at first because of the fact that the helicopter dynamics show a strong coupling among the longitudinal, lateral, vertical and yaw dynamics. Thanks to the mild cross-coupling among channels, however, the SISO approach manages to function reasonably as has been reported by other researchers and will be shown in the following.

On the other hand, there have been a number of attempts [17,18,19,20] to apply modern control theories to the helicopter control problem because the modern control approach offers many superior features over classical controls such as: decoupling, robustness, and sophisticated performance specification. Surprisingly, however, the MIMO modern control approach has not won many practitioners yet. Many of these efforts extend only as far as simulation and very limited works have been performed on actual helicopters.

Our goal in this research is to provide a working autopilot system for our helicopters. Although there are many fancy control theories promising theoretically beautiful results, the reality is, only a handful of these can be actually applied to the complicated helicopter dynamics. Therefore, we choose to deploy linear control theory for its consistent performance, well-defined theoretical background and effectiveness proven by many practitioners. In this research, we apply classical SISO control theory as well as multivariable state-space control theory such as μ-synthesis for the stabilization of the helicopter in the hover mode. In the following, the formal statement of the stabilizing feedback controller design is given:

Problem Statement

Suppose the kinematics and linearized dynamics are given as follows:

$$\begin{aligned}
\dot{\mathbf{X}}^{TP} &= \mathbf{V}^{TP} \\
&= \mathbf{R}_{B\to TP}\mathbf{V}^{b} \\
\frac{d}{dt}\begin{bmatrix}\Phi\\ \Theta\\ \Psi\end{bmatrix} &= \begin{bmatrix}1 & \sin\Phi\tan\Theta & \cos\Phi\tan\Theta\\ 0 & \cos\Phi & -\sin\Phi\\ 0 & \sin\Phi/\cos\Theta & \cos\Phi/\cos\Theta\end{bmatrix}\boldsymbol{\omega}^{b} \\
\dot{\mathbf{x}} &= \mathbf{A}\mathbf{x}+\mathbf{B}\mathbf{u} \\
\mathbf{y} &= \mathbf{C}\mathbf{x}
\end{aligned} \tag{4.1}$$

where

$$\mathbf{X}^{TP} = [p_x \quad p_y \quad p_z]^T$$

$$\mathbf{V}^{TP} = [v_x^{TP} \quad v_y^{TP} \quad v_z^{TP}]^T$$

$$\mathbf{V}^b = [u \quad v \quad w]^T$$

$$\boldsymbol{\omega}^b = [p \quad q \quad r]^T$$

$$\mathbf{x} = [u\ v\ p\ q\ \Phi\ \Theta\ a_{1s}\ b_{1s}\ w\ r\ r_{fb}]^T$$

$$\mathbf{u} = [u_{a_{1s}}\ u_{b_{1s}}\ u_{\theta_M}\ u_{r_{ref}}]^T$$

$$\mathbf{y} = [p_x \quad p_y \quad p_z \quad v_x^{TP} \quad v_y^{TP} \quad v_z^{TP} \quad \Phi \quad \Theta \quad \Psi \quad u \quad v \quad w \quad p \quad q \quad r]^T$$

The goal is to synthesize the control law that stabilizes the vehicle dynamics and steers the vehicle to follow the desired trajectory

$$\mathbf{y}_{ref}(t) = \left(x_{ref}^{TP}(t), y_{ref}^{TP}(t), z_{ref}^{TP}(t), \Psi_{ref}(t)\right) \tag{4.2}$$

As a partial requirement, we need to find a static or dynamic stabilizing feedback law

$$\mathbf{u}_{fb}(t) = \mathbf{f}(\mathbf{y}(t)) \tag{4.3}$$

such that $\mathbf{A} + \mathbf{Bu}$ is Hurwitz.

In the following, the controller design process for Ursa Magna 2 (Yamaha R-50) is presented. A similar procedure had been applied to Ursa Minor 3 (Kyosho Concept 60) earlier.

4.1.1 Classical Controller Design

Since the classical control approach is applicable only to the SISO system, the MIMO helicopter dynamics should be decoupled into SISO sub-systems (Figure 4.2). This is achieved by ignoring the substantial amount of coupling among these systems. This is a rather strong assumption and will be examined in the following. Nonetheless, this is currently the most favored method by military or industry research communities due to the simple and intuitive control system structure and more importantly, the fact is that it has been shown to be effective in numerous flight tests. The system equation in equations (2.63) to (2.67) represents a MIMO system with moderate coupling among the roll, pitch, yaw, and heave channels. For example, the roll and pitch responses show approximately

15-25% coupling and the vertical mode agitates the yaw model due to the persistently varying anti-torque of main rotor. Nonetheless, the system can be considered to be four sub-systems that consist of roll~v_y, pitch~v_x, yaw and heave channels and each can be stabilized by proportional-differential (PD) controllers as will be discussed in the following. The roll and pitch rate dynamics show lightly damped stable responses, which are similar to each other due to the symmetry of the main rotor system. The roll and pitch angle dynamics can be seen as the cascade of integration and the attitude rate dynamics, resulting in marginally stable systems. The feedback scheme to stabilize the longitudinal/lateral dynamics can be conceived by studying the root loci of those as shown later in this section. Stepping one step out to the translational velocity dynamics, the dynamics from the roll/pitch control input to v_x and v_y are clearly unstable as shown in Section 2.2.8 and they cannot be stabilized with proportional feedback of the translational velocity only in each channel. The vertical and yaw dynamics have a strongly coupled nature due to the anti-torque of the main rotor. The inherent dynamics of these channels are stable because of the aerodynamic relationship with the lift and the local inflow. However, further damping of the vertical dynamics is desired because of the sluggish response of the Yamaha R-50. The yaw dynamics is already damped sufficiently by the built-in rate gyroscope system. In this case, assuming the gyro system is tuned properly, only the angle regulation is required.

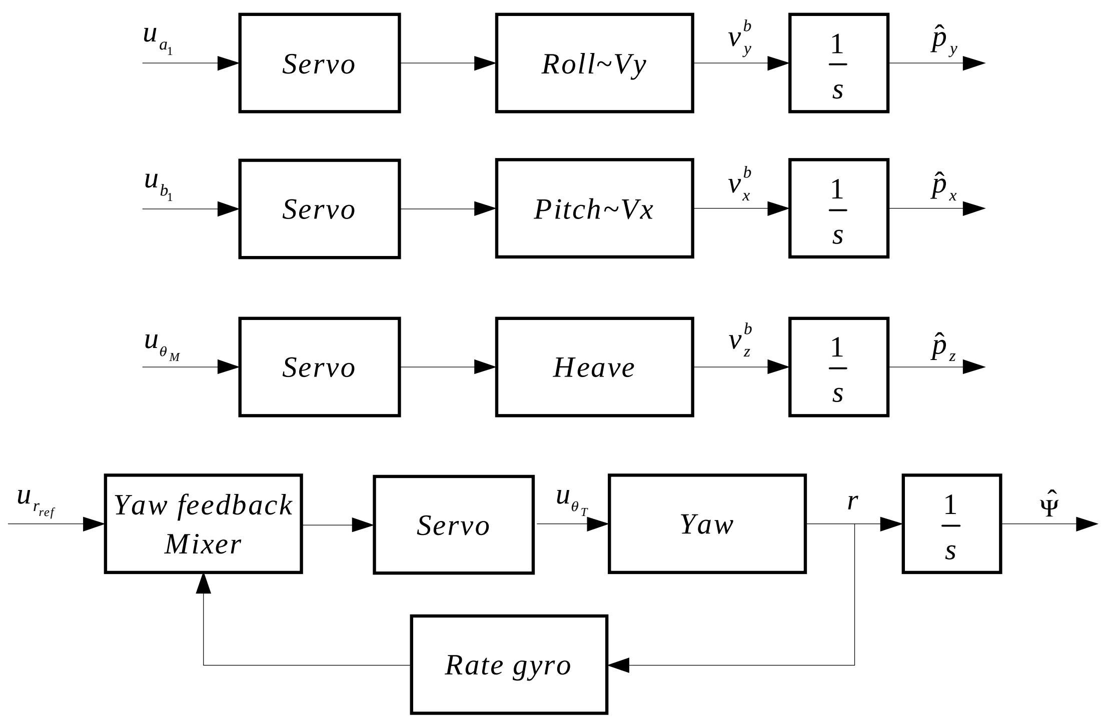

Figure 4.2 SISO representation of helicopter dynamics

Based on these observations, the control law by the classical SISO approach is established as shown in (4.4). The control law is very simple and static. Currently it does not involve any dynamic controllers yet because the static control achieves a reasonable performance and the measurements for feedback do not require any further filtering.

$$\begin{aligned} u_{a_1} &= -K_\Phi \Phi - K_v v - K_{p_y} \Delta_{p_y} \\ u_{b_1} &= -K_\Theta \Theta - K_u u - K_{p_x} \Delta_{p_x} \\ u_{\theta_M} &= -K_w w - K_{p_z} \Delta_{p_z} \\ u_{r_{ref}} &= -K_\Psi \Delta_\Psi \end{aligned} \tag{4.4}$$

- **Attitude Control**

The attitude dynamics indicates the behavior when the translational motion in *x* and *y* direction is constrained. For the design of attitude feedback design, we extract the attitude dynamic model by fixing the state variables of translational velocities in *x, y,* and *z*-direction and the yaw terms to zero.

The eigenvalues of the attitude dynamics of the Ursa Magna 2 are 0, 0, -1.5729±12.2576i (roll) and -1.8706± 8.2616i (pitch). The poles at the origin yield marginal stability. The root-locus suggests that the attitude dynamics may be stabilized by simple attitude feedback only. The proper gains for the roll and pitch loop can be found by the root loci and the step responses with various gains and they are chosen to be $K_\Phi = -0.55,\ K_\Theta = 0.55$.

With the stabilization of the attitude dynamics, it should be noted that we could design a more sophisticated control law involving filters. The structure of the proposed controller has a close relationship with the characteristics of the employed navigation sensors. As commented earlier, the Boeing DQI-NP INS produces attitude estimates with a relatively low bandwidth. Therefore, we do not need to filter high frequency noise for our control problem and the attitude estimates may be directly used for control law computation. We also intentionally avoided introducing angular rate feedback for further modification of the underlying attitude dynamics because the angular rate measurements contain a large portion of noise due to the severe structural vibration of the helicopter. In addition, simpler control laws were preferred in the early stages of the controller experiments. The proposed control laws of proportional gains perform reasonably.

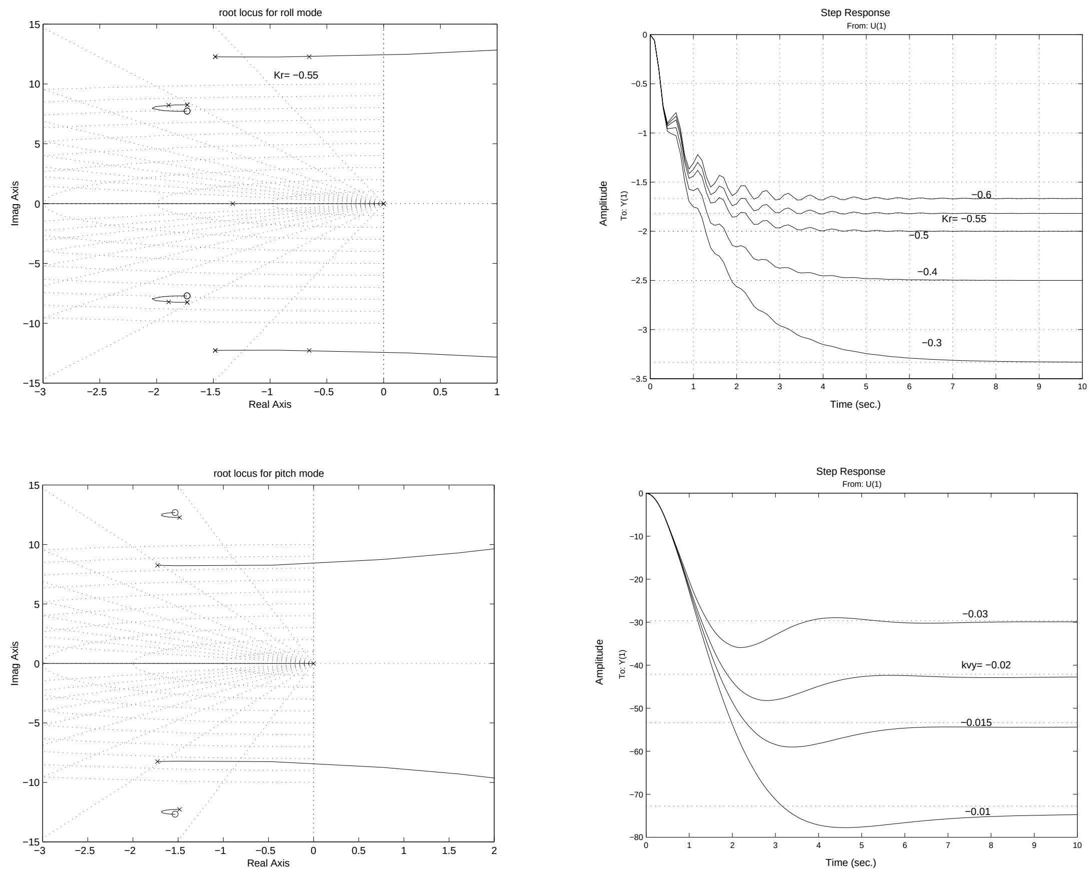

Figure 4.3 Attitude Compensator Design

- **Horizontal Velocity Control**

Once the attitude sub-dynamics are stabilized, we proceed to find the stabilizing feedback gains for the velocity dynamics with the similar approach. Based on the root loci and step responses of the velocity dynamics as shown in Figure 4.4, we find the suitable gains to be: $K_u = -0.02, K_v = -0.02$. The gains in the roll and pitch loops are identical so far due to the very similar dynamic characteristics of these channels. It is expected, if we recall that the roll dynamics has a faster response, that the roll channel will show a faster response than the pitch channel.

With the combined use of proportional feedback for the attitude and the velocity, we could stabilize the longitudinal-lateral dynamics. The proposed controller structure is extremely simple but, as proved in the experiment, very effective in stabilizing the targeted dynamics. The closed-loop dynamics become fully stable so that the manual control in this presence of the stabilizing feedback control becomes very stable and easy.

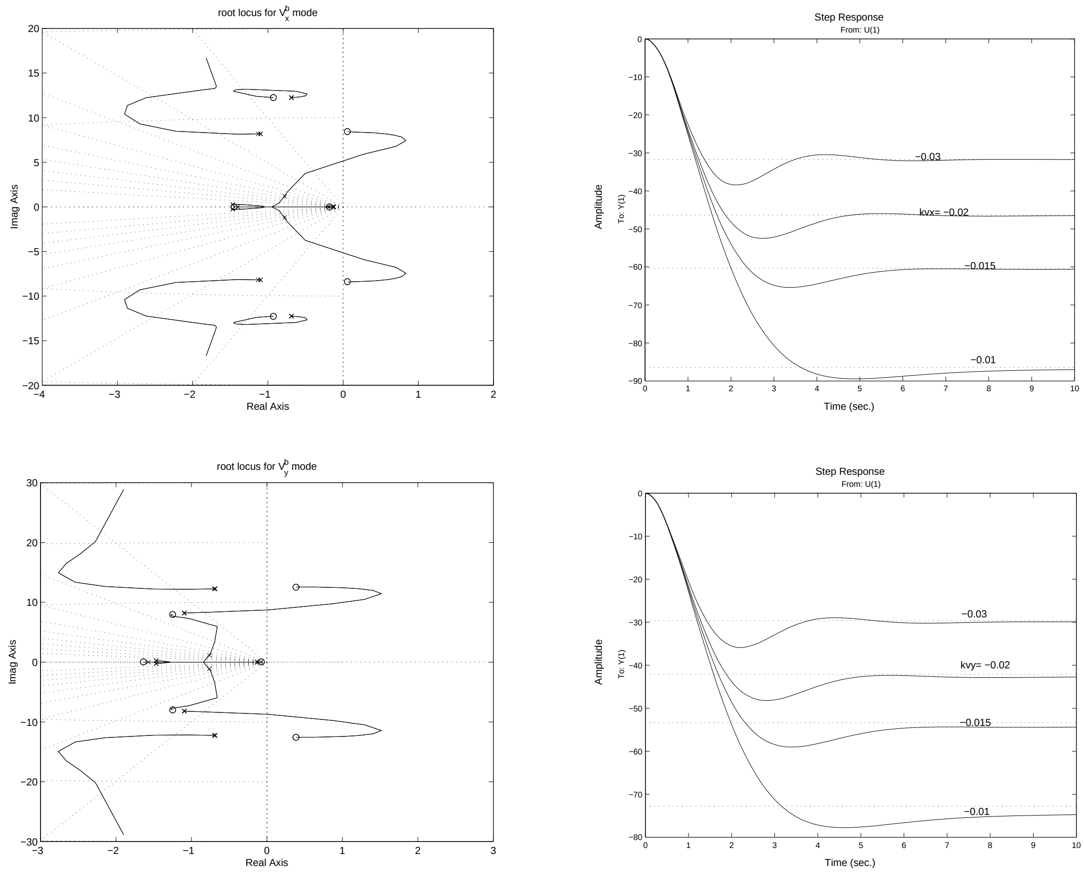

Figure 4.4 Velocity compensator design

- **Horizontal Position Control**

Finally, the position regulation loop gains for the *x* and *y* coordinates are sought. This loop is required for the accurate hovering control at a fixed coordinate in the air. The gains are found using similar SISO root locus method as shown below. The gains are chosen to be $K_{P_x} = -0.01$, $K_{P_y} = -0.01$.

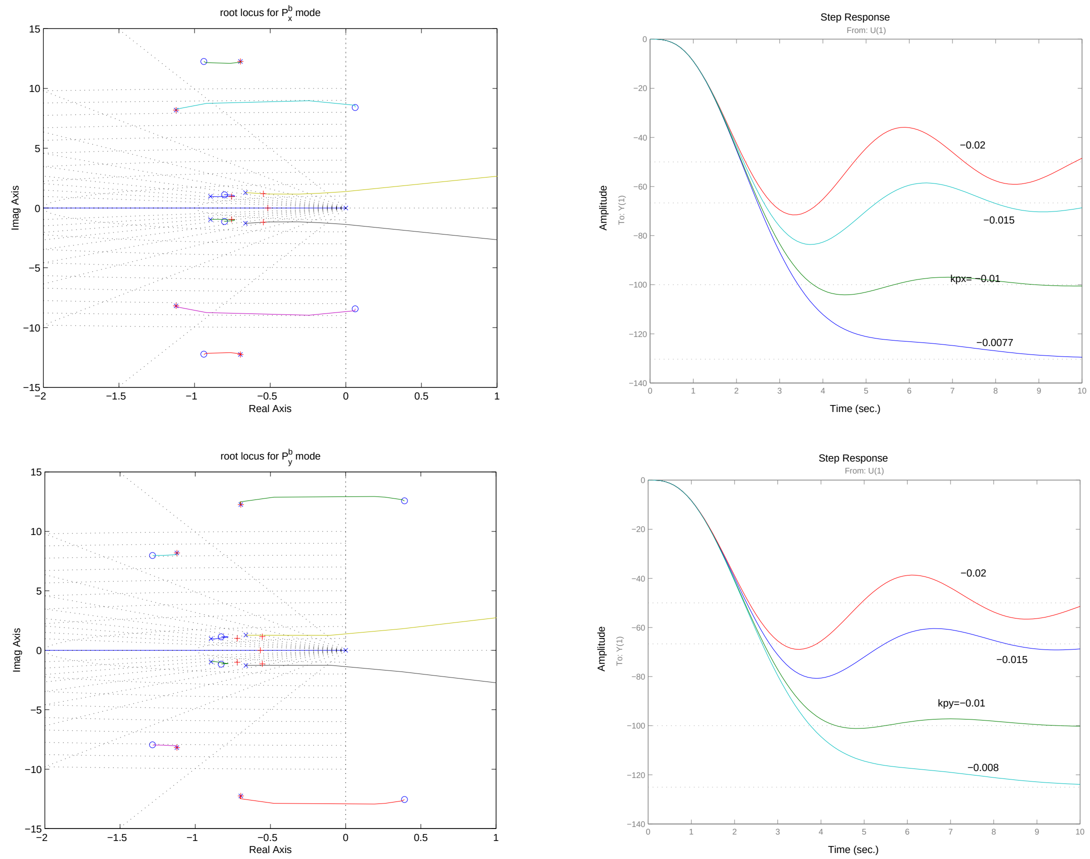

Figure 4.5 Position compensator design

- **Heave and Yaw Control**

We can proceed in a similar way to design the compensators for the heave and yaw dynamics. It should be noted that the heave dynamics is inherently stable due to the aerodynamics of lift generation. Still, introducing further damping by velocity feedback improves the system response considerably. The altitude control can be realized by proportional altitude error feedback. The heave control loop has the architecture of typical motion control because of the base dynamics. The control loop consists of velocity feedback for further stabilization and the altitude deviation feedback. The gains are chosen to be $K_{V_z} = 0.035$ and $K_{P_z} = 0.12$

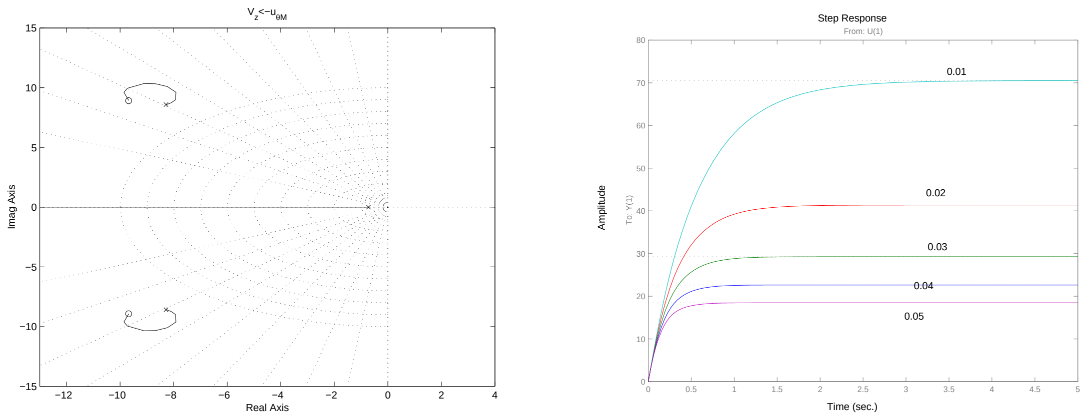

Figure 4.6 Heave dynamics compensator design

The yaw dynamics is also inherently stable for the same reason as the heave dynamics, but it is often desired to introduce further damping on the yaw rate to artificially counteract the anti-torque of the main rotor. For this purpose, almost all small-size radio controlled helicopters are equipped with a simple yaw rate feedback mixer so that the human pilot on the ground can control the helicopter with greater comfort. The Yamaha R-50 also comes with the built-in yaw rate feedback gyro system and its approximated dynamics is included in the system model in (2.63)~(2.67). By keeping the rate-gyro system in the loop, only the heading error feedback is required for the heading control. The yaw gain is chosen to be $K_{\Psi} = 1$.

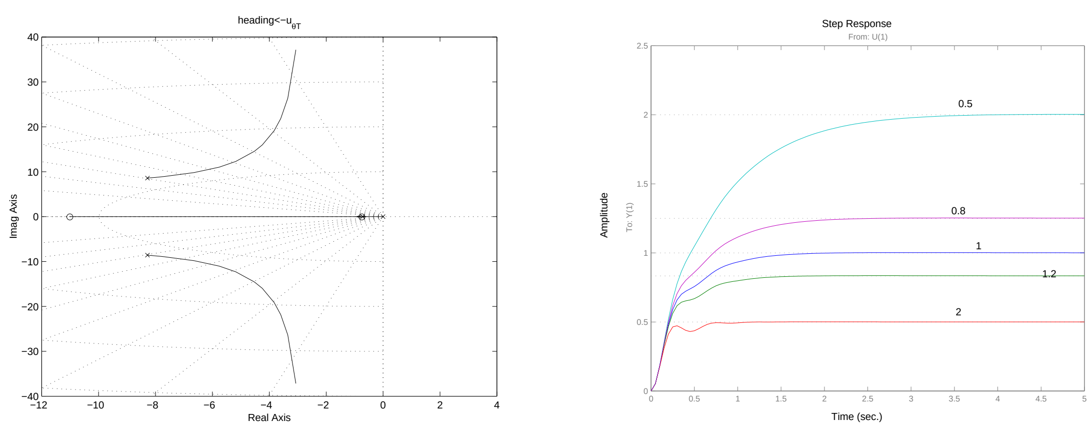

Figure 4.7 Yaw dynamics compensator design

In Figure 4.8, the structure of the multi-loop SISO classical compensator is shown. This simple architecture is advantageous in terms of the efficiency on realtime numerical load and the versatility on the fault-tolerance. Obviously, the control law shown in (4.4) is extremely light in terms of CPU load because it is static and involves very small number of arithmetic operations. In terms of the versatility, the multi-loop architecture can achieve a number of control objectives by switching between proper loops of attitude, velocity, and position control. For attitude control, only the attitude loop is closed. For velocity control, cruise mode for example, the velocity loop as well as the attitude loop are closed. For position control, the position, velocity, and attitude control loops are activated all together. As mentioned above, the velocity and the position loops function correctly only if their inner loops are activated.

A series of experiments have been performed using the proposed controller on Ursa Magna 2. During the repeated experiments, the attitude/velocity controller has shown stable operation even when the helicopter stays on the ground. Therefore, more accurate take-off and landing can be achieved by activating the attitude/velocity controller even before the helicopter takes off from the ground. When operated manually, the pilot engages the attitude/velocity controller using a switch on the transmitter and then takes the helicopter off the ground. At this time, only steady heave reference command is given. Once the helicopter reaches the desired altitude, the hovering controller, i.e., the position/velocity/attitude loop controller is activated.

Figure 4.10 shows the experiment results of the hovering controller tested on the Ursa Magna 2. The RUAV showed a stable response over two minutes with ±0.5m accuracy in x and y directions. The roll, pitch, and translational velocity in the x and y directions are regulated very wel. The altitude regulation shows outstanding performance with ±0.1m error and the heading regulation is also great with a ±3 degree error. Figure 4.11 shows the experiment results of Ursa Minor 3: the hovering accuracy is ±0.2m in x, y, and z directions. The better accuracy of the hovering control of Ursa Minor 3 can be attributed to the faster response of its smaller size.

In Figure 4.9, the photograph of Ursa Magna 2 in hover is shown.

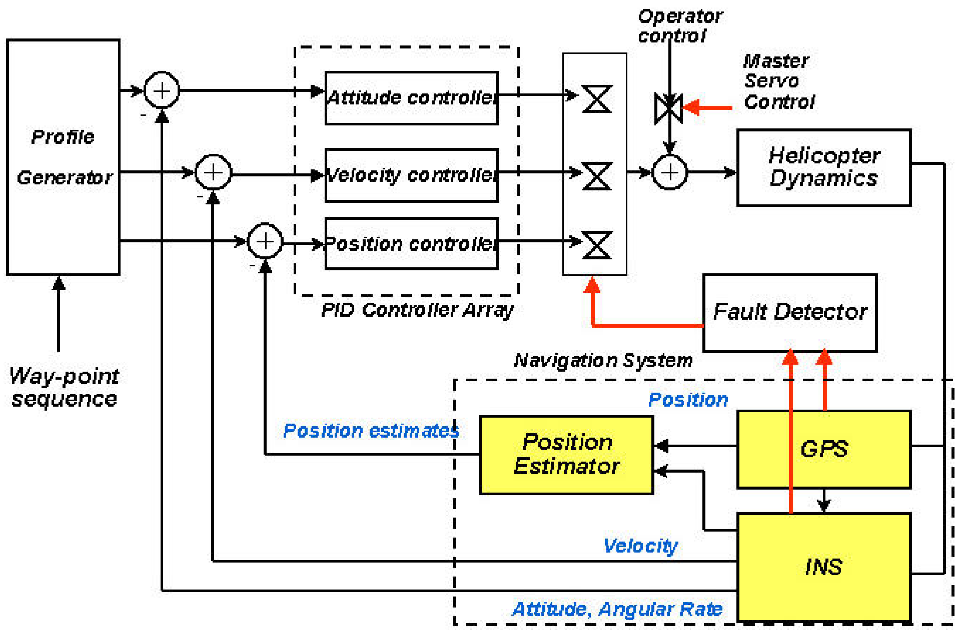

Figure 4.8 The architecture of proposed SISO multi-loop controllers

Figure 4.9 Ursa Magna 2 in automatic hover

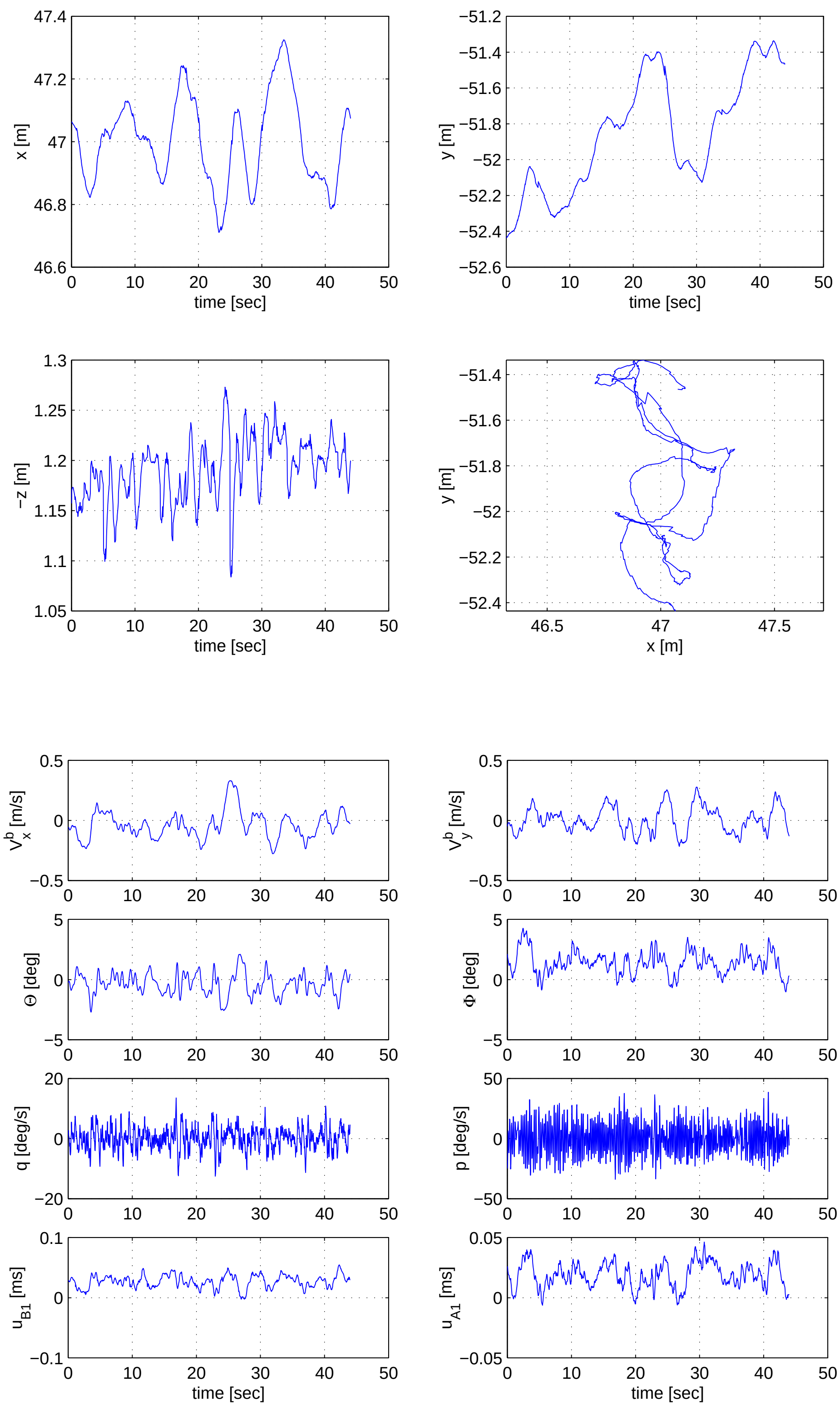

Figure 4.10 Experiment result of autonomous hovering of Ursa Magna 2

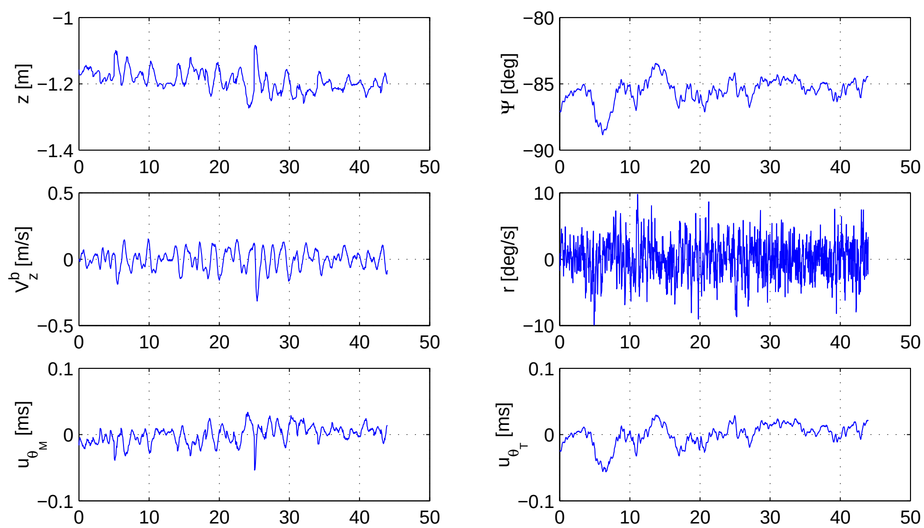

Figure 4.10 (‘cont)

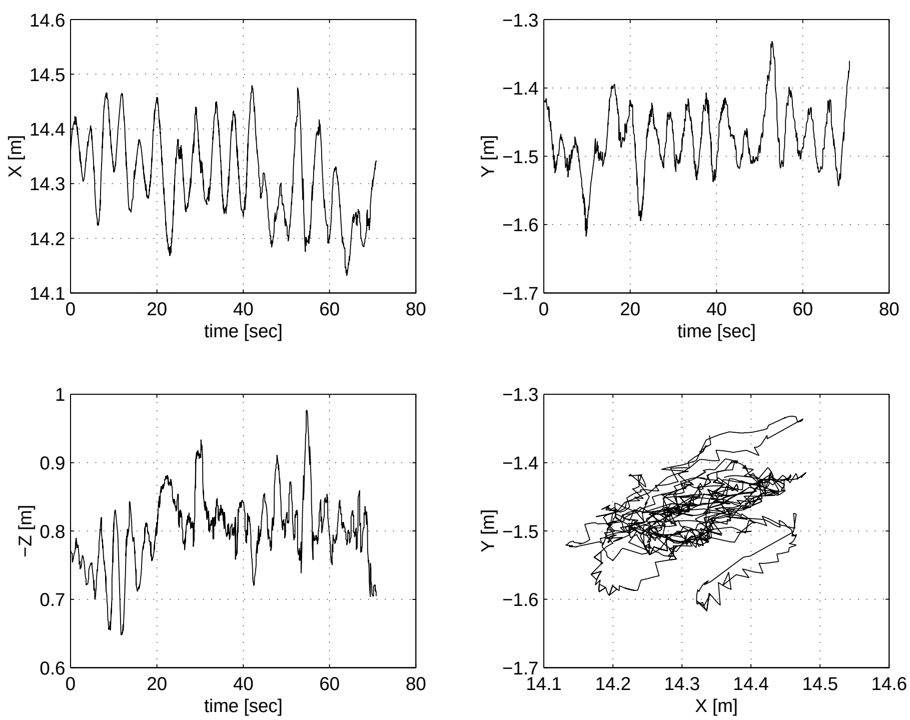

Figure 4.11 Experiment results of autonomous hovering on Ursa Minor 3

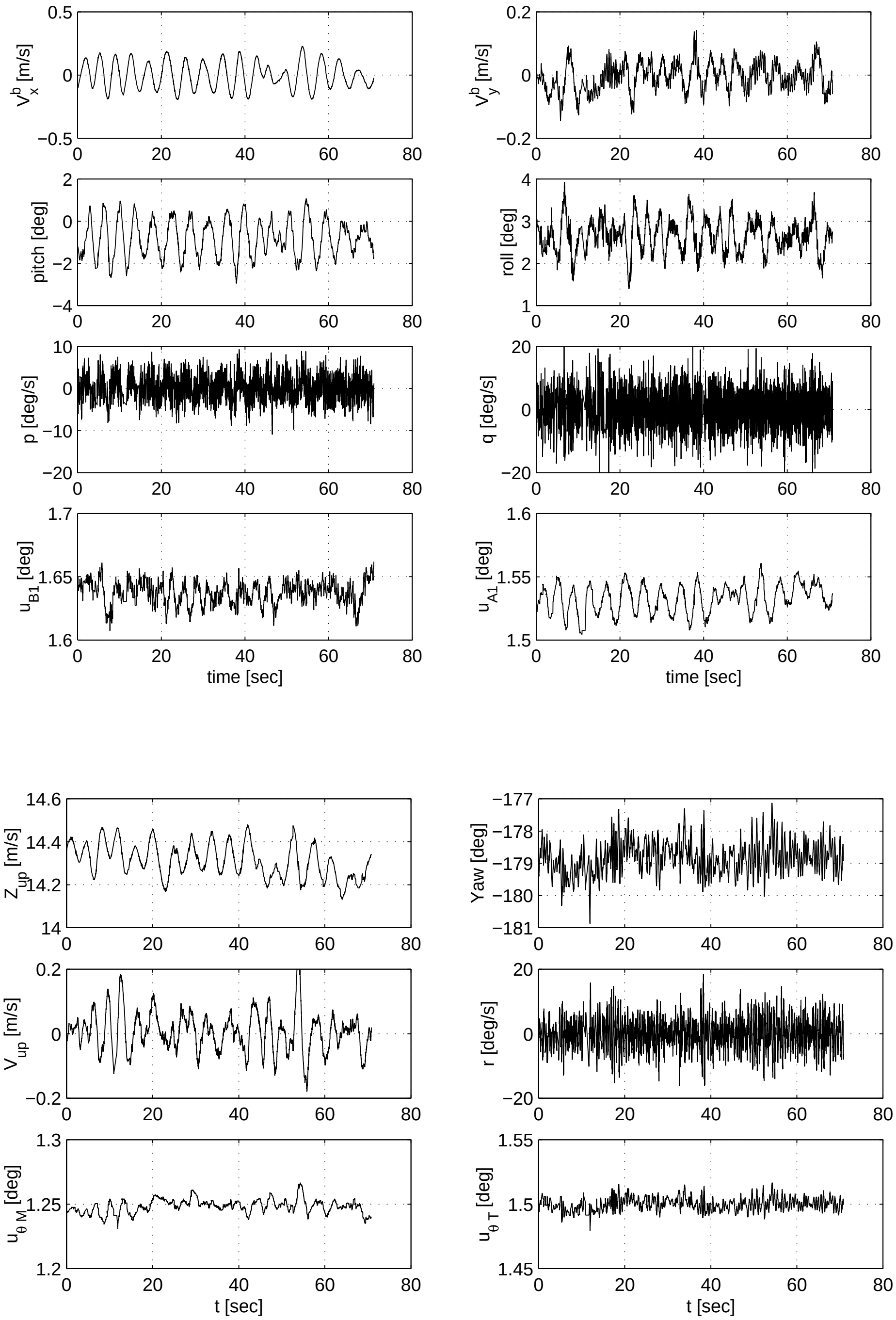

Figure 4.11 (‘cont)

Figure 4.12 Ursa Minor 3 in autonomous hover above the ship deck simulator

4.1.2 μ- Synthesis Controller Design

As an alternative to the classical approach, we apply the modern MIMO linear control theory to the helicopter control problem. Due to the inherent cross-coupling of the rotor dynamics, MIMO control algorithms are more desirable than SISO controllers. The controller must perform stabilization of the nonlinear unstable helicopter system in the presence of uncertain and/or poorly known system dynamics and the severe disturbance and sensor noise. Among the many MIMO control theories, the μ-synthesis control theory is particularly attractive because of its explicit account for the structured uncertainty of a system. The μ-synthesis approach also incorporates a description of the sensor noise model and supports the design of a controller satisfying the performance criterion in the presence of the uncertainty and sensor noise.

Problem Definition [49]

Find an internally stabilizing controller K(s) such that for all perturbations $\Delta_{pert} \in \mathbf{\Delta}_{pert}$, $\max_{\omega} \bar{\sigma}\left[\Delta_{pert}(j\omega)\right] \le 1$ representing the uncertain helicopter dynamics, the closed-loop system is stable and satisfies

$$\left\|T_{e \leftarrow d}\right\|_{\infty} = \left\|F_L[F_U(P, \Delta_{pert}), K]\right\|_{\infty} \le 1 \tag{4.5}$$

The goal of μ-synthesis is to minimize the peak value of $\mu_{\Delta}(\cdot)$ of the closed-loop transfer function $F_L(P, K)$ over all stabilizing controllers K i.e.,

$$\min_{\substack{K \\ stabilizing}} \max_{\omega} \mu_{\Delta}\left(F_L(P,K)(j\omega)\right) \tag{4.6}$$

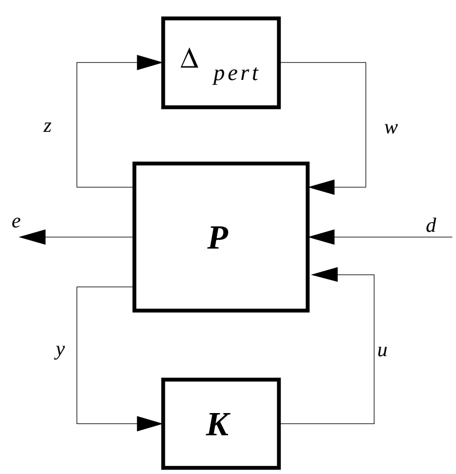

Figure 4.13 LFT representation of μ-synthesis framework

P is the generalized plant, which includes the helicopter linear model and weighting matrix blocks for the sensor noise model and the performance specifications. The structure of the generalized plant should be carefully designed so that the resulting controller K may fulfill all of the robust stability and robust performance requirements. The generalized plant contains the helicopter dynamics, uncertainty weighting, noise weighting, reference response model and performance weighting. The attitude dynamics is extracted from equation (2.63) by discarding the state variables u, v, w, r, and r_{fb}, as shown in the following:

$$\begin{aligned} \dot{\mathbf{x}}_{att} &= \mathbf{A}_{att}\mathbf{x}_{att} + \mathbf{B}_{att}\mathbf{u}_{att} \\ \mathbf{y}_{att} &= \mathbf{C}_{att}\mathbf{x}_{att} \end{aligned} \tag{4.7}$$

where

$$\mathbf{x}_{att} = [p \quad q \quad \Phi \quad \Theta \quad a_{1s} \quad b_{1s}]^T \tag{4.8}$$

$$\mathbf{u}_{att} = [u_{a_{1s}} \;\; u_{b_{1s}}]^T \tag{4.9}$$

$$\mathbf{y}_{att} = [p \quad q \quad \Phi \quad \Theta]^T \tag{4.10}$$

$$\begin{aligned} \mathbf{A}_{att} &= \begin{bmatrix} 0 & 0 & 0 & 0 & L_{a_{1s}} & L_{b_{1s}} \\ 0 & 0 & 0 & 0 & M_{a_{1s}} & M_{b_{1s}} \\ 1 & 0 & 0 & 0 & 0 & 0 \\ 0 & 1 & 0 & 0 & 0 & 0 \\ 0 & -1 & 0 & 0 & -1/\tau_f & A_{b_{1s}} \\ -1 & 0 & 0 & 0 & B_{a_{1s}} & -1/\tau_f \end{bmatrix} \\ \mathbf{B}_{att} &= \begin{bmatrix} 0 & 0 \\ 0 & 0 \\ 0 & 0 \\ 0 & 0 \\ A_{u_{a1s}} & A_{u_{b1s}} \\ B_{u_{a1s}} & B_{u_{b1s}} \end{bmatrix} \end{aligned} \tag{4.11}$$

As discussed above, the helicopter dynamics, when the translational dynamics is constrained, are marginally stable. In the μ-synthesis framework, the interconnection for the generalized plant ***P*** and the weighting functions are the design parameters. The interconnection diagram is given in Figure 4.15, which includes a number of weighting functions categorized as (1) uncertainty model, (2) noise model, (3) control input penalty model, (4) handling quality model, (5) performance weighting model.

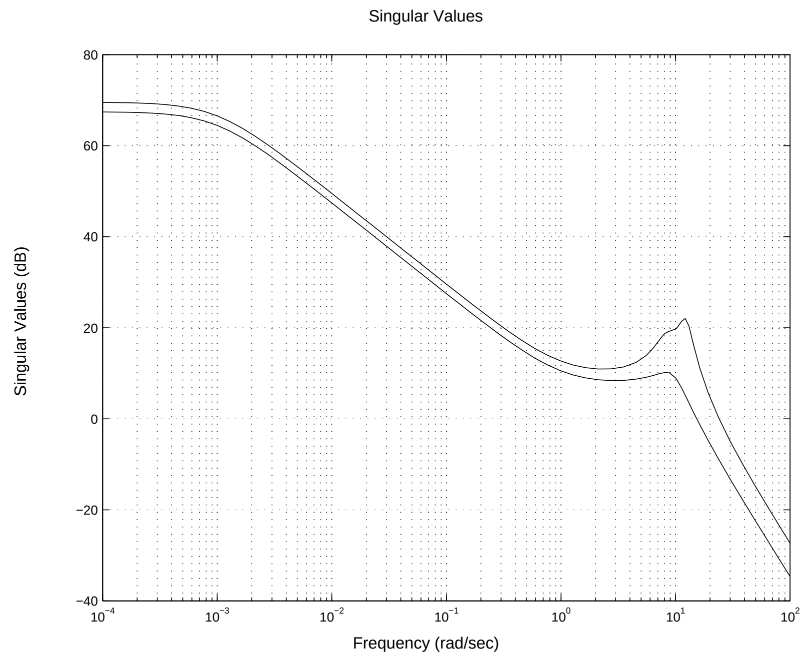

Figure 4.14 Singular value plot of the attitude dynamics of Ursa Magna

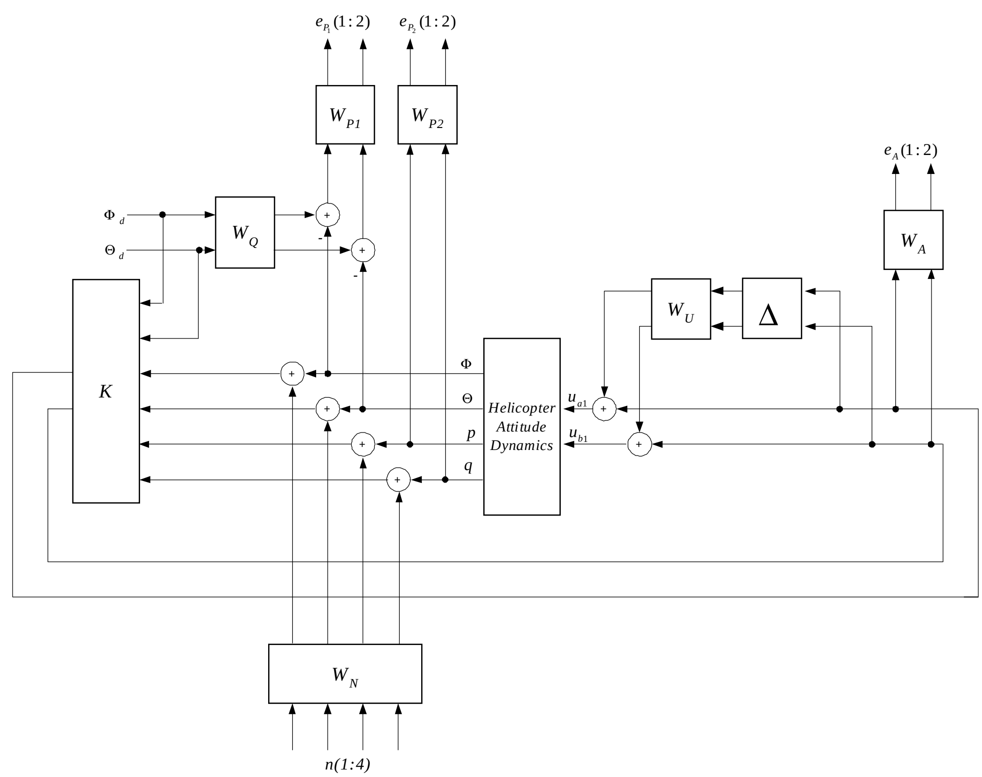

Figure 4.15 Interconnection diagram for μ-synthesis controller design

The weighting functions specify the characteristics of the controller under the framework of the minimization of the closed-loop system input-output infinity norm as shown in (4.5). Roughly speaking, the weighting functions shape the controller so that the input-output ratio is smaller than 1.For example, if a weighting function penalize the deviation of the system response from the model response by 10, the error of the closed-loop system would be around 10%. The actual behavior of the μ-synthesis controller is significantly more complicated than this simplified interpretation.

- **Uncertainty Model**

The uncertainty or unmodeled dynamics of the helicopter system equation may be categorized as: 1) poorly identified or time-varying aerodynamics or inertial quantities, 2) unmodeled higher order dynamics such as the rotor flapping dynamics or the servomotor dynamics and 3) nonlinear effects of the kinematic and dynamic system equations. All of these may perturb the resulting closed-loop linear control systems out of stable region, so the controller should be designed to be robust to those effects. The uncertainty model associated with the helicopter dynamics is usually very hard to establish due to the nonlinear complex behavior of the original helicopter dynamics. Therefore, 10 % of the multiplicative input uncertainty in each channel is assumed as the starting point.

$$W_U = 0.1\frac{s+1}{s/10+1}\mathbf{I}_{2\times 2} \tag{4.12}$$

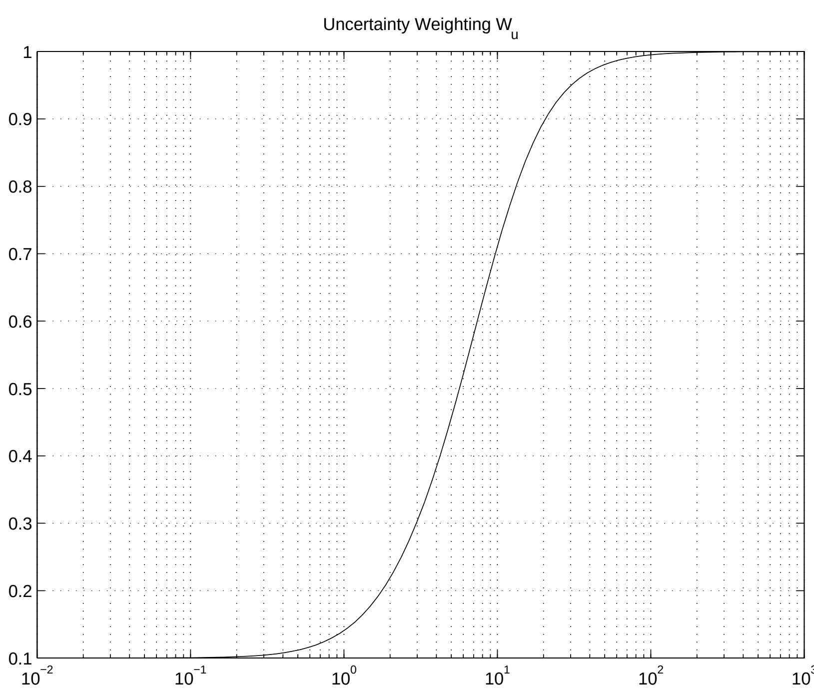

Figure 4.16 Unstructured input uncertainty model

- **Noise Model**

In the attitude regulation, the attitude angle (Φ, Θ) and the angular rates p and q are measurable. These measurements are obtained through the Boeing DQI-NP system. The main rotor flapping angles a_{1s} and b_{1s} are not usually measurable without a special measuring device. The angular rates are the direct measurements of the rate gyroscopes and the attitude is the integration of the angular rates by the kinematic equation in (2.11). The actual measurements obtained during flight are analyzed by FFT and then captured in the form of rational transfer function. Although the identical rate gyroscopes are used, the actual noise characteristics are different in each channel because of the different vibration characteristics of the horizontal support bar on which the INS is mounted.a

$$\begin{aligned} W_N^{\Phi,\Theta} &= 0.006\frac{s+1}{s/10+1}\mathbf{I}_{2\times 2} \\ W_N^p &= \frac{0.371s^2+3.64s+28}{s^2+93.4s+9852} \\ W_N^q &= \frac{0.133s^2+7.05s+60.7}{s^2+181s+21930} \end{aligned} \tag{4.13}$$

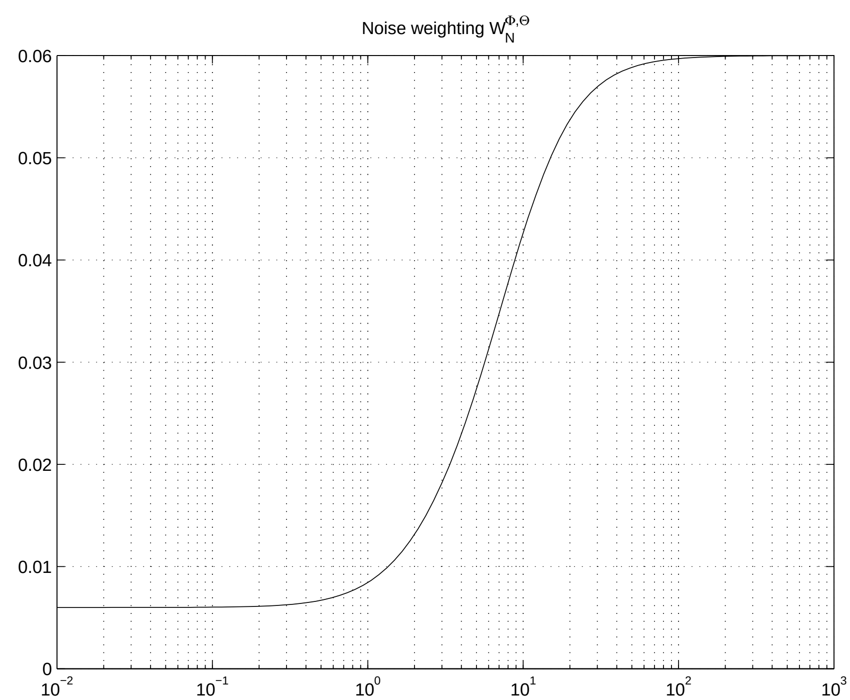

(a) Noise weighting of Φ and Θ

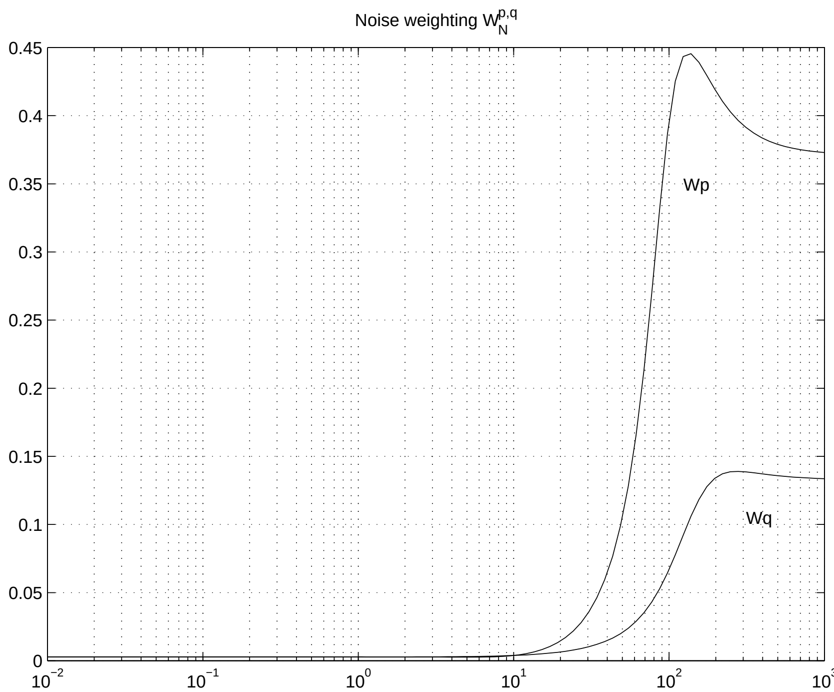

(b) Noise weighting of angular rates *p* and *q*

Figure 4.17 The Noise weighting functions

- **Reference Model**

The reference response model specifies the response profile of the roll and pitch angle to follow. The deviation of the system response from the desired response is penalized by the performance weighting model that will be discussed in the following. The response model can be considered as the handling quality model, which is a concept widely used in the aerospace community. In this research, it is described by 2nd order critically damped transfer function. During the flight test, it was discovered that the weighting on the error has significant effect not only on the response shape but also the overall stability of the overall closed-loop system response. This phenomenon attributes to the mismatch of the linear system model with the nonlinearity of the system model.

$$W_Q = \frac{\omega_n^2}{s^2 + 2\omega_n s + \omega_n^2}\mathbf{I}_{2\times 2}, \quad \omega_n = 0.6\pi \tag{4.14}$$

- **Performance Weighting**

The performance weighting consists of two parts. One part penalizes the deviation of the system response from the reference model to force the helicopter to follow the reference model. The other part penalizes the angular rates so that the Corioli's acceleration and the gyroscopic effects do not become large enough to disturb the linearity regime.

$$W_P^1 = \begin{bmatrix} 120 & 0 \\ 0 & 100 \end{bmatrix} \frac{s/100+1}{s+1}$$
$$W_P^2 = 3\frac{s+1}{s/0.2+1}\mathbf{I}_{2\times 2} \tag{4.15}$$

- **Actuator Weighting**

The purpose of the actuator weighting is mainly to penalize the input to the helicopter in order to prevent saturation. A second-order model is chosen to penalize the control action at higher than 20 rad/s.

$$W_A = \frac{93.25s^2 + 966.5s + 774.3}{s^2 + 33.51s + 784.7}\mathbf{I}_{2\times 2} \tag{4.16}$$

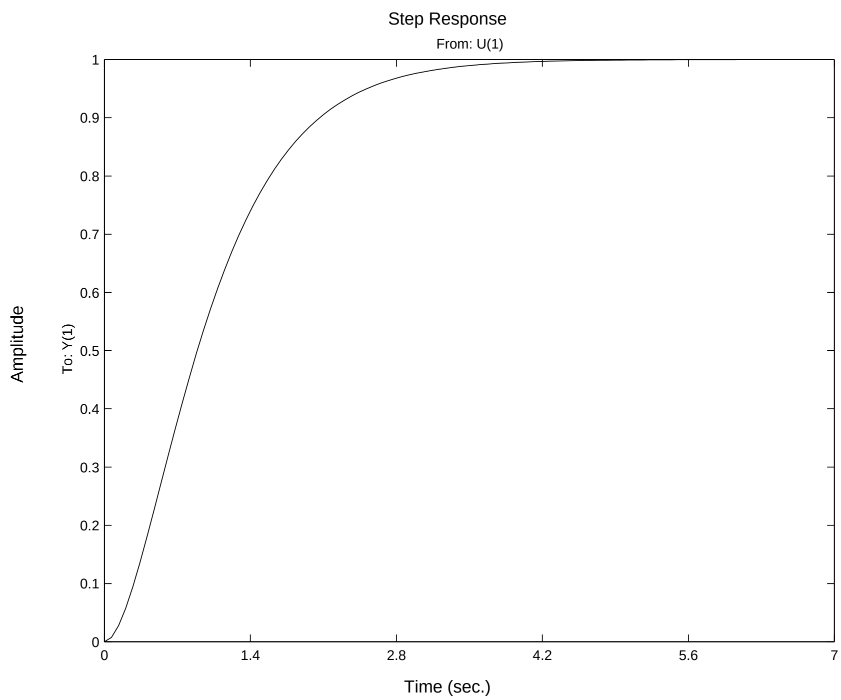

Figure 4.18 The step response of the reference model

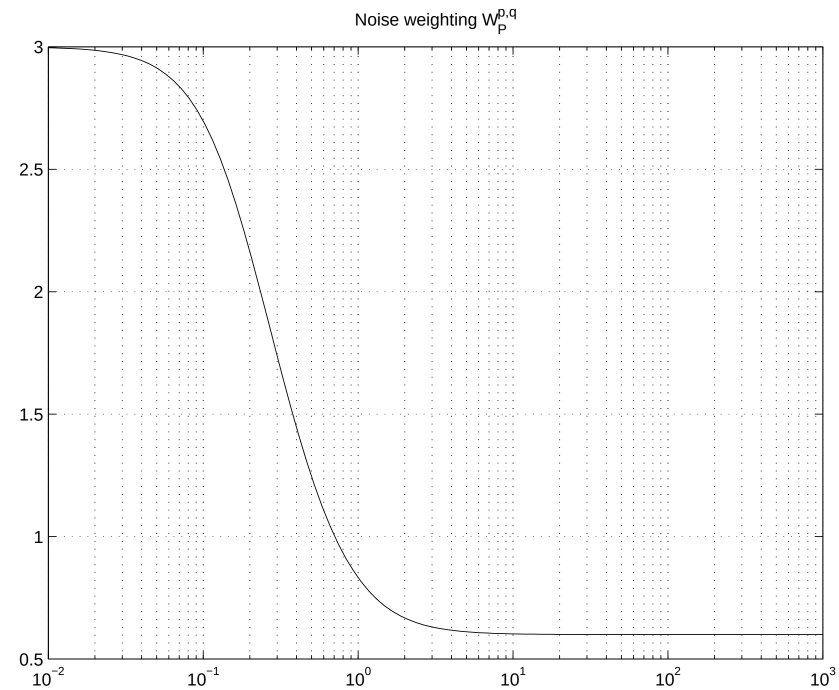

Figure 4.19 Performance weighting

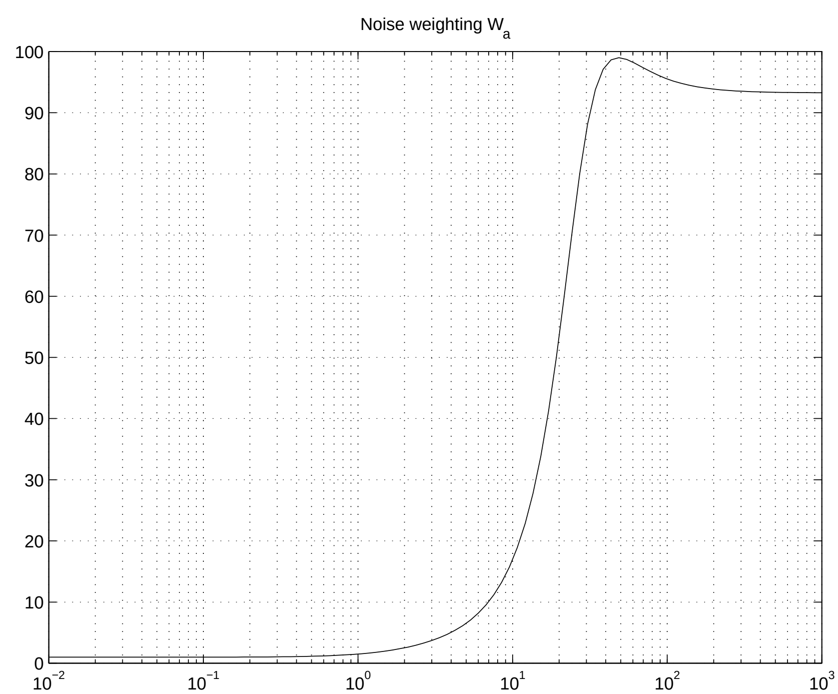

Figure 4.20 The actuator weighting

The controller ***K*** with 6 inputs and 2 outputs is computed using the algorithm known as *D-K iteration*. The minimization problem in (4.6) is not easily solved with the operator of the structured singular value μ. The μ minimization problem is hence replaced with the minimization of the upper bound of the μ such that

$$\mu_{\Delta}(M) \leq \inf_{D \in \mathbf{D}_{\mathbf{\Delta}}} \bar{\sigma}\left(DMD^{-1}\right) \tag{4.17}$$

During this iteration, it is aimed to find the controller K and the input-output scaling matrix D in a alternating manner. At first, with D fixed, the controller K is sought by the $\mathscr{H}_{\infty}$ optimization algorithm such that

$$\min_{\substack{K \\ stabilizing}} \left\| F_L(P_D, K) \right\|_{\infty}$$

Using the resulting K, the scaling matrix D such that

$$\min_{D_{\omega} \in \mathbf{D}} \bar{\sigma}\left[D_{\omega} F_L(P,K)(j\omega) D_{\omega}^{-1} \right]$$

is sought. This process is repeated by a reasonable number until any significant improvement of the peak value of the μ is made or the order of the controller reaches the limit of the reasonable size. The D-K iteration is a heuristic algorithm that does not guarantee any convergence to the local minima, not even the global minima of the minimization problem. Nonetheless, this algorithm yields reasonable results most of the time. In Figure 4.21, the value of μ during the D-K iteration are shown.

The disadvantages of the μ synthesis algorithm are (1) the effort to establish the interconnection of the system and the individual weighting functions, (2) the tremendous off-line computation load, (3) the on-line (realtime) computation load, and (4) the large size of the controller. The drawbacks (1) and (2) are justified if the resulting performance of the μ synthesis controller is superior to other controllers. The drawback (3) as well as some part of (2) are not much of issues these days thanks to the extremely fast and cheap computing capability available even at PC level. The drawback (4) is partially resolved by a number of order-reduction algorithms such as coprime factorization or Hankel-norm minimization.

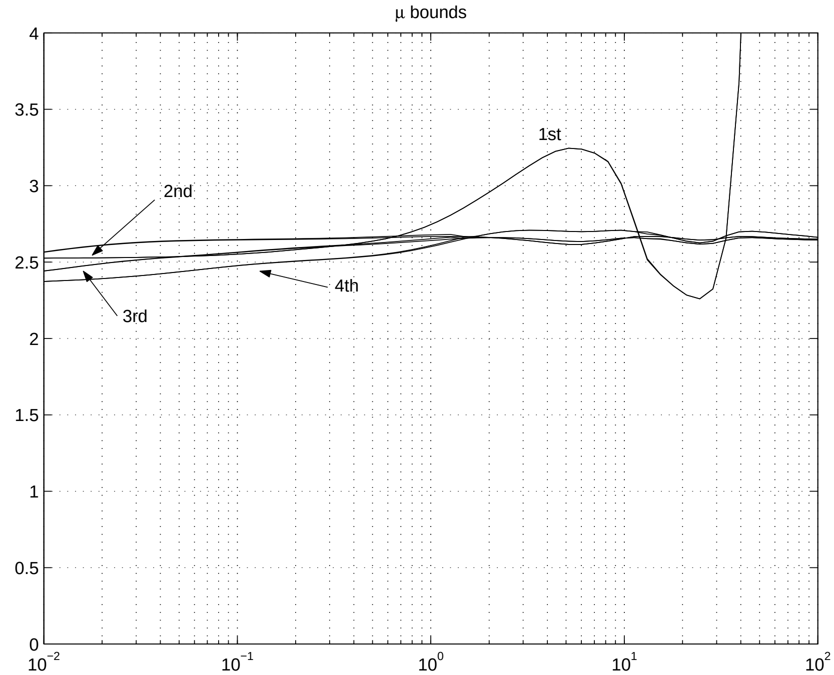

Figure 4.21 μ bounds during the D-K iteration

The resulted controller K is 34th order and its singular value plot is given in Figure 4.22. As a matter of fact, the large size of the resulted controller is one of the major drawback of the μ synthesis algorithm. In our application, the order of the controller has a direct impact on the realtime computation time and the distortion of the controller by the truncation error of the real variables. In terms of the realtime performance, the high order of the controller is not of too much concern any more these days thanks to powerful but common CPUs. It was discovered that, after debugging, the variable to hold the controller system matrix (**A,B,C,D**) should be declared as a double to keep the perturbation of the poles by the truncation error to be minimal.

The resulted continuous-time controller is discretized with the bilinear transform and implemented on the FCS. As mentioned before, the execution time of the 34th order controller was short enough to keep the 21.76 ms sampling time.

In Figure 4.23, the experimental results of the proposed μ-synthesis controller are given. It can be verified that the controller is capable of stabilizing the helicopter system for sufficiently long time. The graph shows that the roll angle is regulated within ± 2 degrees while pitch angle is within ±3~4 degrees. It should be noted that the pitch angle could be more tightly controlled by using larger penalty function W_{Θ}.

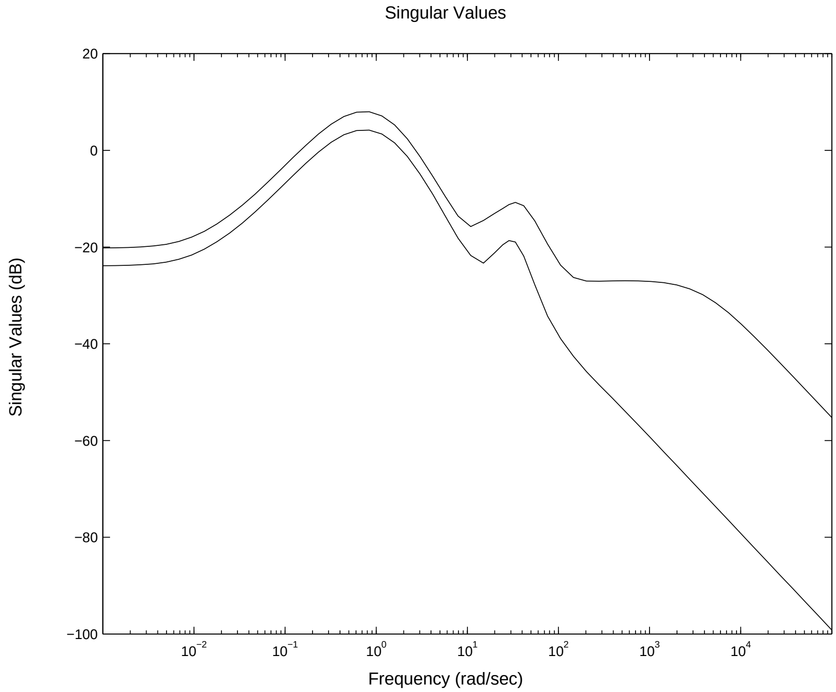

Figure 4.22 The singular value plot of the μ-attitude controller

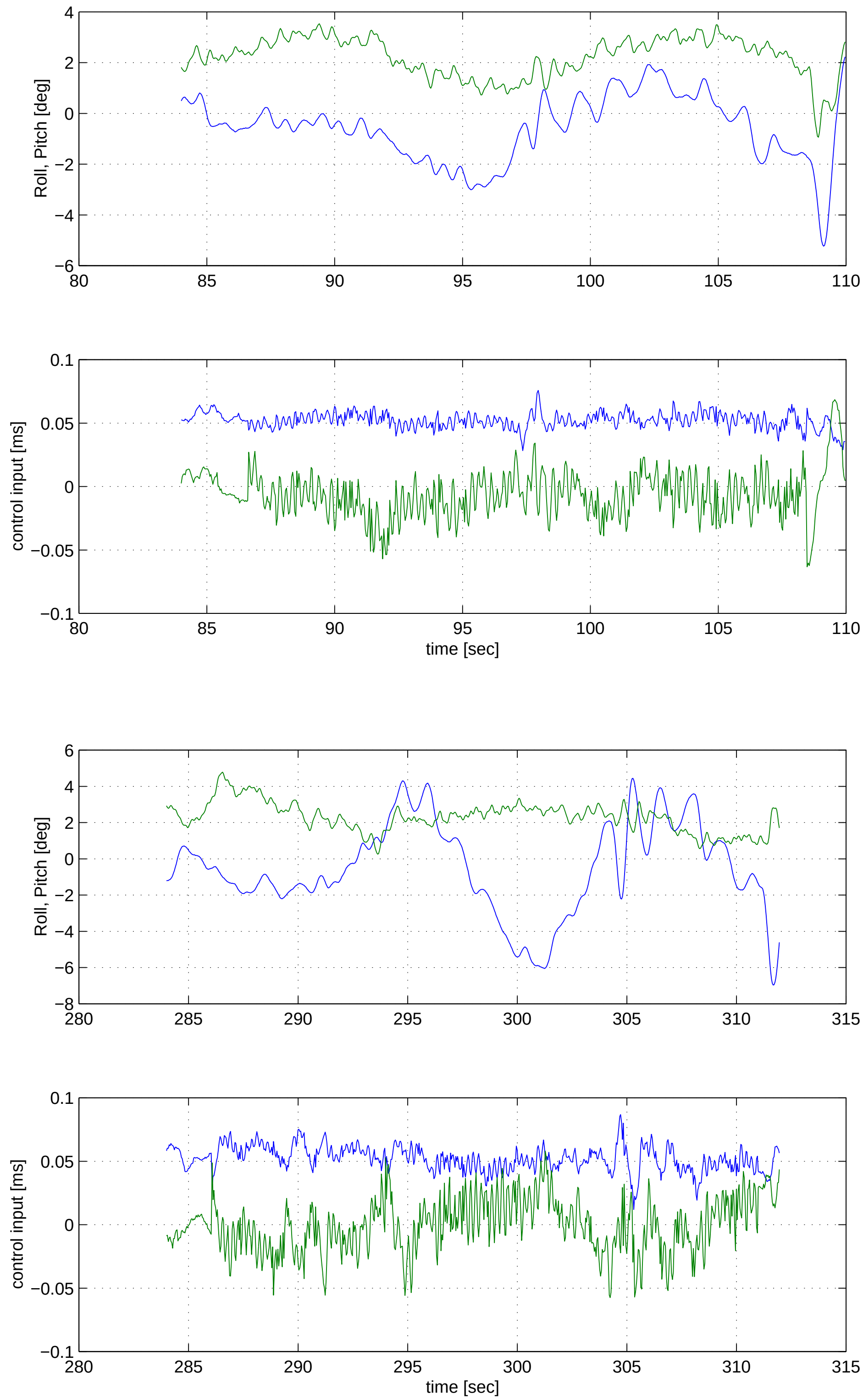

Figure 4.23 Experiment results of attitude regulation by μ-synthesis controller

4.2 Waypoint Navigation

In order for a RUAV to track the given flight paths with the regulation layer that was proposed in the previous section, some supervising control logic should be synthesized for the hierarchical control structure. This layer of supervising logic lies between the strategic planner and the regulation layer. It receives the waypoint request from the strategic planner and reports the execution results of the given request.

In the design of the waypoint navigator, the unique nature of the helicopter maneuverability should be taken into consideration. The flight modes of a RUAV can be categorized as (1) take-off, (2) hover, (3) ascent, (4) descent, (5) forward flight, (6) bank-to-turn, (7) pirouette, and (8) land[1]. The transition relationship among these flight modes is depicted as a state transition diagram in Figure 4.24. According to this diagram, a flight scenario of a RUAV can be understood as a sequential combination of some of these modes. A mission of a helicopter starts with the *Take-off* mode, goes through *Hover* and other flight modes, and ends with the *Land* mode. The *Take-off* and *Land* modes are *terminal nodes,* which means that these modes are either starting or ending nodes. The other modes are *bi-directional,* which means that the sequence can enter or exit this mode. Based on this rule, a given mission scenario is decomposed into a sequence of flight modes either by the strategic planner or by a human operator.

It is worthwhile to compare the flight characteristics of RUAV with that of FUAV. The flight modes of conventional aircrafts can be categorized as (1) take-off, (2) climb, (3) cruise, (4) bank-to-turn, (5) descent, and (6) land[2]. One important factor of any fixed-wing aircraft flight is that the aircraft always has a positive forward velocity higher than the stall velocity. In contrast to the nature of the fixed-wing aircraft, as can be understood from above, the RUAVs feature the superset of flight modes. Whilst the FUAVs always have pass-by waypoints, the RUAVs may have *pass-by* waypoints or *stop-over* waypoints. This versatility of the flight capability requires a more sophisticated waypoint navigation algorithm.

Once the flight sequence is determined, the supervising logic of the waypoint navigator should activate the correct combination of attitude/velocity/position control for the selected flight mode and generate the associated reference trajectory. The output of the waypoint navigator is fed into the

[1] More aggressive maneuvers or some combination of the listed flight modes are possible: the former include barrel-role, split-s, 540-degree stall turn and so on. The latter include forward take-off, cruise while climbing and so on. In this research, we limit our scope to the listed *conventional* flights.

[2] Some type of fixed-wing aircrafts, especially those with thrust-vectoring, can have very versatile flight characteristics. In this research, we will consider more *conventional* flight patterns.

regulation layer. We choose the multi-loop SISO controller proposed in Section 4.1.1 because of its simple structure and acceptable performance that has been validated in a series of test flights.

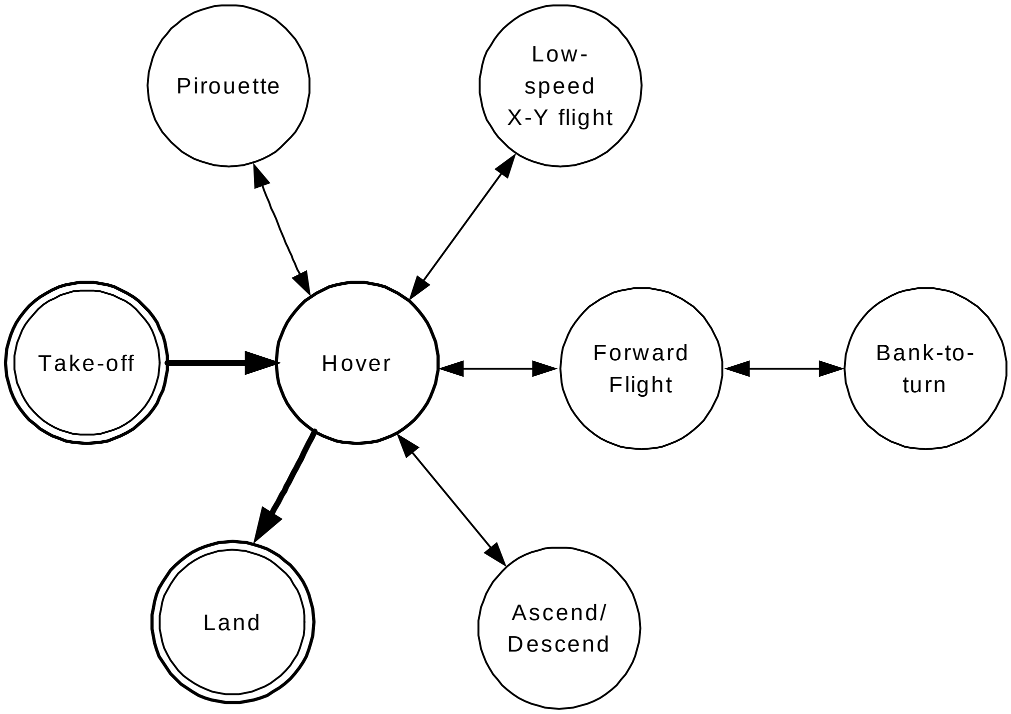

Figure 4.24 State transition diagram of helicopter control

In the following, the detailed definition of these modes are given:

- **Take-off**

Take-off mode is the starting point for all RUAV missions. In the beginning of this mode, the helicopter rests still on the ground with engine on idle. The autopilot commands the aircraft to reach the target altitude while the horizontal deviation is kept minimal. Once the aircraft reaches the target altitude, it is ready to make transition to other possible flight modes. Here follows the formal definition of the take-off mode:

$$\begin{bmatrix} X_0 \\ Y_0 \\ Z_0 \\ \Psi_0 \end{bmatrix}_{t_{initial}} \rightarrow \begin{bmatrix} X_0 \\ Y_0 \\ Z_{Hover} \\ \Psi_0 \end{bmatrix}_{t_{final}} \tag{4.18}$$

where Z_{Hover} is the target hover altitude

Apparently, a more aggressive way such as jump take-off is also possible. In this case, the helicopter gains forward velocity as well as altitude simultaneously. This is in fact the combination of the take-off mode and the forward flight according to our definition. In our study, we exclude this mode for simplicity. Under this assumption, the first flight mode right after take-off is enforced to be the hover mode.

- **Hover**

Hover indicates the state where the RUAV stays in the air with negligible speed and heading change. This is the most essential flight mode to be accomplished by the autopilot system because almost all flight patterns go through the hover mode. During this mode, the requirement given in (4.19) should be satisfied.

From the view of the helicopter dynamics, the hover mode is considered as the state where the influence of inflow on the rotor dynamics is negligible. Our own analysis shows that the influence of the inflow is negligible up to 5 m/s in horizontal direction. Therefore, we may use the hover controller for the control of low-speed forward flight, sideslip, pirouette and ascent/descent by feeding in appropriate reference inputs to the appropriate channels.

$$\begin{aligned}
&\max_t \left| X(t) - X_{ref} \right| \le X_{tol} \\
&\max_t \left| Y(t) - Y_{ref} \right| \le Y_{tol} \\
&\max_t \left| Z(t) - Z_{ref} \right| \le Z_{tol} \\
&\max_t \left| \Psi(t) - \Psi_{ref} \right| \le \Psi_{tol}
\end{aligned} \tag{4.19}$$

$$\text{for } \forall \mathrm{t} \in [\mathrm{t}_{\mathrm{initial},} \mathrm{t}_{\mathrm{final}}]$$

- **Landing**

Landing is the opposite of the take-off mode in most aspects. This mode is entered from hover by initiating a descent. At first, the autopilot system calculates the relative altitude, i.e., the relative distance from the helicopter to the ground downright, using relative sensors such as the ultrasonic altimeter or laser range finder and then generates the landing profile accordingly. The vehicle descends slowly until it touches the ground. The touchdown is detected securely by the four ground contact switches mounted on the landing gear. Once the touchdown is detected, the autopilot system reduces the engine RPM to idle and the main rotor collective pitch to zero. Then the vehicle goes into the wait state until the mission is over or it resumes a new operation. The definition of landing mode is given as:

$$\begin{bmatrix} X_0 \\ Y_0 \\ Z_{Hover} \\ \Psi_0 \end{bmatrix}_{t_{initial}} \rightarrow \begin{bmatrix} X_0 \\ Y_0 \\ Z_{Ground} \\ \Psi_0 \end{bmatrix}_{t_{final}} \tag{4.20}$$

- **Forward Flight**

Forward flight is the state in which the helicopter gains and maintains nonzero forward velocity while the heading is generally kept tangent to the flight path. This is the primary maneuver used to visit the distant waypoints. This mode is divided into three phases: (1) acceleration, (2) cruise with constant velocity, and (3) deceleration to stop if required. When the helicopter enters the forward flight mode from hover, the forward velocity is controlled to follow certain profile while the lateral velocity is regulated to zero. The forward velocity is attained by tilting the thrust of main rotor slightly to forward direction through the longitudinal cyclic pitch control. Then the vehicle starts accelerating in the forward direction. As the main rotor thrust is tilted forward by the longitudinal cyclic pitch, the vertical component decreases, causing the vehicle to lose altitude. To compensate this slight loss in the vertical thrust, the collective pitch would be increased accordingly. In automatic control, the loss of the altitude should be compensated by the separate altitude regulation loop. As the vehicle gains forward velocity, the inflow to the main rotor and tail rotor affect the overall rotor dynamics. The rotor generates more lift, known as translational lift, due to the increased amount of the inflow in unit time. The relative airspeed experienced by the blades becomes asymmetric and induces the flapping.

The forward flight can be categorized as (1) low-speed cruise and (2) high-speed cruise. The determining factor between these two flights is the significance of the influence of the inflow on main and tail rotors. The hover controller may be used if the effect of the local flow due to the forward velocity is negligible. If the vehicle reaches a significant forward speed, the rotor dynamics changes and the contributions of the fuselage, horizontal and vertical stabilizer fins grow together. In this case, a separate controller optimized for the high-speed cruise dynamics should be designed. As for now, we limit our scope to the low-speed forward flight, which can be managed by the hover controller.

The reference trajectory for the forward motion may be generated using sophisticated algorithms such as dynamics inversion. Detailed discussion will be given in the following section.

$$\begin{bmatrix} X_0 \\ Y_0 \\ Z_0 \\ \Psi_0 \end{bmatrix}_{t_{initial}} \rightarrow \begin{vmatrix} X_1 \\ Y_1 \\ Z_1 \\ \Psi_1 \end{vmatrix}_{t_{final}} \tag{4.21}$$

while tracking

$$\begin{aligned} & u(t) \rightarrow u_{ref}(t) \\ & \max_t |v(t)| \le v_{tol} \\ & w(t) \rightarrow w_{ref}(t) \\ & \Psi(t) \rightarrow \text{atan}\,2(V_y^{TP}(t)\big|_{ref}, V_x^{TP}(t)\big|_{ref}) \end{aligned} \tag{4.22}$$

- **Low-speed flight**

This maneuver indicates the low-speed flight in x-and/or y-direction. In this mode, the influence of inflow on rotors, fuselage, and stabilizer fins are small enough to be ignored and hence the use of hover control is justified. In this mode, the helicopter is controlled to have longitudinal as well as lateral velocity to reach the target waypoint. The heading is maintained constant independent from the direction of the flight path. The waypoint navigator generates the reference trajectory as shown in (4.24). Although the rotor dynamics is symmetric because of the symmetric geometry of rotor, the responses in the x and y directions are slightly different due to the asymmetric mass moment of inertia in x and y axis. In the y-direction, the fuselage receives more wind drag and the tail rotor dynamics is affected in a different manner.

$$\begin{bmatrix} X_0 \\ Y_0 \\ Z_0 \\ \Psi_0 \end{bmatrix}_{t_{initial}} \rightarrow \begin{vmatrix} X_1 \\ Y_1 \\ Z_1 \\ \Psi_0 \end{vmatrix}_{t_{final}} \tag{4.23}$$

while tracking

$$\begin{aligned} & u(t) \rightarrow u_{ref}(t) \\ & v(t) \rightarrow u_{ref}(t) \\ & w(t) \rightarrow w_{ref}(t) \\ & \Psi(t) \rightarrow \Psi_{ref}\big|_{\text{constant}} \end{aligned} \tag{4.24}$$

- Pirouette

Pirouette[1] indicates a maneuver of changing the heading with minimal velocity deviation about the main rotor axis. This mode is mainly controlled by the tail rotor collective pitch with compensating inputs from other channels. The unbalanced lateral force of the tail rotor should be canceled by the cyclic pitch of main rotor in roll direction. The engine RPM perturbation due to the tail rotor pitch variation should be regulated by the engine governor.

$$\begin{aligned} &\max_t |u(t)| \le u_{tol} \\ &\max_t |v(t)| \le v_{tol} \\ &\max_t |w(t)| \le w_{tol} \\ &\Psi(t) \to \Psi_{ref}(t) \end{aligned} \tag{4.25}$$

- Ascent/Descent

This flight mode indicates, in a narrow sense, the vertical motion while horizontal velocity and the heading deviation are kept minimal. The vertical mode is dominantly controlled by the main rotor collective pitch. During ascent, the rotor has to generate more lift by increasing the pitch. This alone requires more power from the power plant. The vertical velocity of the helicopter affects the lift generation of the rotor and imposes additional drag on the blade, which requires more power. Therefore, the rate of ascent is limited by the maximum horsepower of the engine.

The behavior with the descent mode is more complicated than ascent. A low-rate descent is achieved by slightly decreasing the main rotor collective pitch and, in turn, main rotor thrust. When the helicopter descends faster to reach the same speed of the induced velocity of main rotor, the blades are unable to push down air and cannot produce thrust any more. This dangerous state is called *vortex ring* and it should be avoided because in this state the control over the vehicle is simply lost. If the vehicle manages to pass this region quickly and descends faster, the rotor enters the windmill state and it begins to *receive* power from the passing air. With the proper collective pitch, the vehicle finds an equilibrium in vertical descent and this state can be sustained. This condition is called *autorotation* and it corresponds to the gliding of fixed-wing aircrafts. In the case of engine malfunction, the pilot can disconnect the dead engine output shaft with the main rotor shaft, let the main rotor enter the autorotation state, and safely land the vehicle.

[1] This French word originally means a full turn on the toe or ball of one foot in ballet. In this paper, the term "pirouette" is favored over "turn" because the latter word may be confusing to indicate "turn" about a fixed axis or "bank-to-turn" at higher forward velocity.

Although we do not need to be concerned too much with this advanced capability of the rotorcraft for now, the autopilot should be programmed to stay off from the unsafe ascent and descent rates. These hard bounds dependent on the helicopter configuration should be considered to generate the reference trajectory by the waypoint navigator.

Ascent and descent modes can be defined as following:

$$\begin{aligned}
&\max_t \left| X(t) - X_{ref} \right| \le X_{tol} \\
&\max_t \left| Y(t) - Y_{ref} \right| \le Y_{tol} \\
&\max_t \left| \Psi(t) - \Psi_{ref} \right| \le \Psi_{tol} \\
&w(t) \to w_{ref}(t) \\
&\Psi(t) \to \Psi_{ref}
\end{aligned} \tag{4.26}$$

In general, ascent or descent may occur while the vehicle has nonzero horizontal velocity or turning rate. From the viewpoint of dynamics and control, the vertical mode is relatively less coupled with horizontal mode so that the simultaneous control of horizontal and vertical velocity may be achieved easily. During ascent or descent, the tail rotor collective pitch should be controlled accordingly to counteract the change in the anti-torque of the main rotor, which is the function of main rotor collective pitch or thrust.

4.2.1 Vehicle Control Language

Vehicle Control Language, or *VCL,* is a framework to describe the given mission with human-understandable form of script language. VCL includes a set of commands to realize the flight modes listed in Figure 4.24 so that a given mission can be described in a sequence of the achievable flight modes. This approach provides the isolation and abstraction between the low-level vehicle control and the mission-level condition. In this framework, the onboard autopilot system can perform any given feasible mission without any reprogramming of the onboard software as the mission changes. The sequence of motion commands is described in a script language form that is understandable to humans.

A VCL command line consists of the command verb, required parameters and optional parameters. VCL flight commands typically take the form:

command <target coordinates> options

- Command

This part of VCL script specifies the type of maneuver. Currently, `TakeoffTo`, `Hover`, `FlyTo`, `MoveTo` and `Land` commands are defined. Among these `Hover`, `FlyTo`, and `MoveTo` commands are implemented in VCL-based waypoint navigator and tested successfully as will be shown in the following section.

- Target coordinates

This part specifies the target coordinate either in absolute coordinates or in relative coordinates in the local Cartesian frame. The type of coordinates is specified by the postfix **`abs`** or **`rel.`** The absolute coordinates are referred to the origin in the test field as defined in Figure C.1 in Appendix. The relative coordinates specify the difference from the last target point specified by the previous line of VCL. If no previous value is set, the current position is taken as the base coordinates by default.

- Optional parameters

This part provides additional specifiers to shape the flight pattern. The available options depend on the preceding command part. If none is provided, the default values stored in the VCL interpreter will be used. The registered optional parameters are shown below.

In the following, the syntax of currently implemented VCL commands is given.

`TakeoffTo` <coord>{abs,rel}

: Initiate take-off maneuver to the target altitude

`Hover` `<coord>{`**`abs,rel`**`} {`**`heading`**`=<heading>{`**`deg,rad`**`}}`
`<duration> {`**`sec,min`**`}`

: hover with given heading angle for given time

`FlyTo` `<coord>{`**`abs,rel`**`}`
`{`**`vel=`**`<velocity>{`**`mps,kmps,fps,knots,mph`**`}} {passby,stopover}`
`{autoheading, heading=<heading>{deg,rad}}`

: cruise to certain waypoint stopping over or passing by

MoveTo <coord>{**abs,rel**}
{**vel=**<velocity>{**mps,kmps,fps,knots,mph**}} {**autoheading**,
heading=<heading>{**deg,rad**}}
: move to certain way point to stopover with fixed heading

BankToTurn <heading change>{**deg,rad**} {{**radius**}<radius>{**m,ft**}}
{{**vel**=<velocity>{**mps,kmps,fps,knots,mph**}
: Perform bank-to-turn during cruise

Land : Perform automatic landing

More detailed descriptions about the actual operation will be given as below.

4.2.2 Operation of VCL-based Waypoint Navigator

VCL described in the previous section is executed in a hierarchical structure as shown in Figure 4.25. The VCL module consists of a user interface part on the ground station, a language interpreter, and a sequencer on the UAV side. When a mission is given, the ground operator specifies a sequence of waypoints with their attributes such as the type of waypoint, heading, velocity, etc. When a mission is given, the corresponding VCL command file is uploaded to the RUAV control system and then executed in a sequential manner. The VCL execution module (VCLEM) selects the proper controller for the flight mode and generates the reference command. VCLEM monitors the vehicle trajectory and determines if one sequence is finished or not. It also monitors the vehicle status for possible troubles in sensor or the vehicle itself. If an error is detected, the fault detection algorithm shown in Figure 4.8 is activated and a proper error handling measure is executed. In the worst case, the VCL releases the automatic vehicle control mode and returns the control to the safety pilot. This routine is repeated until the end of VCL command script is reached and the RUAV returns to its default flight mode. In the following, the keywords and syntax of VCL are shown. Currently the VCL vocabulary covers the basic maneuvers, and it will be expanded as more flight modes are realized.

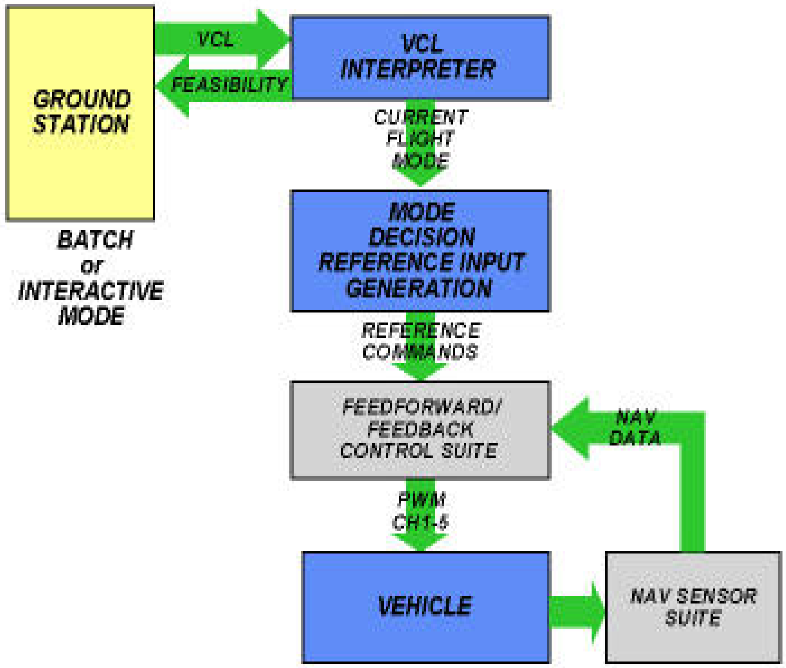

Figure 4.25 Hierarchical architecture of VCL processing

In the following, the descriptions of registered VCL commands are given.

1. **`TakeoffTo`**

This command requests the waypoint navigator to perform the take-off maneuver. To take off, the main rotor should generate enough lift to counteract the weight of the vehicle. The take-off procedure requires a sophisticated coordination of three control inputs: engine throttle, main rotor collective pitch and the tail rotor collective pitch. At the first stage, the engine RPM is increased until the hover RPM while the collective pitch is fixed to a minimal value around 0 degree. Once the engine RPM is kept constant, the main rotor collective pitch is gradually increased so that the vehicle follows the vertical motion profile. The throttle valve of the engine is controlled accordingly to provide enough power to meet the demand of the increasing load of the main rotor at constant RPM. Although tail rotor does not provide the vertical thrust, it should be controlled to counteract the increasing anti-torque of the main rotor so that the heading is kept constant. The take-off mode finishes when it reaches the target altitude and the autopilot automatically makes transitions to the hover mode.

In terms of controller design, it is worthwhile to examine the transition that the helicopter dynamics go through during take-off. As the lift increases, the landing gear receives less support and constraint forces by the ground surface. Before take-off, the ground supports the entire weight of the helicopter.

As the main rotor rotates and generates the lift, the ground supports less portion of the weight. The friction force exerted by the ground also gets smaller and the helicopter starts drifting. The lateral force of the tail rotor acts to tip off the helicopter when on the ground and acts to drift sideway when airborne. The main rotor goes through a transition in terms of the ground effect. When the helicopter is on the ground, the ground effect is strongest and it becomes weaker as the helicopter gains altitude. The take-off controller should be robust or adaptive enough to cope with the uncertainty and the disturbance that the helicopter experiences during this mode.

2. `Hover`

Hover is the most important flight mode to implement because of its significance in many ways. Hover is a very unique and useful maneuver that a rotorcraft is specialized to offer. Although hover indicates the stationary flight in the air, the `Hover` command is also able to perform the heading change by providing the target heading in the VCL. In this sense, the `Hover` command covers the hover and pirouette flight mode defined in Figure 4.24. In `Hover` command, all the loops in multi-loop SISO controller (Figure 4.8) are activated to stay at the given coordinate while tracking the reference heading. When the requested heading in the VCL line is different from the current heading, a smooth heading command is issued by the waypoint navigator as shown in Figure 4.26

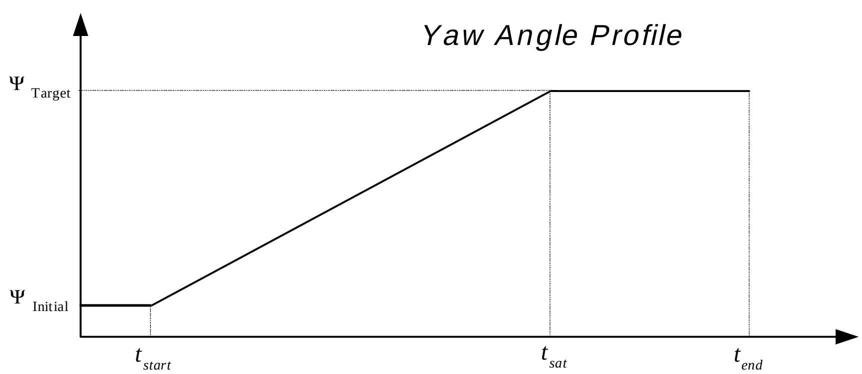

Figure 4.26 Reference yaw angle profile

3. `FlyTo`

FlyTo is the primary command to move between relatively distant waypoints with accuracy. In this flight mode, the vehicle turns to the target waypoint and then goes through (1) acceleration, (2) cruises, and (3) deceleration phases constrained by the predefined or VCL-specified maximum velocity. The heading is constantly controlled during the whole period of this moment to point the target waypoint. Since the helicopter can stop over a point during a flight, the waypoint can be either a *stop-over* or a more conventional *pass-by* waypoint. As implied in the name, the stop-over waypoint is where the helicopter should stop and hover. The pass-by waypoint is where the helicopter should go through without stopping over.

The `FlyTo` maneuver is controlled by the hover controller developed in Section 4.1.1 under the assumption of low-speed flight. The waypoint navigator generates the reference values for velocity, position, and heading and passes them to the low-level controller in realtime. As a starting point, we use a heuristic trajectory profile for forward flight. Typically, the vehicle maintains a constant ground speed while the heading remains fixed. Therefore, the waypoint navigator should generate the reference commands in the following way:

- Altitude: constant
- Heading: constant
- Longitudinal maneuver: follow the trajectory (Figure 4.27)
- Lateral velocity: zero

Explicit coordinate transformation as a function of heading is performed for the linear controller.

4. **`MoveTo`**

`MoveTo` is a special low-speed maneuver developed for ground object tracking in the *pursuit-evasion game* [2,3]. In this game, helicopters, as the aerial pursuers track the ground-based evaders following a sequence of waypoints that is generated by the strategic planner. This maneuver allows sideslip as well as forward/rearward motion with fixed heading so that the coordination of the heading with the flight direction is kept simple. The fixed heading has another advantages in terms of camera frame compensation and emergency take-over by the ground pilot.

For this maneuver, the base hover controller in Section 4.1.1 is again adopted. The controller receives the reference trajectories *both* in x and y direction while the heading is regulated to the requested heading by VCL or the default value if none is specified. The reference trajectories are similar with the one for `FlyTo` command. The following reference commands are passed to the regulation layer.

- Altitude: constant
- Heading: constant
- Longitudinal maneuver: follow the trajectory (Figure 4.27)
- Lateral maneuver: follow the trajectory (Figure 4.27)

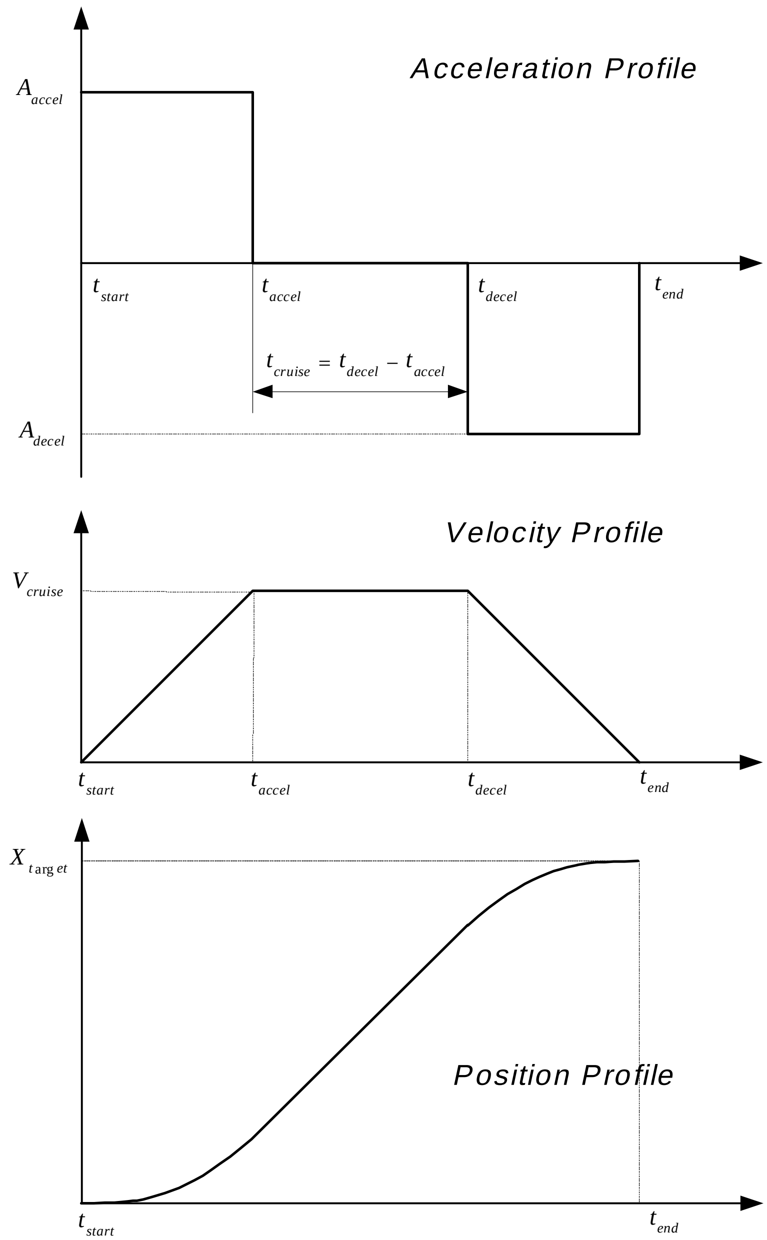

Figure 4.27 The acceleration, velocity, and position profile for low-speed forward flight

The VCL-based navigation can be executed in a batch mode or in an interactive mode. In batch mode, a VCL file is uploaded to the helicopter and the VCLEM sequences through the give command. In interactive mode, the VCLEM waits for the request from the ground station or any authorized source and execute the received VCL line and goes back to stand-by hover maneuver. A flowchart for the batch mode is given in Figure 4.28.

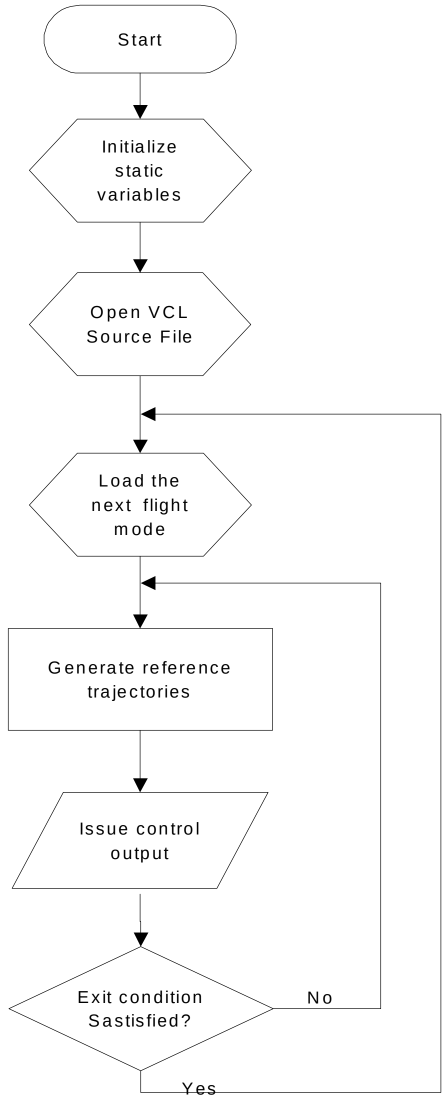

Figure 4.28 Flowchart of VCL-based waypoint navigation in batch mode

4.2.3 Validation of Waypoint Navigator

Validating the waypoint navigation algorithm is a non-trivial problem because some part of the flight control logic cannot be checked during simple ground tests due to flight conditions. For example, reaching some waypoints is simply not reproducible on the ground. Hence, some method should be devised in order to fully validate the navigation algorithm and avoid any fatal consequences during the flight experiments. In this research, an ingenious validation method exploiting the support for the MATLAB/Simulink S-function written in C is developed. This approach exploits the resemblance of the execution mechanism of the S-function in Simulink and QNX FCS. The Simulink integration engine calls the simulation blocks including S-function blocks at certain rates requested by each block. In the QNX FCS, the VCL navigator is called right after the navigation data from the DQI-NP INS is read every 20ms. Based on this observation, the VCL code can be tested in the Simulink environment.

The navigation code is first divided into two parts of the *wrapper* and the core codes for the navigation control logic part. The individual wrapper codes are required for the Simulink environment and QNX RTOS. The wrapper for Simulink interfaces the core code with Simulink numerical integration engine. More specifically, the wrapper decomposes the incoming signal vector into a suitable data structure used in VCL core code, and formats the control command into an outgoing signal vector. Likewise, to maintain compatibility of the VCL core code, a similar wrapper is written for the QNX environment, which performs almost identical tasks differing only in the actual data structure. Once the functionality of these wrappers is fully validated, then we can concentrate on the development of VCL core code by testing various approaches without fatal accidents during the test flights. Another great benefit is that the fully validated VCL by Simulink has a good chance of functioning correctly in the actual test flight when used with high-accuracy simulation model. During a series of flight experiments, this claim turned out to be true because the flight results of VCL implementations showed very similar behavior to the simulation results.

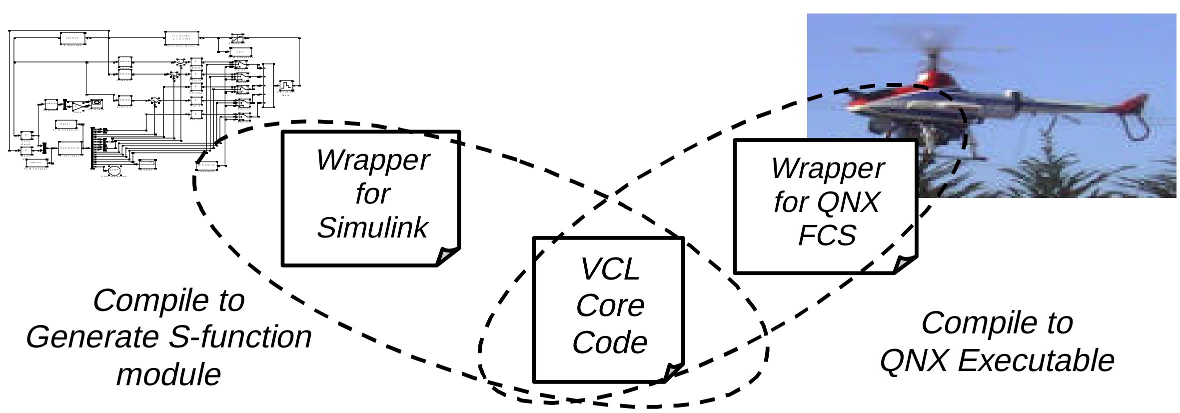

Figure 4.29 The validation method using MATLAB/Simulink

The proposed VCL processor is implemented in the onboard flight software. This software is first validated in MATLAB/Simulink and is then tested in real flight conditions. In the following section, the simulation results and the actual experiments of VCL are given. Figure 4.31 shows some sample VCL code describing a sweeping path of a certain area. Figure 4.34 shows a sequence of `MoveTo` maneuvers, which simulates the waypoint request by a strategy planner for pursuit-evasion game. As those graphs suggests, the VCL processor could execute the requested maneuvers with acceptable accuracy.

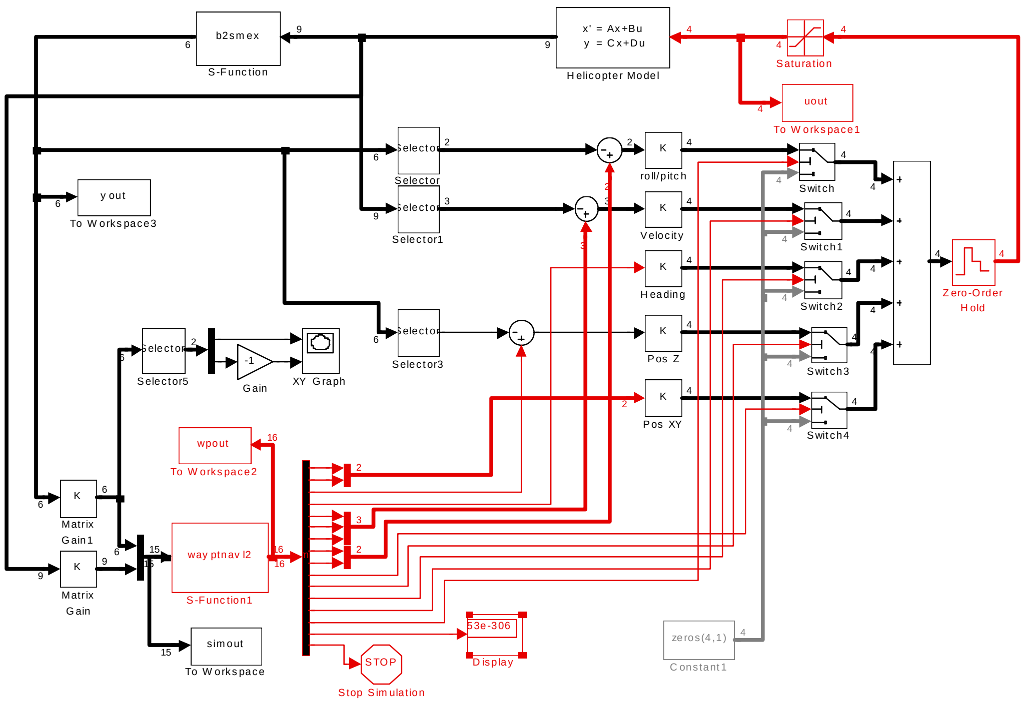

Figure 4.30 Simulink model for waypoint navigation

It should be noted, however, that validation in more detail should be performed by a *hardware-in-the-loop* simulation scheme because the proposed method using Simulink validates only the control and sequencing logic part of VCL in C-code form. The true behavior of FCS software when implemented on a PC board running QNX RTOS is affected by the factors related to hardware-specific problems of sensors and realtime performance of realtime software. Currently, research efforts are being made to construct a hardware-in-the-loop simulator running a realtime simulation model.

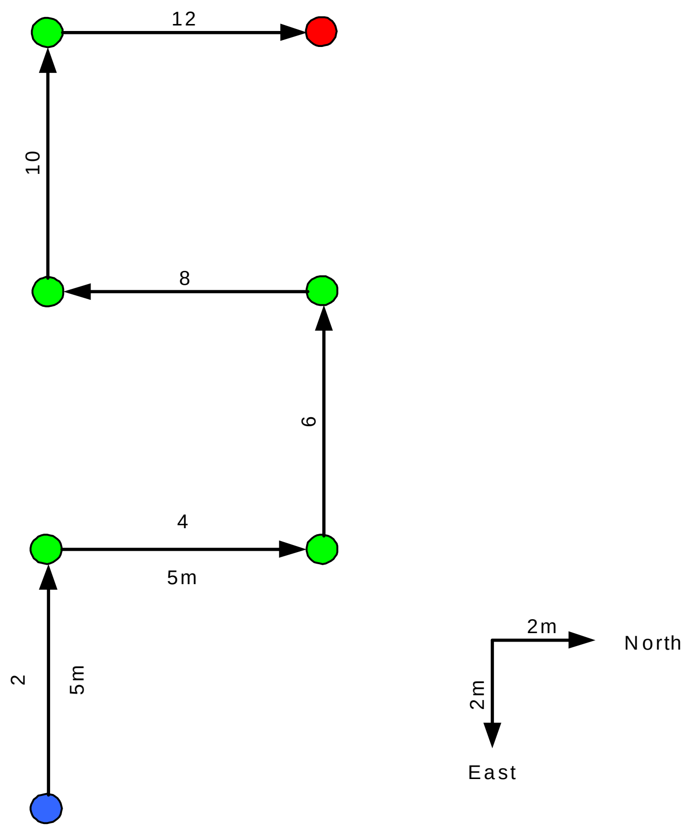


```
 1: Hover (0,0,0)rel heading=270deg duration=10sec;
 2: FlyTo (0,-5,0)rel vel=0.5m/s stopover autoheading;
 3: Hover (0,0,0)rel heading=0deg duration=10sec;
 4: FlyTo (5,0,0)rel vel=0.5mps stopover autoheading;
 5: Hover (0,0,0)rel heading=270deg duration=10sec;
 6: FlyTo (0,-5,0)rel vel=0.5m/s stopover autoheading;
 7: Hover (0,0,0)rel heading=180deg duration=10sec;
 8: FlyTo (-5,0,0)rel vel=0.5mps stopover autoheading;
 9: Hover (0,0,0)rel heading=270deg duration=10sec;
10: FlyTo (0,-5,0)rel vel=0.5m/s stopover autoheading;
11: Hover (0,0,0)rel heading=0deg duration=10sec;
12: FlyTo (5,0,0)rel vel=0.5mps stopover autoheading;
13: Hover (0,0,0)rel heading=270deg duration=10sec;
```

Figure 4.31 Sample VCL code for `FlyTo` maneuvers

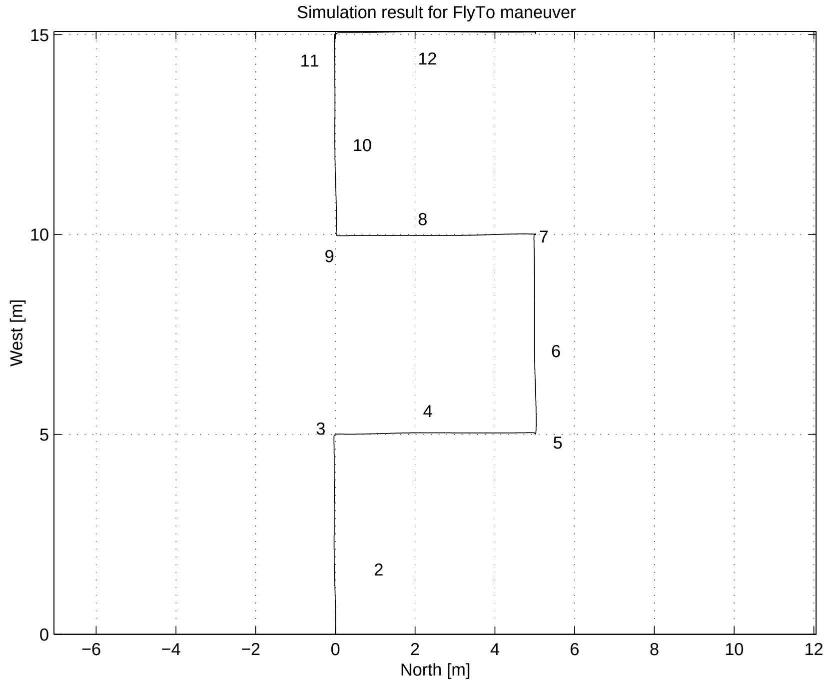

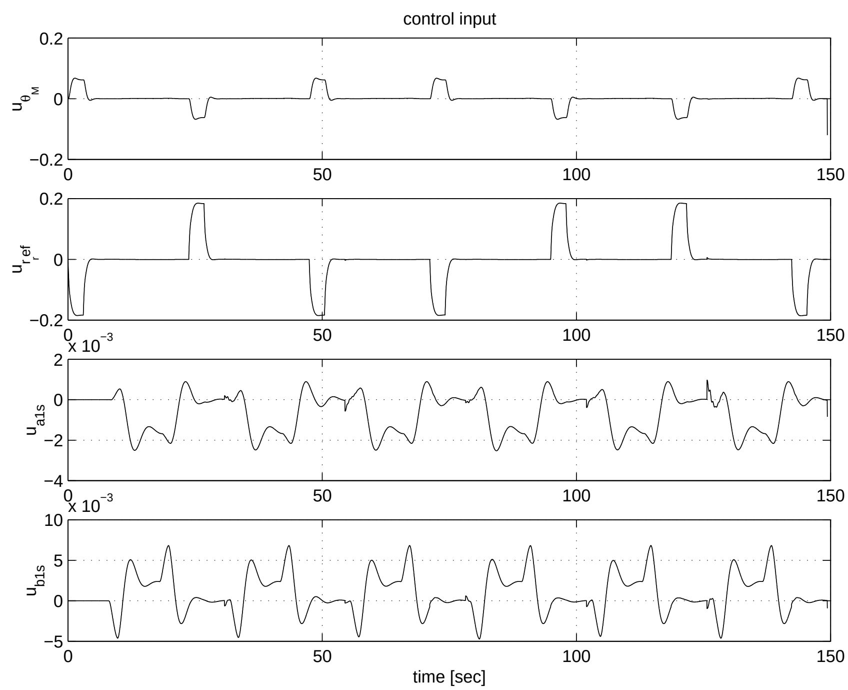

Figure 4.32 Simulation results of `FlyTo` maneuvers

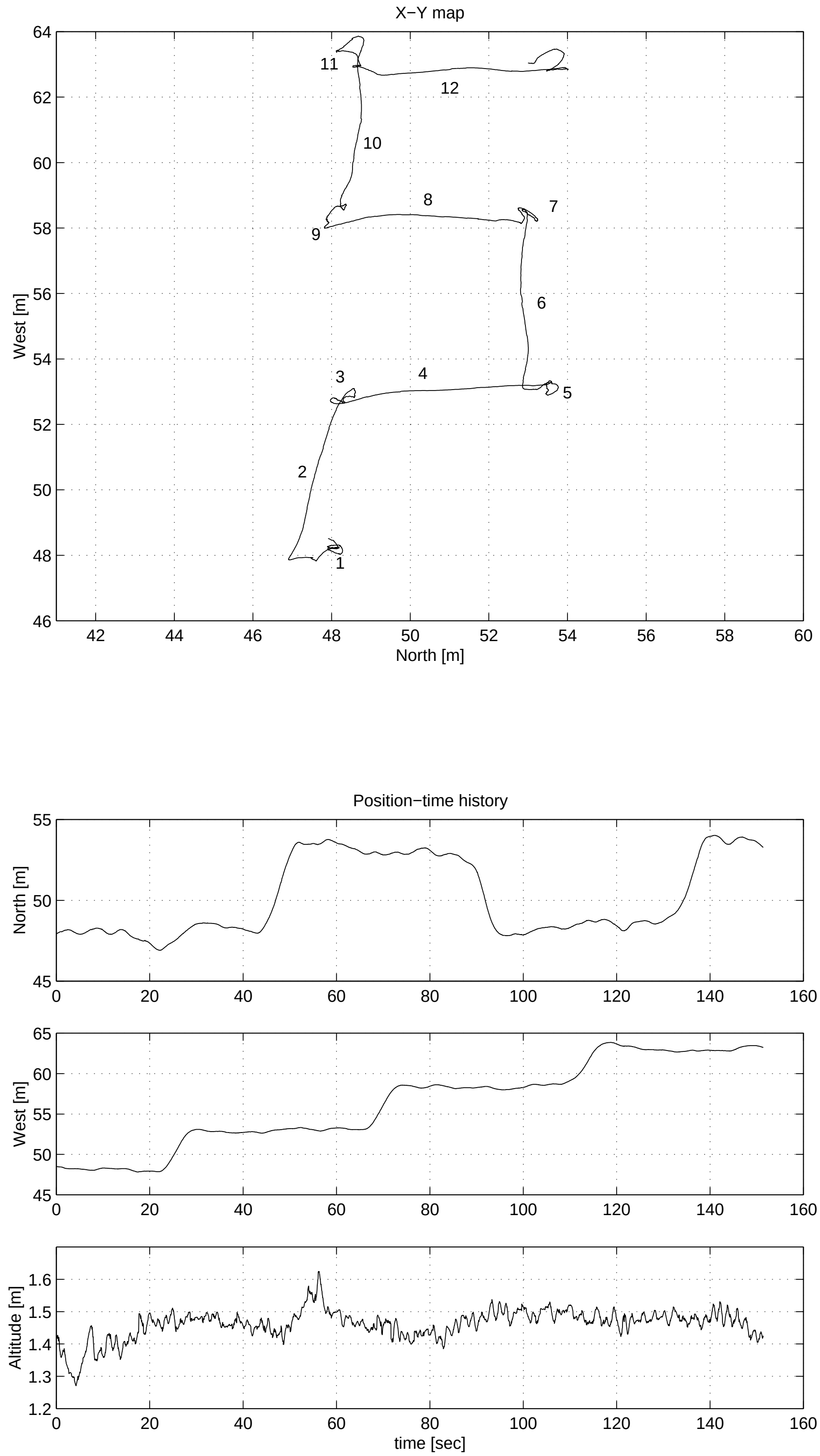

Figure 4.33 Experiment result of `FlyTo` maneuvers

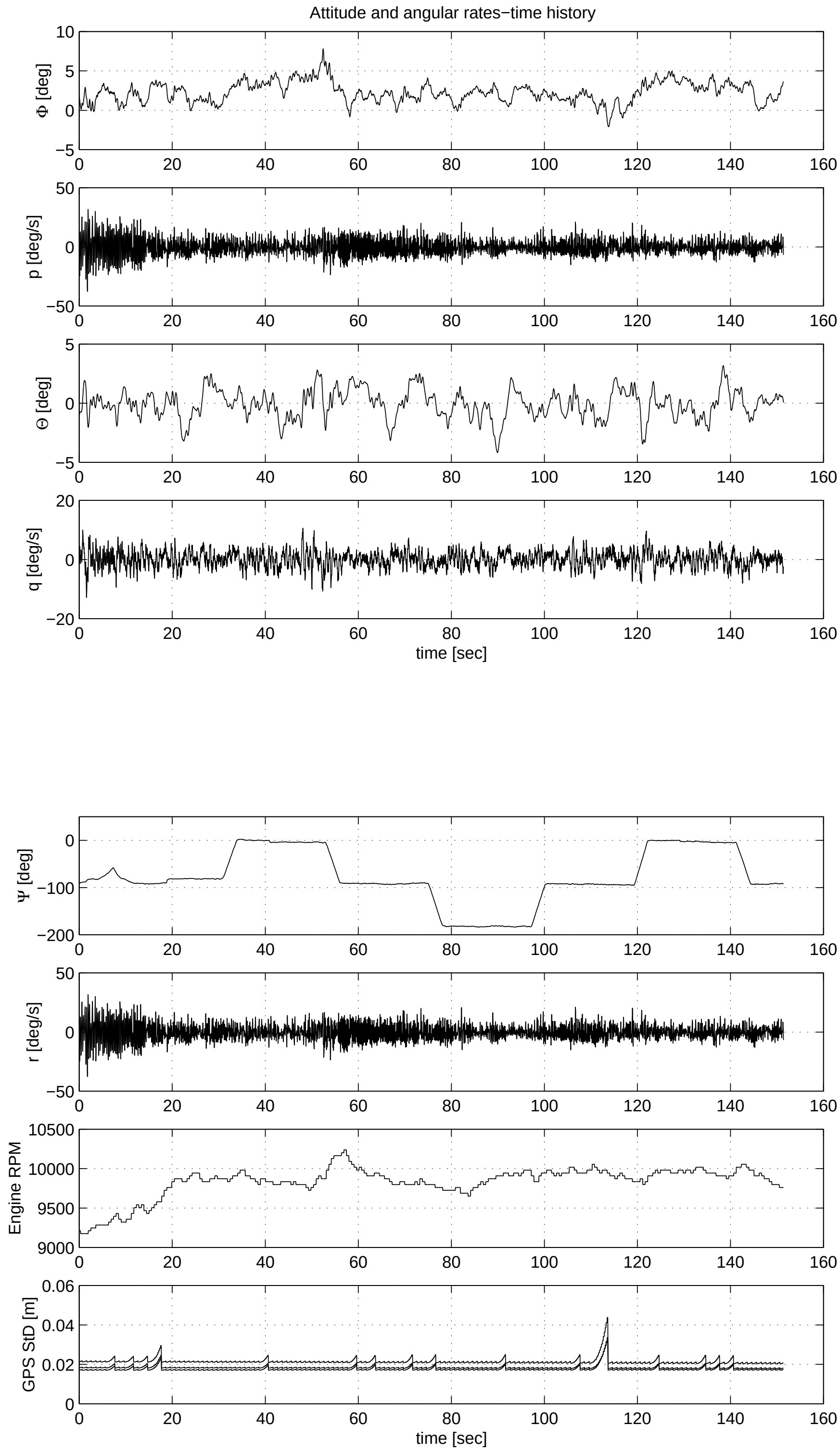

Figure 4.33 ('cont')

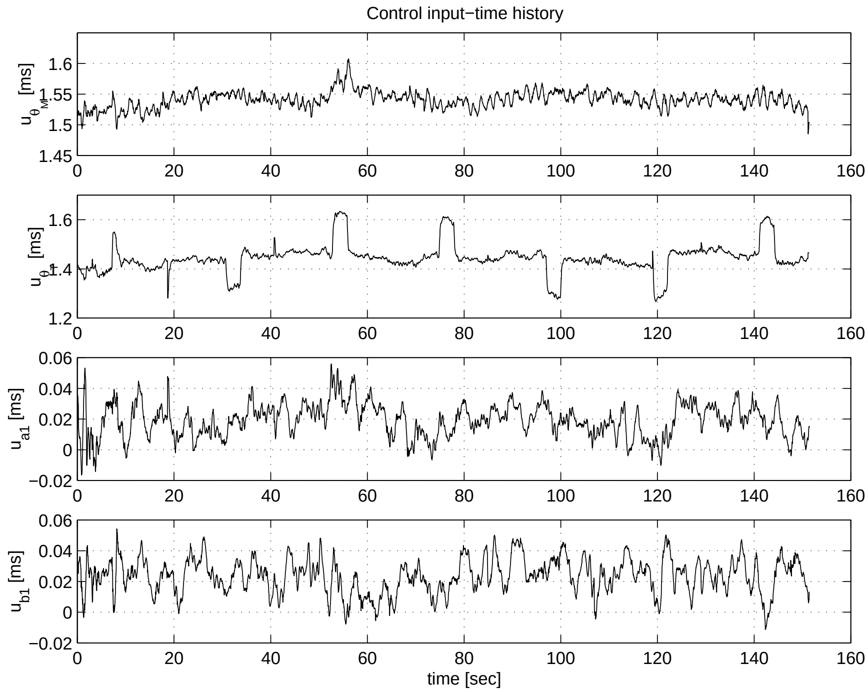

Figure 4.33 ('cont')

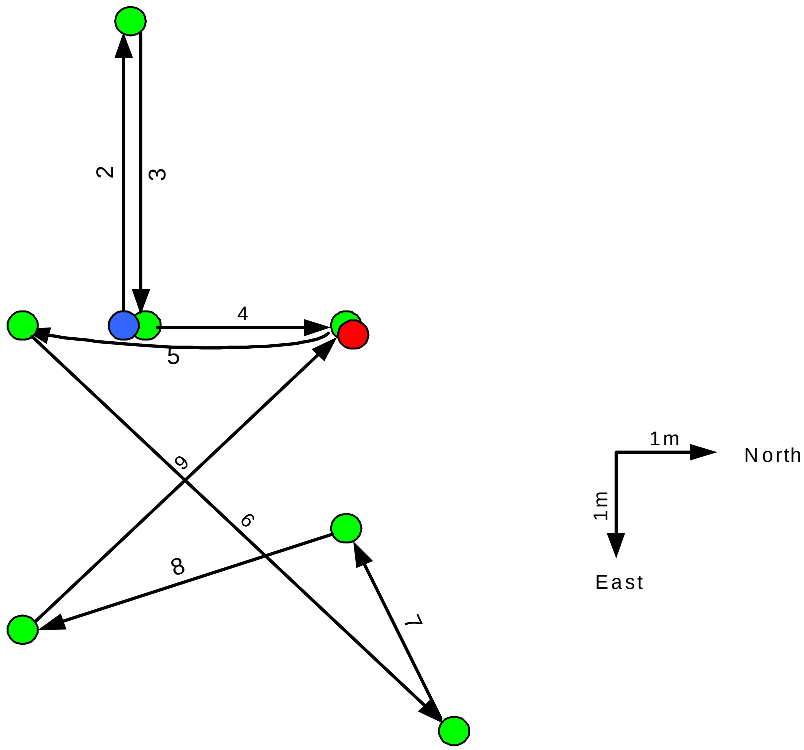


```
 1: Hover (0,0,0)rel heading=180deg duration=7sec;
 2: MoveTo (0,-3,0)rel vel=0.5m/s heading=180deg;
 3: MoveTo (0,3,0)rel vel=0.5m/s heading=180deg;
 4: MoveTo (2,0,0)rel vel=0.8m/s heading=180deg;
 5: MoveTo (-3,0,0)rel vel=0.3m/s heading=180deg;
 6: MoveTo (4,4,0)rel vel=0.2m/s heading=180deg;
 7: MoveTo (-1,-2,0)rel vel=0.2m/s heading=180deg;
 8: MoveTo (-3,1,0)rel vel=0.2m/s heading=180deg;
 9: MoveTo (3,-3,0)rel vel=0.2m/s heading=180deg;
10: Hover (0,0,0)rel heading=180deg duration=7sec;
```

Figure 4.34 Sample VCL code for `MoveTo` maneuvers

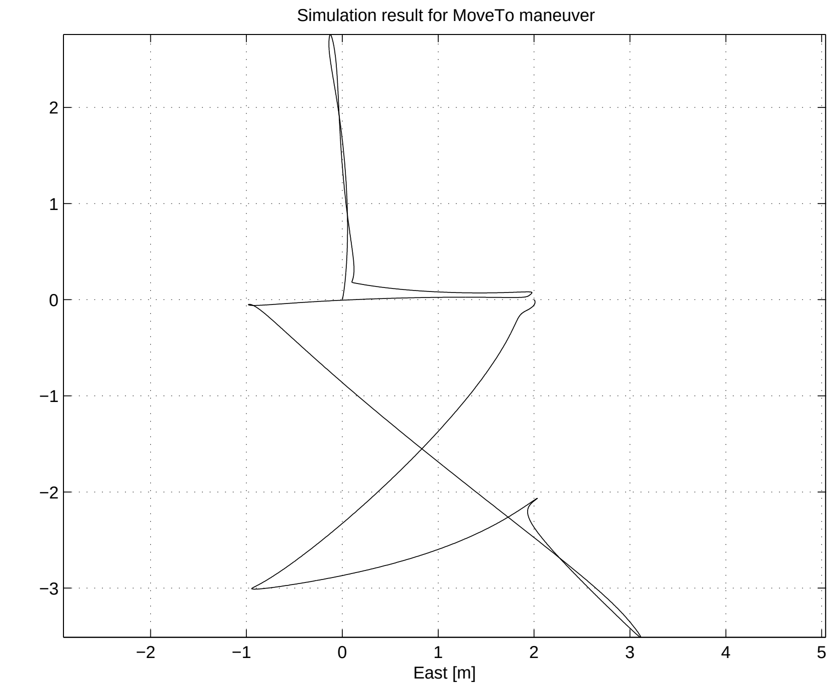

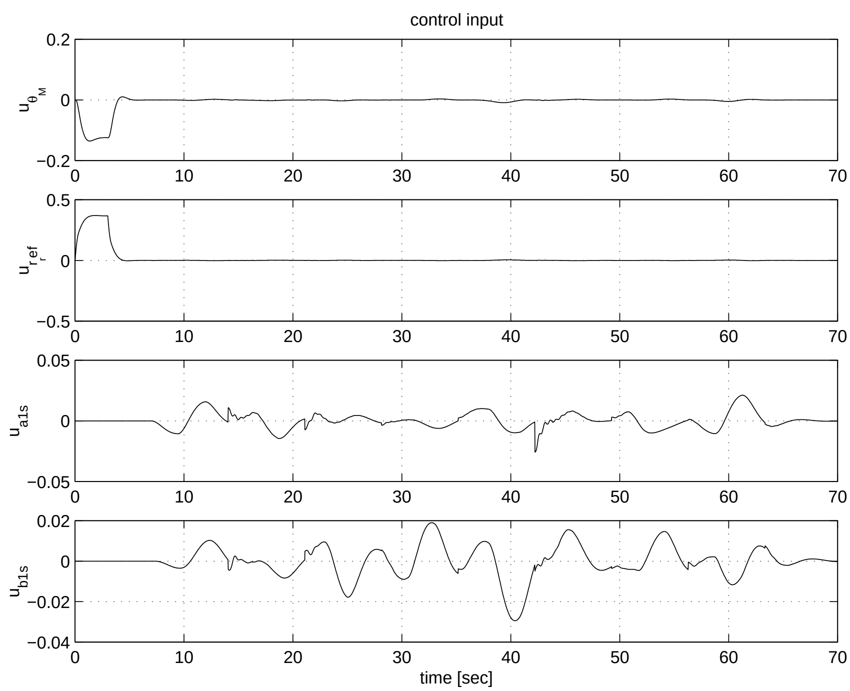

Figure 4.35 Simulation results of `MoveTo` commands

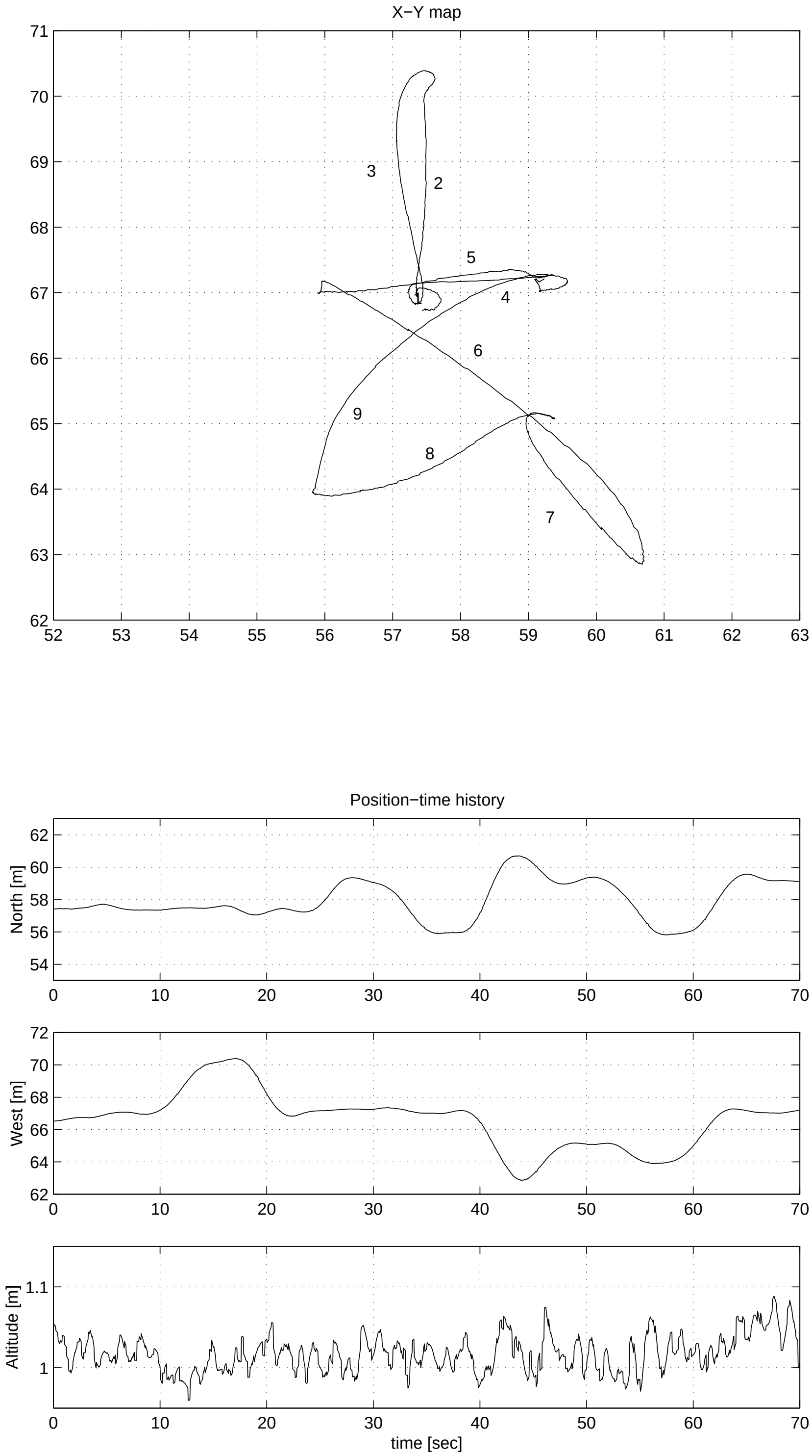

Figure 4.36 Experiment result of `MoveTo` commands in Figure 4.34

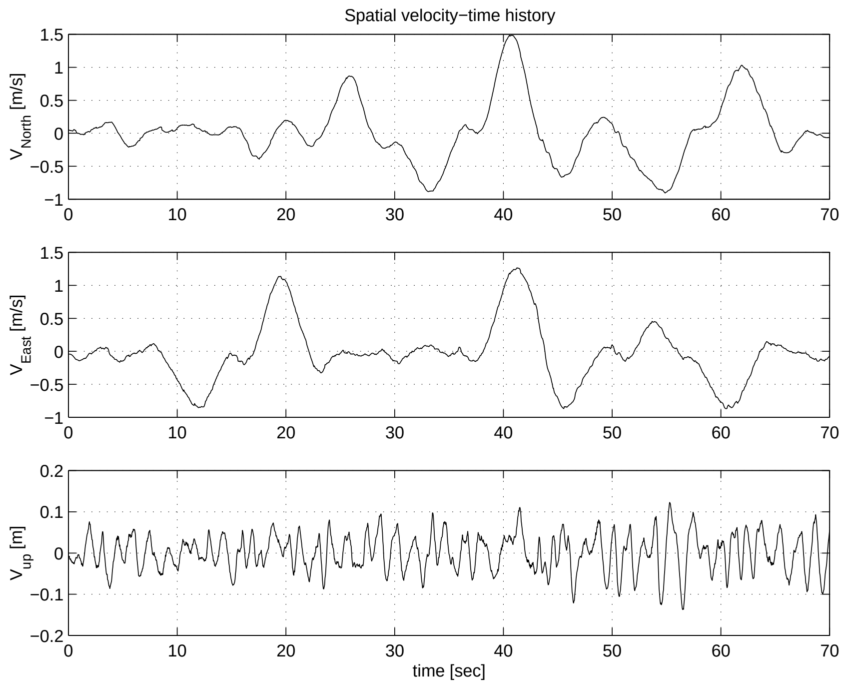

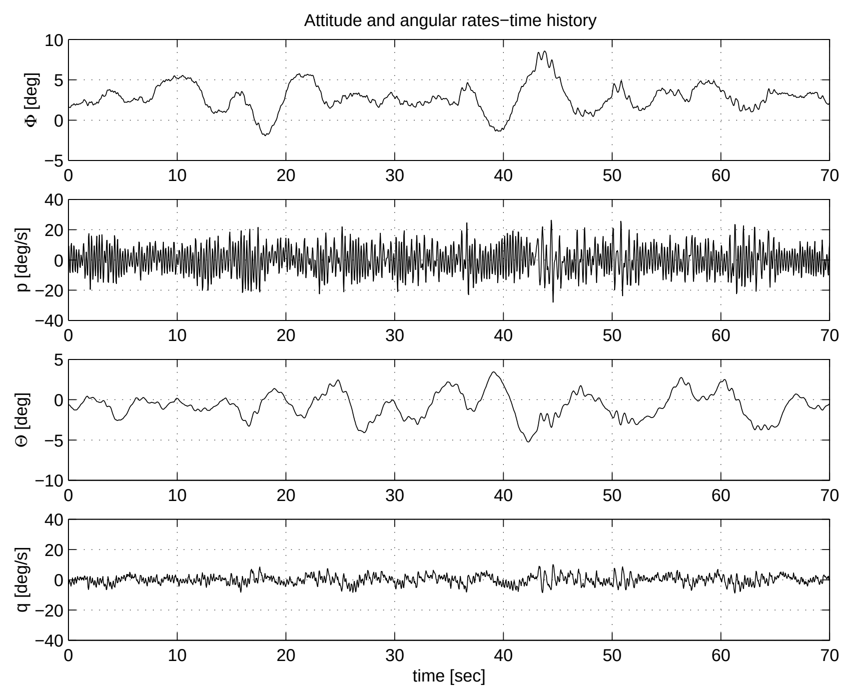

Figure 4.36 (‘cont)

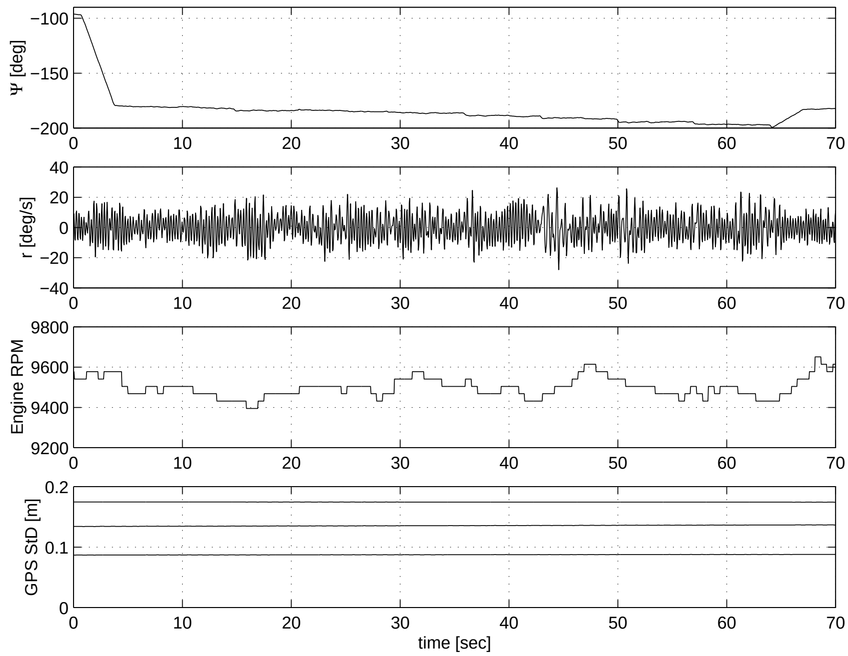

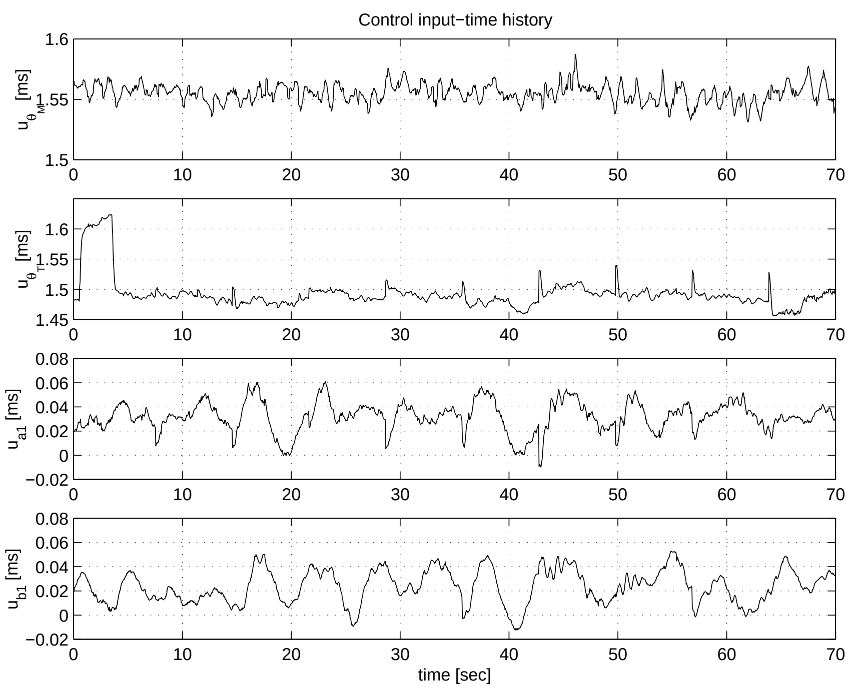

Figure 4.36 (‘cont)

Chapter 5

Conclusion

This dissertation has introduced the development of a hierarchical RUAV autopilot design which has been conducted at the University of California at Berkeley. As our goal is to build the autopilot system hardware and software and integrate these with commercially available radio-controlled helicopters whose dynamic model is not known a priori, the helicopter model, onboard hardware, software, and experimental setup have been established from the bottom to the top during the last three years. The helicopter dynamic model was found using the nonlinear aerodynamic models and was simplified to the linear hover model. Based on this LTI model for hover, two different control theories, classical SISO control and μ-synthesis control, are deployed for vehicle stabilization. Both of these have been tested in real flight experiment and shown reasonable performances. The controller for hover is designed with the linear SISO multi-loop control approach. In addition to the classical approach, the μ -synthesis attitude controller is designed and tested successfully on the Yamaha R-50. Both of these approaches showed satisfactory results. The SISO multi-loop controller is then used as the low-level vehicle stabilization layer in the hierarchical structure and it is integrated with the middle level waypoint navigator. In order to provide mission-independent universal vehicle guidance and control interface, the novel concept of VCL is proposed and implemented in Ursa Magna 2. The first-generation VCL system could perform, as promised, different missions whenever the associated VCL script file is uploaded.

The research presented in this dissertation provides the footsteps for our visionary future works. The methodology developed so far plays a crucial role in the autopilot system and the higher-level mission scenarios will be implemented and tested on top of this work in real scale. The developed methodology can be repeatedly applied to different helicopters with only minor modification and we will be able to implement a fleet of RUAV in a networked system.

As of now, the following research topics are being investigated as the ongoing effort:

- Pursuit-evasion game

The Pursuit-evasion game is a scenario that involves a multiple number of autonomous ground-based and aerial autonomous vehicles that are guided by central or distributed controllers. The goal of this game is to find the evaders in a field. The pursuer should actively build a map of the terrain and a probabilistic map to find the evaders. On the other hand, the evaders move in the field by random rule or by active evasive motion using similar map building technology. The work proposed so far makes it possible for the aerial vehicle to follow the waypoint commands received from the strategy planner, whose goal is to guide the pursuers through the optimal trajectory. Currently, the VCL command for the pursuit-evasion game is already implemented and will be integrated into the hierarchical control system for the pursuit-evasion games.

- Vision-based navigation

As mentioned, the Ursa Magna 2 is equipped with a dedicated vision processing unit (VPU). The VPU is now capable of color tracking and motion estimation using the color pan-tilt-zoom (PTZ) camera and the frame grabber. The FCS is connected with the VPU via RS-232 and sends flight information upon the request of the VPU. When the vision-based navigation is enabled, the VPU will send the navigation command to the FCS. Currently, the color tracking and motion estimation algorithm have been tested in real flight tests and the vision-based servoing algorithms are being developed and tested in the simulation environment.

- Testbed for advanced wireless communication protocol

Modern autonomous agents operate solely with wireless communication links. A clumsy umbilical cord is a thing of the past and simply unacceptable for advanced operations. Therefore, wireless communication is vital for the operation of unmanned autonomous vehicles. As the number of agents increases, the management of the wireless network also becomes an important issue to address. Currently, a joint research with Stanford Research Institute International is in progress. The unique feature of this work is that any node can be the active agent or repeater depending on the situation of the network. Therefore, if the some agents go out of the communication range of the base, the communication link can still be established if there are agents between them. The in-between agents automatically arm themselves as the repeaters and the communication packets can be relayed to/from the base in a *multi-hop*.

Another important part is the quality of service (QoS) of the network system. Among many aspects of the general term QoS, we are interested in the realtime nature of the wireless communication. The QoS of the CSMA/CD protocol, which is used currently, degrades quickly if the number of agents or the amount of data transferred increases. In some applications such as coordinated flight, the demand for realtime communication is very high and some alternative protocols are being sought.

- Coordinated flight

When multiple numbers of UAVs fly in a close range or in a potentially conflicting course, the situation has to be resolved in some way. There must be some way to know the current position of the agents in the vicinity and to estimate potential conflicts in near future. Active sensors such as vision systems or laser range finders would be one solution to detect the nearby agents. Another way is to exchange the information of the position of the participating agents via reliable realtime wireless network.

- Testbed for advanced control law

As mentioned many times, the control of a helicopter is a very challenging problem. Currently, the classical SISO approach is more widely accepted than any other advanced control theory. However, significant improvements are expected if more advanced control theories are applied with an accurate system model.

- Testbed for Open-Control Platform (OCP)

The current control system is implemented as proprietary system. Although there are many research efforts on similar helicopter control problems, the actual implementations are not compatible at all. The motivation of the OCP is the development of a unified software development and execution platform that enables formal validation and reuse of previous work. Currently, collaboration with the Boeing OCP team is underway and the new Ursa Maxima is planned to be the first UAV that flies with the OCP realtime software.

As reviewed so far, the original single UAV control problem has diversified into numerous challenging research topics. The groundwork presented in this work will enable the validation of these research topics mentioned above through actual flight tests.

Appendix A Hardware Configuration of Berkeley RUAVs

A.1 Ursa Minor 3

The key design concept of Ursa Minor 3 is a low-cost, small-size and easy-to-maintain RUAV testbed suitable for basic navigation and controller testing. The airframe itself is relatively cheaper than other larger size RUAVs and maintenance and repair work is very easy because replacement parts are readily available and not expensive. Limited by the small payload, the onboard hardware is kept minimal for basic autonomous navigation solely based on INS and GPS. At first, the communication of Ursa Minor 3 relied on the wireless modem and later it gave its way to Lucent WaveLAN(later renamed Orinoco). The flight computer consists of single stack of PC104, consisting of main CPU board, serial port extender, counter/timer board, custom take-over board,

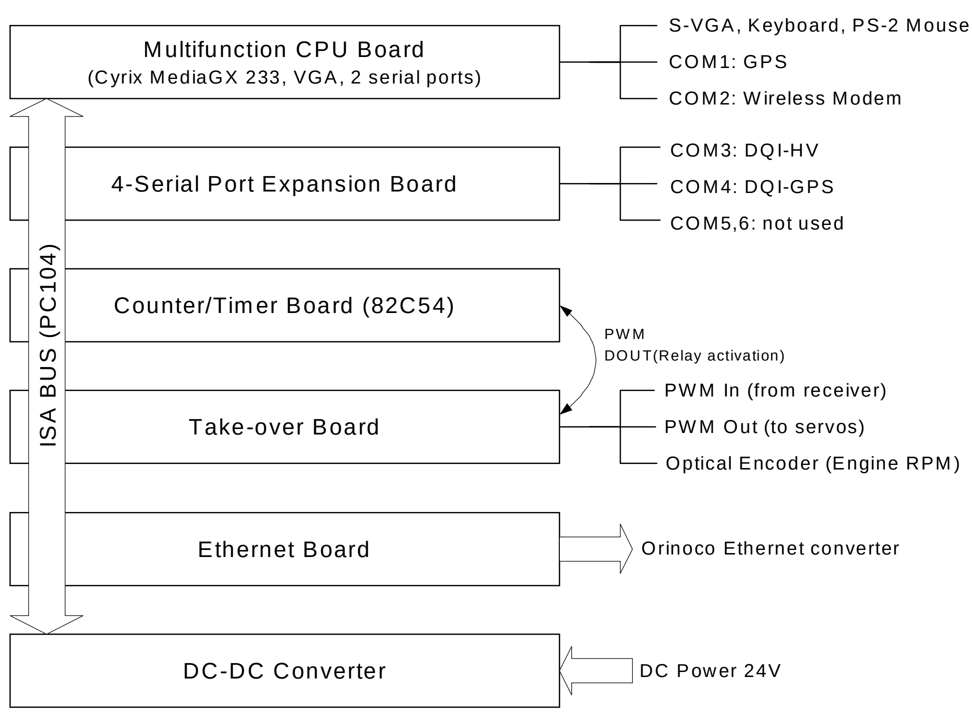

Figure A.1 Flight computer layout of Ursa Minor 3

Table A-1 Interrupt and base address setting of Ursa Minor 3 FCS

Device	Base Address	IRQ
/dev/ser1	0x3F8	3
/dev/ser2	0x2F8	4
CTC: PWM reading	0x240-0x244	5
TOB: reserved	Not Assigned	7
/dev/ser4, /dev/ser6	0x2E8, 0x2A8	10
/dev/ser3, /dev/ser5	0x3E8, 0x3A8	12
Ethernet	0x320	
LPT1	0x378	

A.2 Ursa Magna2

The Ursa Magna 2 is the primary platform for most flight tests of Berkeley RUAV research now. The Ursa Magna 2 was constructed to serve as a testbed for low-level to high-level control algorithm, vision-based navigation, and an aerial agent for pursuit-evasion game. It contains two Intel Pentium LittleBoard®, one for flight control and the other for vision processing. These boards are larger and heavier than the CPU board used for Ursa Minor 3 but offers more powerful computing capability. Due to the different board setup, a slightly different set of PC104 peripheral cards is used as shown in Figure A.2.

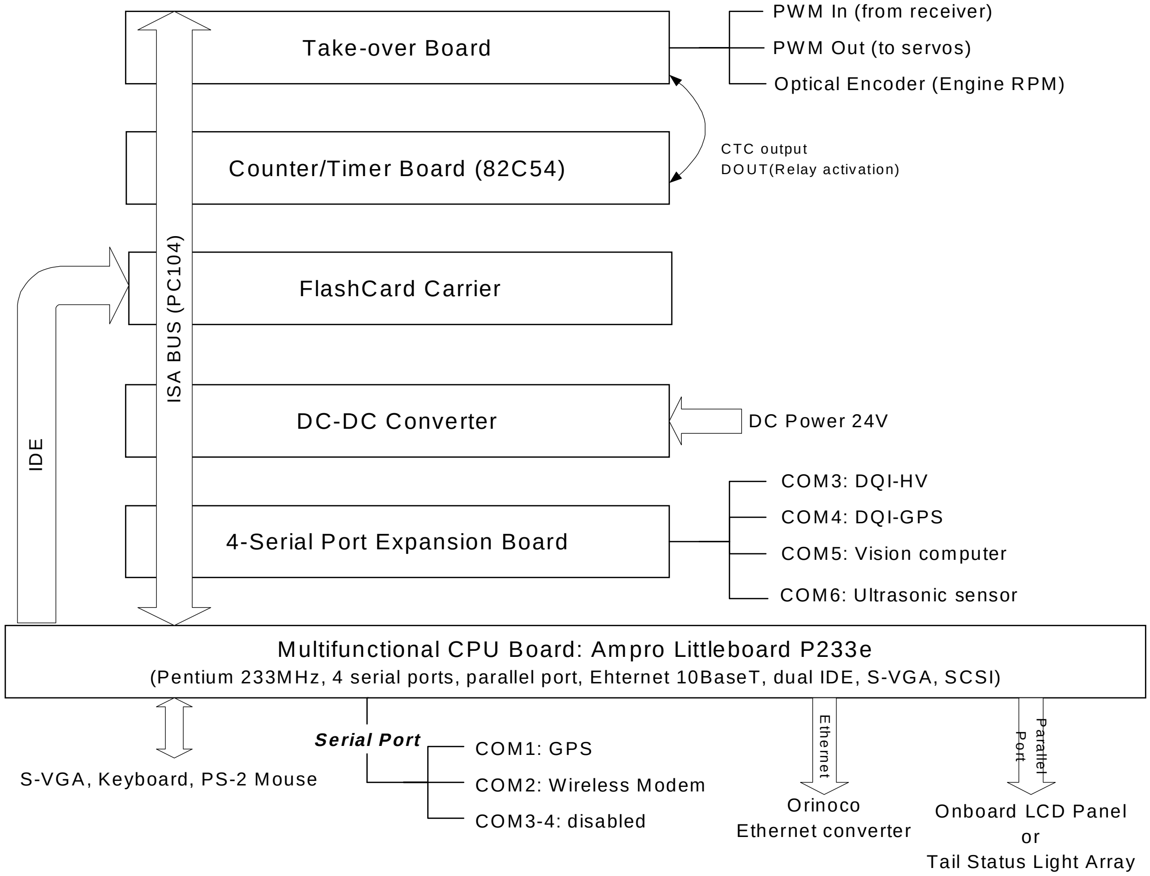

Figure A.2 Flight computer layout of Ursa Magna 2

Table A-2 Interrupt and base address setting of Ursa Magna 2 FCS

Device	Base Address	IRQ
/dev/ser1	0x3F8	3
/dev/ser2	0x2F8	4
CTC: PWM reading	0x240-0x244	5
TOB: reserved	Not Assigned	7
/dev/ser4, /dev/ser6	0x2E8, 0x2A8	10
/dev/ser3, /dev/ser5	0x3E8, 0x3A8	12
Ethernet	0x320	
LPT1	0x378	

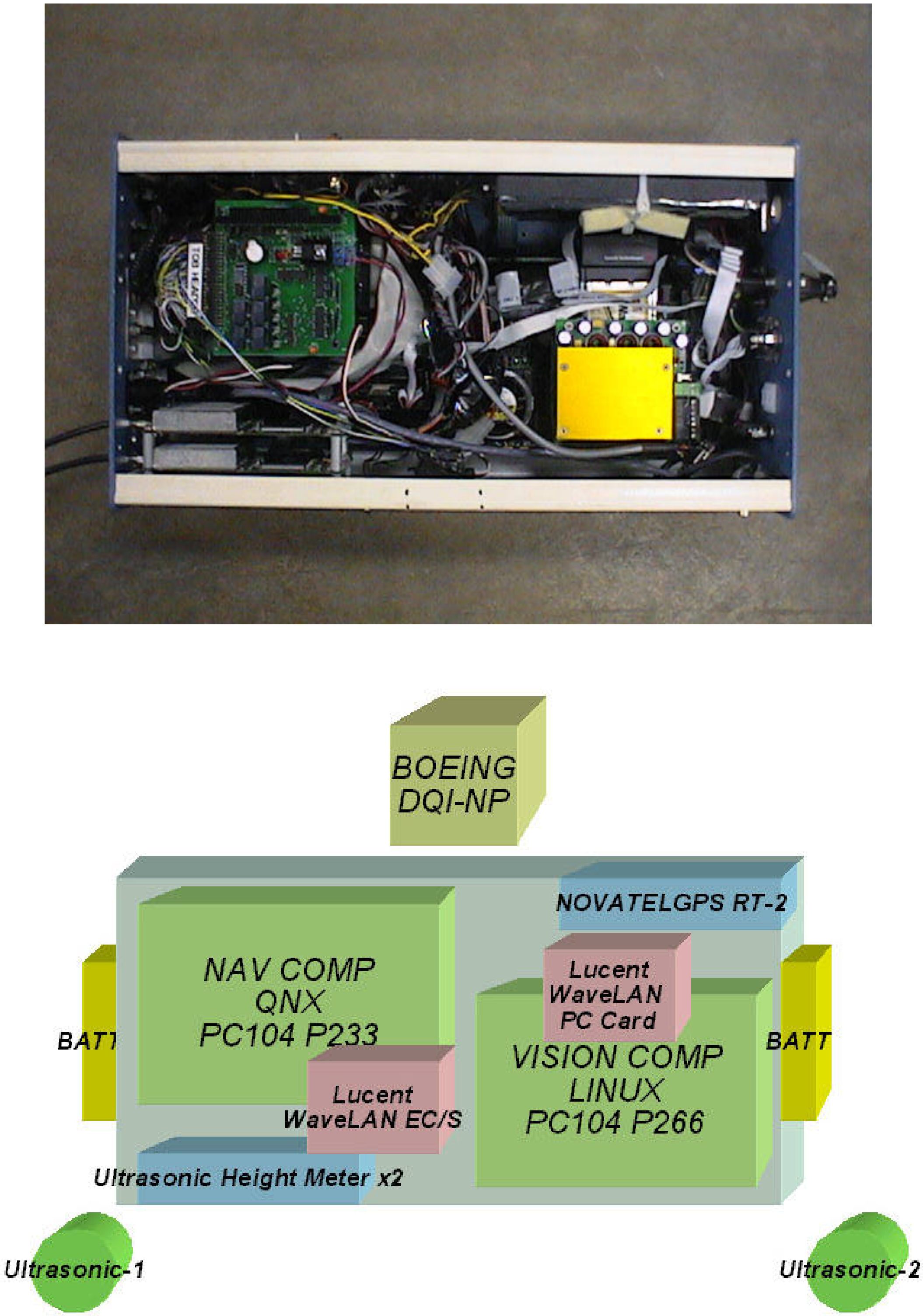

Figure A.3 Inside view of Ursa Magna 2 FCS

A.3 Ursa Maxima2

The avionics of the Ursa Maxima 2 is designed to serve as the testbed for latest research topics such as online identification, fault tolerance, unfalsification, advanced dynamic multi-hop communication and realtime high QoS communication system. Fully taking advantage of the ample payload of Yamaha RMAX, the avionics contains up to four PC104 computers. In the current design, two computers are dedicated to the flight control and background optimization. One computer is for vision processing and another is for advanced wireless communication. These four computers communicate one another through the onboard Ethernet hub and the communication computer serves as the gateway of the advanced wireless communication using the Lucent Orinoco system.

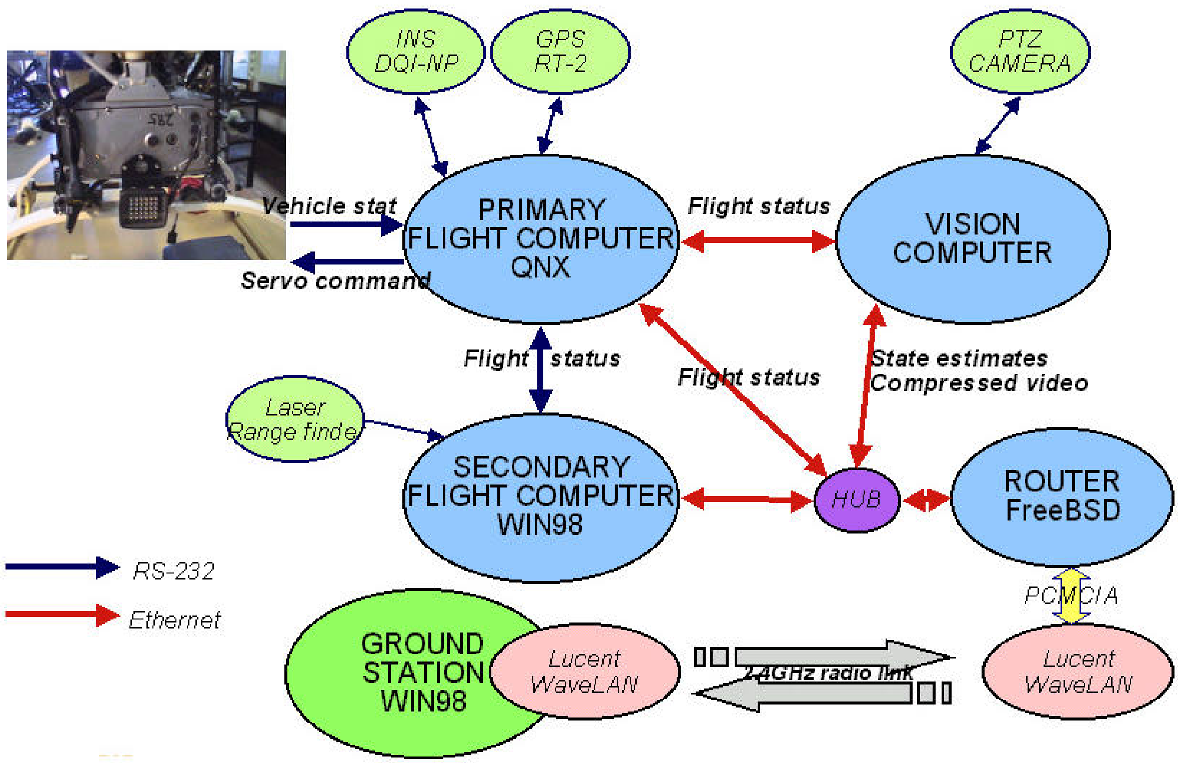

Figure A.4 The information flow in the avionics of Ursa Maxima 2

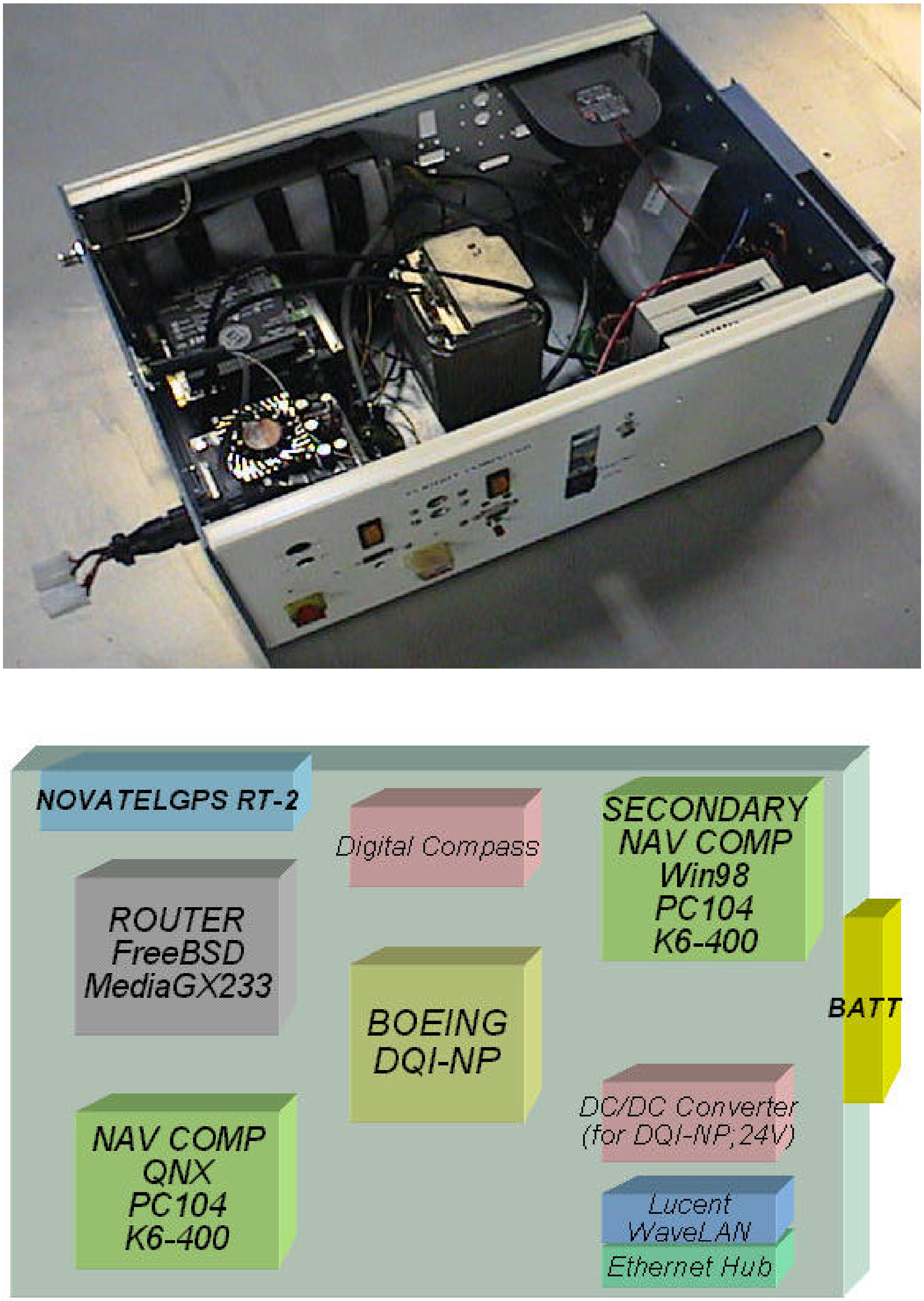

Figure A.5 Avionics for Ursa Maxima 2

A.4 Servomotor Control

A servomotor is a compact electromechanical device consisting of a DC motor with a built-in feedback circuit. These servomotors accept pulse-width modulation (PWM) signals as the reference input. The PWM signal has fixed period and the duration of on-duty varies from 0.8 ms ~ 2.4 ms as shown in Figure A.6.

The controlled output shaft angle is proportional to the on-duty duration of the PWM signal. The midpoint value of 1.6 ms corresponds to the neutral position of the servo. A potentiometer that is geared with the output shaft measures the shaft angle. This measurement is fed through a comparator and motor driver circuit, which minimizes the difference between the actual shaft angle and the commanded angle. In this manner, the output shaft of the servomotor is actuated to the target angle proportional to the on-duty period while resisting the external torque.

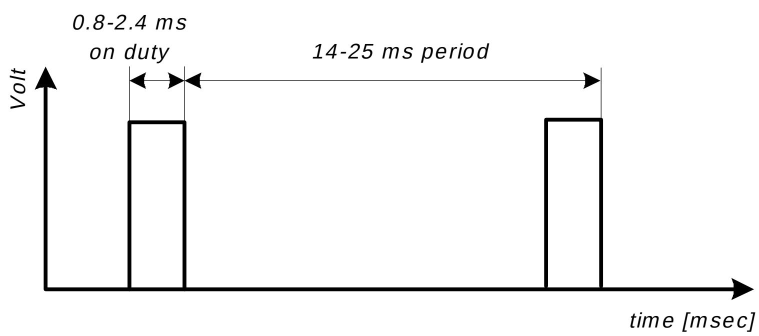

Figure A.6 The characteristics of PWM signal for servomotors

The five-servo configuration is the common setup of all Berkeley RUAVs. The differences come from the PWM characteristics of each receiver. The Kyosho and Bergen helicopters are equipped with the receiver/servomotor system by Futaba Inc. Japan. When operated in PCM (Pulse Coded Modulation), the period of the PWM signal is 14ms while the on-duty duration is identical to the specification shown in Figure A.6. The PWM signals of all channels are synchronized so that the rising edge of the PWM signals occurs at the same time. In Yamaha helicopters, however, the period of the PWM signal is measured as 21.78 ms and the PWM signals are not synchronized as shown in Figure A.11. The Yamaha RMAX does not require PWM signal interception because it offers a more sophisticated interface though serial ports. The receiver status and the servo command are transmitted by RS-232. This approach improves the reliability of the overall system because the wires transmitting the PWM signal for the servo control are not intercepted by any external custom circuits. However, the real time performance is degraded due to the transmission time of the control data over the serial communication channel, which is approximately 14ms. The PWM signal from the receiver has the direct correspondence with the stick manipulation of the radio transmitter by the ground pilot. This capability is essential for the system identification using an input-output sampled data set (Section 2.2.8). The circuit diagram to read and generate the PWM signal for servomotor is shown in Figure A.7. There are many different ways to implement PWM generation circuit. In this research, rather traditional but versatile Intel 8254 counter/timer chip [44] is used. One Intel 8254 chip contains three independent counters. Each counter has one 16-bit read/write register and is controlled by three lines CLK, GATE, and OUT. The counter can operate in one of six user-selectable modes. In this research, modes 0, 1, and 3 are used. Mode 0 works as a simple counter, decrementing the register value by one when the falling edge of CLK is detected and GATE is pulled up high. Hence, mode 0 is used for the engine counter by polling the number of pulses during a constant time interval. Mode 1 is called "hardware retriggerable one-shot" and is used for the PWM signal generation. The CLK is connected to a known accurate clock source, which is set to 2MHz. GATE is connected to the trigger source, which is different among helicopters.

The take-over board (TOB) is a custom print circuit board in PC104 format. This board performs a number of functions vital for autonomous RUAV flight. It resides in the PC104 and operates in cooperation with a Counter-Timer Board (CTB)[1], which has twelve 16-bit counter units, and one 8-bit input and 8-bit output buffered digital I/O port. The TOB consists of the following components:

- Five sets of electromechanical relays
- Opto-isolator at input and output side
- Step-down counter with interrupt selection jumper
- Buzzer
- Isolated 5V regulator power supply for receiver power

The primary task of TOB is switching the source of the PWM signal for the servomotors on the helicopter. The TOB is connected with the CTB, radio receiver output, servo input, and engine encoder. When the vehicle becomes unstable by the PWM signal generated by the onboard controller for any reason, we need to recover the vehicle by the radio control of the human safety pilot on the ground. This is performed by the insertion of five relays in parallel, which switch the servo control from manual radio control to the computer control. The electromechanical relays are chosen so that the control can be automatically recovered when the onboard battery power is drained and

[1] Diamond Systems Cooperation (http://www.diamondsys.com)

consequently the relays de-energize. During manual flights, the relays are turned off and the output of the radio receiver is connected directly to the servos without going through optoisolators. When some or all channels of servo controls should be taken over by the flight computer, the relay control signal is output through the digital output port of CTB and the PWM output from the CTB is injected into the servomotors through the opto-isolators.

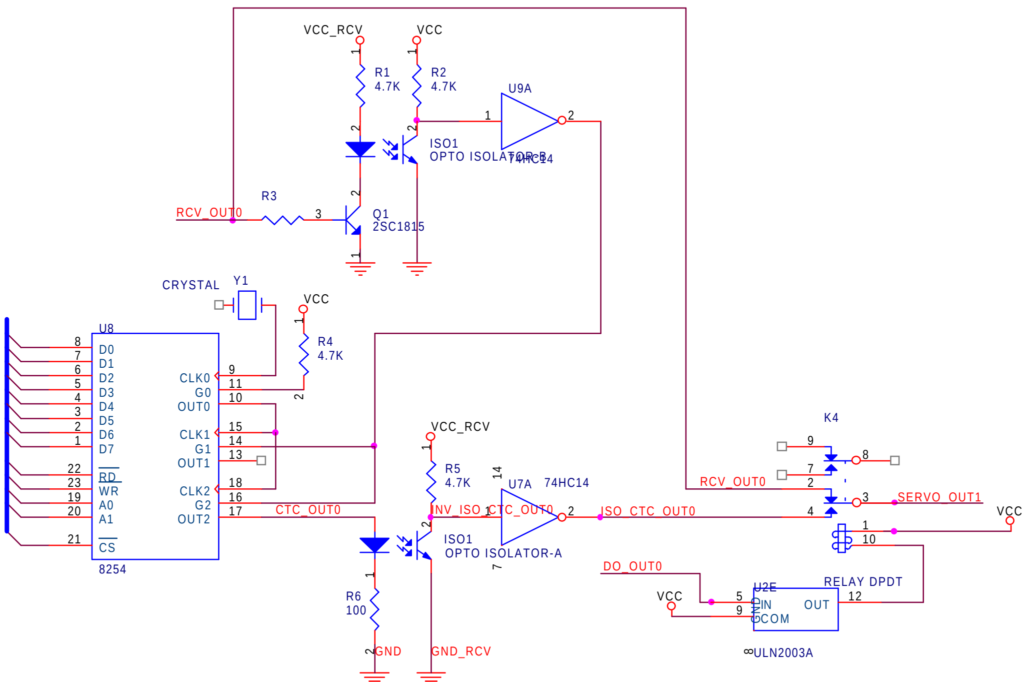

Figure A.7 Schematic diagram of one channel in TOB

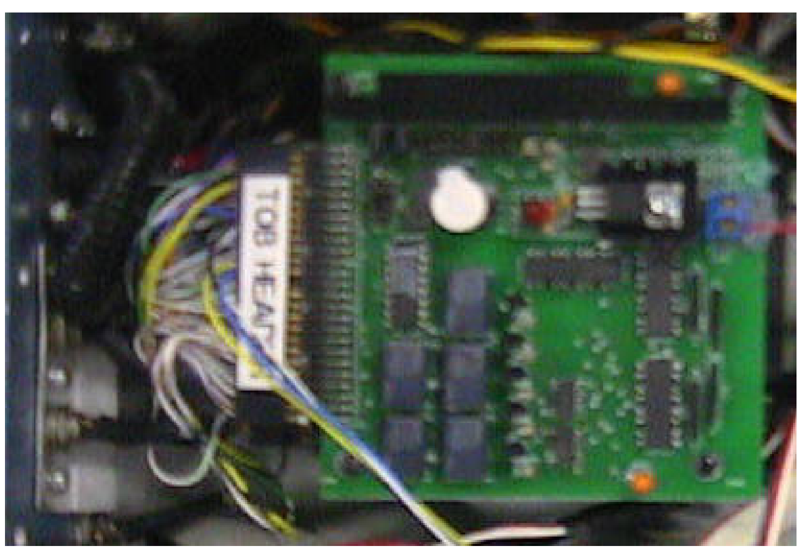

Figure A.8 Take-over board for Ursa Magna 2 FCS

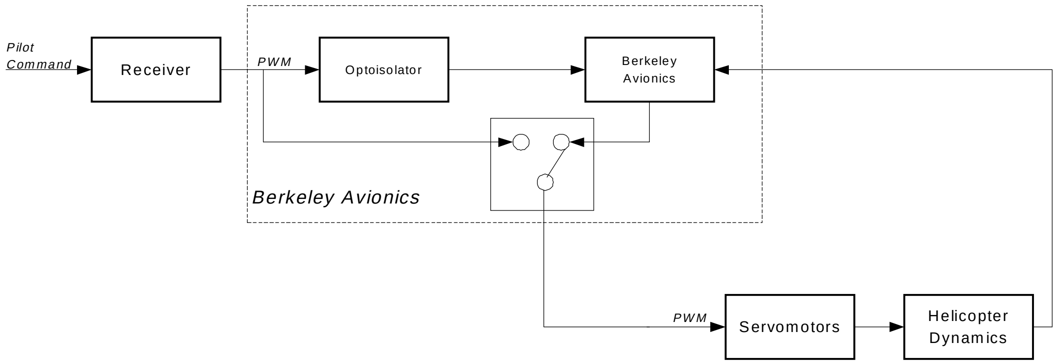

Figure A.9 Signal flow in Ursa Minor 3

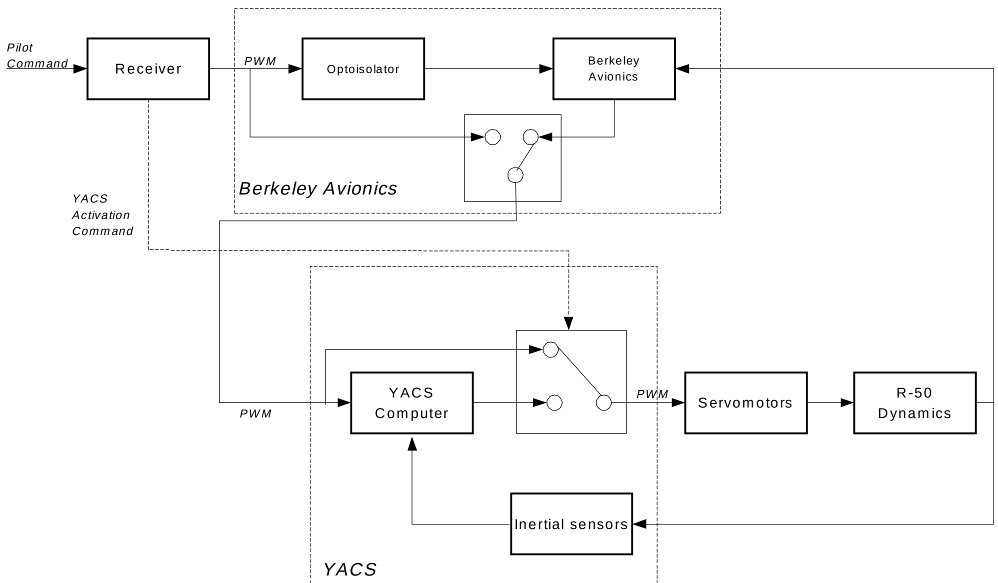

Figure A.10 The signal flow in Ursa Magna 2

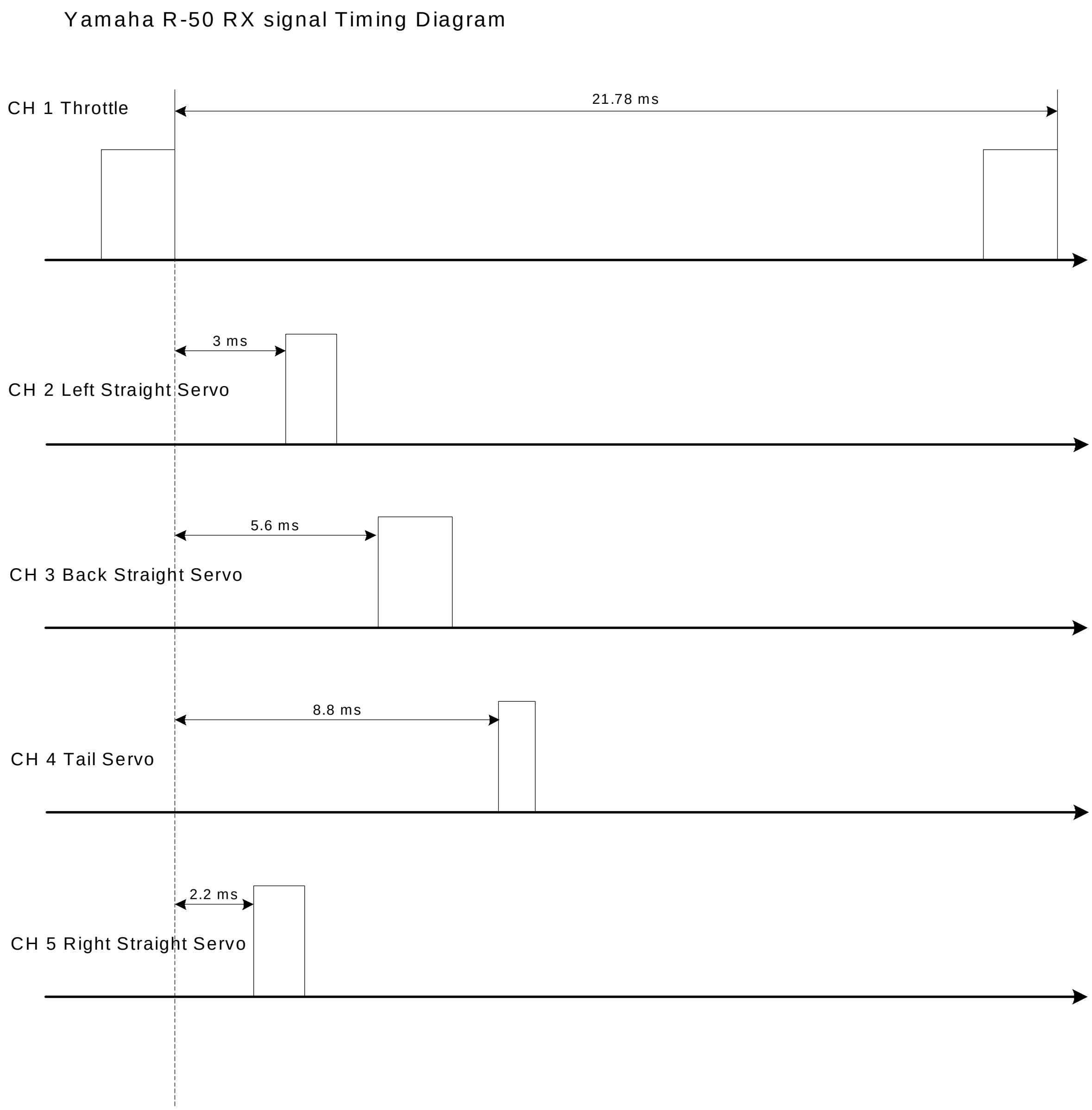

Figure A.11. PWM signal diagram for Yamaha R-50

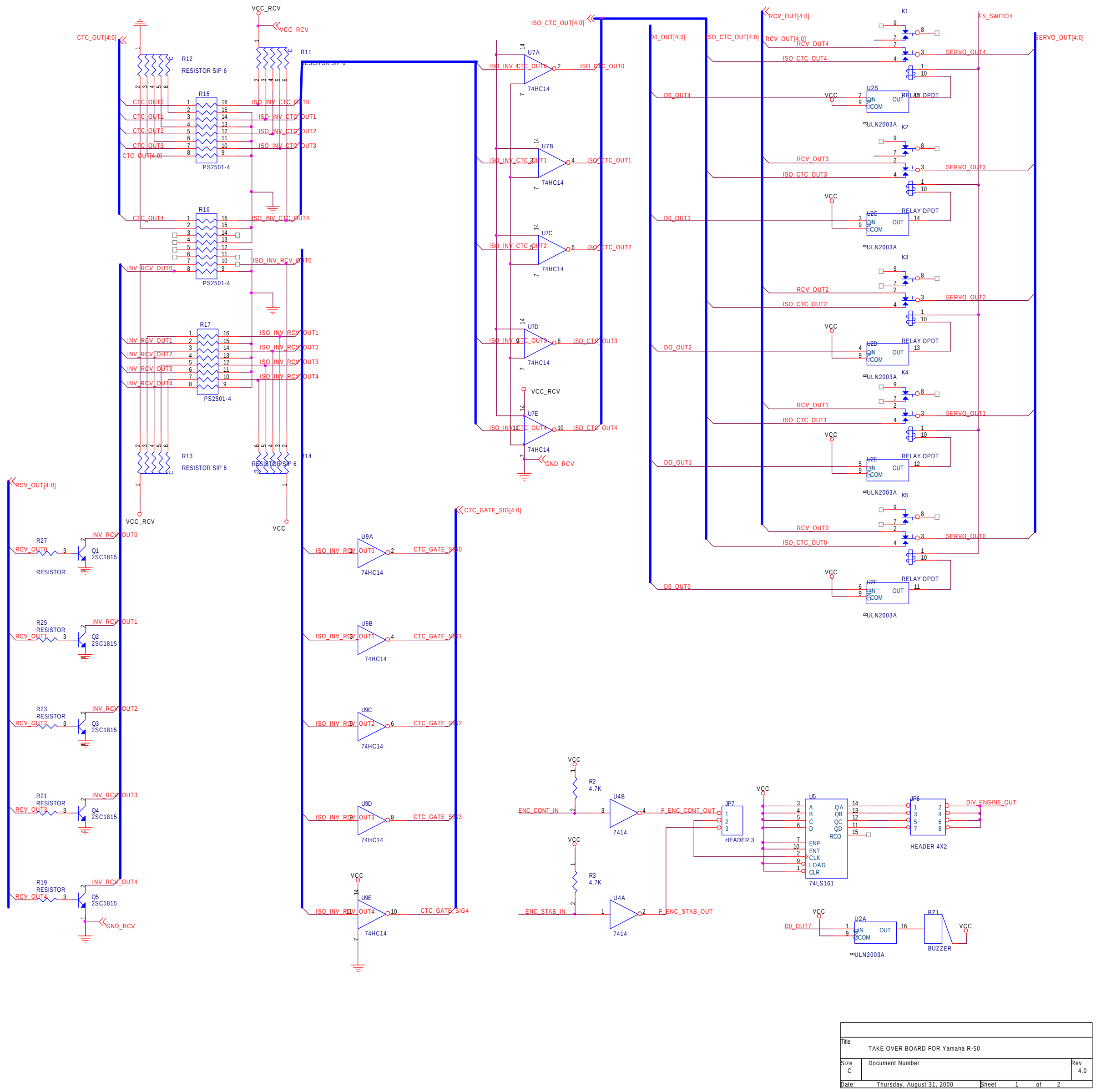

Figure A.12 Schematic diagram of Take-over Board

Appendix B Data Structure

A number of message formats are defined for the communication among aerial vehicles, ground vehicles, vision processing units, and ground monitoring station. The custom messages deliver navigation sensor reading, control output, vehicle status and so on. A message format consists of header and body and each part has its own checksum for extended robustness and security. This type of the data format originated from the Boeing DQI-NP and it was intended to work under streaming data communication channel. This characteristic suits our application because our primary communication channels are either serial communication or streamed TCP. In the following, the general data structure and the format of individual messages are given.

- General data structure

Type	Offset (byte)	Data field type	Description	Content (Example)
Header	0	WORD[1]	Starting marker	0X81FF (always)
	2	WORD	Message ID	1101(decimal)
	4	WORD	Data field size	
	6	WORD	Flags	
	8	WORD	Header checksum	
Body	10	Any type	Data field 1	
	N	Any type	Data field N	
	N+2	WORD	Data checksum	

Every message starts with the marker 0x81FF. Then the message identification number, data field size, flags and the header checksum follow and constitute the header. The data filed size is the number of words of the body except for the data checksum. The flag specifies various handshaking attributes of individual message such as the acknowledge request. The checksums are computed by the following equations:

Header checksum=-0x81FF-(Message ID)-(Data field size)-(Flags)

Data chekcsum=-(Data field 1)-….-(Data field N)

In the following, the data structures for various messages used in our research are listed

[1] In this case, it is defined as 2 byte integer. (`typedef short int WORD`)

- **Message 1001**

Content: PWM reading of receiver and control output, engine RPM, digital input/output

Offset from Body	Data field type	Description	Unit
0	WORD	Receiver Chan #1	0.5 µs
2	WORD	Receiver Chan #2	0.5 µs
4	WORD	Receiver Chan #3	0.5 µs
6	WORD	Receiver Chan #4	0.5 µs
8	WORD	Receiver Chan #5	0.5 µs
10	WORD	Control output Chan #1	0.5 µs
12	WORD	Control output Chan #2	0.5 µs
14	WORD	Control output Chan #3	0.5 µs
16	WORD	Control output Chan #4	0.5 µs
18	WORD	Control output Chan #5	0.5 µs
20	WORD	Engine RPM	Pulse count per 500ms
22	WORD	Digital Input/Output	
24	WORD	Data checksum	

- **Message 1002**

Content: Ultrasonic sensor readings up to four sensors.

Offset from Body	Data field type	Description	Unit
0	float	Ultrasonic sensor #1	m
4	float	Ultrasonic sensor #2	m
8	float	Ultrasonic sensor #3	m
12	float	Ultrasonic sensor #4	m
16	WORD	Data checksum	

- **Message 1101**

Content: Vehicle navigation information from Boeing DQI-NP and the high rate position Kalman estimator

Offset from Body	Data field type	Description	Unit
0	Fixed[3][1]	Difference of roll, pitch, yaw since last measurement (10ms interval)	degree
12	Fixed[3]	Difference of velocity in north, east, up since last measurement (10ms interval)	m/s
24	Fixed[3]	Attitude (pitch, roll, yaw)	degree
36	Fixed[3]	Velocity (north, east, up)	m/s
48	double[3]	Position w.r.t. Local Cartesian coordinate	m
72	double	Reserved; originally intended for single ultrasonic sensor reading	
80	WORD	Data checksum	

- **Message 2001**

Content: Control action request from ground post. The Control ID field contains the control type requested by the ground operator through the monitoring program

Offset from Body	Data field type	Description	Unit
0	WORD	Control ID	
2	WORD	Reserved	
80	WORD	Data checksum	

[1] Non-IEEE standard floating point representation [45]

Control ID	Value	Description
CEM_INIT	0	The controller is just boot up and running idle
CEM_SMANUAL	1	The helicopter is being controlled manually
CEM_SMODE1	2	Controller Mode 1 is being executed
CEM_SMODE2	3	Controller Mode 2 is being executed
CEM_VCL_BATCH	11	VCL is now executed in batch mode
CEM_VCL_INTERACTIVE	12	VCL is now executed in interactive mode
CEM_ABORT	-1	Abort the current control mode

- **Message 4001**

Content: the vehicle position, attitude, and the time stamp.

Issued by the flight computer when requested by the onboard vision computer. The navigation information is referenced for camera coordinate computation.

Offset from Body	Data field type	Description	Unit
0	double	UTC	sec
8	double[3]	Position w.r.t. Local Cartesian coordinate	m
32	double[3]	Attitude (roll, pitch, yaw)	degree
56	WORD	Data checksum	

Appendix C Helicopter Operation

Actual flight test is the crucial stage to validate the proposed algorithms for guidance, navigation, control, hardware, software and so on. Conducting a test flight is by nature a very dangerous process because of the dangerous operating condition of the helicopter-type airframes used in this research. Careful experiment design, equipment check, software debugging, and any and every effort for perfection is required. The experiment is also heavily dependent on the circumstantial factors such as GPS signal characteristics, weather, geography, and other surrounding factors. In this section, the detailed information about the experimental setup and test flight procedures is presented.

Proper setup of RUAV is required for safe and correct operation of a RUAV. A RUAV is operated in the following order:

1. Careful inspection of onboard hardware/software
2. Onboard system battery check
3. Pre-flight RUAV checkup following a checkup list
4. Position of the RUAV in the flight test field
5. Setup of the ground station
6. Start of the ground station and onboard flight computer
7. Start of the flight computer software
8. Initialization of the navigation sensors
   - GPS lockup
   - Initialization of INS
9. Start of the radio transmitter and receiver
10. Start of the helicopter engine
11. Check of the airframe with low-speed and low-altitude manual flight
12. Performing of the intended flight
13. Landing and recovery of the vehicle
14. Switching off the electronics equipments
15. Cleanup of the experiment
16. Post-flight inspection of the RUAV

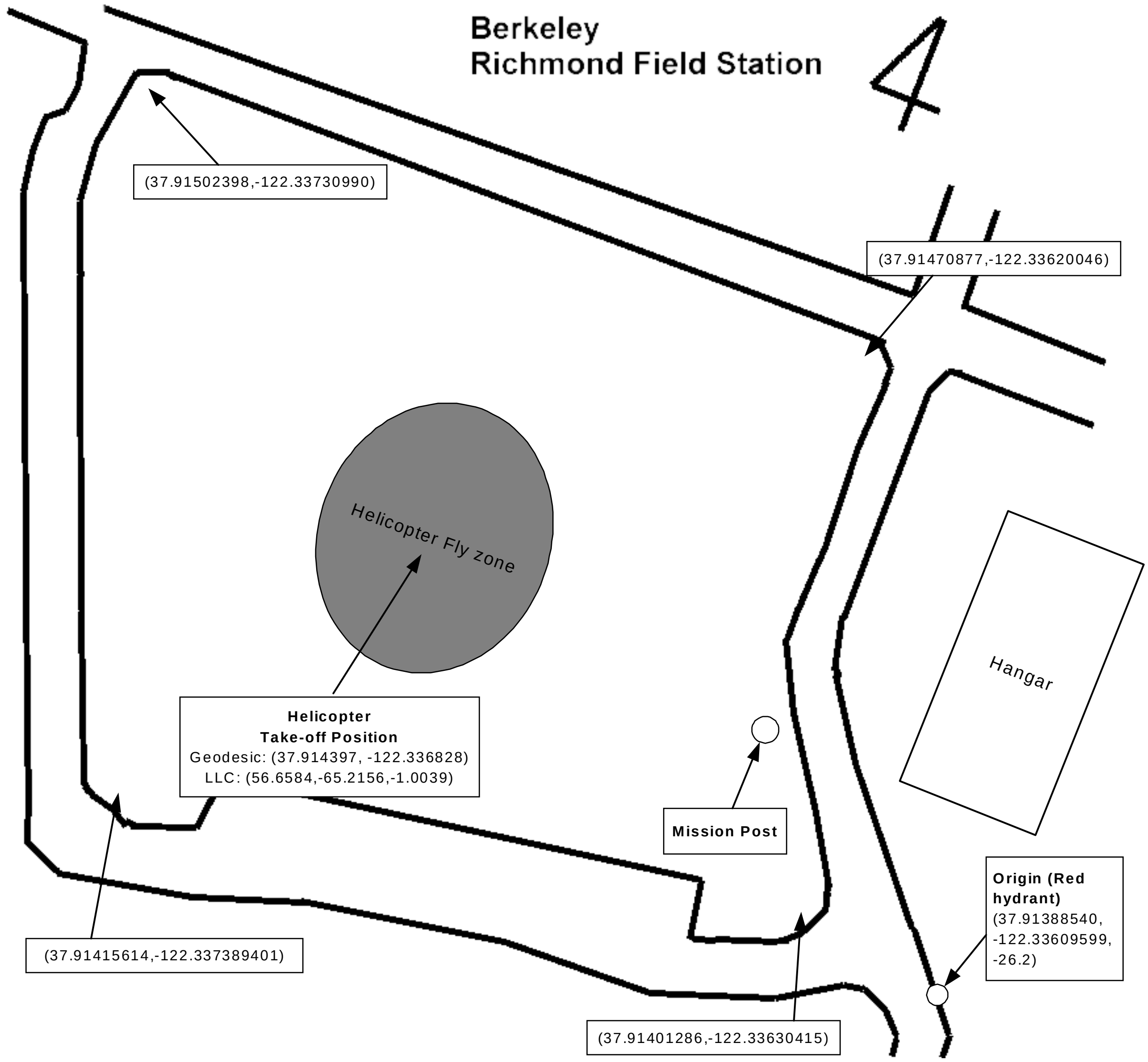

Figure C.1 Aerial view of the test flight site in Richmond, California

Figure C.2 The operation of the ground station for Berkeley UAV research
(left: notebook computer with wireless network capability, monitored by Hoam Chung;
right: ground safety pilot with radio controller; the author)

Appendix D Glossary

AGC	Automatic Gain Control
CSMA/CD	Carrier Sensing Medium Access/Collision Detection
COTS	Commercial Off-The-Shelf
CTC	Counter/Timer Chip
DQI-NP	Digital Quartz Instrument-Navigation Processor
DSP	Digital signal processing
ECEF	Earth-Centered Earth-Fixed
FCS	Flight Control System
FUAV	Fixed-wing-based Unmanned Aerial Vehicle
GPS	Global Positioning System
IMU	Inertial Measurement Unit
INS	Inertial Navigation System
IP	Internet Protocol
LAN	Local Area Network
LTI	Linear Time-Invariant
MIMO	Multi-Input Multi-Output
OCP	Open Control Platform
PC	Personal Computer
PCM	Pulse-Coded Modulation
PEG	Pursuit-Evasion Game
PEM	Prediction-Error Method
PID	Proportional-Integral Differential
PWM	Pulse-Width Modulation
RTOS	Real-Time Operating System
RUAV	Rotorcraft-based Unmanned Aerial Vehicle
QoS	Quality of Service
S/A	Selective Availability
SAS	Stability Augmentation System
SISO	Single-Input Single Output
SSD	Solid-State Disk
TCP	Transmission Control Protocol
TDMA	Time-Division Medium Access
UAV	Unmanned Aerial Vehicle
UDP	User Diagram Protocol
UGV	Unmanned Ground Vehicle
VCL	Vehicle Control Language
VCLEM	Vehicle Control Language Execution Module
VPU	Vision Processing Unit
WGS	World Geodetic System
YACS	Yamaha Attitude Control System

Bibliography

[1] J. Lygeros, *Hierarchical, Hybrid Control of Large Scale Systems,* Ph. D. thesis, Department of Electrical Engineering and Computer Sciences, University of California, Berkeley, 1996.

[2] J. Hespanha, H. J. Kim, S. Sastry, "Multiple-Agent Probabilistic Pursuit-Evasion Games,"*39th IEEE Conference on Decision and Control,* pp. 3511-3516, 1999.

[3] H. Jin Kim , D. H. Shim, S. Rashid, S. Sastry, "Hierarchical System for Multiple-agent Scenarios," submitted to *International Conference on Robotics and Automation*, 2001.

[4] D. H. Shim, H. J. Kim, S. Sastry, "Hierarchical Control system Synthesis for Rotorcraft-based Unmanned Aerial Vehicles," *AIAA Guidance, Navigation, and Control Conference,* August 2000, Denver, CO.

[5] D. H. Shim, H. J. Kim, S. Sastry, "Control System Design for Rotorcraft-based Unmanned Aerial Vehicles using Time-domain System Identification," *Proceedings of the 2000 IEEE International Conference on Control Applications*, pp. 808-813, Anchorage, Alaska, 2000.

[6] H. Shim, T. J. Koo, F. Hoffmann, S. Sastry, "A Comprehensive Study of Control Design for an Autonomous Helicopter," *37th IEEE Conference on Decision and Control,* pp. 3653-3658, 1998.

[7] B. Mettler, M. B. Tischler, T. Kanade, "System Identification of Small-Size Unmanned Helicopter Dynamics," *American Helicopter Society 55th Forum,* Montreal, Quebec, Canada, May 1999.

[8] D. N. Godbole, *Hierarchical Hybrid Control of Automated Highway Systems,* Ph. D. thesis, Department of Electrical Engineering and Computer Sciences, University of California, Berkeley, December, 1994.

[9] C. J. Tomlin, *Hybrid Control of Air Traffic Management Systems*, Ph.D. thesis, Department of Electrical Engineering and Computer Sciences, University of California, Berkeley, Fall, 1998.

[10] R.W. Prouty, *Helicopter Performance, Stability and Control*, Krieger Publishing Company, 1995.

[11] R. K. Heffley and M. A. Mnich, *Minimum-Complexity Helicopter Simulation Math Model,* NASA Contractor Report 177476, April, 1988.

[12] R. D. Murphy, K. S. Narendra, "Design of Helicopter Stabilization Systems Using Optimal Control Theory," *Journal of Aircraft,* Vol. 6, No. 2, March-April 1969.

[13] N. K. Gupta and A. E. Bryson Jr., "Near-Hover Control of a Helicopter with a Hanging Load," *Journal of Aircraft,* Vol. 13, No. 3, March 1976.

[14] M. B. Tischler, J. D. Colbourne, M. R. Morel, D. J. Biezad, W. S. Levine and V. Moldoneanu, "CONDUIT- A New Multidisciplinary Integration Environment for Flight Control Development," *NASA Technical Memorandum 112203,* June 1997.

[15]J. K. Peiper, S. Balillie, and K. R. Goheen, "Linear-Quadratic Optimal Model-Following Control of a Helicopter in Hover," *Proceedings of the American Control Conference,* Baltimore, MD, June 1994, pp. 3470-3474.

[16] W. L. Garrad, E. Low, and S. Prouty, "Design of Attitude and Rate Command Systems for Helicopters using Eigenstructure Assignment," *Journal of Guidance,* Vol. 12, No. 6, Nov.-Dec. 1989.

[17] I. Postlethwaite, A. Smerlas, D. J. Walker, A. W. Gubbels, S. W. Baillie, M. E. Strange, and J. Howitt, "H_∞ Control of the NRC Bell 205 Fly-by-Wire Helicopter," *Journal of the American Helicopter Society,* October 1999, pp. 276-284.

[18] D. J. Walker, and I. Postlethwaite, "Advanced Helicopter Flight Control using Two-Degree-of-Freedom H_∞ Optimization," *Journal of Guidance, Control, and Dynamics,* Vol. 19, No. 2, March-April 1996, pp. 461-468.

[19] M. D. Takahashi, "H_∞ Helicopter Flight Control Law Design With and Without Rotor State Feedback," *Journal of Guidance, Control, and Dynamics,* Vol. 17, No. 6, November-December 1994, pp. 1245-1251.

[20] D. Maclay, S. J. Williams, "The Use of mu-Synthesis in Full Envelope Helicopter Flight Control System Design,"

[21] W. E. Hall Jr. and A. E. Bryson Jr., "Inclusion of Rotor Dynamics in Controller Design for Helicopters," *Journal of Aircraft*, Vol. 10, No. 4, April 1973.

[22] M. D. Takahashi, "Rotor-State Feedback in the Design of Flight Control Laws for a Hovering Helicopter," *Journal of the American Helicopter Society,* Jan. 1994, pp. 50-62.

[23]S. J. Ingle, and R. Celi, "Effects of Higher Order Dynamics on Helicopter Flight Control Law Design," 48*th* *Annual Forum of the American Helicopter Society,* Washington, D. C., June 1992, pp. 12- 23.

[24] K. Furuta and T. Shiotsuki, "Training Simulator of Radio Control Helicopter," *10th IMACS World Congress on System Simulation and Scientific Computation*.

[25] J. Pallet, B. J. Wolfert, and S. Ahmad, "Real Time helicopter Flight Control Test Bed," *Technical Report TR-EE 91-28,* School of Electrical Engineering, Purdue University, 1991.

[26] H. Shim, *A Study on the Design of Hovering Flight Controller for a Model Helicopter*, Master's Thesis, Seoul National University, Seoul, Korea, 1993.

[27] J. C. Morris, M. van Nieuwstadt, and P. Bendotti, "Identification and Control of a Model Helicopter in Hover," *Proceedings of the American Control Conference,* Baltimore, MD, June 1994, pp. 1238-1242.

[28] H. Sira-Ramirez, M. Zribi, and S. Ahmad, "Dynamical Sliding Mode Control Approach for Vertical Flight Regulation in Helicopters," *IEE Proceedings of Control Theory Applications,* Vol. 141, January, 1994, pp. 19- 24.

[29] P. Bendotti and J. C. Morris, "Robust Control for a Model Helicopter," *Proceedings of the American Control Conference,* Seattle, Washington, June 1995, pp. 682-687.

[30] A. R. Conway, *Autonomous Control of an Unstable Model Helicopter Using Carrier Phase GPS Only,* Ph. D. Thesis, Department of Electrical Engineering, Stanford University, March 1995.

[31] C. P. Sanders, P. A. DeBitetto, E. Feron, H. F. Vuong, N. Leveson, "Hierarchical Control of Small Autonomous Helicopters," *37th IEEE Conference on Decision and Control,* pp. 3629-3634, 1998.

[32] J. E. Corban, A. J. Calise, J. V. R. Prasad, "Implementation of Adaptive Nonlinear Control for Flight Test on an Unmanned Helicopter," *37th IEEE Conference on Decision and Control*, pp. Pp. 3641-3646, 1998.

[33] R. T. N. Chen, M. B. Tischler, "The Role of Modeling and Flight Testing in Rotorcraft Parameter Identification," The 1986 AHS Forum, System Identification Session, Washington, D.C., 1986.

[34] L. J. Ljung, *Matlab System Identification Toolbox User's Guide* , The Math Works, Inc.,1997.

[35] L. J. Ljung and E. J. Ljung, *System Identification: Theory for the User*, 2nd ed., Prentice-Hall, 1998.

[36] J. A. Farrell and M. Barth, *The Global Positioning System & Inertial Navigation*, McGraw Hill, 1998.

[37] G. M. Siouris, *Aerospace Avionics Systems,* Academic Press, Inc., 1993.

[38] J. A. Schroeder, M. B. Tischler, D. C. Watson, and M. M. Eshow, "Identification and Simulation Evaluation of a Combat Helicopter in Hover," *Journal of Guidance, Control and Dynamics*, Vol. 18, No. 1995, pp. 31-38.

[39] E. A. Fradenburgh, "The Helicopter and the Ground Effect Machine," *Journal of American Helicopter Society*, 1960, pp. 24-33.

[40] M. Sargent, and R. L. Shoemaker, *The Personal Computer from the Inside Out,* 3rd edition, Addison-Wesley, 1995.

[41] R. Krten, *Getting Started with QNX® 4*, PARSE Software Devices, 1998.

[42] *QNX Operating System- Installation & Configuration,* QNX Software Systems Ltd. 1996.

[43] *QNX Operating System- System Architecture*, QNX Software Systems Ltd. 1996.

[44] *Intel 8254 counter/timer chip user guide*, Intel Press

[45] *DQI-NP Integrated INS/GPS User's Guide*, Boeing Electronic Systems & Missile Defense, 1999.

[46] R. K. Mehra, S. Mahmood, and R. Waissman, "Identification of Aircraft and Rotorcraft Aeroelastic Modes using State Space System Identification," *IEEE ????*, 1995, pp. 432-437.

[47] F. L. Lewis, *Optimal Estimation*, John Wiley & Sons, 1986

[48] X. D. Sun, and I. Posltethwaite, "Affine LPV Modelling and Its Use in Gain-scheduled Helicopter Control," *UKACC International Conference on CONTROL '98,* September, 1998, pp. 1504-1509.

[49] G. J. Balas, J. C. Doyle, K. Glover, A. Packard, R. Smith, μ*-Analysis and Synthesis Toolbox User's Guide*, The MathWorks Inc., 1995